National Library of Canada
Acquisitions and Bibliographic Services Branch
395 Wellington Street
Ottawa, Ontario
K1A 0N4

Bibliothèque nationale du Canada
Direction des acquisitions et des services bibliographiques
395, rue Wellington
Ottawa (Ontario)
K1A 0N4

Your file Votre référence

Our file Notre référence

NOTICE

The quality of this microform is heavily dependent upon the quality of the original thesis submitted for microfilming. Every effort has been made to ensure the highest quality of reproduction possible.

If pages are missing, contact the university which granted the degree.

Some pages may have indistinct print especially if the original pages were typed with a poor typewriter ribbon or if the university sent us an inferior photocopy.

Reproduction in full or in part of this microform is governed by the Canadian Copyright Act, R.S.C. 1970, c. C-30, and subsequent amendments.

AVIS

La qualité de cette microforme dépend grandement de la qualité de la thèse soumise au microfilmage. Nous avons tout fait pour assurer une qualité supérieure de reproduction.

S'il manque des pages, veuillez communiquer avec l'université qui a conféré le grade.

La qualité d'impression de certaines pages peut laisser à désirer, surtout si les pages originales ont été dactylographiées à l'aide d'un ruban usé ou si l'université nous a fait parvenir une photocopie de qualité inférieure.

La reproduction, même partielle, de cette microforme est soumise à la Loi canadienne sur le droit d'auteur, SRC 1970, c. C-30, et ses amendements subséquents.

Canada

Viscoelastic Properties of Paper in a Calender Nip

by

Thomas Carl Browne

Department of Chemical Engineering

McGill University

Montreal

August 1994

A thesis submitted to the Faculty of Graduate Studies and Research
in partial fulfillment of the requirements for the
degree of Doctor of Philosophy

ISBN 0-612-05681-3

Canada

In memory of

Lawrence and Roula

Table of Contents

Abstract

Paper in a calender nip is subjected to a compressive pressure pulse which reduces its thickness and roughness, thus improving the product quality. Strain recovery after the nip is time-dependent, and some permanent strain remains. The material behaviour is viscoelastic; recovery depends on the pulse magnitude and duration, and does not occur immediately on exiting the nip. An improved description of the viscoelastic response to a calender pulse would allow design of adaptive control systems using feedforward techniques.

Measurements of paper thickness in the nip, immediately after the nip and 24 hours after calendering were made with newsprint sheets running through an experimental calender operating at industrial conditions. The calculated strains were first related to the operating conditions using empirical curve-fitting methods, then using linear viscoelastic models. Empirical results describe the data well, and can be used to design improved control systems. Linear viscoelastic modeling was less successful since the material behaviour is not linear. Photomicrographs of sheet cross-sections were taken, and the observed non-linearities were discussed qualitatively in terms of paper and fibre properties.

Résumé

Dans une calandre, l'épaisseur et la rugosité d'une feuille de papier sont réduites par l'application d'une charge en compression. Ce procédé améliore la qualité du produit. La feuille subit une grande déformation dans la pince, puis recouvre une partie de l'épaisseur originale à la sortie. Cette récupération n'est pas instantanée, mais requiert un certain temps. Le papier se comporte donc de façon viscoélastique. Une description améliorée des caractéristiques viscoélastiques du papier servirait à la conception de systèmes de contrôle adaptifs pour l'épaisseur de la feuille à la sortie de la calandre.

Les déformations dans la pince, à deux endroits immédiatement après la pince et 24 heures après le calandrage ont étés mesurées sur une calandre échèlle laboratoire reproduisant des conditions industrielles typiques. Le papier en question était un papier journal du Québec. Les déformations sont décrites en premier lieu avec des relations empiriques, puis avec des modèles viscoélastiques linéaires. Les relations empiriques décrivent bien les déformations, et peuvent maintenant servir à la conception de systèmes de contrôle améliorés. Par contre, les modèles viscoélastiques se sont montrés moins utiles puisque le papier ne se prête pas facilement à une analyse linéaire. Des photomicrographies de sections de feuilles ont été prises, et l'aspect non-linéaire du papier est discuté en termes qualitatifs à partir des propriétés fondamentaux du papier et de la fibre.

Acknowledgements

It is now my pleasant duty to thank all the people who had a hand, however indirect, in the completion of this research project. Hopefully, I haven't forgotten anyone; if I have, please accept my apologies.

First, I wish to thank my advisors, Dr. R.H. Crotogino and Dr. W.J.M Douglas, for their continued technical and financial support, without which this thesis would not have been possible.

The calendering specialists at Paprican's Pointe Claire laboratory invariably had time for discussion. For their time and encouragement, I wish to extend my thanks to Dave McDonald, Michel Gratton, Jean Hamel, Larry Gee and Steve Smallwood.

James Drummond, of Paprican's Vancouver laboratory, prepared the samples and took the micro-photographs presented in Chapter 5.

The electronics and machine shop staffs at McGill University's Department of Chemical Engineering and at Paprican's Pointe Claire laboratory were unfailingly helpful in maintaining the complex experimental equipment necessary for this work.

The following people offered continuous moral support and encouragement, and their various contributions are gratefully acknowledged:

Anne Abbey, Sue Adams, Korkor Amarteifio, Jean-François Bond, Catherine Browne, Marie Carlson Browne, Michael Browne, Robert Browne, Anna Cicciarelli, Charles Dolan, Johanne Duchêne, Joseph Grassi, Dr. R.J. Kerekes, Bill Kreklewetz, Spiros Lazaris, Rebecca MacIntyre, Rob McCleave, Roula Najjar, Antoinette Paventi, Dr. I.I. Pikulik, Dr. I.T. Pye, Lawrence Ramsay, Patti Turner, Michael Weir, Domenico and Angela Zampini, Lucy Zampini, Phil Zampini, Rita Zampini.

Last but certainly not least, I wish to thank my family, Mary, Tara and Alexander, for their moral support and understanding. I would not have been able to finish this project without their help.

Nomenclature

The number in parentheses gives the Chapter where the variable is defined.

a	Ingoing nip length, mm (2.2)
a_c	Roughness compensated ingoing nip length, mm (5.3.2)
A	Intermediate variable for Burger's model (5.2.2)
A_{ij}, a_{ij}	Calendering equation coefficients (2.1) Subscripts: *i*: o offset, L Load, M Moisture content, P Pressure, S Sheet speed, R Radius, t time, θ temperature. *j*: n in-nip, r recovered, p permanent.
A_1	Second order calendering equation coefficient (4.1.1)
A_2, a_{o2}, a_{L2}, a_{R2}, a_{S2}	Coefficients for density equation (4.1.1)
B_i, B_p	Initial and permanent (fully recovered) paper bulk, cm^3/g (2.1)
b	Outgoing nip length, mm (4.2.1)
b_{max}	Largest possible value of b, mm (4.2.1)
C	Roll circumference, m (3.2)
CD	Cross-machine direction in a paper machine (1)
C_V	Coefficient of variation (4.1.1)
c, c_0, c_1	Curve fitting coefficients (4.2.3)
E	Elastic modulus, Pa (2.1)
E_{xx}, E_{yy}, E_{zz}	Elastic moduli, GPa (2.2)
$F(\varepsilon)$	Shape factor (2.1)
G, G_e	Spring moduli, Pa (2.2)
G_K, G_M	Spring moduli, Pa (5.2.2)
G_{xx}, G_{yy}, G_{zz}	Shear moduli, GPa (2.2)
K_1, K_2	Intermediate variables for Burger's model (5.2.2)
k_1, k_2, k_3	Curve fitting coefficients (5.2.3)
L	Nip load, kN/m (2.1)
L_{lim}	Curve fitting constant (4.2.2)
M	Paper moisture content, % (2.1)
M_{50}	Paper moisture content corrsponding to 50% R.H., % (3.2)
MD	Machine direction in a paper machine (1)
m, n	Curve fitting constants (4.2.1)
m_1, m_2	Curve fitting constants (4.2.2)
p_1, p_2	Intermediate variables for Burger's model (5.2.2)
P	Nip pressure, Pa (2.1)
P(x,z)	Point on the roll surface with coordinates x,z (5.2.1)
q_1, q_2	Intermediate variables for Burger's model (5.2.2)
R	Roll radius, m (2.1)
r_1, r_2	Intermediate variables for Burger's model (5.2.2)
S	Sheet speed, m/min (2.1)

S.E.	standard error (4.1.1)
T	Total data acquisition time, s (3.2)
T_o, T_n, T_r	Initial, in-nip and recovered paper thicknesses, μm (2.1)
t	Elapsed time, s (2.1)
t_1, t_2	Dwell times, s (2.2)
t_e	Nip dwell time, s (5.2.2)
t'	Variable of integration (2.2)
u, u_o	Upper roll position, μm (3.1.2)
v, v_o	Lower roll position, μm (3.1.2)
v_a, v_f	Volume of air or fibre in a paper sheet (5.3.3)
V	Sheet velocity, m/s (4.2.1)
W	Machine width, m (5.2.3)
$W_{\Delta r}$	Roll deformation width, mm (2.1)
x	Distance in the machine direction, m (3.2)
x_1	An arbitrary in-plane direction (5.3.2)
z	Thickness direction in a paper machine (1)
$z(t)$	Paper surface position, μm (5.2.1)
z_c	Roughness-compesnated sheet half-thickness, μm (5.3.2)
z_i, z_n, z_e, z_p	Initial, in-nip, exit and permanent sheet half-thickness, μm (4.2.1)
z_o	Roll indentation, μm (5.2.1)
z_r	Roughness height, μm (5.3.2)
β, β_{max}	Nip length ratios (5.2.2)
Γ	Machine drive torque, N m (5.2.3)
$\delta(t)$	Unit impulse function (5.2.2)
Δr_p	Peak roll radius deformation, μm (2.1)
ΔT	Change in paper thickness, μm (2.1)
ε_c	Roughness compensated initial strain (5.3.2)
ε_{corr}	Corrected paper strain (3.2)
ε_e	Paper strain at the nip exit (4.2.1)
ε_{el}	Instantaneous elastic strain recovery (5.2.3)
ε_K	Strain in a Kelvin element (5.2.3)
ε_n, ε_r, ε_p	In-nip, partially recovered and permanent paper strains (2.1)
ε_N	Critical strain (2.1)
ε_0, ε_1	Step strain input (2.2)
ε_o, ε_∞	Curve fitting constants (4.2.2)
ε_R	Recoverable strain (4.2.2)
$\varepsilon_1(t)$	In-nip strain history (5.2.1)
$\varepsilon_2(t)$	Post-nip strain history (5.2.1)
η	Viscosity, Pa s (2.2)
η_K, η_M	Viscosities, Pa s (5.2.2)
θ	Sheet temperature, °C (2.1)
μ	Nip intensity coefficient (2.1)
μ_n, μ_r, μ_p	In-nip, recovered and permanent intensity coefficients (2.1)

μ_{p1}, μ_{p2}	Second order calendering equation nip intensities (4.1.1)
μ_2	Nip intensity for density equation (4.1.1)
ξ	Devorah number (2.2)
ξ_1, ξ_2	Devorah numbers for Burger's model (5.2.2)
ξ_K, ξ_M	Devorah numbers for Burger's model (5.2.2)
ρ	Paper density, g/cm^3 (4.1.1)
ρ_f, ρ_p	Fibre and paper paper density, g/cm^3 (2.1)
ρ_o, ρ^*	Initial and maximum paper density, g/cm^3 (2.1)
$(\rho_n)_{max}$, $(\rho_p)_{max}$	Maximum in-nip and permanent paper densities, g/cm^3 (4.1.2)
ρ_{xy}, ρ_{xz}, ρ_{yx}, ρ_{yz}, ρ_{zx}, ρ_{zy}	Poisson's ratios (2.2)
σ	Compressive stress, Pa (2.1)
σ_0, σ_1	Step stress input, Pa (2.2)
$\sigma_K(t)$	Stress imposed on a Kelvin element, Pa (5.2.3)
$\sigma_V(t)$	Stress imposed on a viscous component, Pa (5.2.3)
$\phi(t)$, $\phi_1(t)$, $\phi_2(t)$, $\phi_3(t)$	Strain retardation functions, Pa^{-1} (2.2)
$\psi(t)$, $\psi_1(t)$, $\psi_2(t)$, $\psi_3(t)$	Stress relaxation functions, Pa (2.2)
τ	Time constant, s (2.2)
τ_1, τ_2	Time constants for Burger's model (5.2.2)
τ_K, τ_M	Time constants for Burger's model (5.2.2)

Figures and Tables

a) Figures:

b) Tables:

1. Introduction

For most grades of paper, the last processing step is calendering. This operation reduces paper thickness and roughness by pressing the sheet between two or more large cast iron rolls. The high loads encountered in the nip between two smooth calender rolls flatten high spots in the rough sheet by permanently deforming wood fibres on the surface of the sheet, thus reducing the roughness of the sheet. Fibres inside the sheet are also deformed, reducing the thickness. The process is the papermaker's last chance to reduce thickness variations along the length and width of the finished sheet. A smoother sheet results in improved print quality, while more uniform thickness profiles improve the winding process and reduce sheet breaks in printing presses. The calendering operation thus improves the quality of the finished product.

In the Cartesian coordinate system defined for paper machines, the direction of paper travel is called the machine direction (MD), the direction across the width of the machine the cross-machine direction (CD), and the direction perpendicular to the paper plane the *z*-direction. Specific volume, referred to in the paper industry as paper bulk, cm^3/g, is the ratio of thickness (or *z*-direction dimension, in μm) to basis weight (mass per unit area, in g/m^2), and is the inverse of apparent density. Thickness is typically reduced by calendering; since MD and CD dimensional changes due to calendering are typically several orders of magnitude smaller than the corresponding *z*-direction strain, basis weight changes are usually small and the thickness reduction is essentially equal to the bulk reduction.

While surface properties are mainly of interest to the printer, the papermaker can most easily measure thickness or bulk on-line. The relationships between thickness reduction and surface properties such as roughness and gloss have been well documented in the past [19, 24, 26]; thus any change in thickness reduction can be related to changes in paper properties by referring to published work. The present work therefore refers only to thickness reduction, bulk reduction and strain.

The amount of bulk reduction depends on several process variables. Load,

machine speed and roll radius define the magnitude and duration of the applied pressure pulse. These variables, along with the number of nips, determine the work done on the paper. Bulk reduction also depends on paper properties such as initial bulk, moisture content and in-nip temperature, which determine paper response to a calender pulse. The effects of these calendering variables on the CD average bulk reduction have been quantified and can be calculated by means of the calendering equation [18, 22, 23, 24, 76].

Paper bulk at the entrance to a calender may vary both in the machine and cross-machine directions. Machine direction variations can be reduced in the calender by altering the average cross-direction load. Hydraulic loading systems respond relatively quickly, so real-time control of long-wavelength machine direction thickness or bulk variations is straight-forward.

Cross-machine variations can be minimized by varying the local roll radius profile, thus changing the local pressure profile. Commonly, a larger local roll radius for more bulk reduction is obtained by heating the roll locally using impinging hot air jets, induction coils or infrared heaters. Higher local temperatures result in small radial deformations of the roll surface. While roll diameter is typically of the order of 1 meter, paper thickness entering the calender is of the order of 10^{-4} m; thus a radial roll deformation of a few microns, corresponding to a radial strain of the order of 10^{-6}, is very small compared to the scale of the roll but enormous when measured on the scale of the paper, where the same roll deformation imposes a z-direction strain on the paper of the order of 10^{-2}. The cross-direction radius profile resulting from a given temperature profile can be calculated [41, 42, 68, 69] given details of the heating system and the roll geometry. Unlike hydraulic loading systems, thermal methods for CD control are slow due to the high thermal inertia of a typical calender roll, leading to significant delays in implementing a control action.

Web temperature and moisture content can vary across the width of a paper web as it enters the calender, often due to uneven conditions in the dryer section. These variations can cause roll temperature variations as the sheet wraps around the roll, in turn

causing further local roll radius changes. Along with variations in initial bulk and control actions taken by the papermaker, these thermal deformations result in cross-direction variations in the load distribution which cannot be taken into account using the calendering equation since local values of roll radius and nip load are not easily measured. In order to determine the local bulk reduction or the final bulk profile using the calendering equation, either the load distribution or the radius distribution and its effect on the load must be known.

The roll temperature profile required for a given radius profile can be calculated; the means of achieving the desired profile is also known. However it has not been possible to determine the radius profile required to create a desired bulk profile since the rheological properties of paper in a rolling nip have not been known. A relationship between local stress and strain for paper in a calender nip is the final element required for a complete explicit description of cross-machine calender control.

This stress-strain relationship cannot easily be determined using simple methods since the behaviour of paper under compression is neither elastic nor viscous, but viscoelastic. Both the strain under load and the permanent residual strain after removal of the load depend not only upon the magnitude of the load, but also on the dwell time during which it was applied. Since the calendering process applies a roughly parabolic pressure profile which reaches peaks of several megapascals and lasts for only a few hundred microseconds, equipment such as bench-top platen presses are inadequate for this purpose.

The present work describes part of an ongoing research project whose goal is the development of a cross-machine control system for bulk leaving a calender. The project consists of three distinct but complementary steps. The first step focused on the unsteady state and steady state response of a rotating calender roll to heat transfer from an array of impinging hot air jets, and on the radius profile resulting from thermal deformation of the roll [41, 42, 68, 69]. The second step focused on describing the paper response to local variations in calendering conditions, and was itself divided into two parts: the first part [8, 9] was the design and construction of a new experimental paper calender

allowing accurate and repeatable measurement of the in-nip paper thickness under industrially relevant calendering conditions; the second part, the topic of this thesis, was a complete experimental program to make these local, in-nip thickness measurements using the new equipment, followed by empirical and viscoelastic modeling of paper response to local calendering conditions. The final step, now underway as the topic of a future thesis, is the combination of the two previous steps, actuator design and material response to an actuator input, into a complete description of cross-direction calender control.

2. Literature review

2.1 Paper calendering

Paper is compressed by a pressure pulse in a calender nip, then exhibits time-dependent partial recovery of its initial thickness. The in-nip and permanent deformations and their dependence on this pulse are the subject of the current work. Peel [66, 67] compiled comprehensive reviews of calendering practice and theory, updating an earlier review by Baumgarten et al. [3]. This first section of the literature review examines some of the more important results described by Peel and subsequent researchers.

The effect of a pressure pulse on paper thickness was investigated by Chapman and Peel [15] using a platen press. They derived empirical relationships for compressed and recovered paper thicknesses as functions of maximum pressure and pulse duration, which they called master creep relationships:

$$\frac{T_o - T_n}{T_o} = A_n (1 + \tanh \mu_n)$$
$$\frac{T_o - T_r}{T_o} = A_r (1 + \tanh \mu_r) \qquad [2.1]$$

where the nip intensity coefficients μ_n and μ_r are given by

$$\mu_n = a_{on} + a_{Pn} \log_{10} P + a_{tn} \log_{10} t$$
$$\mu_r = a_{or} + a_{Pr} \log_{10} P + a_{tr} \log_{10} t \qquad [2.2]$$

and where T_o, T_n, T_r are the initial, in-nip and recovered paper thicknesses. The constants A, a_o, a_P and a_t were obtained by curve fitting, and describe the effects of maximum applied pressure P and dwell time t. The shortest pulse duration was about 6 ms, which is an order of magnitude or more greater than the dwell time in a commercial calender, and the pressures applied were fairly constant over that duration; the results therefore describe the creep characteristics of paper rather than the response to a

calendering pulse. Furthermore, the effect of successive compressions was not analyzed. The work was extended by Colley and Peel [17] to include the effect of web temperature and moisture content.

Kerekes et al. [44, 46] modified these relationships to predict directly the thickness reduction in a calender in terms of nip load, roll radius and machine speed rather than maximum pressure and pulse duration, an advantage to the papermaker since load, speed and radius are easily measured on-line while maximum pressure and dwell time are not. The predictions were based on assumptions regarding the viscoelastic behaviour of paper, which will be discussed subsequently, and were verified using a laboratory-scale calender at speeds approaching industrial values. The equipment thus produced a pressure pulse much more typical of a commercial calender than the platen press used by Peel et al. [15, 17].

Haglund and Robertson [34] used optical methods to measure paper thickness in the nip of a small laboratory calender run at low speeds. Their roll diameters and sheet speeds were both extremely small compared to industrial practice, which limits the applicability of their results; nonetheless they found (in agreement with Colley and Peel [17]) that while initial density had an effect on bulk reduction, initial thickness did not. They suggested rewriting Equations 2.1 and 2.2 to include the ratio of initial density ρ_o to the maximum density obtainable in the nip ρ^*:

$$\frac{\Delta T}{T_o} = \frac{1}{2}\left(1 - \frac{\rho_o}{\rho^*}\right)(1 + \tanh \mu) \qquad [2.3]$$

They show that this expression along with measured values of the parameter A from Chapman and Peel's work consistently predicts ρ^* to be similar to accepted values for the density of cellulose, which is presumably the limit in paper densification.

Crotogino [18] extended Kerekes' work [44] to include the effects of initial bulk. His calendering equation is an empirical relationship giving the average cross-machine recovered bulk reduction in terms of web speed, roll radius, CD average nip load and

CD average initial paper properties. Since it accounts for initial bulk, this CD average calendering equation may be used successively for multiple nips.

Much of the work of preceding authors is summarized in the calendering equation. The present work extends the CD average calendering equation to an in-nip calendering equation. The nature of the calendering equation will therefore be described in greater detail.

Permanent bulk reduction ε_p is a measure of strain:

$$\varepsilon_p = \frac{B_i - B_p}{B_i} \qquad [2.4]$$

where B_i and B_p are initial and permanent recovered bulks. Baumgarten [4], Krenkel [47], and Gay et al. [29] have shown that CD paper dimensional changes in calendering are small, reaching at most 1 % under the most severe conditions of load and speed; work described in Section 4.5 will show that MD changes in length are equally small. The surface area and therefore the basis weight of a sheet are thus essentially unchanged by calendering even at high loads and low speeds. Recalling that bulk is thickness divided by basis weight, and that basis weight is essentially constant, ε_p as defined by Equation 2.4 is an engineering strain, with positive values corresponding to a thickness reduction. The calendering equation, illustrated in Figure 2.1, relates bulk reduction in terms of either B_i or ε_p to the nip load L in kN/m, machine speed S in m/min, roll radius R in m, paper temperature θ in °C and moisture content M in %:

$$\varepsilon_p = A + \mu B_i \qquad [2.5]$$

where

$$\mu = a_o + a_L \log_{10} L + a_S \log_{10} S + a_R \log_{10} R + a_\theta \theta + a_M M \qquad [2.6]$$

The constants are all furnish dependent and must be determined experimentally.

Equations 2.5 and 2.6 are valid for a range of B_i defined by

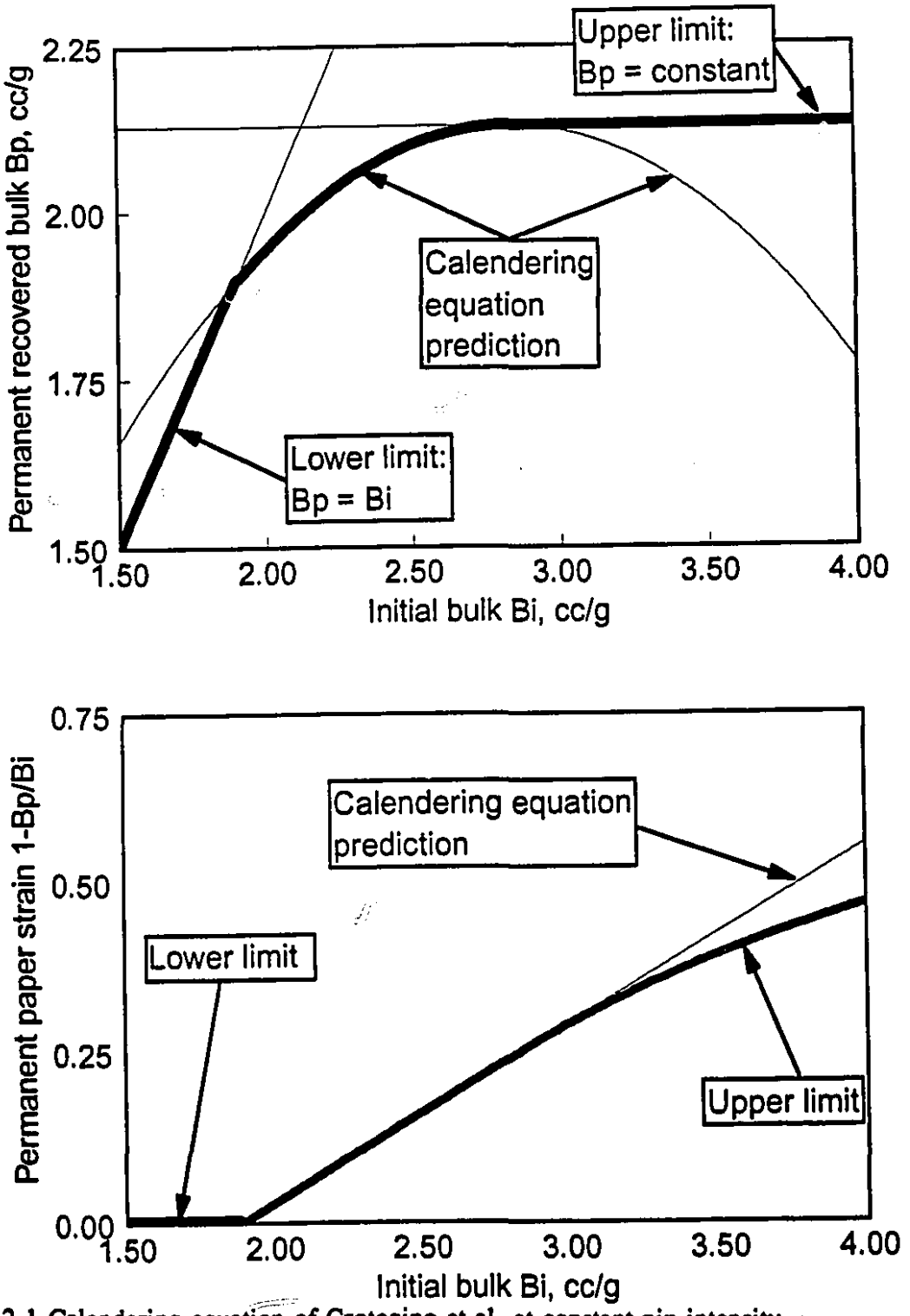

Figure 2.1 Calendering equation of Crotogino et al. at constant nip intensity μ.

$$-\frac{A}{\mu} \leq B_i \leq \frac{1 - A}{2\mu} \qquad [2.7]$$

The lower limit is the point below which, for a given nip intensity μ, no bulk reduction will occur, and corresponds to a line of slope 1 on a plot of B_p vs. B_i:

$$B_p = B_i \quad \textit{when} \quad B_i \leq -\frac{A}{\mu} \qquad [2.8]$$

Below this limit the calendering equation predicts $B_p > B_i$, or $\varepsilon_p < 0$, which is not applicable.

The upper limit of applicability of the calendering equation is the point beyond which an increase in initial bulk has no significant effect on bulk reduction, and arises from the fact that the calendering equation, which is the result of empirical curve fitting, predicts the recovered bulk B_p as a parabolic function of B_i. Above this limit, B_p is independent of B_i:

$$B_p = \frac{(1-A)^2}{4\mu} \quad \textit{when} \quad B_i \geq \frac{1-A}{2\mu} \qquad [2.9]$$

The calendering equation may be applied successively for multiple nips, with the final bulk from the previous nip serving as the new initial bulk. As well, once the coefficients are known it may be used to predict the new bulk reduction arising from a change in calendering conditions. The calendering equation has been used extensively to calculate the cross-direction average thickness reduction as a function of cross-direction average calendering variables [18, 22, 23, 24, 35, 76]. However, the bulk reduction predicted by the calendering equation is a cross-machine average, since local loads and strains across the width of the machine are unknown.

Timms [76] has reported successful use of the calendering equation in an industrial setting to optimize calender performance and troubleshoot problems using inexpensive laboratory results instead of more expensive machine trials. Hamel et al. [35] used the calendering equation to calculate the nip load distribution from the recovered

thickness profiles of paper calendered at low speeds. The procedure is useful for locating misaligned or poorly ground rolls; however, it does not provide any information about the nip shape or thickness of the paper in the nip, and thus cannot yield an in-nip stress-strain relationship or provide the missing link between roll radius profile and final thickness profile.

Browne et al. [8, 9] performed an initial set of measurements of in-nip paper thickness in a calender operating under industrial conditions using a laboratory calender with a web width of only 70 millimetres in order to maintain constant radius and pressure profiles across the width of the calender. Their calender, which was also used for this study and which is described in greater detail in Chapter 3, consists of a differential slice out of an industrial calender. It can therefore be used to measure local values of the calendering conditions and in-nip strains. From this data an in-nip calendering equation, complementing the CD average calendering equation, may be obtained. Their results confirmed the validity of the calendering equation, and showed that an empirical relation of the form of Equations 2.5 and 2.6 applies for in-nip strain ε_n:

$$\varepsilon_n = A_n + \mu_n B_i \qquad [2.10]$$

where

$$\mu_n = a_{on} + a_{Ln} \log_{10} L + a_{Sn} \log_{10} S \qquad [2.11]$$

Equations 2.10 and 2.11 do not include terms for radius, moisture content or temperature since these were not varied; the effect of these variables is included in the term a_{on}. As well, limits of the in-nip calendering equation were not evaluated since the range of calendering intensities was not extensive enough.

While previous work described so far concerns empirical descriptions of paper strain during and after calendering, a number of authors have proposed theoretical descriptions of paper response to a compressive stress. Kerekes [45] predicted the pressure pulse in a calender nip would be approximately parabolic with a certain amount of skew due to the time-dependent response of paper, as shown in Figure 2.2. The

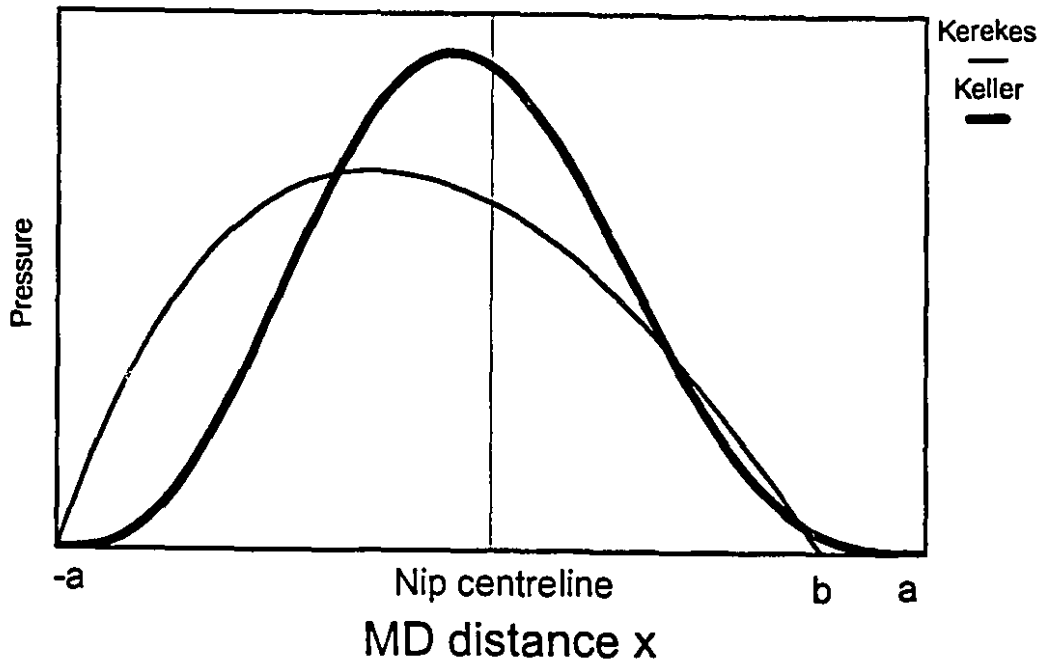

Figure 2.2 Pressure profiles in a calender nip for the same line load.

analysis was based on work by May et al. [53], Hunter [37] and Alblas and Kuipers [2], and modeled paper under compression as a standard linear solid. As will be detailed in Section 2.2, this model is based on the assumption that the permanent paper deformation of the sheet is small compared to the initial thickness. Since permanent compressive strains are often in the range of 10% to 30%, this is a poor approximation.

Keller [43] experimented with a calender using a soft roll and a pressure sensor embedded in a matching hard roll. In-nip pressure profiles (illustrated in Figure 2.2) show the skew predicted by Kerekes [45]. In spite of difficulties determining where the nip begins and ends, Keller's work also showed a nip contact area which is not symmetrical about a line through the roll centres. This asymmetry is expected given both the large permanent paper deformations encountered in calendering and the longer contact area due to the elastic nature of the soft roll. Keller's measured pressure profiles also deviate markedly from the skewed parabola predicted by Kerekes at the entrance and exit of the nip. At the entrance, the pressure increases much more slowly than predicted; at

the exit, the pressure drops quickly before tapering off. There are two possible causes for these deviations: first is elastic deformation of the soft roll, whose modulus of elasticity and Poisson's ratio are both large compared to those of paper [54], but small compared to the hard roll; second is the finite MD length of the pressure sensor (0.56 mm) compared to the MD nip length (2 to 7 mm).

Ionides et al. [38] used a Poisson model of fibre distribution together with an exponential relationship between stress and strain to model paper compression. The results are shown to reproduce published experimental results in a narrow range of loads and speeds. Their model predicts the in-nip strain as a linear function of the permanent strain; as will be seen in Chapter 4, an exponential fit describes the data over a wider range of calendering conditions.

Rodal [73] proposed separating the compressive stress-strain curve for paper into three more or less distinct phases. Under extremely low loads, Hooke's law applies and Young's modulus $E = \partial\sigma/\partial\varepsilon$ is a constant. At higher loads the fibre network begins to collapse, leading to a much lower modulus $\partial\sigma/\partial\varepsilon$. Finally, very large loads result in little additional strain as the fibres themselves collapse; the modulus E here approaches infinity as the curve of stress vs. strain becomes vertical. These three regimes are described using a modified version of Hooke's law, in which the proportionality between stress and strain is modified by a nonlinear term $F(\varepsilon)$:

$$\sigma = E\varepsilon\, F(\varepsilon) \qquad [2.12]$$

The so-called "shape factor" $F(\varepsilon)$ is further decomposed into two additive parts, one due to buckling of the fibre network and one to collapse of the fibres themselves, which are then derived in terms of a critical strain ε_N at which buckling of the fibre network begins. The model is shown to fit data from the literature in the high stress regimes, but requires estimated values for critical strain and several other parameters. Finally, Rodal suggests the best results are obtained when calendering in the low modulus region.

Osaki et al. [61, 62] investigated compressive properties of paper. Based on the

assumption that there are two compressive regimes, one due to fibre network collapse and one due to fibre crushing, they derive separate stress-strain relationships for the two regimes using statistical descriptions of fibre distributions. Theoretical results were tested using a platen press. Loads and dwell times were not given, and the pulp type and basis weight were not specified. Compression rates were very low compared to those attained in commercial calenders, ranging up to 85 μm/s where a typical industrial rate is 50,000 μm/s, but good agreement with theory was found.

While paper response to a load input is a key element in building a complete CD caliper control system, another essential element is the ability to predict the roll radius deformation, and thus the calender nip profile, due to a given heating profile. Pelletier et al. [68, 69] and Journeaux et al. [41, 42] described how to vary the radius profile of a calender roll using heating or cooling impinging air jets. Arrays of impinging jets are often used as actuators in CD bulk control systems. Journeaux determined the relationships between the roll and jet geometry, jet Reynolds number and temperature, and roll dimensions and speeds on the one hand, and heat transfer rates to the roll on the other. The corresponding transient and steady-state thermal deformations of the roll radius were then estimated using finite element methods. At steady state, a peak radius deformation Δr_p and a measure of the width of the deformation $W_{\Delta r}$ were reported for various roll types and various thermal conditions.

In order to calculate a cross-direction thickness profile, CD local values of all calendering variables must be known. CD local initial bulk, moisture content and web and roll temperatures can all be measured online. Roll diameter does not vary on a level that would significantly affect the radius term $a_R \log_{10} R$. However, as pointed out in Chapter 1, a roll deformation which is small on the scale of the roll can be enormous on the scale of the paper; the small radius changes described by Journeaux [41, 42] alter the CD nip shape significantly from the point of view of the paper, producing a non-uniform CD load profile. Since load is the variable having the greatest influence on bulk reduction, the result is a significant change in the cross-machine bulk profile. Roll diameter variations across the width of the machine can be estimated using Journeaux's

work, but the local nip load cannot be calculated from the roll radius profile without a stress-strain relationship for paper in a rolling nip.

In conclusion, paper is pressed in a calender where it is deformed to an extent dependent on the process variables. Local paper deformation is controlled by local thermal deformation of the roll which alters the local radius and pressure profiles. The CD control actuator settings generating a desired radius profile are known, but the pressure profile and thus the CD bulk reduction profile resulting from that radius profile are not known since the viscoelastic properties of paper in a rolling nip are not known. The goal of the work described here was the measurement of local in-nip paper thicknesses at different loads, leading to quantitative and qualitative descriptions of paper response to a calendering pulse.

2.2 Linear viscoelastic models for paper compression

When a load is applied to a body, energy is either stored or dissipated (Tschoegl [79]). Dissipation may be modeled using viscous elements, while storage may be described in terms of elastic or inertial elements. In the case of paper under compression, the inertial terms are small and can be ignored, leaving elastic elements as the only storage media. Paper compression is not accompanied by significant expansion in the MD or CD; calendering essentially imposes a compressive load on paper. Therefore, the review of stress analysis presented here concentrates on the uniaxial case, as the more general treatment of stress and strain as tensor quantities is not relevant here.

The simplest form of linear viscoelastic model is a single elastic element described using Hertzian elastic theory [39, 40], as proposed for use with paper by Lyons and Thuren [52]. However, this model does not account for the time-dependent behaviour of paper, and further predicts no permanent deformation of the sheet. Thus Hertzian theory remains an approximation to true paper behaviour; its usefulness lies in predicting the new paper strain resulting from a small change in calendering conditions. In order to predict both time-dependent recovery and permanent deformation, a viscoelastic model using a combination of elastic and viscous elements is necessary. Lee [48], Lee and Radok [49], Štok and Kranjec [75], Radok [72] and Carini and de Donato [11], among others, point out that once a solution for an elastic material and a given geometry has been found using Hertzian theory, a viscoelastic solution may be found by substituting viscoelastic operators for the elastic material constants. A model made up of one or more elements may be described in terms of its response to a step input, whether stress σ_0 or strain ε_0, cf. Findley et al. [27]:

$$\begin{aligned} \varepsilon(t) &= \phi(t)\ \sigma_0 \\ \sigma(t) &= \psi(t)\ \varepsilon_0 \end{aligned} \qquad [2.13]$$

where the retardation function $\phi(t)$ and the relaxation function $\psi(t)$ depend on the

particular model. If the material behaves in a linear fashion, the retardation and relaxation functions are material properties unaffected by the applied strain or strain rate, and the response to a second step input σ_1 or ε_1 added to the first at a later time t_1 is

$$\begin{aligned} \varepsilon(t) &= \phi(t)\ \sigma_0 + \phi(t-t_1)\ \sigma_1 \\ \sigma(t) &= \psi(t)\ \varepsilon_0 + \psi(t-t_1)\ \varepsilon_1 \end{aligned} \qquad [2.14]$$

The response at any time t to an arbitrary sequence of earlier step inputs beginning at time t=0 is then the sum of the responses to these individual inputs. In the limit Equations 2.14 become the Boltzmann superposition integrals:

$$\varepsilon(t) = \int_0^t \phi(t-t')\ \frac{\partial \sigma(t')}{\partial t'}\ dt' \qquad [2.15]$$

$$\sigma(t) = \int_0^t \psi(t-t')\ \frac{\partial \varepsilon(t')}{\partial t'}\ dt' \qquad [2.16]$$

The claim of Lee and Radok [49] that Equations 2.15 and 2.16 are viscoelastic operator forms of a Hertzian solution can be verified by setting $\psi(t)$ equal to the elastic modulus E and integrating Equation 2.16, which yields Hooke's law.

Two basic models may be assembled from ideal mechanical elements. The Maxwell model consists of a spring and damper in series. If the spring has modulus G and the damper viscosity η, the relaxation function is given by Tschoegl [79]:

$$\psi(t) = G\ e^{\left(\frac{-tG}{\eta}\right)} \qquad [2.17]$$

As illustrated in Figure 2.3, the stress in a Maxwell unit subjected to a step strain decays to zero at sufficiently long times. When the strain is removed at earlier times, a Maxwell element exhibits instantaneous partial recovery of the initial thickness.

The Kelvin unit, a parallel spring and damper, has retardance given by

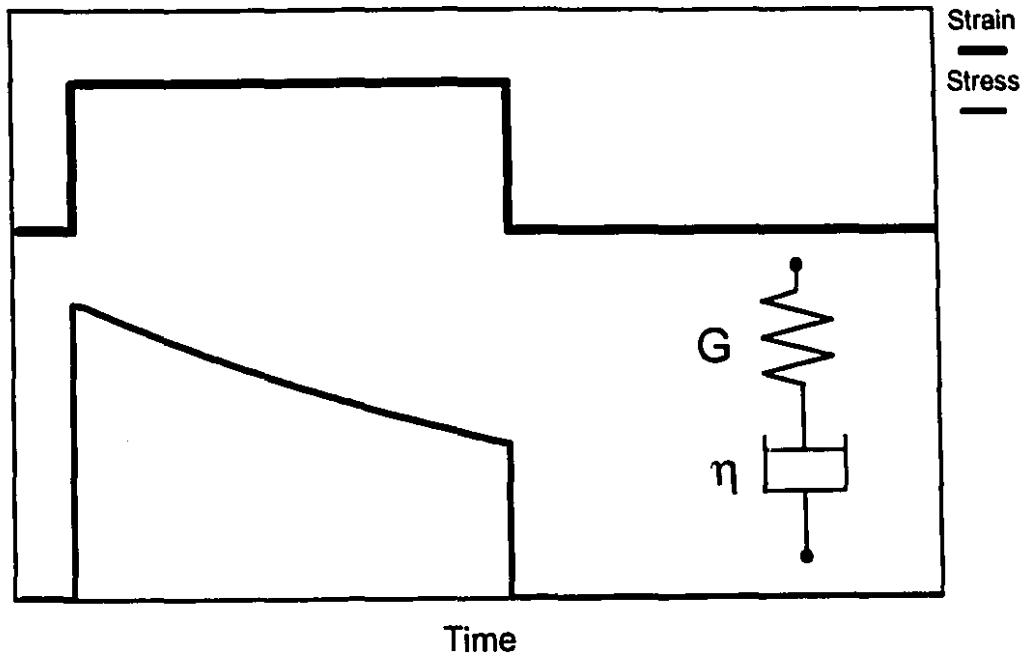

Figure 2.3 Maxwell unit response to a step strain.

$$\phi(t) = \frac{1 - e^{\left(\frac{-tG}{\eta}\right)}}{G} \qquad [2.18]$$

Strain in a Kelvin unit subjected to a step stress eventually reaches a constant value, as illustrated in Figure 2.4. There is complete time-delayed recovery once the stress is removed.

More complex behaviour can be approximated by combining three or more elements. Several authors [37, 45, 53] have used the standard linear solid, a spring in series with a Kelvin model, to describe a thin viscoelastic sheet pressed between two rolls. If the additional spring, which models instantaneous elastic response, has modulus G_e, the retardation function is

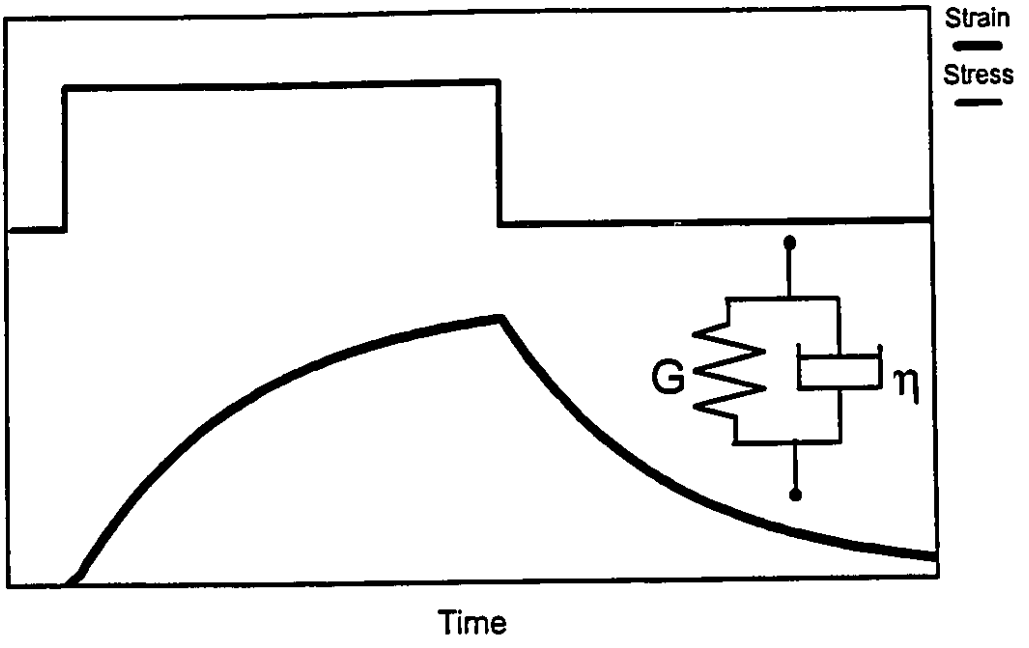

Figure 2.4 Kelvin unit response to a step stress.

$$\phi(t) = \frac{1}{G_e+G}\left\{1 + \frac{G\left(1 - e^{(-t/\tau)}\right)}{G_e}\right\} \qquad [2.19]$$

where $\tau = \eta(1/G + 1/G_e)$. If the standard solid is subject to a step stress σ_0 at time t=0 which is removed at time t_2, the strain for times later than t_2 is found by substituting Equation 2.19 into Equation 2.15:

$$\varepsilon(t>t_2) = \sigma_0 \frac{G}{G_e}\left(e^{t_2/\tau} - 1\right) e^{-t/\tau} \qquad [2.20]$$

At large enough times, Equation 2.20 (illustrated in Figure 2.5) predicts that permanent strain approaches zero. As this is not the case with paper, the model remains an approximation when applied to calendering.

Given the geometry of the nip, and based on the assumption that the initial thickness of the material is small compared to the roll radius, May et al. [53] and Kerekes [45] derived expressions (described in greater detail in Chapter 5) for the strain

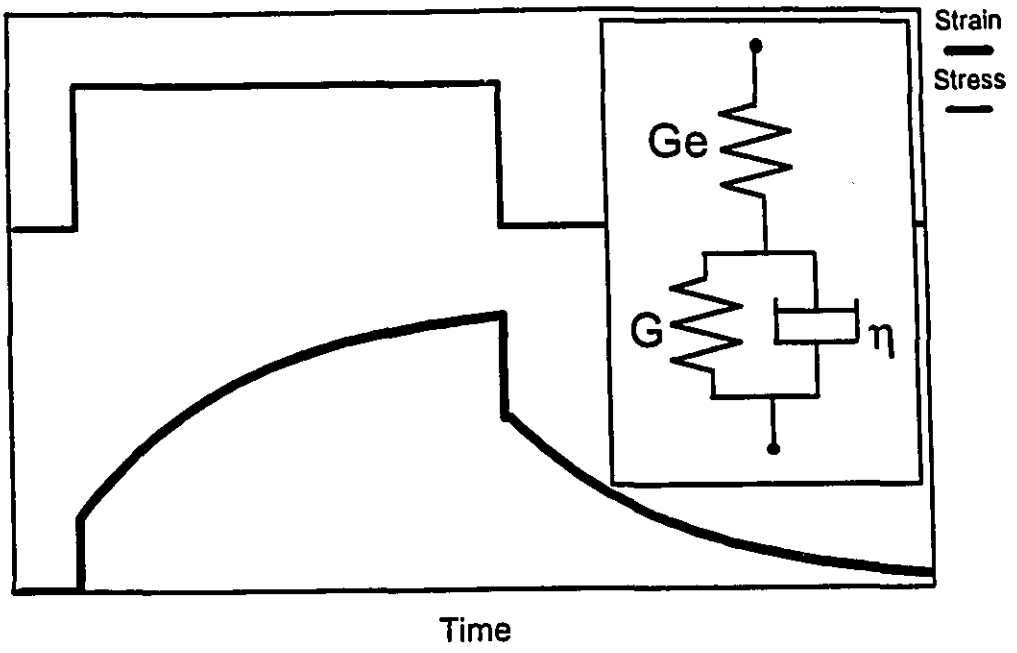

Figure 2.5 Standard linear solid response to a step stress.

$\varepsilon(t)$ and strain rate $\partial\varepsilon(t)/\partial t$ in a calender nip. Kerekes also calculated the stress profile for a standard linear solid in a rolling nip using the Boltzmann superposition principle. This profile, illustrated in Figure 2.2, is parabolic with a certain amount of skewing towards the ingoing side of the nip. Kerekes showed that the factor controlling the skew is the ratio of the material relaxation time τ to the time a/S required for the web to cover the distance a from the nip entrance to the nip centreline. When this ratio, also known as the Deborah number ξ, is close to 1, the behaviour of the material is viscoelastic. When ξ is very much greater than 1, the processing time a/S is much shorter than the material property τ, and behaviour appears viscous since any recovery occurs over a time equal to many processing times. There will be eventual full elastic recovery of the initial thickness, but that recovery is significantly delayed compared to the dwell time in the nip. Similarly when ξ is very small the processing time is much longer than the material property, and what recovery there is occurs immediately since the rate at which the pressure is removed at the nip exit is slower than the rate at which the material can

recover. At both extremes the amount of skew is small, reaching a maximum only when $S\tau/a \approx 1$. It should be noted that viscoelastic behaviour will be observed for any standard linear solid (described by its time constant τ) and any nip geometry (described by the ingoing half-length a) at a sheet speed $S \approx a/\tau$.

Beginning with elastic descriptions of the stress-strain properties of paper, Mann et al. [54] have measured all nine orthotropic elastic constants for paper using ultrasonic methods. The paper was a thick (680 μm), dense (520 g/m^2) milk carton stock. Castagnede et al. [12, 13] extended the work to include a 240 g/m^2 kraft sheet. The experimental method is based on measurement of the speed of propagation of an ultrasonic pulse through the material. Since the speed of the pulse is very high, the stresses are applied for a very short time, the resulting strains are very small, and the measured values of elastic and shear moduli are thus independent of viscoelastic effects. The results of Mann et al. [54], listed in Table 2.1, show the strong anisotropy of paper; for example, the z-direction elastic modulus E_{zz} is two orders of magnitude less than the in-plane moduli, and the Poisson's ratios for a load in the z-direction are one order of magnitude smaller than the in-plane ratios ρ_{xy} or ρ_{yx}. Castagnede et al. [13] point out that measurements of elastic constants obtained with mechanical methods tend to be significantly different from acoustical measurements: moduli are typically 20% to 30% higher, and Poisson's ratios are 20% to 40% lower, when acoustic methods are used. The discrepancy in moduli is explained by the short duration of the acoustic tests, which effectively eliminates any viscous contribution to the general stiffness tensor. The discrepancy in Poisson's ratios is attributed to propagation of error in calculating ρ from the measured quantities. They conclude that the assumptions of symmetry inherent in the definition of the orthotropic stiffness tensor are only approximations, especially for paper in the z-direction.

Watanabe and Amari [80] have proposed modeling paper compression using a four-element model, called a Burger's model by Tschoegl [79], made up of a Maxwell and a Kelvin model in series. The Maxwell model predicts instantaneous elastic deformation (due to the spring) and permanent deformation once the load is removed

TABLE 2.1: Orthotropic elastic constants, from Mann et al.

Young's modulus, GPa		Shear modulus, GPa		Poisson's ratio			
E_{xx}	7.44	G_{xy}	2.04	ρ_{xy}	0.32	ρ_{yx}	0.15
E_{yy}	3.47	G_{xz}	0.137	ρ_{xz}	1.52	ρ_{zx}	0.008
E_{zz}	0.039	G_{yz}	0.099	ρ_{yz}	1.84	ρ_{zy}	0.021

(due to the dashpot), while the Kelvin element predicts the viscoelastic behaviour, in particular the time-dependent recovery. They measured paper strain in the nip of a laboratory-scale printing press by pasting a sheet of paper between two sheets of aluminum foil; the foil acted as a capacitor whose dielectric constant was related to paper thickness. The method thus yields a continuous strain profile of the nip. Roll radius, sheet speed and line load were small, and typical dwell times were large compared to a commercial calender; nonetheless the strain profile resembles the stress profile of Keller [43], a skewed parabola with entrance and exit effects superimposed. From the strain vs. time profile they determined an approximate retardation time for the Kelvin element of 2.5 ms, and predicted the spring rate of the Maxwell element (which they link to the compressive modulus of a single wood fibre) to be about 217 MPa, independent of line load or moisture content. This value is higher than the value of 39 MPa reported by Mann et al. [54]; the difference may be due to the different paper types used. Equations governing the behaviour of a Burger's model are derived in Chapter 5.

More complex models may also be used to give a closer approximation to nonlinear materials. Among these, the short time approximation proposed by Huang and Lee [36] and modified by Lubliner [51] may be applied to calendering of paper at high speeds. The first step is to use a polynomial series to approximate nonlinear behaviour, replacing Equations 2.13 with new expressions for response to an input step stress σ_0 or

strain ε_0:

$$\varepsilon(t) = \phi_1(t)\,\sigma_0 + \phi_2(t)\,\sigma_0^2 + \phi_3(t)\,\sigma_0^3 + \ldots$$
$$\sigma(t) = \psi_1(t)\,\varepsilon_0 + \psi_2(t)\,\varepsilon_0^2 + \psi_3(t)\,\varepsilon_0^3 + \ldots \qquad [2.21]$$

Additional time-dependent material functions $\phi_2(t)$, $\phi_3(t)$, etc., need to be determined from either experiment or theory. In principle, increasing accuracy is obtained by including more terms in Equation 2.21. In the limit, for a given stress or strain history, Equations 2.21 become integrals analogous to the Boltzmann integrals, illustrated here for strain:

$$\varepsilon(t) = \int_0^t \phi_1(t-t_1)\,\frac{\partial\sigma(t_1)}{\partial t_1}\,dt_1$$
$$+ \int_0^t\int_0^t \phi_2(t-t_1,\, t-t_2)\,\frac{\partial\sigma(t_1)}{\partial t_1}\,\frac{\partial\sigma(t_2)}{\partial t_2}\,dt_1\,dt_2 \qquad [2.22]$$
$$+ \int_0^t\int_0^t\int_0^t \phi_3(t-t_1,\, t-t_2,\, t-t_3)\,\frac{\partial\sigma(t_2)}{\partial t_1}\,\frac{\partial\sigma(t_2)}{\partial t_2}\,\frac{\partial\sigma(t_3)}{\partial t_3}\,dt_1\,dt_2\,dt_3$$
$$+ \ldots$$

Truncating the series after three terms and integrating by parts gives an expression containing terms which are negligibly small for short times (cf. Lubliner [51]); ignoring these gives

$$\varepsilon(t) = \phi_1(0)\,\sigma(t) + \phi_2(0,0)\,\sigma^2(t) + \phi_3(0,0,0)\,\sigma^3(t)$$

$$- \int_0^t \left[\frac{\partial \phi_1(t-t_1)}{\partial t_1}\,\sigma(t_1) + 2\frac{\partial \phi_2(t-t_1,0)}{\partial t_1}\,\sigma(t)\,\sigma(t_1) \right] dt_1 \qquad [2.23]$$

$$- \int_0^t \left[3\,\frac{\partial \phi_3(t-t_1,0,0)}{\partial t_1}\,\sigma^2(t)\,\sigma(t_1) \right] dt_1$$

The first three terms give the instantaneous nonlinear elastic deformation, while the integrals give the time-dependent history.

Finally, the various integral forms may be used with material functions ϕ or ψ which are dependent on the stress or strain rate as well as time; Equations 2.15 and 2.16 are then nonlinear. Determining the form of $\phi(t,\varepsilon,\partial\varepsilon/\partial t)$ or $\psi(t,\sigma,\partial\sigma/\partial t)$ requires stress-strain data for step stress or step strain inputs over a large range of times. In a calender nip, the strain input is not a step but a modified parabola, and the range of industrially-relevant dwell times is very small; thus the extra effort expended in determining $\phi(t,\varepsilon,\partial\varepsilon/\partial t)$ or $\psi(t,\sigma,\partial\sigma/\partial t)$ may not be worth the additional precision of the results.

As models become more complex, the constitutive equations can more closely approximate stress-strain behaviour over a larger range of dwell times, thus providing a more complete description of material behaviour for a broader range of processing conditions; however, this improvement comes at the cost of increasing complexity. More complex models require substantially increased computational effort and more extensive experimentation in order to determine numerical values or functional forms of the material response functions $\phi(t,\varepsilon,\partial\varepsilon/\partial t)$ or $\psi(t,\sigma,\partial\sigma/\partial t)$. The duration of the loading becomes a particularly important independent variable in models with significant viscous behaviour. In calendering of paper, the dwell times are very short and vary by at most an order of magnitude, so the additional work required to obtain a better description of the time dependency of ϕ or ψ is not justified by the added precision of the results. The simplest model exhibiting all the observed stress-strain properties of paper in a calender

nip, such as creep under load and time-dependent partial recovery, will be the most useful for purposes of improving CD control systems.

3. Experimental procedures

3.1 Equipment overview

3.1.1 Mechanical systems

The experimental equipment, a modified version of that used recently by Browne et al. [8, 9], is designed to reproduce industrial conditions of nip load, web speed and roll radius while allowing accurate and repeatable measurements of the separation of the rolls. To this end all sources of cross-direction thickness variation had to be minimized. This goal was attained by making the calender as narrow as possible, thus eliminating errors due to roll bending or bearing deflection. Figure 3.1 is an overall view of the calender, which has a face width of 75 mm and a maximum paper width of 70 mm.

The calender layout, Figure 3.2, is designed to take continuous webs from a reel of up to 1.0 m in diameter, and to feed them through a single calender nip to a rewinder at speeds of up to 1000 m/min. Nip loads are varied using a hydraulic pump and cylinder, and range up to 210 kN/m. The hydraulic system can be used for nip relief, allowing loads less than those due to the gravity loading applied by the mass of the upper roll alone. Three pairs of rolls are provided, with diameters of 404, 508 and 711 mm. The shoulder machined into the side of each roll, Figure 3.3, serves as the target for a displacement sensor recording the position of both rolls relative to a fixed stand. Signals from these sensors are used to calculate in-nip paper thicknesses.

A computerized data acquisition system records sheet tensions and speeds before and after the nip, nip load, upper and lower roll positions relative to a fixed point, and paper caliper at two positions immediately after the nip. The acquisition rate is keyed to the web speed and roll radius: 150 to 200 data points are acquired per roll revolution over a total of 10 to 15 roll revolutions, thus keeping the distance along the sheet between samples approximately constant. As an example, at 1000 m/min with a 404 mm diameter roll, 150 samples are acquired per roll revolution over about 14 revolutions; the acquisition rate is thus about 2000 Hz, with 2048 samples acquired roughly every 8.5 mm over a total distance of about 17 m along the sheet. At 90 m/min with a 711 mm

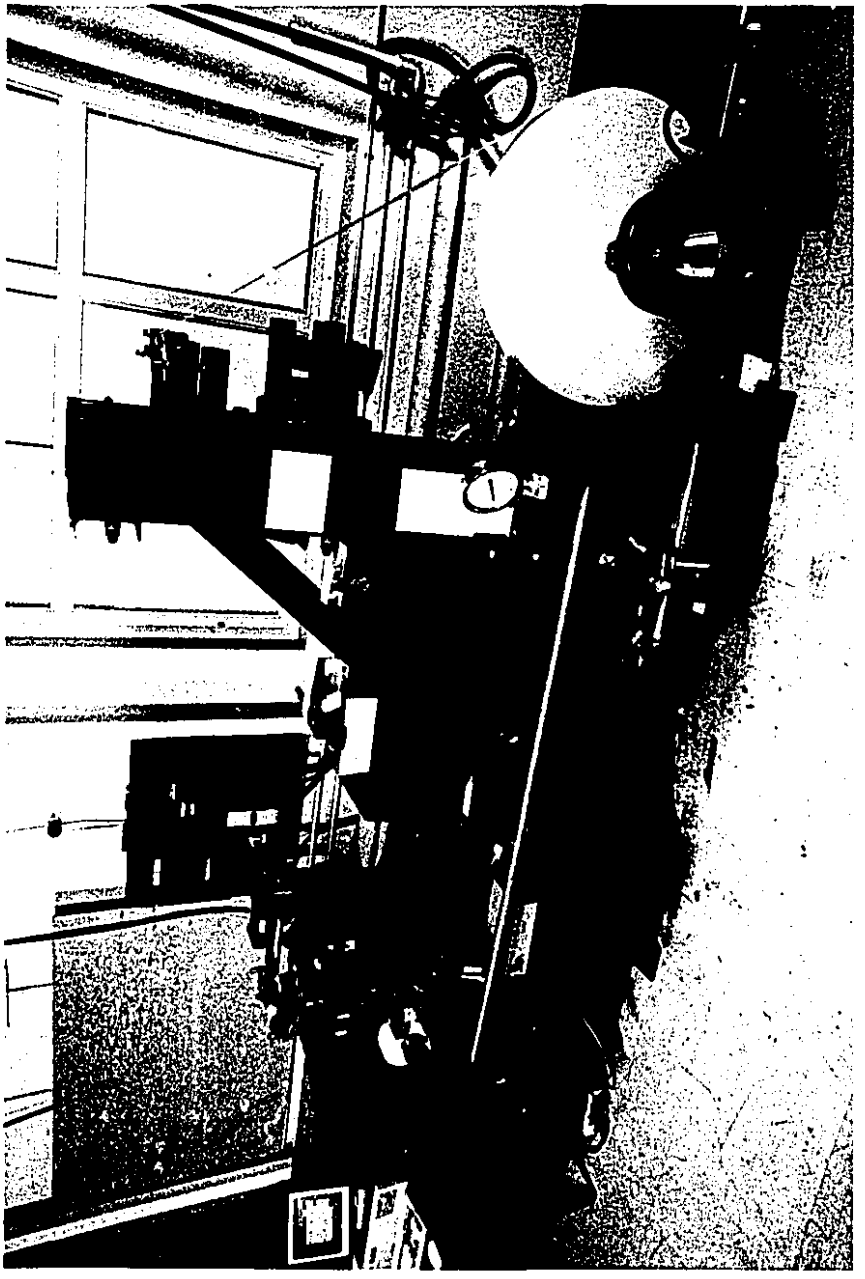

Figure 3.1 Overall view of calender; 202 mm radius rolls shown.

diameter roll, 300 samples are acquired per roll rotation, one every 7 mm over 15 m of paper for an acquisition rate of about 200 Hz.

In the present study the loading mechanism was revised from that described by Browne et al. [8, 9] so that the hydraulic cylinder now pulls down on the upper roll supporting arm, instead of pushing from above. As well, the frame was stiffened. The purpose of these modifications was to reduce the bending loads applied to the main calender stand and thus reduce the movement of the upper roll relative to the measurement sensors as nip loads are increased. Other modifications include the addition of computer control over the nip load and winder sheet tension to simplify operation of the equipment and to reduce the frequency of sheet breaks.

The most important modification was to the sensors which measure roll position, or nip gap, Figure 3.3. Previously these were contact devices riding on shoulders machined in the sides of the rolls. While these sensors had a high electrical natural frequency, allowing data acquisition at high rates, the mechanical natural frequency was low, causing the gauges to bounce at certain combinations of roll radius and web speed. As well the carbide contact tips were subject to wear, leading to frequent re-calibration.

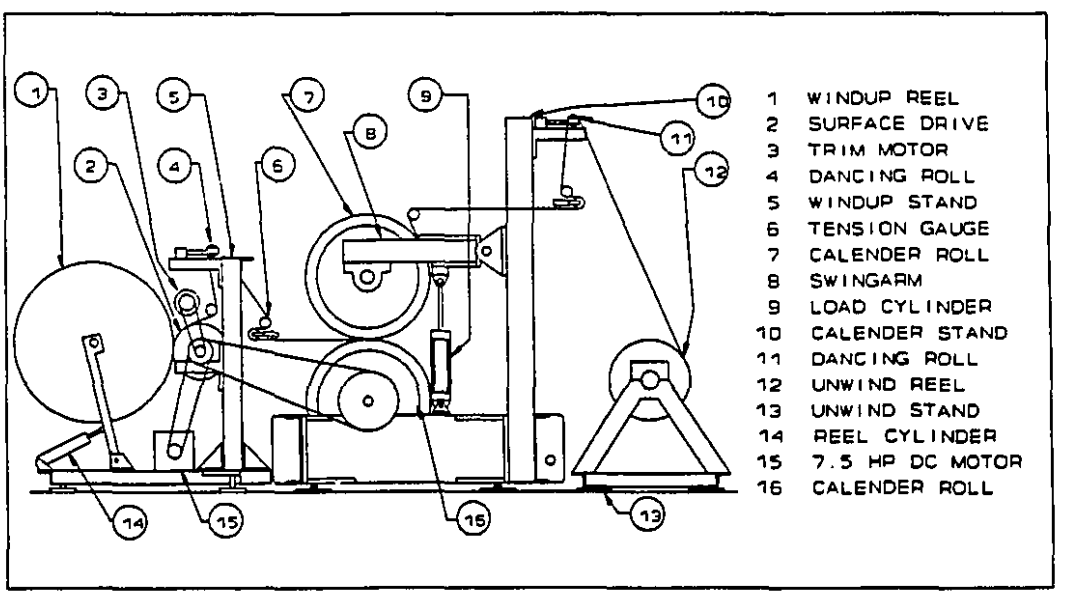

Figure 3.2 Layout of experimental calender. Length ≈ 4 m, height ≈ 2 m.

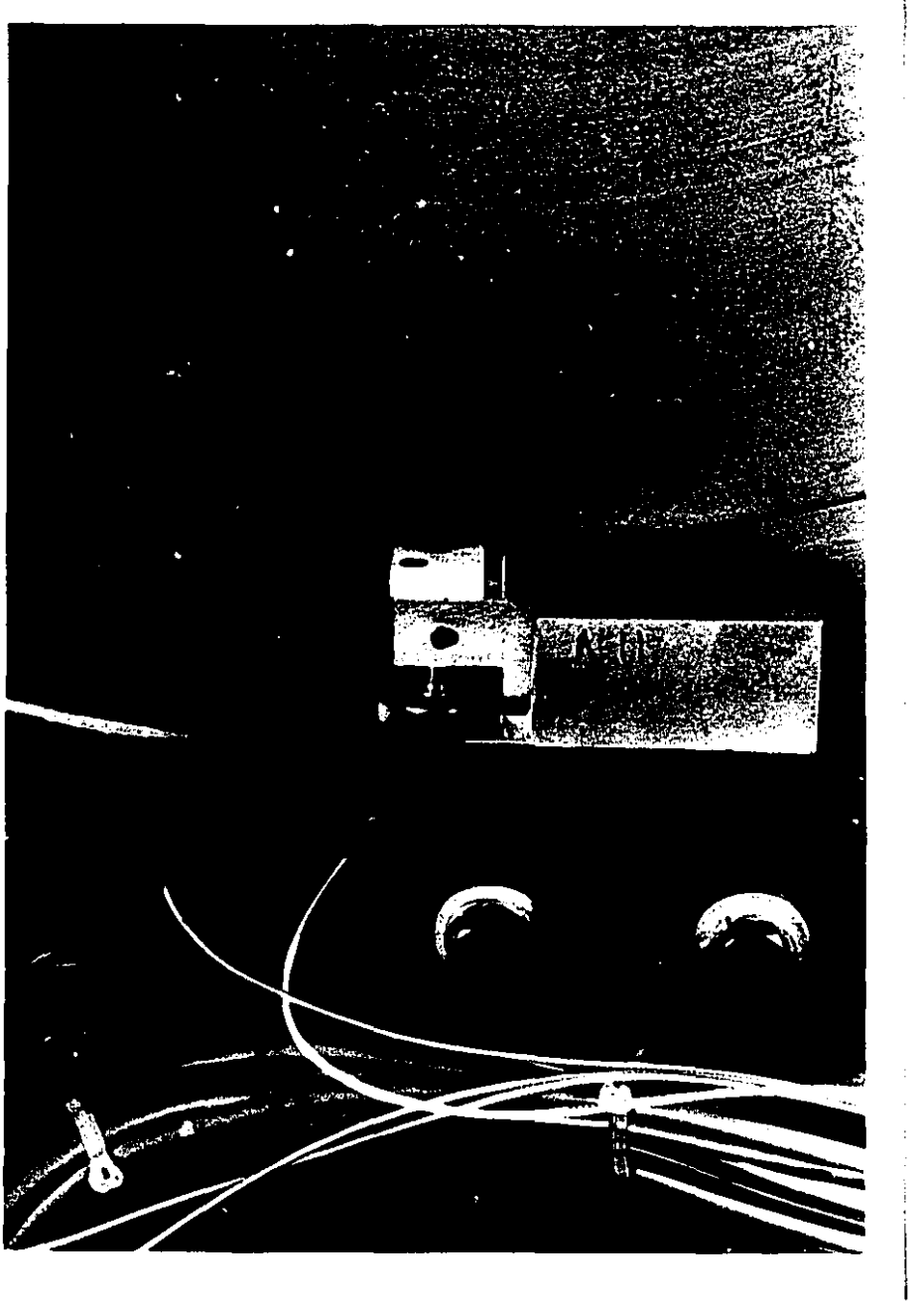

Figure 3.3 Roll displacement sensors; 355 mm radius rolls shown.

The contact gauges were replaced with non-contact inductive type sensors which react to the presence of a metallic mass, in this case the surface of the roll shoulder. The new gauges have better resolution at all speeds and do not require frequent re-calibration. As well, since the new gauges are non-contact devices, the problem of bounce has been eliminated, resulting in less wasted experimental time. Roughly half the data presented here was acquired using the older setup.

Paper caliper is now measured at two positions, 296 mm and 1050 mm after the nip, using inductive sensors buried in a ceramic anvil; the target for the sensor is an aluminum disc carried in the floating head of a modified industrial caliper gauge. Illustrated in Figure 3.4, these sensors are more reliable than the type described previously [8], but since they still involve a contact element a certain amount of bounce can occur under certain conditions. The advantage of the new system is better dynamic control of the floating head.

Sheet speed is now measured in three ways. A tachometer on the main drive motor is used to calculate the surface speed of the lower (driven) calender roll. This is the value used in all calculations and plots, and is unchanged from the method used previously.

In order to measure machine-direction strain imposed by the calender, the change in sheet speed from the unwind stand to the winder at a constant set of calendering conditions was computed from two additional measurements of sheet speed. Two idler rolls, one before and the other after the nip, were covered with 10 alternating strips of matte black paint and shiny aluminum tape. One of these devices is illustrated in Figure 3.5. Facing each roll was an optical sensor which responded to the different optical properties of the paint and tape by generating a square wave. The diameters of the idlers were 63.35 mm before the nip and 63.34 mm after; each rotation of the idlers thus corresponded to a length along the sheet of about 199 mm, and generated 10 cycles of a square wave. The output was filtered using a Schmidt trigger, and the pulses were counted using the counter/timer function on the A/D board. The total number of pulses in a given time, divided by the number of pulses per rotation and multiplied by the idler

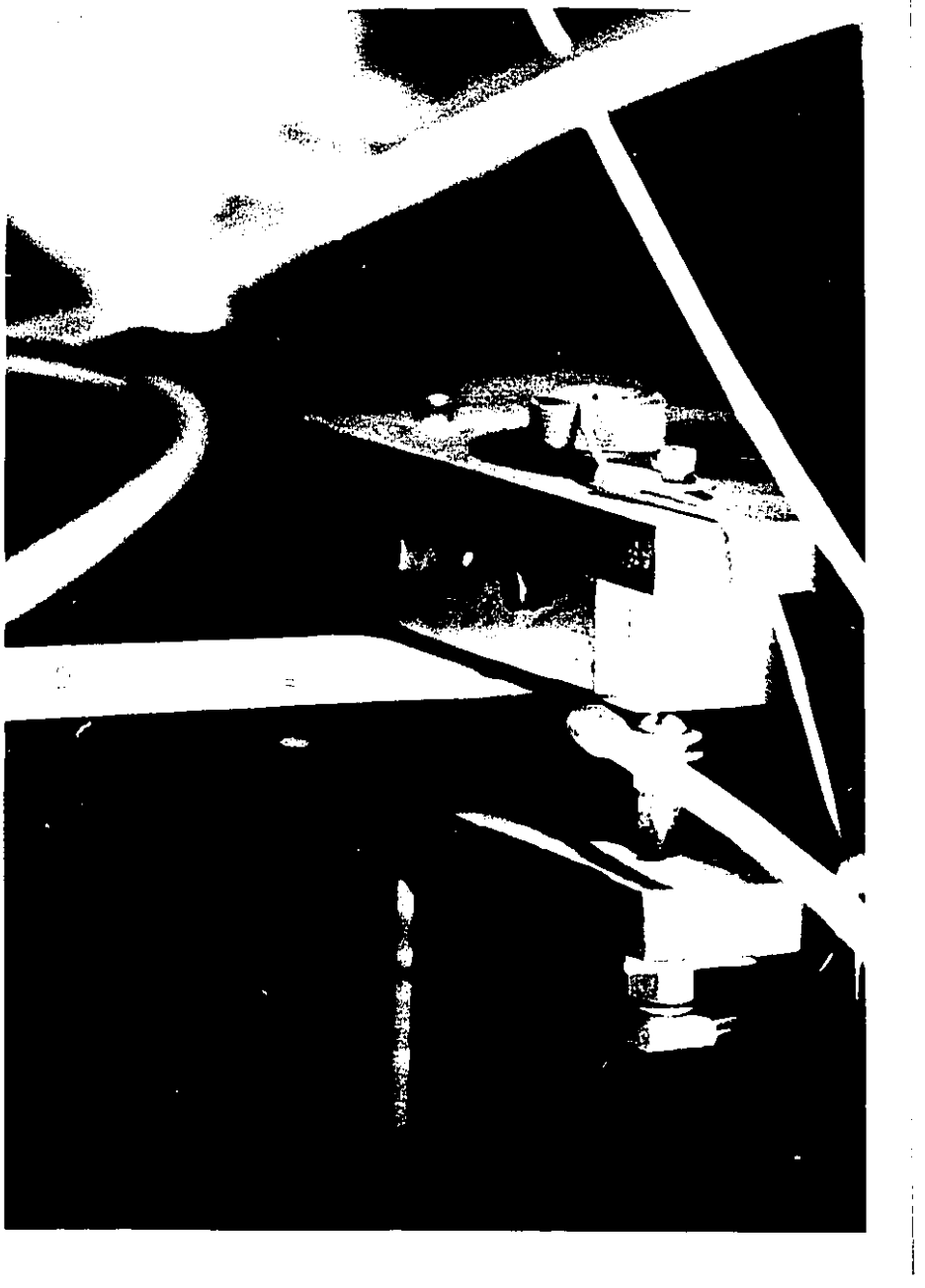

Figure 3.4 Online caliper gauge 296 mm after the nip.

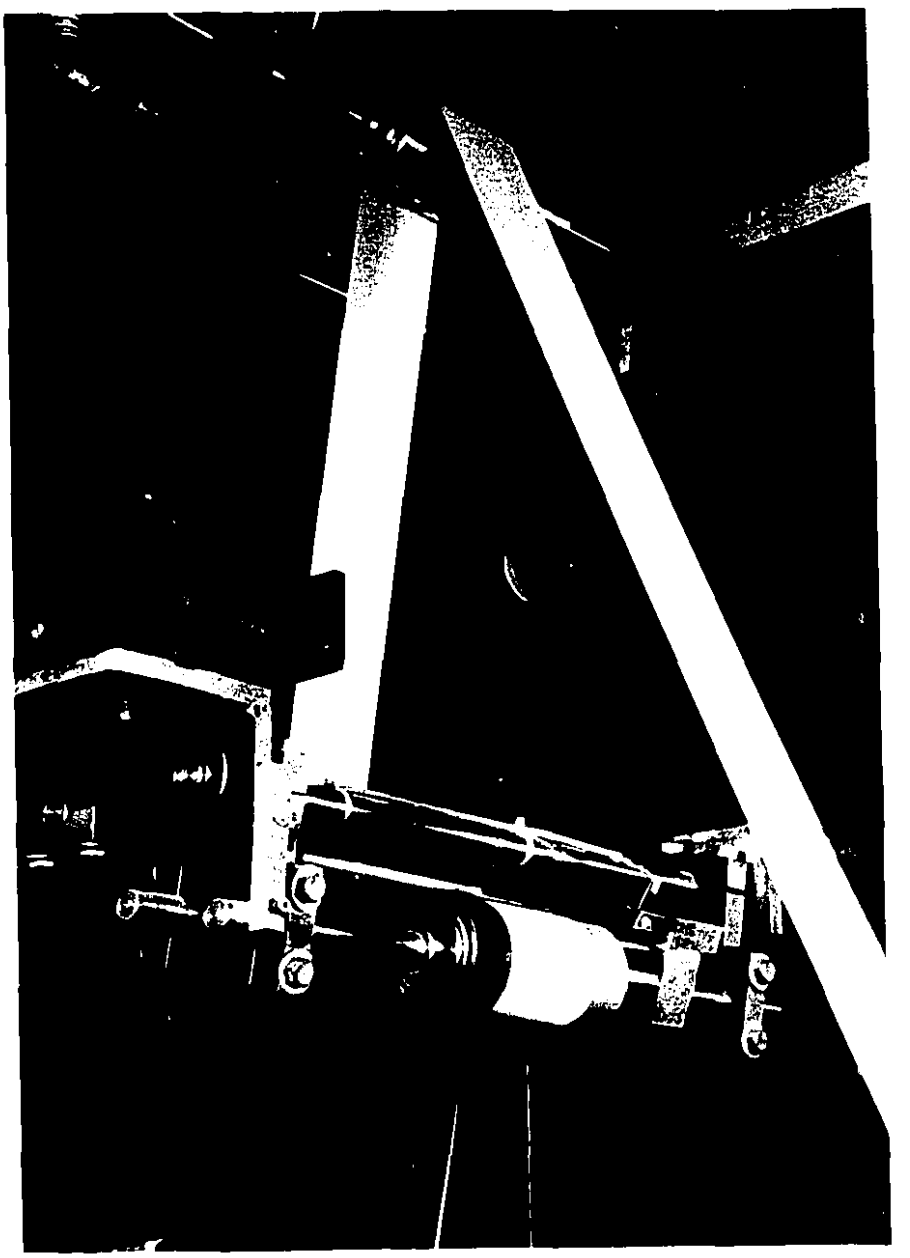

Figure 3.5 Sheet speed sensors.

circumference, is proportional to the sheet speed at that idler. Comparison of the speed before and after the nip yields an estimate of the percent speed increase, which is equal to the MD stretch.

To minimize the possibility of slip between the sheet and idler, the idlers were roughened by sandblasting and were installed so that the sheet wrap was a full 180 degrees. Pulse counting using the A/D counter function was initiated sequentially for the two counters just before acquisition of the in-nip thickness data was started; the counters were stopped in the same sequence immediately after the end of the in-nip data acquisition. The MD stretch data was thus typically computed over a distance of about 17 meters of paper, or about 1000 pulses from each sensor.

Sheet tension is another factor influencing sheet stretch; although the target tension was low at 600 N/m, the measured tension was often either lower or higher, and occasionally varied substantially within a set of data. Thus all sheet extension measurements made when either unwind or winder tension was excessively variable, or when the two tensions were not within 20% of one another, were discarded. In other words if the tension is sufficient to cause additional stretch, the effect is assumed to be similar on both sides of the nip when the tensions are similar.

3.1.2 Data acquisition and processing systems

All analog sensor outputs were filtered using a simple RC filter with a cutoff frequency of 34 Hz to eliminate interference from 60 Hz supply circuits. The filtered signals were then connected to a pair of 12 bit analog-to-digital conversion boards installed in an IBM-compatible personal computer. The boards also included digital input/output ports as well as digital-to-analog conversion, which were used to control the equipment. After acquisition, initial processing included taking a moving average of each digitized signal; in this process, each data point was replaced with the average of the four preceding points, the current point and the four following. Since every fourth point then included information about the three intervening points, only the fourth point was saved, reducing the data set from 2048 points to 512. Acquisition, control and initial processing were performed using a custom program written using Microsoft's QuickC programming language; a listing appears in Appendix A2.

The most important aspect of the data processing concerns the treatment of the output from the nip thickness gauges. The calibration of these gauges, whether the older contacting type or the new non-contact devices, is crucial to the acquisition of reliable in-nip paper thicknesses. Ideally, the lower roll remains fixed relative to the gauge, and the upper roll is deflected upwards by the presence of paper in the nip. Assuming a linear relationship between sensor output and roll position, the paper thickness in the nip T_n is then the difference between the upper roll position as seen by the sensor with paper in the nip, u, and the position without, u_0. The relationship between roll position and sensor output was indeed linear; however, there are two problems with this simple approach.

First, the lower roll is not fixed relative to the gauges, but moves vertically in its bearings which have a small amount of radial play. As the load is increased at constant speed, grease is forced from the lower ball races in the bearings, allowing the lower roll to drop as much as 20 μm when the load is increased from lowest to highest. Since the paper sheet and upper roll ride on the lower roll, both are thus displaced downwards. On the other hand, hydrodynamic forces between the ball bearing and race cause the lower

roll to lift over a range of about 10 μm as speed is increased from lowest to highest at constant load. Since paper thicknesses in the nip are less than the initial thickness, and since that initial thickness was about 120 μm for the paper used in this study, these errors are substantial.

The solution was to fit a second gauge facing the lower roll. The in-nip paper thickness is then the sum of the distances from the gauges to the two rolls with paper in the nip, compared with the same distances measured when there is no paper in the nip. If v and v_o are the position of the lower roll respectively with paper and at rest, the true in-nip paper thickness is then

$$\begin{aligned} T_n &= (u - u_o) + (v - v_o) \\ &= (u + v) - (u_o + v_o) \end{aligned} \qquad [3.1]$$

where the second form has been used to reduce the error in subtracting v_o from v.

The second problem is due to the fact that both roll surfaces and shoulders are all slightly eccentric with respect to their bearing axes. The signals from the gauges are thus superimposed on a sinusoidal wave whose period is the rotation period of the roll, and whose amplitude is the magnitude of the eccentricity. (The eccentricities of the roll surfaces were measured relative to the bearing centerlines and found comparable in both amplitude and phase to those of the roll shoulders). Further, the signal from the gauge locating the upper roll is the sum of two sinusoidal waves, since the upper roll rides on top of the lower one and is thus deflected by an amount depending on the sum of the amplitudes and the relative angular position of the two rolls. Since the eccentricity ranges from 25 to 40 μm for the different rolls, this effect is also significant, and has been eliminated by using averages (as described in the previous Section) of 2048 values of u, u_o, v and v_o taken over a minimum of 10 revolutions of the lower roll. At 1000 m/min with a 404 mm diameter roll, this works out to a minimum distance of about 17 m of paper.

The final problem involves a slight shift in the paperless reading ($u_o + v_o$)

depending on whether the hydraulic system is providing load or relief. This was ascribed to a slight twisting effect of the calender stand due to the difficulty of aligning the load cylinder perfectly with the machine-direction centerline of the paper, bringing a different circumference of the roll shoulders into position in front of the sensors as the frame twists. The difference between paperless readings varied by about 3 μm from loading to relieving, and was constant over the rest of the range of loads; on the assumption that readings with paper would vary by the same amount, values of $(u_o + v_o)$ were routinely obtained for both loading and relieving situations, the appropriate one being used to compute T_n. The assumption was a fair one since the position of the lower roll depended only on load and speed, and not on the presence or absence of paper.

The slight twist of the frame described above did not result in measureable deformation of the nip; this was verified by taking paper thickness measurements of calendered sheets and computing the average cross-machine variation in paper thickness. The measured variation did not vary from loading to relieving, but remained constant for all loading conditions.

Readings from the load cell giving the nip load also showed a small sinusoidal variation due to the eccentricities of the rolls adding and trying to lift the upper arm. Sheet speed was also affected, since the variable nip load causes a variable load to be put on the DC drive. In both these cases the amplitude of the oscillation was small, of the order of 1 kN/m and 5 m/min respectively, and was eliminated by averaging over the same distance as with the nip gauges.

3.2 Experimental conditions and procedures

The main experimental aspect of this work was the measurement of paper thickness before, during and after calendering under a variety of conditions, and the computation of in-nip and permanent strain. Modified versions of the calendering equation were then fitted to the strain data.

Two types of newsprint were used: a specialty newsprint from Boise-Cascade, Fort Frances, Ontario, and a newsprint from thermo-mechanical pulp (TMP) made by F. Soucy, Rivière-du-Loup, Québec. Both papers were obtained wound in 1.2 m wide rolls which were then cut into several narrow rolls, 70 mm wide and 1.0 m diameter. Properties of these papers before calendering are listed in Table 3.1. All properties were measured after conditioning for 24 hours at 23°C and 50% relative humidity.

The specialty newsprint was made from a furnish containing 71.5% semi-bleached groundwood pulp and 28.5% bleached kraft pulp. It had been lightly calendered at the mill, resulting in a low initial bulk of 1.97 cm^3/g. This paper was calendered here to compare results with those published by Browne et al. [8, 9] using the same equipment before the modifications described in Section 3.1.1. The calendering conditions were extended beyond those reported earlier to include a larger range of loads and speeds, and experiments were performed using different roll diameters. Experiments were performed using most combinations of independent variables, with replicates performed only at a few points.

The largest part of the work involved calendering the TMP newsprint. The three basis weights had essentially the same initial bulks. Most experiments were performed using the uncalendered bulk as received of 2.65 to 2.90 cm^3/g, but several lower bulks were obtained by precalendering a roll to a bulk in the range 2.0 to 2.25 cm^3/g, then recalendering.

A full range of loads, speeds and roll diameters was investigated using a full factorial experimental design, and several replicates were performed at most conditions. Calendering conditions for both paper types are listed in Table 3.2.

TABLE 3.1: Paper properties as received.

Paper type	Boise-Cascade	F. Soucy		
Basis weight, g/m^2,	52.0	42.3	44.4	46.6
standard deviations		0.42	0.39	0.44
Caliper, μm,	102	117	122	131
standard deviations		3.11	2.71	3.12
Bulk, cm^3/g,	1.97	2.65	2.75	2.91
standard deviations		0.10	0.08	0.10
Moisture content, %	9.0	7.93	7.89	7.36
Parker Print Surf,	4.78, 5.17	5.04, 5.91	5.18, 6.27	5.53, 6.53
μm, top/wire side,	0.14, 0.14	0.14, 0.18	0.17, 0.20	0.16, 0.38
standard deviations				

Experimental procedure was as follows. After allowing all sensors to warm up for a minimum of 2 hours, the calender was started up with no paper in the nip to obtain the calibration offset ($u_o + v_o$) as described in Section 3.1.2. Calibrating tests had shown that this reading was insensitive to sheet speed, but depended slightly on whether the loading system was operating in loading or relieving. This so-called zeroing run was therefore repeated at several loads but at only one speed, typically 90 m/min.

After taking an uncalendered sample, paper from a new roll was threaded through the calender. In some cases this paper had previously been calendered to a lower bulk. The computer was used to accelerate the main motor slowly up to 90 m/min under a light load while tracking and tension of the sheet were checked. The motor was then accelerated to the desired speed, the desired load was applied, and once speed and

TABLE 3.2: Calendering conditions.

Load, kN/m	10 to 210
Roll Radius, mm	202, 254, 355
Sheet Speed, m/min	90 to 950
Bulk, cm^3/g (specialty newsprint)	1.97
Bulk, cm^3/g (TMP newsprint)	2.01 to 2.25; 2.55 to 2.90

tension were reasonably stable the complete set of sensors was scanned 2048 times at a rate determined using the reasoning described in Section 3.1.1. The location in the wound roll corresponding to the data set was marked using a slip of paper inserted in the winder nip, the data was saved to disk, and the speed and load were then adjusted to the next condition. The process was repeated until the experiment was ended either by the operator, by the end of the unwind roll, or by a sheet break.

Raw data were then smoothed using a moving average method. In the method selected, each data point was replaced with the average of 9 points: the current point and the 4 preceding and following. Every fourth point was saved, for a total of 512; the remainder was discarded. Since a minimum of 150 in-nip thickness readings were acquired for every roll revolution, the eccentric signature of the roll was still easily identifiable after this process.

Sufficient paper usually remained on the unwind roll for another uncalendered sample to be taken. Samples were never taken from the first or last few meters of paper on a roll, but always a minimum of several centimeters radially from the core or rim of the roll. Once the wind-up reel was full, the roll of calendered paper was cut up and samples corresponding to each data set were retrieved. All paper samples were cut to a length corresponding to one circumference of the calender roll in use at the time in order

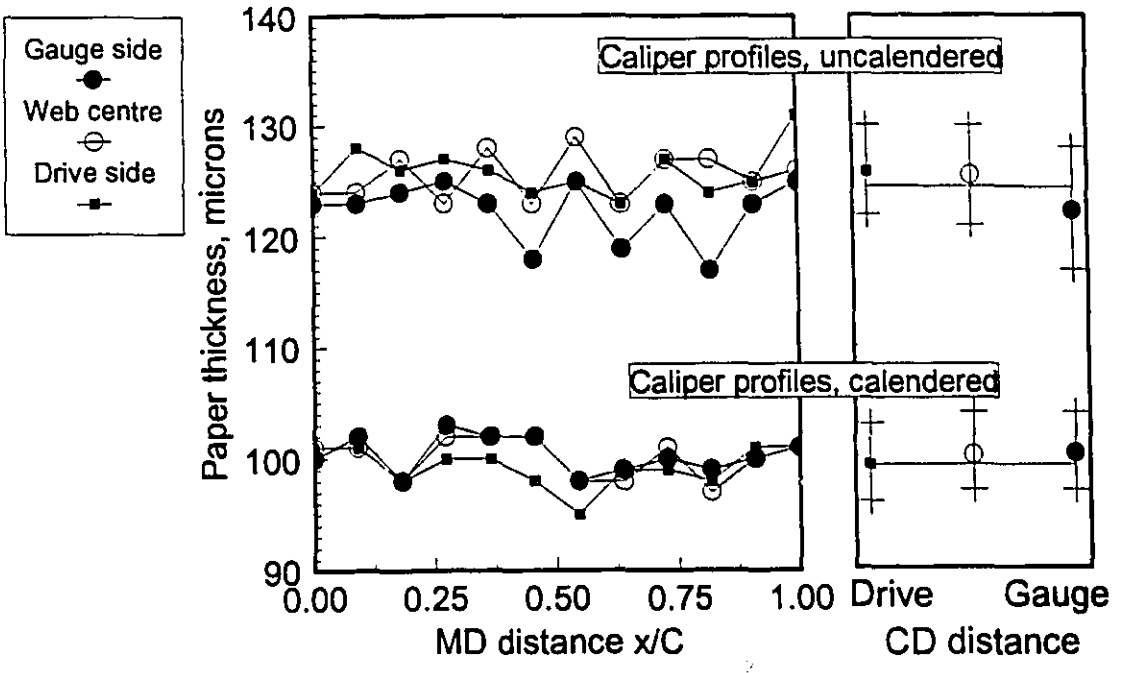

Figure 3.6 Machine-direction thickness profiles, TMP newsprint (run #895E) Calendering conditions: 202 mm, 65 kN/m, 554 m/min, 2.54 cm^3/g.

to average out any machine direction variations due to roll crowns or eccentricities. Calendered and uncalendered samples were conditioned for 18 to 24 hours at 23°C and 50% relative humidity. Paper thickness was determined according to TAPPI Standard 411 (CPPA standard D.4) using a standard electronic micrometer, at 36 points in three rows of 12 along the machine direction of each strip, one row in the center of the 70 mm wide sheet, and the other two 15 mm from each edge. Where the average cross-direction variation in the recovered thickness exceeded 2 μm, the data were discarded and the roll alignment was checked; otherwise the average of all 36 thicknesses was used as the sample paper thickness. Typical machine direction thickness profiles and averages are shown in Figure 3.6 for uncalendered and calendered samples from the same roll; the machine direction x is normalized by dividing by the roll circumference C. Average paper thicknesses and standard deviations for the 36 measurements in this example were 124.6 μm, 2.77 μm (uncalendered) and 99.9 μm, 1.76 μm (calendered), showing that in

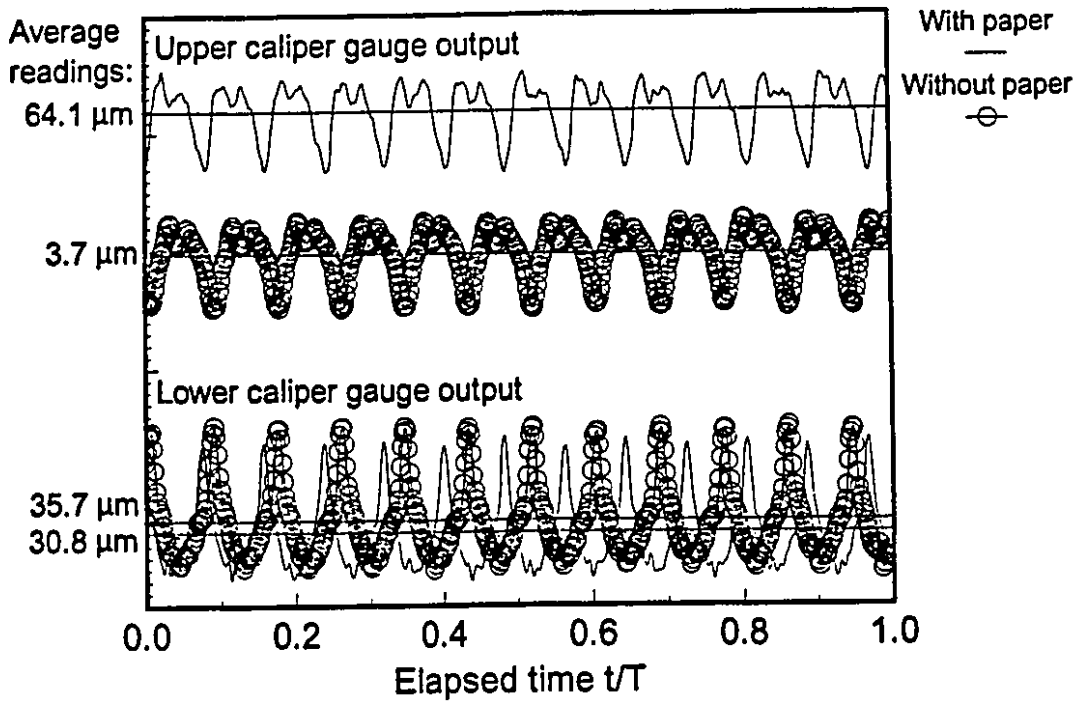

Figure 3.7 Typical caliper gauge output (runs #894B and #895E).

this case calendering improved the CD caliper profile. It appears from the individual averages that the thick side of the ingoing web was calendered heavily enough to become the thin side afterwards; however, the thickness measurements are for samples taken from different MD positions in the roll.

The in-nip thickness data were processed as described in Section 3.1.2. In particular, the reading with paper ($u + v$) was obtained by averaging the 512 values of u and v before adding. This was repeated for ($u_o + v_o$), and the in-nip paper thickness obtained by Equation 3.1. Figure 3.7 shows typical values of u, v, u_o and v_o, with the elapsed time t normalized by dividing by the total acquisition time T. Readings with no paper were obtained at a calendering speed of 90 m/min and a nip load of 65 kN/m, while those with paper were obtained at 554 m/min and 65 kN/m. The slight difference in the frequency of the roll eccentricities between the two sets of curves is due to the different data acquisition rates not quite correcting for the different rotational velocities.

The upper gauge output shows that the upper roll, after removing the roll eccentricities by averaging, was deflected upwards by the presence of paper in the nip from an average position u_o = 3.7 μm from a fixed reference point to another position u = 64.1 μm from the same reference point, a displacement (u - u_o) = 60.4 μm, while the lower roll was also deflected upwards (due to the increased speed) from a position v_o = 35.7 μm from another reference point (fixed relative to the first one) to a new position v = 30.8 μm, a displacement (v - v_o) = -4.9 μm. The average in-nip gap, equal to the average in-nip paper thickness, was therefore (u - u_o) + (v - v_o) = 55.5 μm in this case.

A second paperless reading was often obtained after one or more experimental runs to verify that no changes had occured in the position of the rolls relative to the gauges. A typical variation in the value of (u_o + v_o) was $\pm$1 μm with the newer inductive gauges, $\pm$3 μm with the older contact gauges. Where this was larger than 2 μm (4 μm for the older gauges), the cause was investigated and the data set discarded.

The experimental program was designed to minimize roll changes, as these required time-consuming alignment and re-calibration procedures. Furthermore, sheet breaks were more frequent at higher speeds; higher speeds were thus attempted first to ensure acquisition of sufficient data at these speeds.

The first set of measurements were made with the 202 mm radius set installed, using the contact type of in-nip thickness gauge described in Section 3.1.1. Rolls were then changed for the 254 mm pair and the acquisition process was repeated. Next, the contact-type in-nip caliper gauges were replaced with the inductive type at the same time the 355 mm rolls were installed. Once a full set of data had been acquired using all three sets of rolls, the 202 mm pair was reinstalled and a complete data set acquired again. No significant changes in in-nip or permanent strains were noted between the first and last runs using the 202 mm roll set, in spite of the fact that the earlier data set was acquired using a different type of in-nip displacement sensor. The new gauges resulted in less scatter and fewer data points being discarded, especially at high speeds.

The time required to change roll pairs and acquire a new data set was typically

several months. As the equipment was not installed in a controlled environment room, large seasonal changes in relative humidity and thus paper moisture content tended to mask the effect of roll radius on paper strain. After the statistical analysis described in Chapter 4 was performed, the effect of moisture content on the strain data was estimated, and the analysis repeated. The permanent moisture content coefficient was estimated from data published by Crotogino et al. [22] to be $a_{Mp} = 0.005$. The in-nip coefficient was estimated using data published by Colley and Peel [17], where it appears that $a_{Mn} \approx 0.85\ a_{Mp}$. In-nip and permanent strain data were then adjusted by adding the following quantity, where $M_{50} = 7.69$ is the percent moisture content corresponding to 50% relative humidity:

$$\varepsilon_{corr} = B_i a_M (M - M_{50}) \qquad [3.2]$$

This processing step was not applied to the specialty newsprint, since data were acquired with only one roll radius.

In-nip and recovered thickness were determined for the same strip of paper, since the location in the wound roll corresponding to the acquisition of a set of in-nip thickness data was marked and could be retrieved later by unwinding or cutting up the roll. Initial thickness, on the other hand, was measured at only a few points distributed over the 6 to 8 km of paper wound on each roll; these samples were thus not the same ones which were eventually calendered. Initial thickness was assumed to remain constant throughout the roll from sample to sample. Occasionally the initial thickness of a strip taken from the beginning of the roll differed from one taken towards the end, sometimes by as much as 5 μm; when this occurred strains for the first half of the data acquired with that roll were computed using the earlier initial thickness, and for the last half using the later one. A linear interpolation method was not used because at least one of the rolls was found to have a thickness change of 5 μm occuring over a machine-direction distance of only 1 m. Since the narrow rolls were all cut from a single 1.2 m wide roll, it was assumed that adjacent slices must also exhibit the same step change, presumably due to the action of a control mechanism at the mill at the time of manufacture.

Finally, initial and final paper thickness were obtained using a standard paper micrometer and are thus subject to a smaller random error than in-nip thickness, which was obtained dynamically while the calender was running.

4. Experimental results

4.1 In-nip and permanent strain measurements

4.1.1 The calendering equation

All of the strain data described previously were processed using SYSTAT, a statistical analysis package running on IBM personal computers. In-nip and permanent versions of the calendering equation were fitted to the strain data:

$$\begin{aligned} \varepsilon_n &= A_n + \mu_n B_i \\ \varepsilon_p &= A_p + \mu_p B_i \end{aligned} \qquad [4.1]$$

where the nip intensity coefficients μ_n and μ_p are

$$\begin{aligned} \mu_n &= A_{on} + a_{Ln}\log_{10} L + a_{Sn}\log_{10} S + a_{Rn}\log_{10} R + a_{\theta n}\theta + a_{Mn}M \\ \mu_p &= A_{op} + a_{Lp}\log_{10} L + a_{Sp}\log_{10} S + a_{Rp}\log_{10} R + a_{\theta p}\theta + a_{Mp}M \end{aligned} \qquad [4.2]$$

and ε_n, ε_p are the in-nip and permanent strains, B_i is the initial bulk, L the nip load, S the machine speed, and R the roll radius R. The web temperature θ and moisture content M were not measured in this study, but corresponded to equilibrium conditions in the laboratory, which varied from 23°C and 75% R.H. in the summer to 18°C and 30% R.H. in the winter. The effect of these variables is therefore included with the coefficients A_{on} and A_{op}, and the modified calendering equation as given by Equation 4.3 was used in the curve fitting:

$$\begin{aligned} \mu_n &= a_{on} + a_{Ln}\log_{10} L + a_{Sn}\log_{10} S + a_{Rn}\log_{10} R \\ \mu_p &= a_{op} + a_{Lp}\log_{10} L + a_{Sp}\log_{10} S + a_{Rp}\log_{10} R \end{aligned}$$

where

$$\begin{aligned} a_{on} &= A_{on} + a_{\theta n}\theta + a_{Mn}M \\ a_{op} &= A_{op} + a_{\theta p}\theta + a_{Mp}M \end{aligned} \qquad [4.3]$$

The variation of moisture content and temperature thus contributed to the random

error, as their effect was not accounted for explicitly. As described in Section 3.2, the effect of moisture content was estimated for the TMP data set, strains adjusted to a relative humidity of 50% were calculated, and the curve-fitting was repeated. (The effect of temperature was small due to the small range of ambient temperatures; the data set was thus not corrected for this variable.) These results are presented later in this Section.

The effect of initial bulk was not investigated in the case of the specialty newsprint from Boise-Cascade, so in this case the coeficients a_{on} and a_{op} are zero, and their effect is included in the coeficients A_n and A_p. As well, there was insufficient data to determine the radius coefficient for this paper. The intercepts for the two papers are thus not comparable, but the load and speed coefficients a_L and a_S are.

Equations 4.1, 4.2 and 4.3 are valid for a range of B_i defined by

$$-\frac{A_{n,p}}{\mu_{n,p}} \leq B_i \leq \frac{1 - A_{n,p}}{2\mu_{n,p}} \qquad [4.4]$$

The limits, described in Section 2.1, were also used as input to the analysis program, which decided on the basis of least squares which portion of the calendering equation applied for a given set of conditions. The lower limit applies only to the permanent strain, since at no time in this study was an in-nip strain of zero measured:

$$\left.\begin{aligned} B_p &= B_i \\ \varepsilon_p &= 0 \end{aligned}\right\} \quad \textit{when} \quad B_i \leq -\frac{A_p}{\mu_p} \qquad [4.5]$$

The upper limit was applied to both in-nip and permanent strain:

$$\left.\begin{aligned} B_n &= \frac{(1-A_n)^2}{4\mu_n} \\ \varepsilon_n &= 1 - \frac{(1-A_n)^2}{4\mu_n B_i} \end{aligned}\right\} \quad when \quad B_i \geq \frac{1-A_n}{2\mu_n} \qquad [4.6]$$

$$\left.\begin{aligned} B_p &= \frac{(1-A_p)^2}{4\mu_p} \\ \varepsilon_p &= 1 - \frac{(1-A_p)^2}{4\mu_p B_i} \end{aligned}\right\} \quad when \quad B_i \geq \frac{1-A_p}{2\mu_p} \qquad [4.7]$$

SYSTAT offers two methods for non-linear function minimization. The first method, known as a Quasi-Newton method, was described by Fletcher [28]. The method is an extension of Newton's method for root-finding, using the gradient of the function to decide the direction and magnitude of the change at each iteration. The second method, called the Simplex method, is described by O'Neill [59]. In this method, the function to be minimized, which depends on N independent variables, is evaluated at N+1 points in N dimensions, the points forming a simplex about an initial user-supplied approximation to the solution. In two dimensions, the simplex is a triangle; in three, a tetrahedron. Then the simplex is reflected, expanded or contracted by replacing the largest point with a new smaller one, either outside (reflection or expansion) or within the simplex (contraction). The method is slow, but it requires no estimate of the derivatives, as the Quasi-Newton method does, and is therefore more robust. As well it is more likely to find a global minimum to a function, rather than the closest local minimum, especially when the initial estimate is poor.

SYSTAT allows the user to specify the loss function to be minimized; the function selected here was the classical least-squares error estimate.

Both analysis methods yielded essentially similar results. Where results differed significantly, typically one method or the other converged to a solution whose 95%

confidence interval allowed the possibility that one or more coefficients were zero. These results were discarded.

The raw data, typical command scripts submitted to the program and typical program output are given in Appendix A1, and are summarized next.

Specialty newsprint results using the calendering equation

The coefficients determined from the Boise-Cascade specialty newsprint data are given in Table 4.1; typical data are plotted with the previously published data of Browne et al. [8, 9] along with the predicted curve in Figure 4.1. Figure 4.1 illustrates well the reduction in the scatter obtained with the new gauges. Raw data is given in Table A1.1, the command script in Table A1.2, and the program output in Table A1.3. It should be pointed out that the logarithm operator in Table A1.2 is the natural logarithm, so that the coefficients in Table A1.3 need to be changed to base 10 logarithm for comparison with previous work. This has been done in Table A1.7.

Data were obtained only for the purpose of comparing with previous work, so only certain combinations of load and speed were investigated, and few replicates were performed.

Compared to the data presented previously by Browne et al. [8, 9], the 95%

Table 4.1: Calendering coefficients, specialty newsprint (Boise-Cascade).

	In-nip	Permanent
A	-0.3874	-0.0740
S.E.	0.0362	0.1461
$a_{Ln,Lp}$ (g/cm^3)	0.2597	0.0882
S.E.	0.0117	0.0097
$a_{Sn,Sp}$ (g/cm^3)	-0.0111	-0.0272
S.E.	0.0023	0.0046
r^2	0.995	0.94

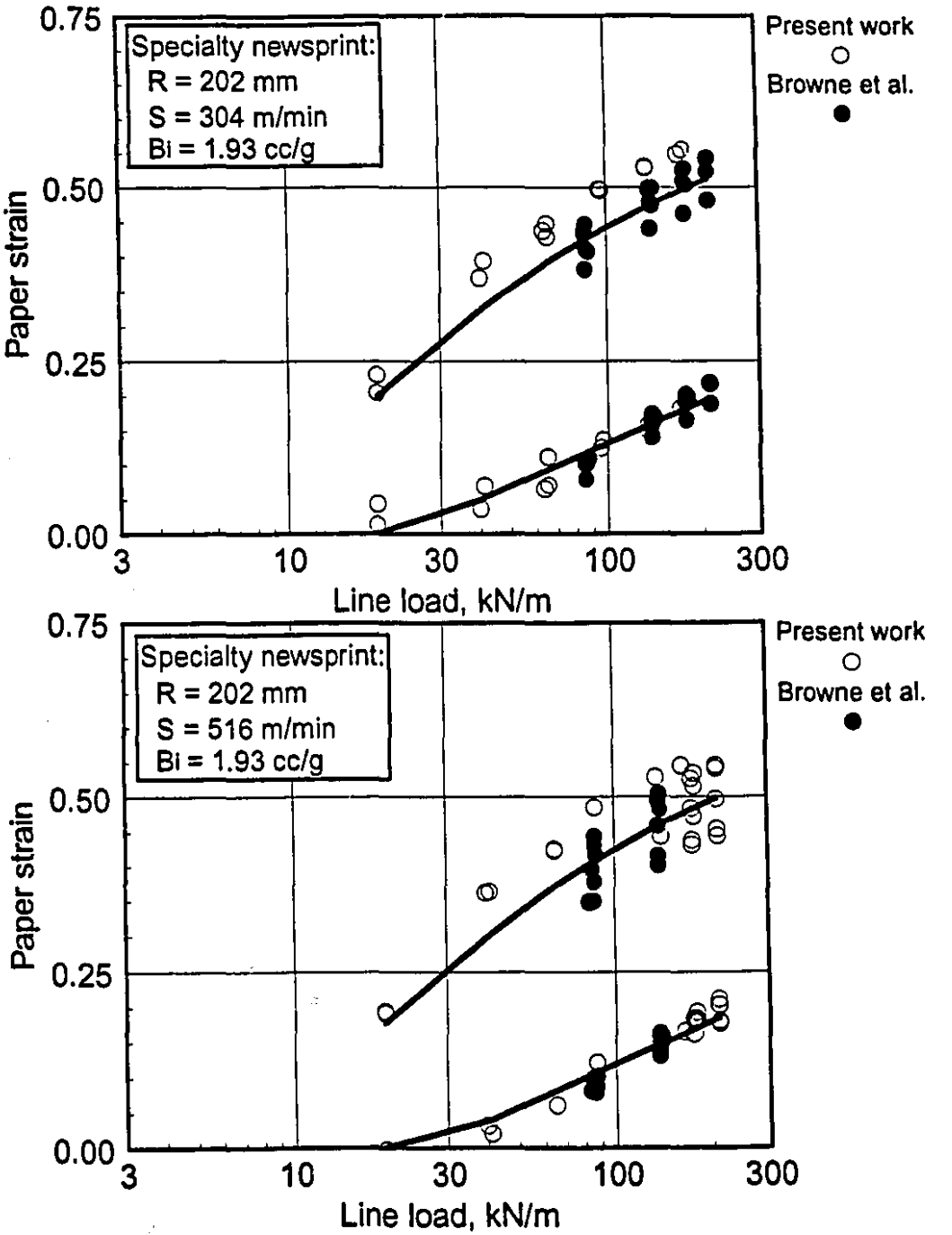

Figure 4.1 Strain vs. load, specialty newsprint: a) 304 m/min; b) 516 m/min. Curve fitting using the calendering equation.

confidence intervals of the permanent load coefficients a_{Lp} do not overlap, with the newer value being significantly lower. This is due to the acquisition of new data at lower loads, as seen in Figure 4.1, which displaces the limits of the calendering equation as determined by the statistical analysis program. Similarly in the in-nip case, the sum-of-squares is minimized if the linear portion of the curve corresponds to the steeper region at low loads, resulting in a substantially larger in-nip load coefficient a_{Ln}.

The permanent velocity coefficient a_{Sp} is slightly larger, for the same reason the load coefficients have changed; the in-nip coefficient a_{Sn} appears smaller but is statistically similar due to large standard errors in both coefficients.

TMP results using the calendering equation

The strain data set acquired with the paper made from TMP contains 1380 data points distributed over 312 unique combinations of load, speed, roll radius and initial bulk. Only one or two replicates exist for several of these combinations, while many replicates exist for the combinations which were easily attainable given the dynamics of the machinery. In other words, using all replicates in the curve-fitting process tends to weight those experimental conditions which imposed no extreme stresses on the equipment. In order to give equal weight to all replicates, combinations with three or more replicates were replaced by single average values of independent and dependent variables, while for combinations with only one or two replicates, all replicates were saved without averaging. The result was a summary data set of 359 data points, containing all the information in the larger set but in a more compact form. This set was used as input to the statistical analysis package.

Calendering coefficients for the TMP are presented in Tables 4.2 and 4.3, and typical data and curves are plotted in Figures 4.2 to 4.7. Along with the estimates, the tables give the standard error (S.E.), the coefficient of variation C_V and the 95% confidence limits. The overall standard error is the root mean square residual computed by comparing measured and predicted bulks in cm^3/g.

Data points plotted in the figures come from the full set of all 1380 replicates, not the averaged summary set used to calculate the regression coefficients. In Figure 4.2, the complete data set for one roll radius has been divided into subsets of low and high initial bulk; the scatter in these curves is thus due to sheet speed. Conditions used to generate the curves with the calendering equations are given. Subsequently data subsets corresponding to unique combinations of roll radius, sheet speed and initial bulk are plotted along with the calendering equation prediction and the 95% confidence limits on that prediction. The upper limit of the calendering equation is indicated on each curve with an arrow; the lower limit occurs for ε_p when the predicted value of ε_p is less than zero.

Raw data, SYSTAT command scripts and SYSTAT output are given in Tables

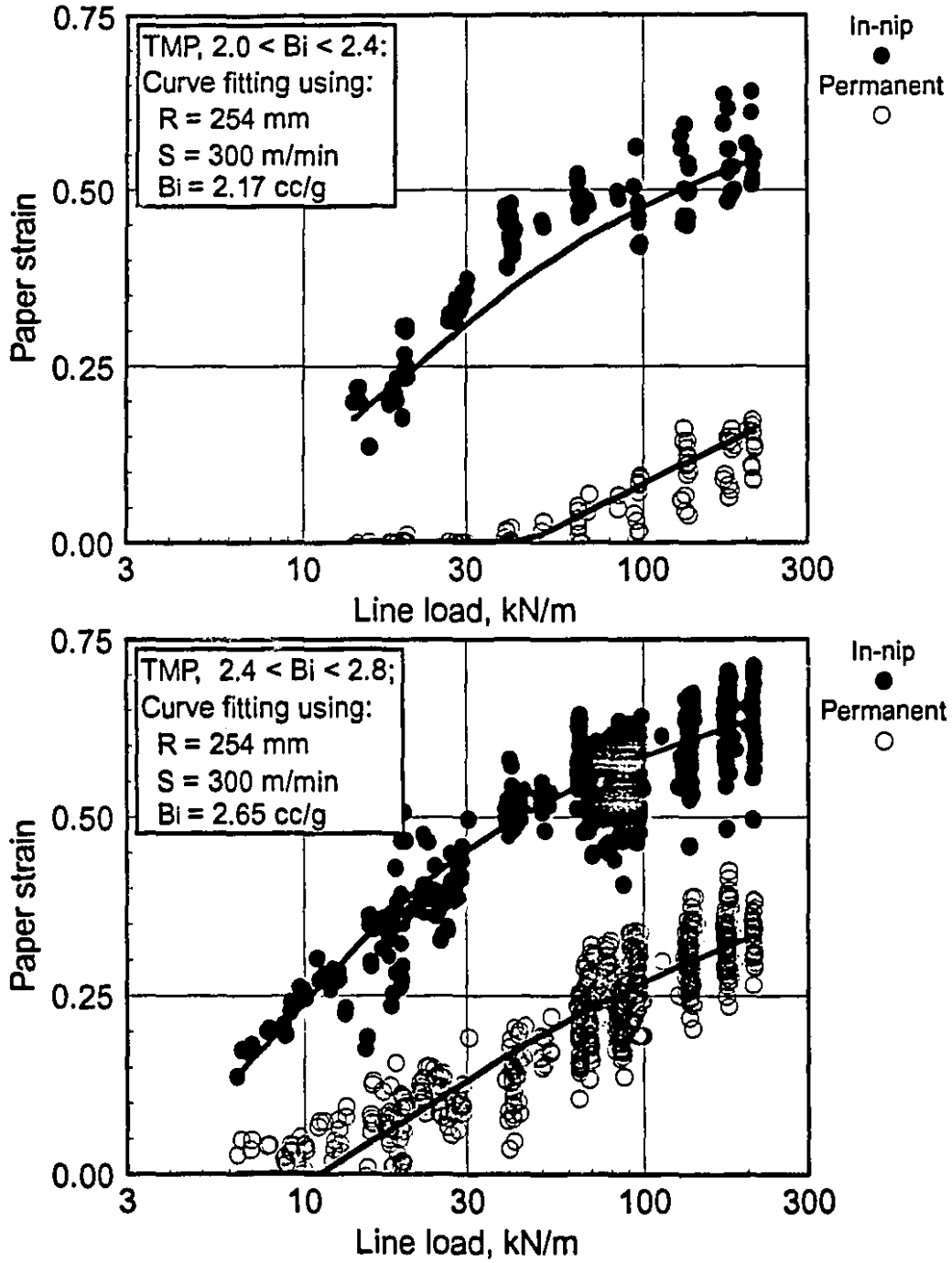

Figure 4.2 Strain vs. load, 202 mm, all data, TMP: a) low initial bulks; b) high initial bulks. Curve fitting using the calendering equation.

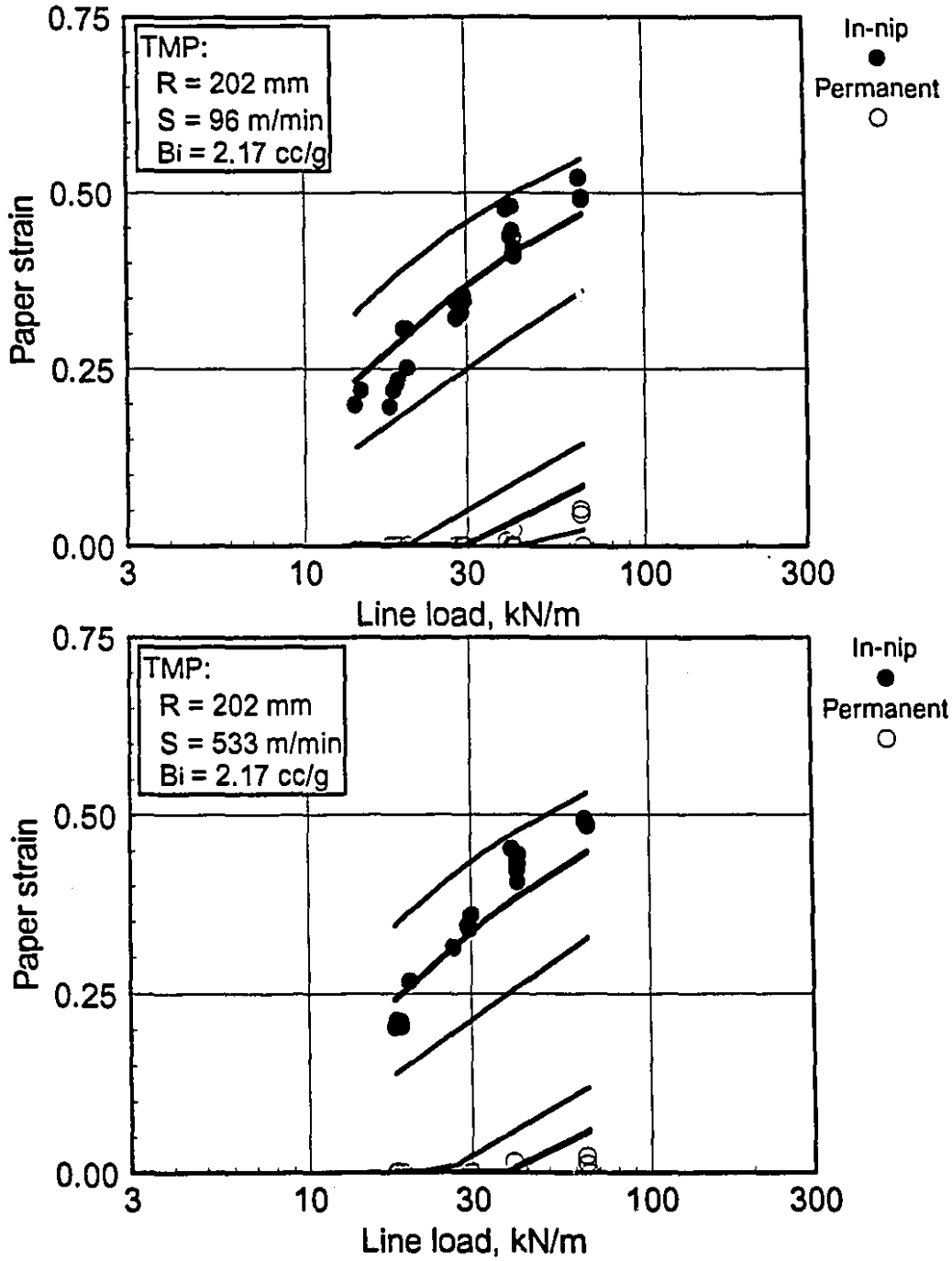

Figure 4.3 Strain vs. load, low initial bulks, TMP: a) 96 m/min;
b) 533 m/min.
Curve fitting using the calendering equation.

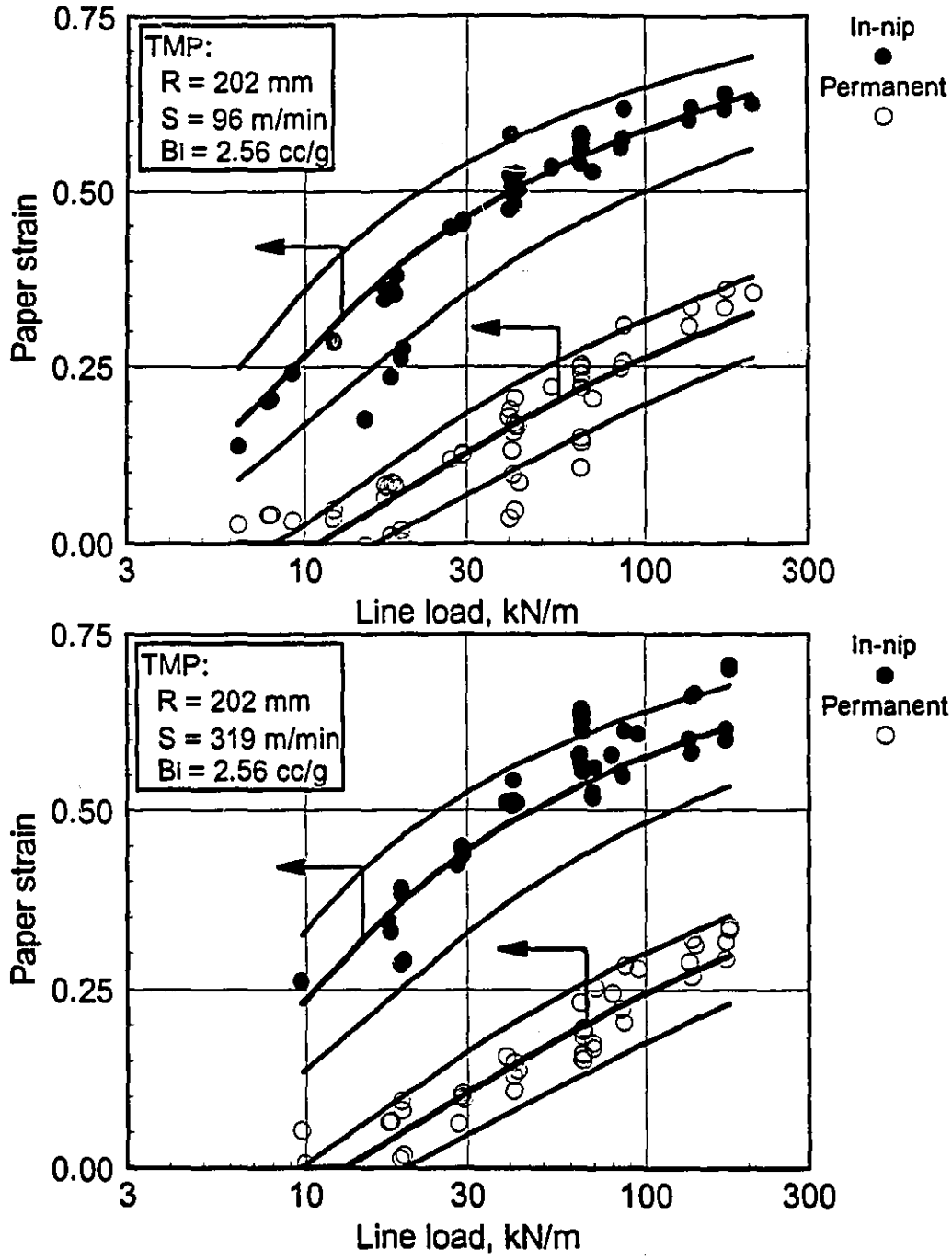

Figure 4.4 Strain vs. load, 202 mm, 2.56 cm^3/g: a) 96 m/min;
b) 319 m/min.
Curve fitting using the calendering equation.

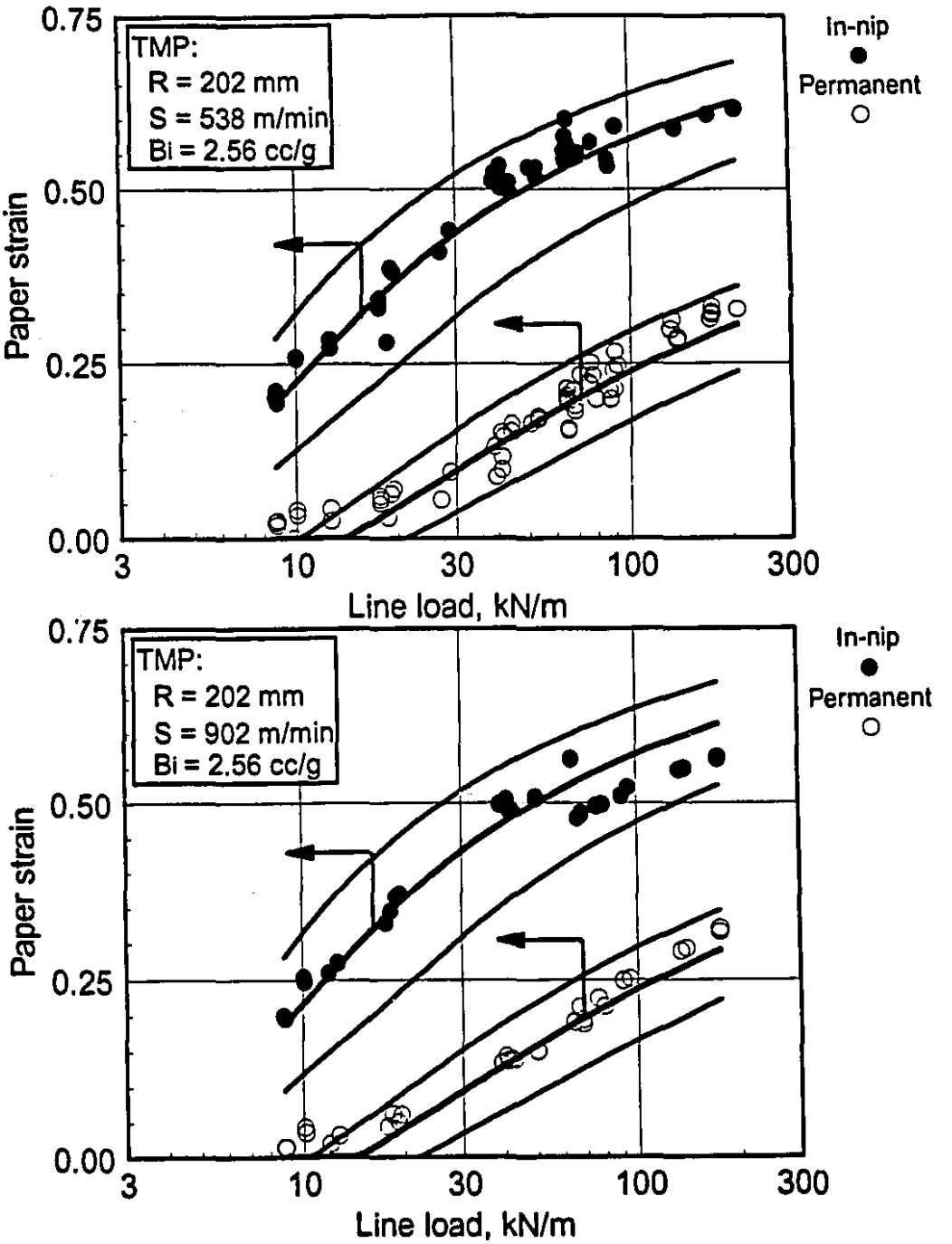

Figure 4.5 Strain vs. load, 202 mm, 2.56 cm^3/g: a) 538 m/min; b) 902 m/min.

Curve fitting using the calendering equation.

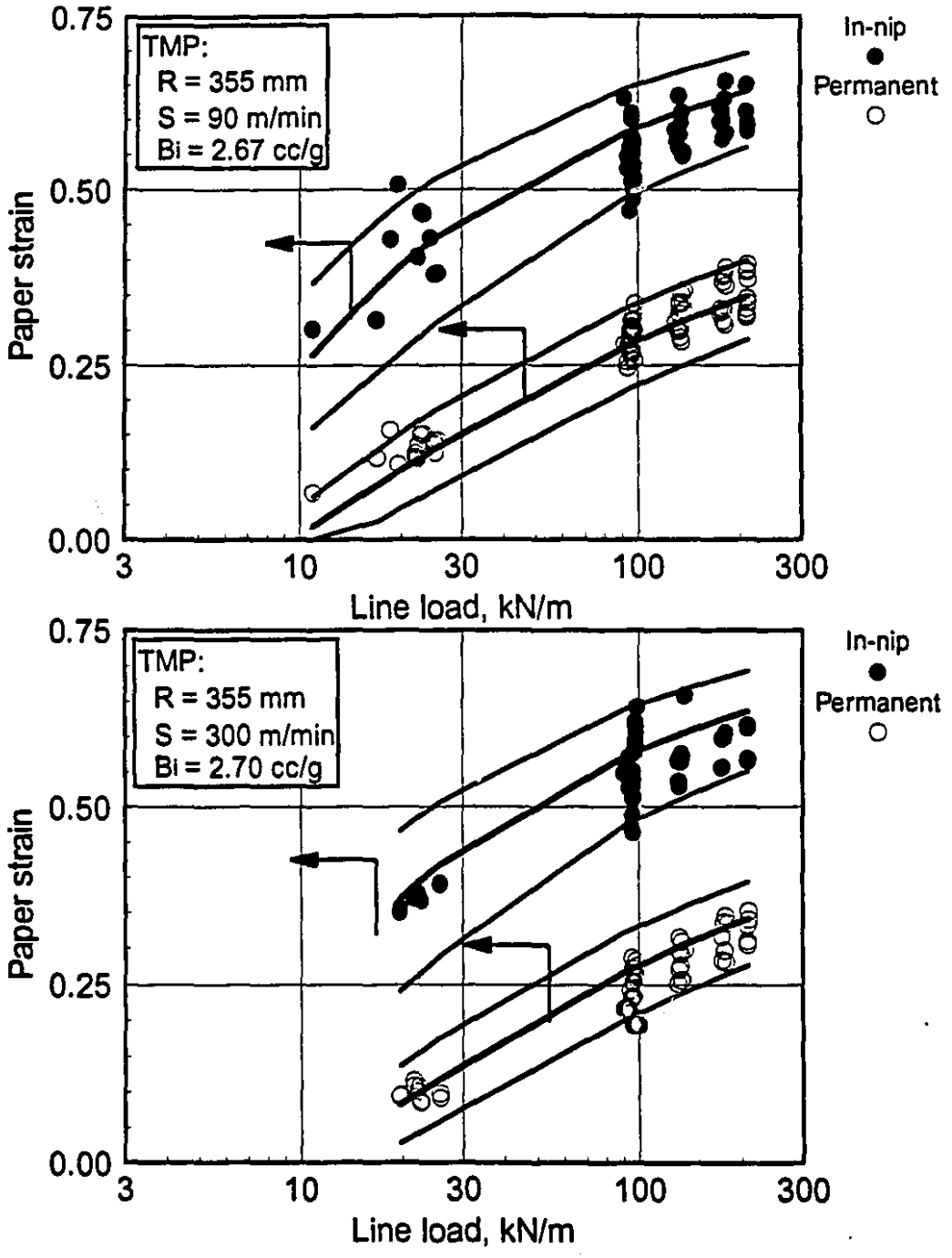

Figure 4.6 Strain vs. load, 355 mm, 2.69 cm^3/g: a) 90 m/min; b) 300 m/min.
Curve fitting using the calendering equation.

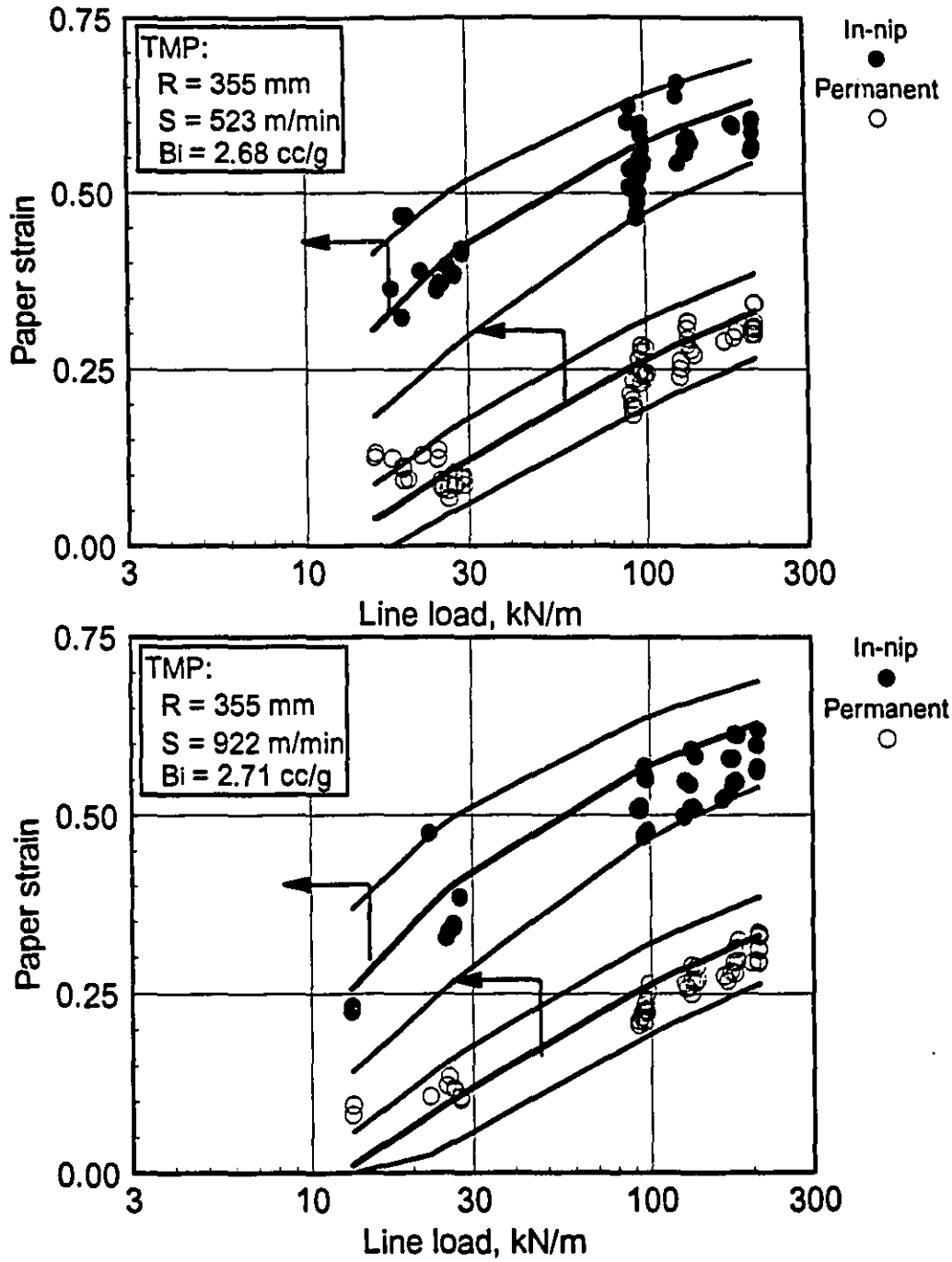

Figure 4.7 Strain vs. load, 355 mm, 2.69 cm^3/g: a) 523 m/min; b) 922 m/min.
Curve fitting using the calendering equation.

TABLE 4.2: In-nip calendering coefficients, TMP (F. Soucy).

Parameter	Estimate	S.E. (C_V)	Lower 95%	Upper 95%
A_n	-0.3629	0.0764 (0.21)	-0.5131	-0.2127
a_{on} (g/cm^3)	0.0418	0.0202 (0.48)	0.0021	0.0815
a_{Ln} (g/cm^3)	0.1936	0.0193 (0.10)	0.1557	0.2319
a_{Rn} (g/cm^3)	-0.0771	0.0173 (0.22)	-0.1112	-0.0431
a_{Sn} (g/cm^3)	-0.0219	0.0058 (0.27)	-0.0332	-0.0108
r^2	0.8703			
S.E., cm^3/g	0.119			

A1.4, A1.5 and A1.6. Results converted to base 10 logarithm are given in Table A1.8.

In-nip coefficients, presented in Table 4.2, have not been determined in the past. The values reported are statistically different from zero, and show that the magnitudes of the effect of the various independent variables on in-nip strain is the same as for the permanent strain, i.e. load has the greatest effect, followed by roll radius, then sheet speed.

Crotogino et al. [18, 22] proposed the calendering equation and measured permanent coefficients for a variety of newsprints. The permanent coefficients in Table 4.3 can thus be compared directly with their coefficients, which are given in Table 4.4.

Comparing the intercepts A_p and a_{op} first, it can be seen that the magnitude of A_p as reported here is slightly higher. This coefficient is a measure of the ease with which a permanent strain can be imposed. For given calendering conditions and initial bulk, the term μB_i will be constant; if the absolute value of A_p is larger the permanent deformation will be smaller. The coefficient A_p is thus a paper property, and the higher

TABLE 4.3: Permanent calendering coefficients, TMP (F. Soucy).

Parameter	Estimate	S.E.	Lower 95%	Upper 95%
A_p	-0.7017	0.0625 (0.09)	-0.8246	-0.5788
a_{op} (g/cm^3)	0.1743	0.0176 (0.10)	0.1398	0.2089
a_{Lp} (g/cm^3)	0.1135	0.0078 (0.07)	0.0981	0.1289
a_{Rp} (g/cm^3)	-0.0187	0.0092 (0.49)	-0.0368	-0.0005
a_{Sp} (g/cm^3)	-0.0158	0.0021 (0.13)	-0.0200	-0.0115
r^2	0.9141			
S.E., cm^3/g	0.094			

magnitude presented here means that this paper is less easily deformed than those used in the earlier work. This confirms previous work by Mitchell et al. [56], which showed that papers made from TMP pulps are more difficult to calender.

The coefficient a_{op} varies quite a lot in the previous study, to the point where the sign changes for different pulp types. No physical explanation for the significance of this coefficient has been found, although it can be suggested that it corrects for all the other effects not already included in the calendering equation, such as freeness, formation, pressing and drying conditions, etc. In this study, a_{op} also includes the terms $a_\theta\theta$ + a_MM.

The load coefficient a_{Lp} reported here is slightly higher than those given previously by Crotogino et al.; however this coefficient also appears to be a paper property, since Crotogino et al. [18, 22] have reported values ranging from 0.117 to 0.148. Thus the value of 0.1135 given here is not unreasonable.

The sheet speed coefficient a_{Sp} is 25% lower in the present study. The range of

TABLE 4.4: Permanent calendering coefficients, from Crotogino et al.

	Trial #1	Trial #2	Trial #3	Trial #4
A_p	-0.500	-0.334	-0.289	-0.417
a_o (g/cm^3)	0.0498	-0.00102	-0.00209	0.0568
a_L (g/cm^3)	0.0988	0.0922	0.0914	0.0912
a_R (g/cm^3)	-0.0390	-0.0374	-0.0353	-0.0354
a_S (g/cm^3)	-0.0208	-0.0175	-0.0208	-0.0204
a_T (g/cm^3 °C)	0.000943	0.000876	0.000567	0.000863
a_M (g/cm^3)	0.00545	0.00462	0.00529	0.00520
r^2	0.928	0.939	0.930	0.887
S.E., cm^3/g	0.107	0.109	0.105	0.117

earlier results shows that a_{Sp}, like the other coefficients, is a paper property which varies from furnish to furnish.

Finally, the root mean square of the residual error reported by Crotogino et al. [22] is similar to the error reported here. Its magnitude can be attributed, firstly, to the random nature of paper structure which subjects strain measurements to a certain unavoidable variation, and secondly, to the uncertainty in the uncontrolled independent variables temperature and moisture content. Of the two, Crotogino et al. [22] have shown that moisture content has the larger effect; in this study its value depended on ambient relative humidity, which varied over a wide range. Using a_M = 0.005, the increase in predicted permanent strain for an initial bulk of 2.65 cm^3/g, as moisture content increases from 5% to 10%, is 0.066.

The permanent data may also be compared with work published by Kerekes [44, 46], who measured a load coefficient of 0.090 and a speed coefficient of -0.018 after correction for the effect of initial bulk. Kerekes also published estimates of a_L and a_S based on the work of Colley and Peel [17]; these values are 0.102 and -0.012, respectively. The load coefficients are slightly smaller than the new value of 0.1135, but both speed coefficients are statistically similar to the value of -0.0158 measured here.

Radius and moisture effects

Radius effects have only been measured once in the past, as described below. Generally, radius coefficients have been calculated from the average of the load and speed coefficients, as suggested by Kerekes [45]:

$$a_R = -\left(\frac{a_L + a_S}{2}\right) \qquad [4.8]$$

Using the results from Table 4.3, Equation 4.8 predicts $a_{Rp} = -0.0489$, which is more than double the measured value reported. In the in-nip case, it can be seen from Table 4.2 that Kerekes' prediction gives $a_{Rn} = -0.0859$, which is not statistically different from the measured value of -0.0771.

Baumgarten and Göttsching [5] measured permanent calendering coefficients for a variety of newsprints. Their load and speed coefficients agree with those presented here once the effect of bulk is removed. However, their roll radius coefficient agrees with Kerekes' prediction rather than the value in Table 4.3.

The standard errors for the two radius coefficients presented here are large, particularly for the permanent data where the 95% confidence interval just barely excludes the possibility of $a_{Rp} = 0$. As mentioned in Chapter 3, the equipment was not located in a controlled environment. As well, roll changes involved a time-consuming rebuild of the calender. For this reason, roll sets were not changed until a full data set had been acquired, a process often requiring several months. By the time the next roll pair had been installed, seasonal changes in relative humidity had caused significant changes in the paper moisture content, and thus its compressibility. This resulted in the possibility of a significant systematic error due to the combined effect of roll radius and sheet moisture content.

Strain data was therefore corrected to 50% relative humidity as follows. Equilibrium moisture content was estimated from the ambient relative humidity using published data for kraft, Bond et al. [6], and for newsprint, Crotogino [20]. Next, the

TABLE 4.5: In-nip calendering coefficients after moisture content corrections, TMP (F. Soucy).

Parameter	Estimate	S.E. (C_V)	% change in estimate
A_n	-0.3647	0.0753 (0.21)	0.5
a_{on} (g/cm^3)	0.0247	0.0194 (0.79)	-40.9
a_{Ln} (g/cm^3)	0.1920	0.0189 (0.10)	-0.8
a_{Rn} (g/cm^3)	-0.1068	0.0184 (0.17)	38.5
a_{Sn} (g/cm^3)	-0.0216	0.0058 (0.27)	-1.4
r^2	0.86		
S.E., cm^3/g	0.119		

moisture coefficients for the calendering equation were estimated from data published by Crotogino et al. [22], who measured $a_{Mp} = 0.005$; this value was essentially the same for four different pulp types. Colley and Peel [17] measured the effect of moisture content on compressed thickness; from that work it can be deduced that $a_{Mn} \approx 0.85 a_{Mp}$. From these, the following amount was calculated and added to each strain measurement:

$$\varepsilon_{corr} = B_i a_M (M - M_{50}) \qquad [4.9]$$

where M is the moisture content corresponding to ambient conditions, and $M_{50} = 7.69\%$ is the moisture content corresponding to 50% R.H. The regressions performed for the original data set were repeated on the new set; results are given in Tables 4.5 and 4.6. Along with the standard error and coefficient of variation, the tables give the percent change in the estimate from those given in Tables 4.2 and 4.3.

The only coefficients which are statistically different are the radius coefficients

TABLE 4.6: Permanent calendering coefficients after moisture content corrections, TMP (F. Soucy).

Parameter	Estimate	S.E. (C_V)	% change in estimate
A_p	-0.6095	0.0188 (0.03)	-13.1
a_{op} (g/cm^3)	0.1256	0.0101 (0.08)	-27.9
a_{Lp} (g/cm^3)	0.1085	0.0041 (0.04)	-4.4
a_{Rp} (g/cm^3)	-0.0530	0.0085 (0.16)	183.4
a_{Sp} (g/cm^3)	-0.0170	0.0018 (0.11)	7.6
r^2	0.90		
S.E., cm^3/g	0.093		

a_R and the intercepts A and a_o. Of the four intercepts, a_{on} is no longer statistically different from zero; however, published values of a_{op} range from -0.002 to +0.057 for different furnishes (Crotogino et al. [22] and Table 4.4). This coefficient accounts for all the pulp properties and paper machine parameters not explicitly included in the calendering equation, and so can vary substantially from case to case.

Using the new correlation, Kerekes' prediction is now verified for both in-nip and permanent strains at the 95% confidence level. As well, the coefficients of variation for the radius coefficients are reduced significantly, especially for a_{Rp}. Thus it appears that the moisture content correction eliminates a large portion of the unexplained error in the first set of results.

The calendering equation revised

Residual bulks computed from the full set of all TMP replicates are plotted in terms of initial bulk in Figure 4.8 for both in-nip and permanent data. As can be seen, there is a slight tendency for the residuals to be positive at low and high bulks, and negative at medium values. (Plots of residuals versus other independent variables show no such trends). In the permanent case, this implies that the basic form of the calendering equation, which is linear in B_i, is not entirely correct. Assuming it is not the result of a systematic error in bulk measurements, several methods can be proposed for dealing with the trend in the residuals. One alternative is to add a second order term to the calendering equation:

TABLE 4.7: Permanent calendering coefficients for Equation 4.10.

Parameter	Estimate
A_1	-0.5503
a_o (g/cm^3)	0.1145
a_L (g/cm^3)	0.1056
a_R (g/cm^3)	-0.0167
a_S (g/cm^3)	-0.0141
μ_{p2} (g/cm^3)^2	0.0014
r^2	0.9188
S.E., cm^3/g	0.094

$$\varepsilon = A_1 + \mu_{p1}B_i + \mu_{p2}B_i^2 \qquad [4.10]$$

The results of fitting this equation to the permanent data yields a value of μ_2 which is statistically different from zero, as shown in Table 4.7, but which is an order of magnitude smaller than the other coefficients. Given a large initial bulk of 3.2 cm^3/g, the change in ε_p due to $\mu_{p2}B_i^2$ is small at 0.014 when typical permanent strain values of 0.100 and up are considered. Compared with the normal calendering equation, the root mean square of the residuals is unchanged and the value of r^2 is slightly lower. Finally, there is no obvious theoretical basis for stating that ε_p should be a parabolic function of

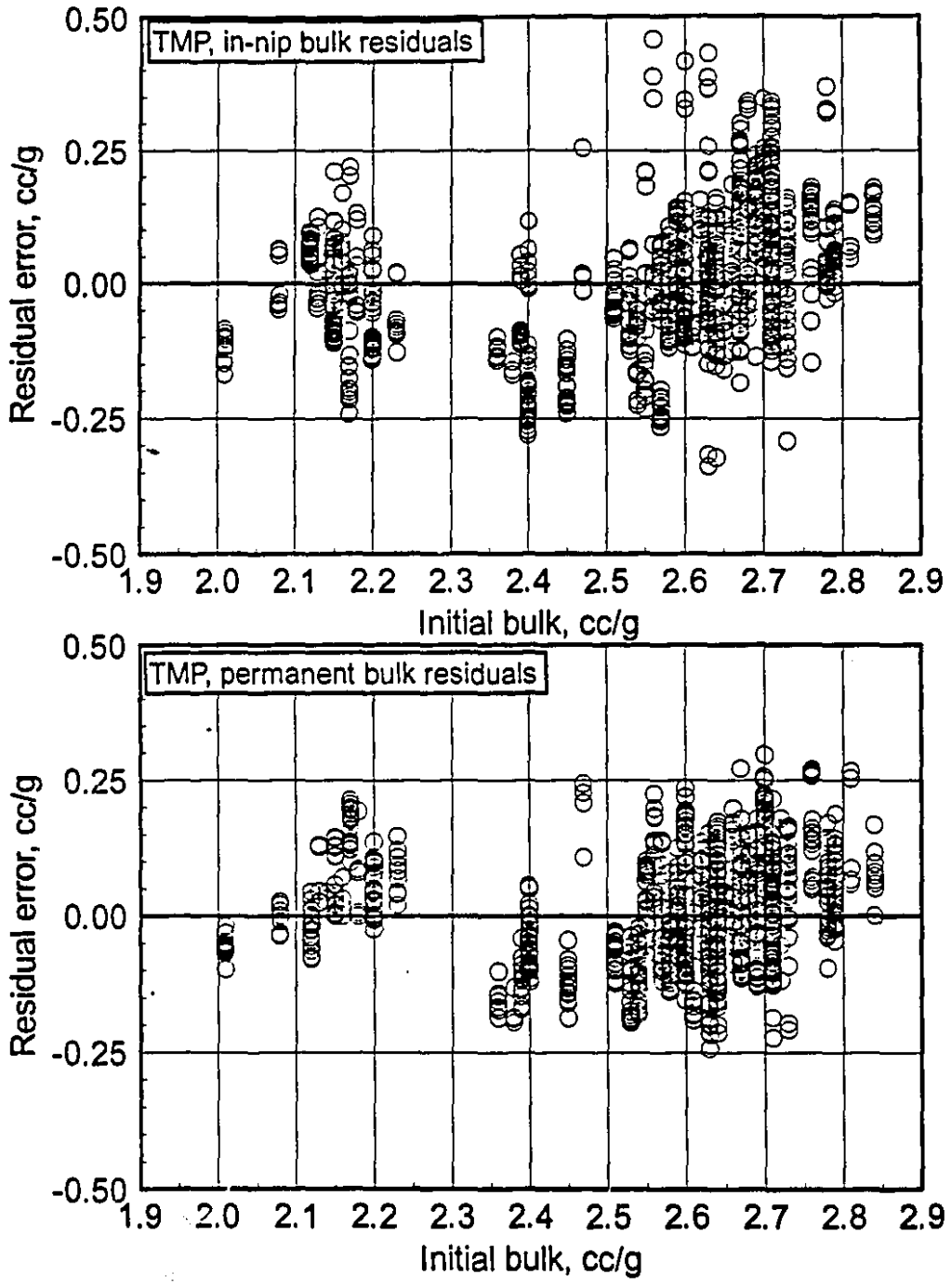

Figure 4.8 Bulk residuals vs. initial bulk, a) In-nip data;
b) Permanent data
Calculated using the calendering equation.

B_i. The increased computational effort associated with the addition of a second-order term may not therefore be offset by any significant improvement.

It can also be suggested that one or more of the coefficients contained in the nip intensity factor μ_p may themselves be functions of B_i. Both in-nip and permanent load coefficients were found to change slightly when low bulk data is ignored. However, the range of initial bulks was too small and there was insufficient data at lower bulks to be able to extract statistically meaningful relationships between the coefficients and B_i. As well, there is no theoretical basis for suggesting any of the coefficients are functions of B_i since the calendering equation itself is not based on any theoretical considerations but on curve fitting results. The benefits resulting from the addition of a second curve-fitting exercise are therefore doubtful.

Another alternative to the calendering equation is suggested by classifying the data reported here according to which portion of the calendering equation applies. For each data point in the full TMP set, the in-nip and permanent nip intensity factors μ_n, μ_p were computed using the coefficients determined by SYSTAT. Regimes based on the limits of the calendering equation were defined next:

$$\textit{Regime } 0: \qquad B_i \le -\frac{A}{\mu} \qquad \varepsilon = 0$$

$$\textit{Regime } 1: \qquad -\frac{A}{\mu} \le B_i \le \frac{1-A}{2\mu} \qquad \varepsilon = A + \mu B_i \qquad [4.11]$$

$$\textit{Regime } 2: \qquad B_i \ge \frac{1-A}{2\mu} \qquad \varepsilon = 1 - \frac{(1-A)^2}{4\mu B_i}$$

Data in Regime 0 falls below the lower limit of the calendering equation, as described in Section 2.1; there is no permanent deformation. In Regime 1 the calendering equation applies, and in Regime 2 the upper limit has been exceeded. The number of data points in each Regime is given in Table 4.8, from which it will be seen that 74% of the permanent strain data, and 95% of the in-nip data fall above their respective upper limits.

TABLE 4.8: Distribution of data according to calendering equation limits.

	Regime 0	Regime 1	Regime 2
ε_p	90 (6.5%)	270 (19.5%)	1021 (74%)
ε_n	--	75 (5.4%)	1305 (94.6%)

(Note that there is no in-nip data in Regime 0, since there were no experimental conditions yielding an in-nip strain of zero.)

Most of the permanent data and virtually all of the in-nip data falls above the upper limit, where strain is proportional to $1/\mu B_i$. The expression for strain in Regime 2 was thus rewritten in a linear form:

$$\frac{1}{1-\varepsilon} = \frac{4\mu B_i}{(1-A)^2} \qquad [4.12]$$

Recalling that apparent density ρ is the inverse of bulk, and defining new constants, Equation 4.12 can be rewritten:

$$\frac{\rho}{\rho_i} = A_2 + \frac{\mu_2}{\rho_i} \qquad [4.13]$$

where

$$\mu_2 = a_{o2} + a_{S2}\log_{10}S + a_{L2}\log_{10}L + a_{R2}\log_{10}R \qquad [4.14]$$

Equation 4.13 is linear in its coefficients, and can therefore be fitted using any linear regression package, such as the one included in most spreadsheets; iterative methods are not necessary. Comparing Equation 4.13 with Equation 4.12 gives an expression relating the coefficients of μ_2 to those of the calendering equation, illustrated with the load coefficient:

TABLE 4.9: Coefficients for Equations 4.13 and 4.14.

	A_2, S.E.	a_{O2}, S.E.	a_{L2}, S.E.	a_{S2}, S.E.	a_{R2}, S.E.	r^2, S.E.
ρ_n/ρ_i	1.3371 0.1968	-0.4742 0.0765	0.4304 0.0148	-0.0534 0.0129	-0.2129 0.0432	0.74 0.123 cc/g
ρ_p/ρ_i	1.1684 0.0397	-0.2582 0.0317	0.1870 0.0063	-0.0334 0.0031	-0.0612 0.0110	0.82 0.177 cc/g

TABLE 4.10: Calendering coefficients given by Equation 4.15.

	a_L	a_S	a_R
ε_n	0.2004	-0.0249	-0.0991
ε_p	0.1211	-0.0216	-0.0397

$$a_L = \frac{(1-A)^2}{4} a_{L2} \qquad [4.15]$$

Given A_n = -0.36 and A_p = -0.60, as generated by SYSTAT, Equation 4.13 can be fit to the data in Regime 2, then the calendering coefficients can be determined using Equation 4.15. This was done using the summary data set of 359 data points after data points in Regimes 0 and 1 were identified and removed; results are given in Tables 4.9 and 4.10 and are plotted in Figures 4.9 to 4.12.

All coefficients are significant at the 95% level, and the calendering equation coefficients are correctly predicted. However, Equation 4.13 fits the data less well than

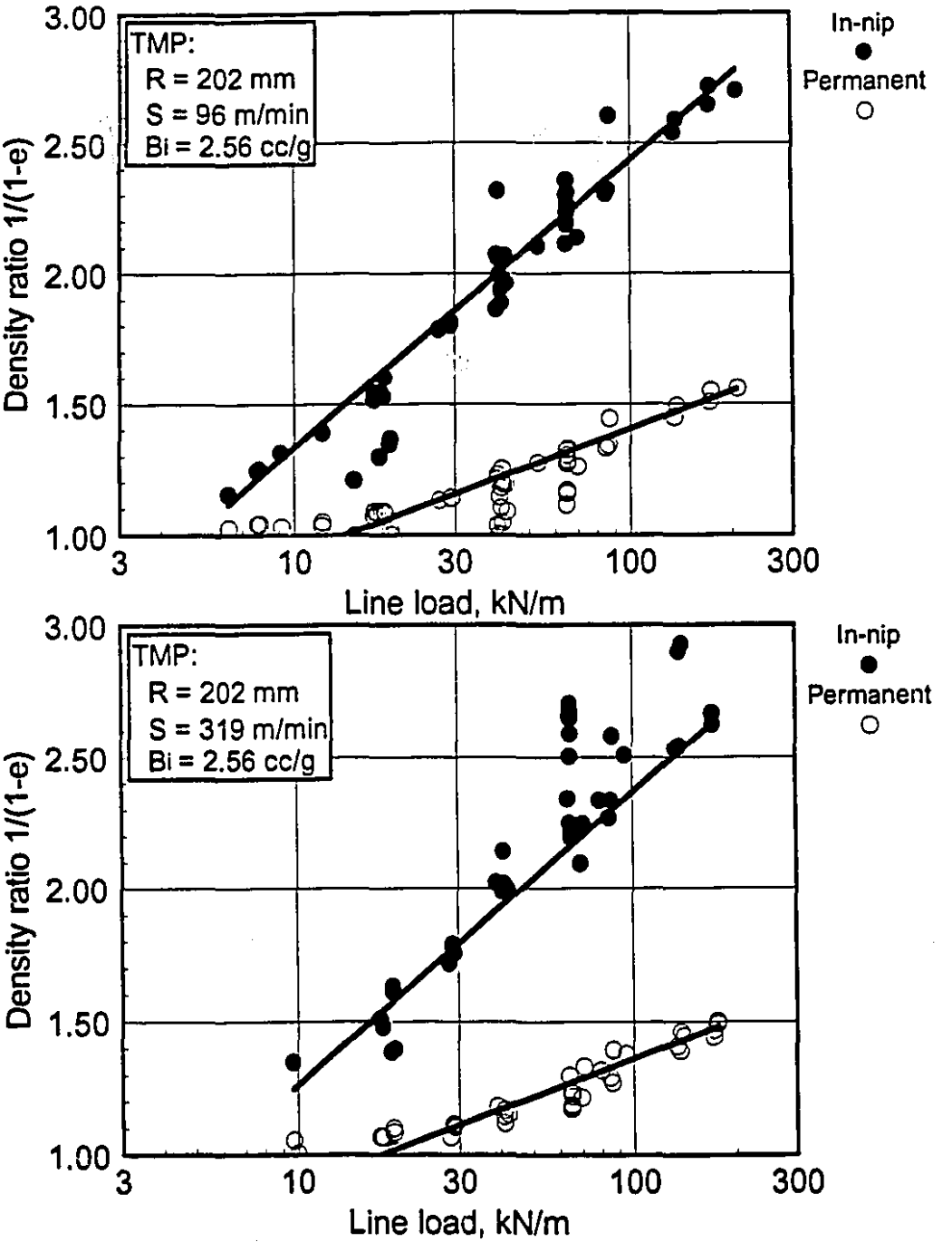

Figure 4.9 Density ratio vs. load, 202 mm, 2.56 cm^3/g: a) 96 m/min; b) 319 m/min.
Curve fitting using Equation 4.13.

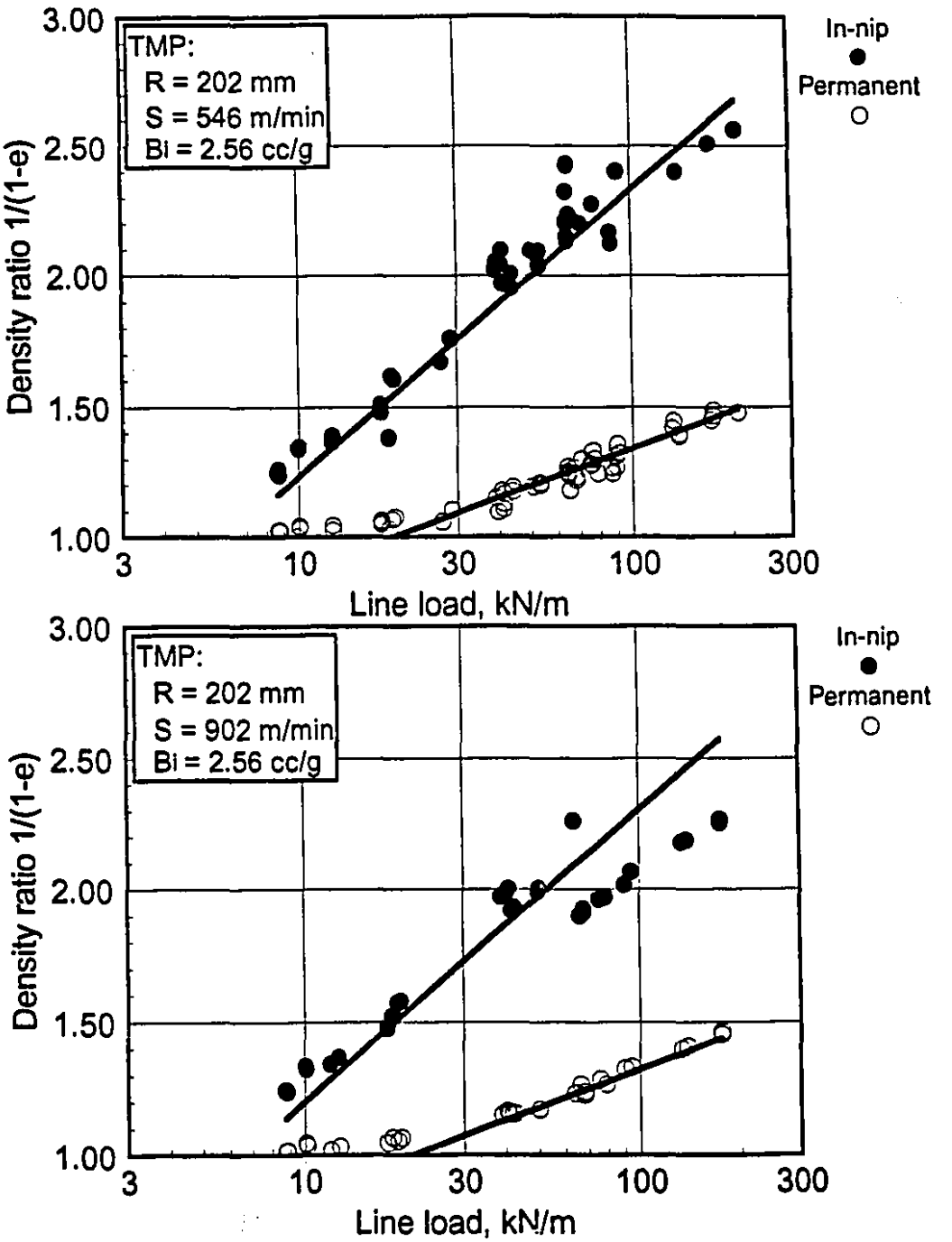

Figure 4.10 Density ratio vs. load, 202 mm, 2.56 cm^3/g: a) 546 m/min; b) 902 m/min

Curve fitting using Equation 4.13.

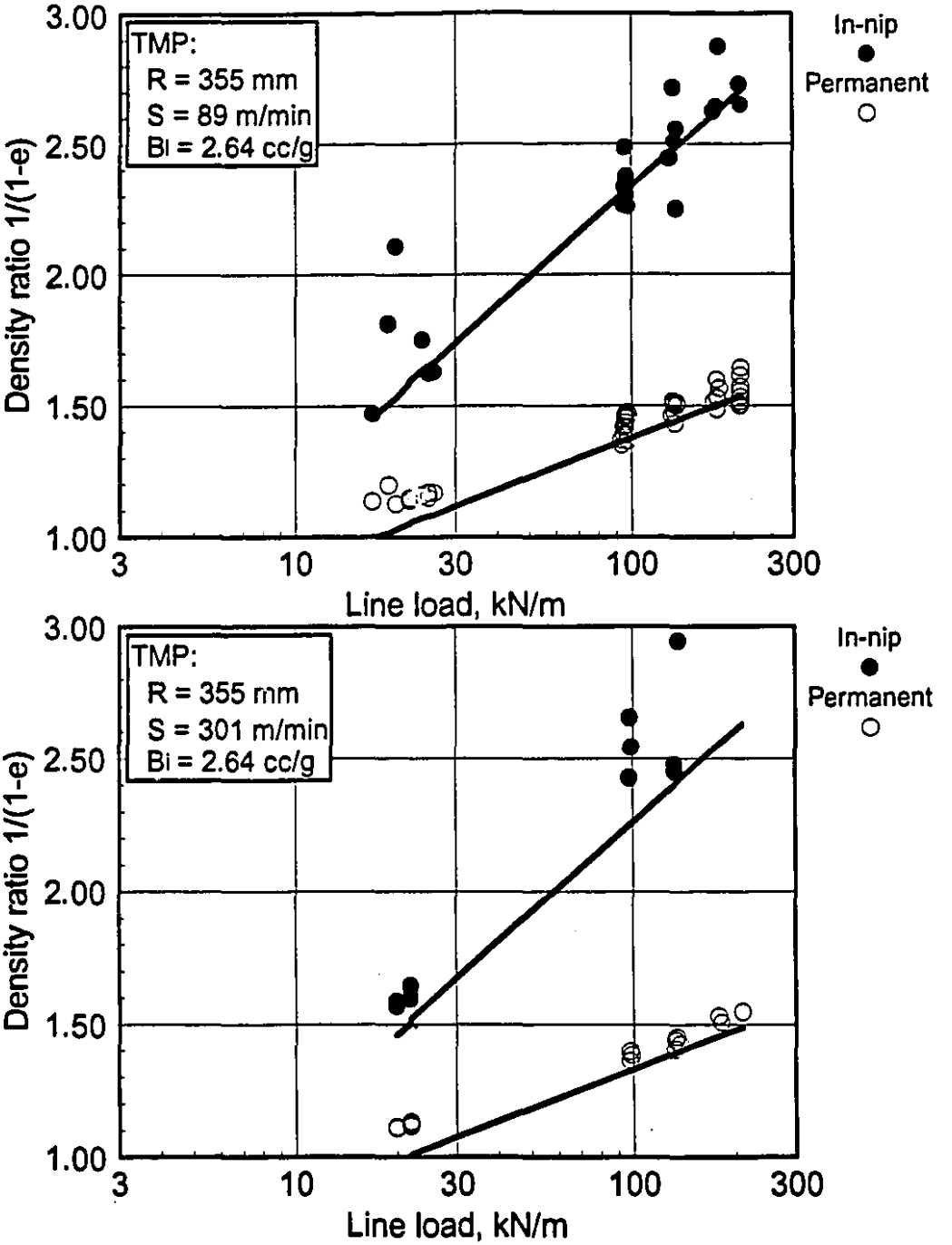

Figure 4.11 Density ratio vs. load, 355 mm, 2.64 cm^3/g: a) 89 m/min; b) 301 m/min.

Curve fitting using Equation 4.13.

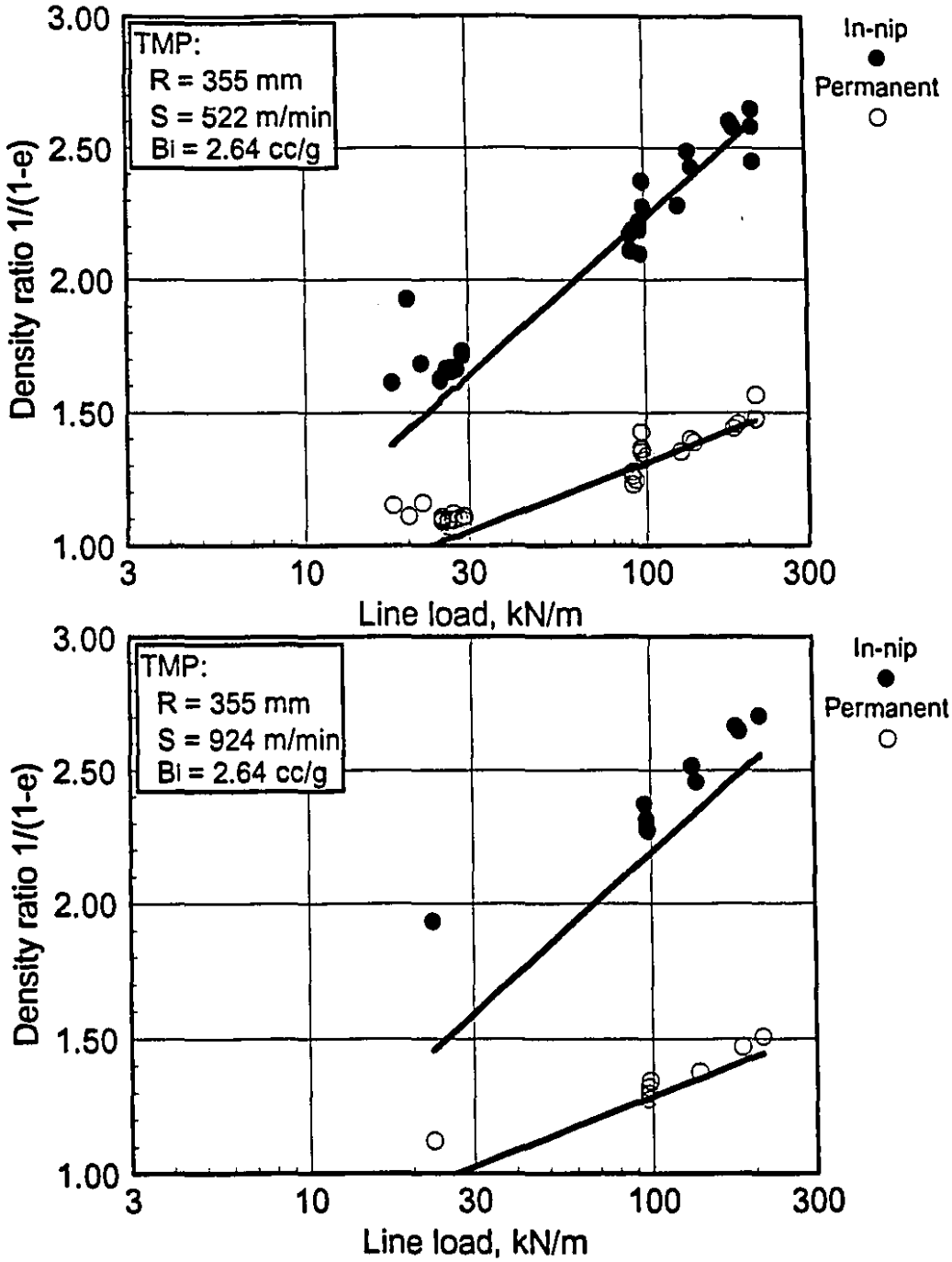

Figure 4.12 Density ratio vs. load, 355 mm, 2.64 cm^3/g: a) 522 m/min; b) 924 m/min.

Curve fitting using Equation 4.13.

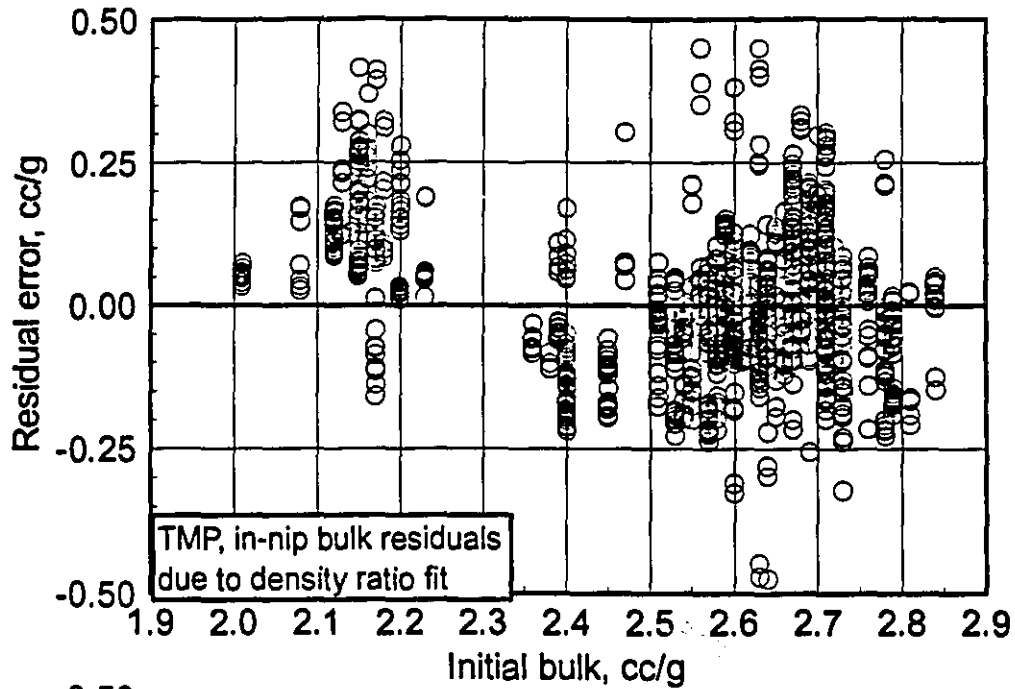

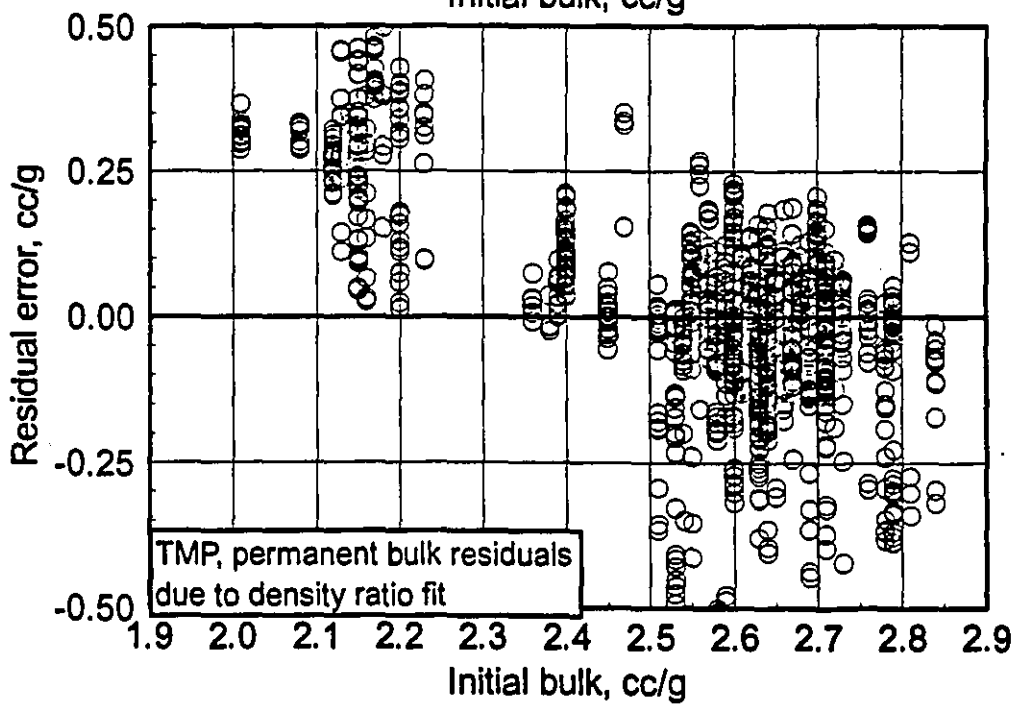

Figure 4.13 Bulk residuals vs. initial bulk, a) In-nip data, b) Permanent data

Curve fitting using Equation 4.13.

the calendering equation itself, with lower values of r^2 and higher standard errors, as seen in the plot of the residuals, Figure 4.13, and the numerical values in Table 4.9. The plot of the residual bulk also shows that the apparent effect of initial bulk has not been accounted for; this is sensible, since Equation 4.13 is simply an algebraic manipulation of the calendering equation.

The benefit of this method thus lies in the use of linear instead of non-linear regression methods, and it may be most useful in estimating in-nip strains since very little load is required to exceed the upper limit of the in-nip calendering equation.

High basis weight streaks in a light weight sheet

It has been suggested by Haglund [33] that a thick streak in a lightweight sheet might be deformed in a nip to the extent that it winds up thinner after calendering than the surrounding, initially thinner sheet. The reasoning proposed was that the thicker area, carrying most of the load in the nip, would see much higher pressures than the adjoining area and would thus be the only portion of the sheet to be calendered. This proposed behaviour can now be tested using the in-nip and permanent calendering equations. Haglund [33] took roll bending into account; the analysis here will first assume an infinite roll bending strength, then a qualitative assessment of the effect of roll bending will be made.

Two cases of a thick streak in a thin sheet are illustrated in Figure 4.14 and in Table 4.11. The in-nip and permanent calendering equations, complete with limits as described in Section 4.1.1 (Tables 4.5 and 4.6), were used to generate strain curves at an initial bulk of 2.4 cm^3/g (Figure 4.14a) or 3.0 cm^3/g (Figure 4.14b). Conditions used in the simulation were a sheet speed of 300 m/min and a roll radius of 254 mm. In Figure 4.14a, the variation from low to high weight was assumed small (45 to 55 g/m^2), while a large variation was used in Figure 4.14b (30 to 60 g/m^2). If the sheet is then compressed to a thickness of 60 μm in the nip, the two areas see different strains (point A and B) due to the different initial calipers. Permanent strains are higher in the heavier spots (point D), but the lighter spots (point C) are still thinner.

This is illustrated again in Figure 4.15, where the same data has been re-plotted in terms of thickness rather than strain. Both spots are compressed to the same 60 μm thickness in-nip, at points A and B. After the nip, point A recovers to point C, while B recovers to D. In both cases the initially thicker spot is still thicker after the nip, although the calendering process has been succesful in reducing the variation. There is no obvious combination of two points A and B on a horizontal line which yield a thickness at D less than that at C, at least for this paper type. A paper with a permanent strain curve closer to the in-nip curve, i.e. a paper which recovers less after the nip,

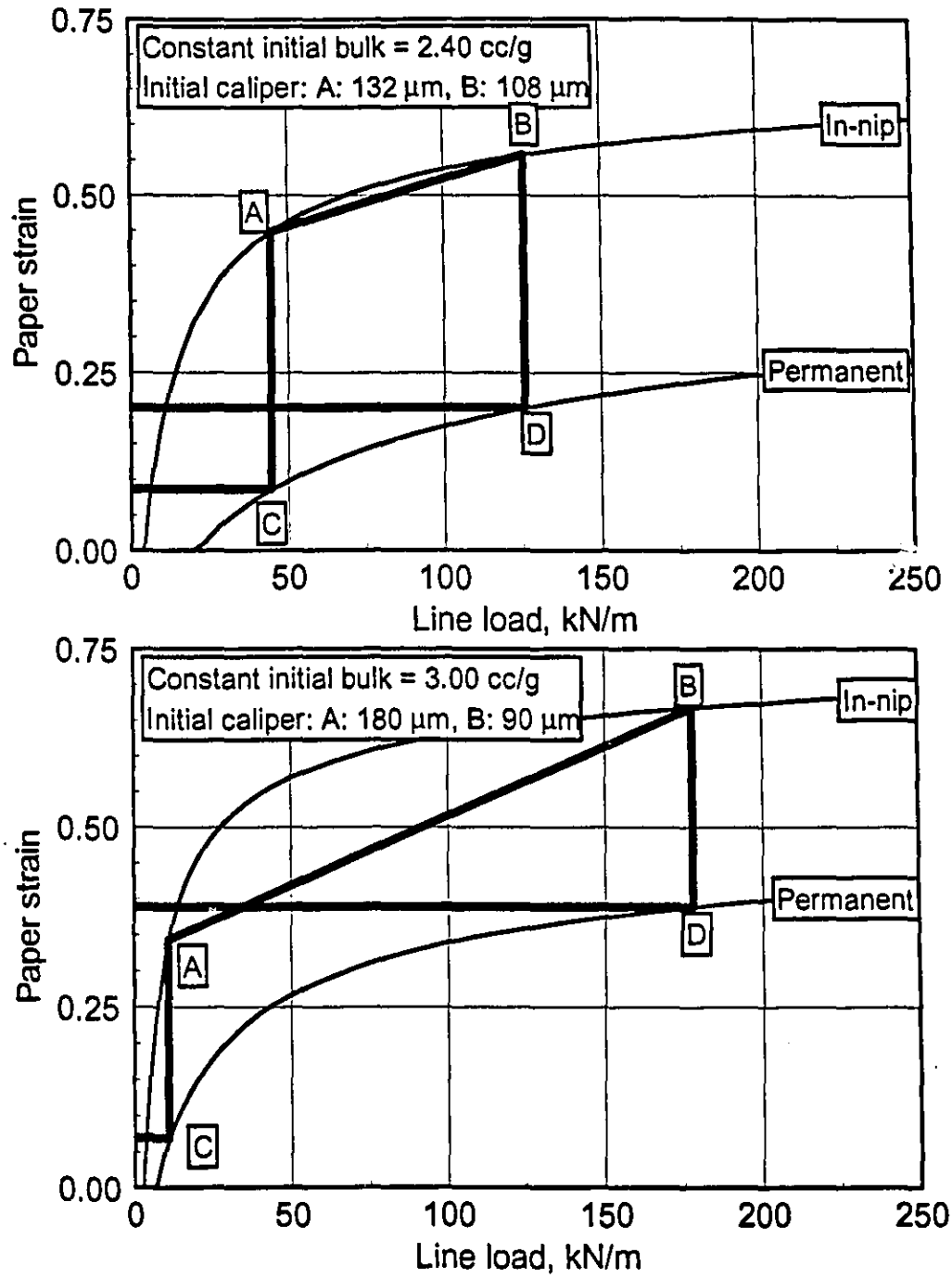

Figure 4.14 Strain in a calender for a thick streak in a thin sheet:
a) low variation; b) high variation.
Curve fitting using the calendering equations for TMP.

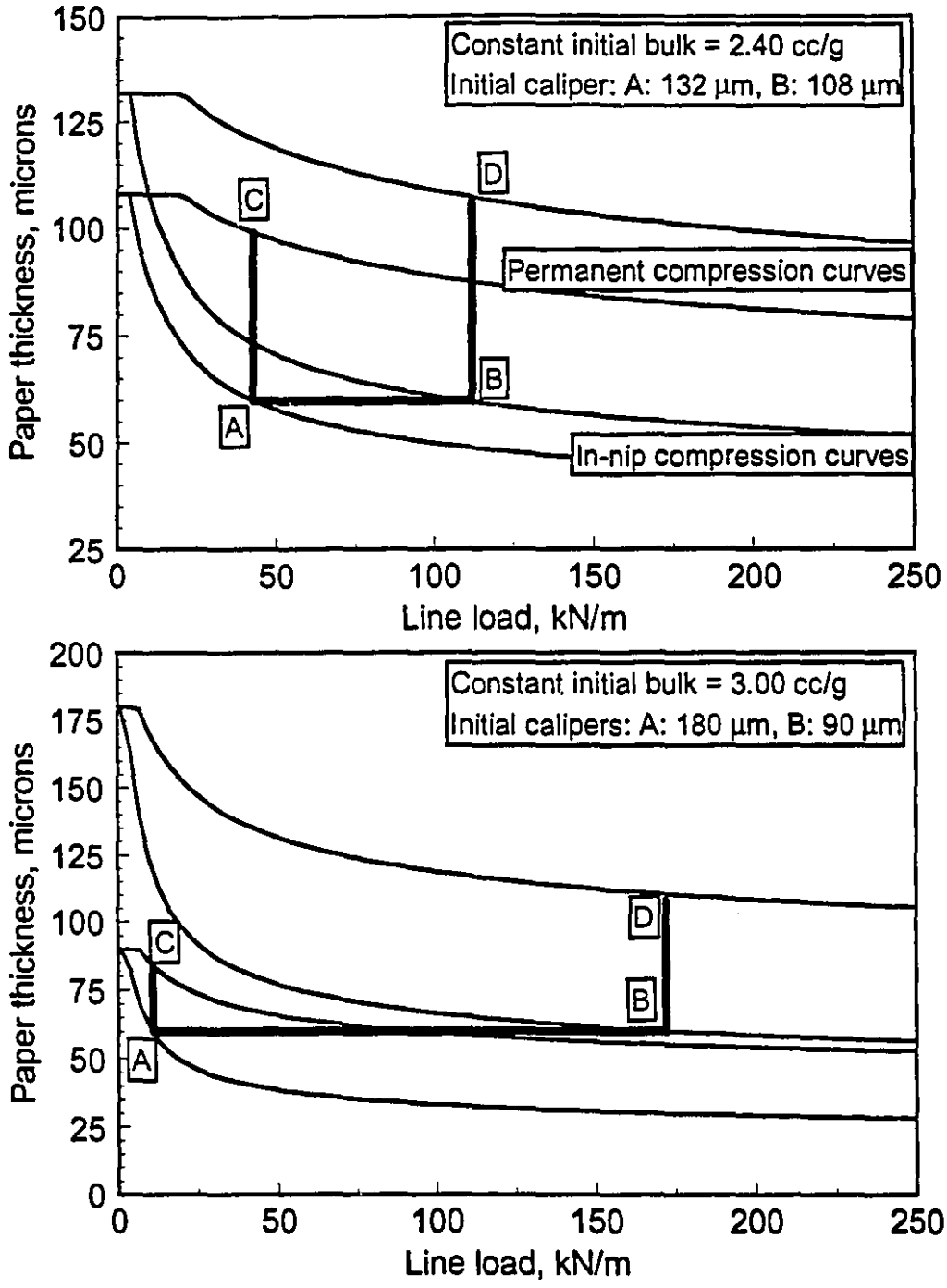

Figure 4.15 Thickness in a calender for a thick streak in a thin sheet:
a) low variation; b) high variation.
Curve fitting using the calendering equations for TMP.

might exhibit this behaviour when the in-nip strain at A is low enough for the permanent strain at C to be zero and the strain at D is high enough that the thickness there is lower than at C.

The effect of roll bending is to alter the nip profile so that nip thickness is not a constant across the width of a calender. This results in point A in Figure 4.15 being displaced slightly along the compression curve so that line AB is no longer horizontal. Line AC must remain vertical, however, so that point C is displaced an equal amount horizontally. There is still no possible set of points A and B yielding D less than C.

A "high basis weight streak" is defined in terms of bulk and caliper. A heavy

TABLE 4.11: Conditions in a calender for a thick streak in a thin sheet.

	Heavy spot (55 g/m^2) (Figures 4.14a, 4.15a)			Light spot (45 g/m^2) (Figures 4.14a, 4.15a)		
	Bulk	Caliper	Strain	Bulk	Caliper	Strain
Initial	2.40	132	--	2.40	108	--
In-nip	1.08	60	0.55	1.33	60	0.45
Final	1.92	106	0.20	2.21	99	0.09
	Heavy spot (60 g/m^2) (Figures 4.14b, 4.15b)			Light spot (30 g/m^2) (Figures 4.14b, 4.15b)		
	Bulk	Caliper	Strain	Bulk	Caliper	Strain
Initial	3.00	180	--	3.00	90	--
In-nip	1.00	60	0.67	2.00	60	0.33
Final	1.80	108	0.39	2.76	83	0.07

streak can thus be made up of a taller stack of identical fibres, as above, or it can consist of an equally thick stack of denser fibres. The case of a dense streak is illustrated in Table 4.12. When the sheet is compressed to 60 μm in the nip, both areas see the same strain (0.50) since the initial thicknesses were the same. The heavy spot now sees less permanent strain and is thus still thicker than the surrounding area after calendering.

For this particular type of TMP pulp, then, a heavy streak may see more strain, which is a relative measure of deformation, but in absolute terms will always be as thick or thicker than a surrounding lightweight area. In the most likely case, where the same type of fibre is deposited in a thicker stack due to variations at the headbox, the heavy spot sees greater permanent strain, but this is not enough to make it thinner than the surrounding, lighter area.

TABLE 4.12: Conditions in a calender for a dense streak.

	Heavy spot (55 g/m^2)			Light spot (45 g/m^2)		
	Bulk	Caliper	Strain	Bulk	Caliper	Strain
Initial	2.18	120	--	2.67	120	--
In-nip	1.09	60	0.50	1.34	60	0.50
Final	1.96	108	0.10	1.65	74	0.38
	Heavy spot (60 g/m^2)			Light spot (30 g/m^2)		
	Bulk	Caliper	Strain	Bulk	Caliper	Strain
Initial	2.00	120	--	4.00	120	--
In-nip	1.00	60	0.50	2.00	60	0.50
Final	1.94	110	0.08	2.80	84	0.30

4.1.2 Master creep relationship

The summary data set extracted from the TMP raw data set as described in the previous section was also fitted to a modified version of the master creep equation proposed by Colley and Peel [17] for data obtained in a platen press:

$$\varepsilon_{n,p} = A \left[1 + \tanh \left(a_P \log_{10} P + a_t \log_{10} t + a_M M + a_\theta \theta + a_o \right) \right] \qquad [4.16]$$

where P is the maximum applied pressure in MPa, t the dwell time in seconds, M the sheet moisture content in percent, and θ the temperature in degrees Celsius. Kerekes [45] proposed a relationship between the coefficients of the variables P, t and L, V, R:

$$\begin{aligned} a_L &= a_P \\ a_S &= -a_t \\ a_R &= \frac{a_t - a_P}{2} \end{aligned} \qquad [4.17]$$

Values for a_L and a_S as computed from data of Colley and Peel [17] and

Table 4.13: Master creep coefficients, from Kerekes and Colley and Peel.

	Colley & Peel		Kerekes
	In-nip	Permanent	Permanent
A	0.33	0.33	--
a_L	1.090	0.900	0.890
a_S	-0.063	-0.130	-0.165
a_R predicted by Equation 4.17	-0.514	-0.385	-0.363

TABLE 4.14 In-nip coefficients, master creep equation, TMP (F.Soucy).

Parameter	Estimate	S.E.	Lower 95%	Upper 95%
$(\rho_n)_{max}$ (g/cm^3)	1.2807	0.0668	1.1471	1.4143
a_{on}	-1.4197	0.1043	-1.6248	-1.2147
a_{Ln}	1.0076	0.0659	0.9344	1.1937
a_{Rn}	-0.4340	0.0905	-0.6120	-0.2560
a_{Sn}	-0.0976	0.0286	-0.1536	-0.0417
r^2	0.87			
S.E., cm^3/g	0.116			

measured by Kerekes [44, 46] are given in Table 4.13.

Haglund and Robertson [34] proposed that since A(1 + tanh x) is asymptotic to 2A for large x, there should be a relationship between A and the maximum density obtainable either in the nip, $(\rho_n)_{max}$, or after, $(\rho_p)_{max}$. In the current study, Equation 4.16 was modified by substituting Kerekes' relationship, Equation 4.17, and Haglund and Robertson's relationship for limiting densities:

$$\varepsilon_{n,p} = \frac{1}{2}\left(1 - \frac{\rho_i}{\rho_{max}}\right)_{n,p} (1 + \tanh \mu_{n,p}) \qquad [4.18]$$

where the nip intensity factors μ_n, μ_p are defined as for the calendering equation.

Curve fitting results were obtained for the TMP data using SYSTAT as described earlier for the calendering equation, with the limitation on initial bulk just given, and are listed in Tables 4.14 and 4.15.

TABLE 4.15: Permanent coefficients, master creep equation, TMP (F. Soucy).

Parameter	Estimate	S.E.	Lower 95%	Upper 95%
(ρ_p)max (g/cm^3)	0.5930	0.0074	0.5784	0.6077
a_{op}	-3.1502	0.2553	-3.6524	-2.6481
a_{Lp}	1.8863	0.3339	1.6876	2.0850
a_{Rp}	-0.8294	0.1932	-1.2095	-0.4490
a_{Sp}	-0.2729	0.0541	-0.3792	-0.1665
r^2	0.88			
S.E., cm^3/g	0.107			

Since SYSTAT lacks a built-in hyperbolic function, the exponential definition was used:

$$\tanh \mu = \frac{e^{\mu} - e^{-\mu}}{e^{\mu} + e^{-\mu}} \qquad [4.19]$$

Figures 4.16 to 4.19 show typical TMP data with the master creep equation superimposed; it can be seen that the predicted strain curves are smoother than those predicted by the calendering equation, especially for permanent strains at low loads. This is due to the continuous nature of the function.

The limiting density in the nip is 1.28 g/cm^3, slightly more than Haglund and Robertson's value of 1.20 but less than the accepted value for the density of cellulose of 1.50 g/cm^3, which is presumably a limiting factor in compression. For a sheet with a certain number of large pores, the limiting density in the nip would be less than the density of fibre, so limiting values of 1.2 to 1.3 make sense.

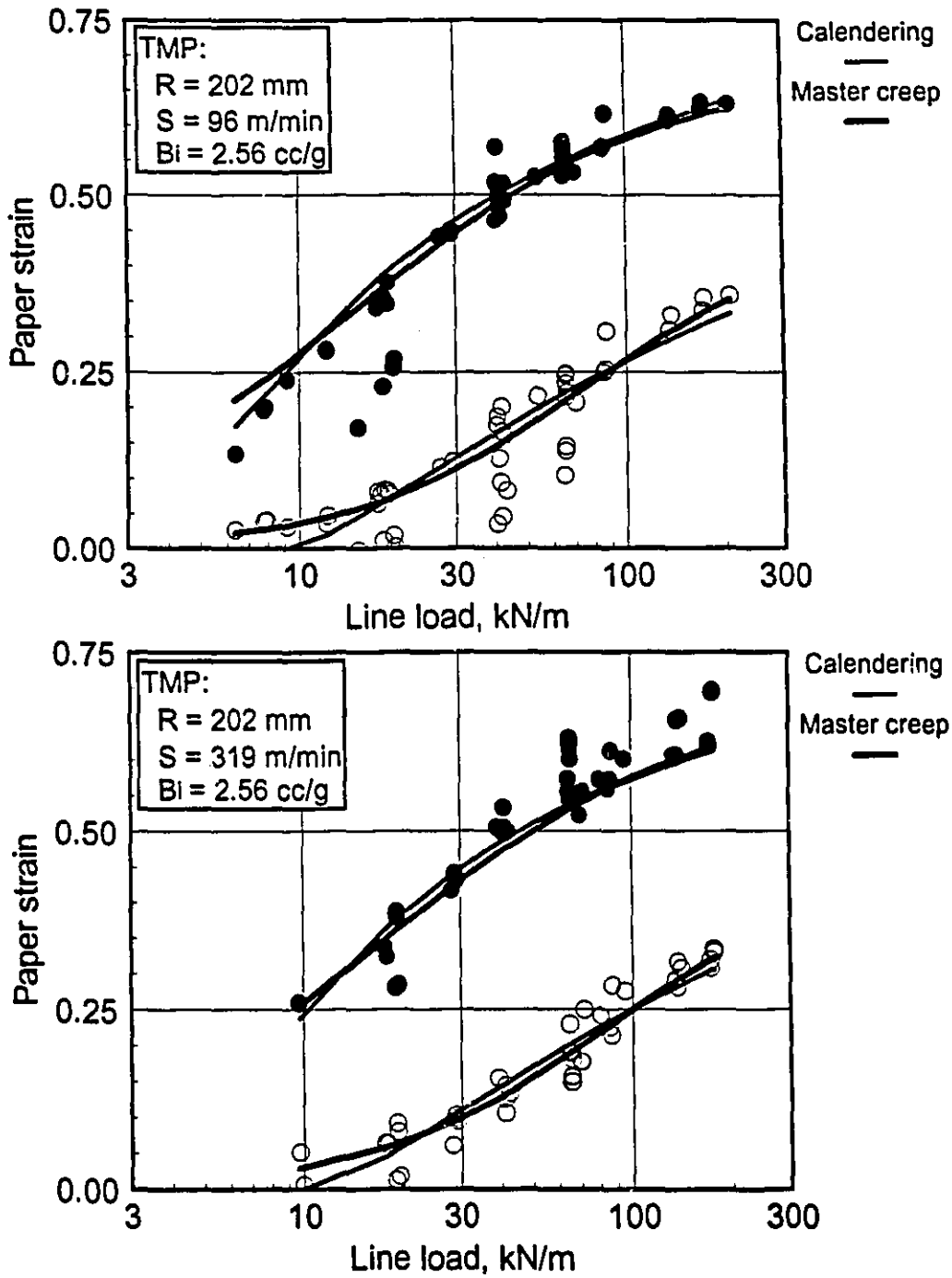

Figure 4.16 Strain vs. load, 202 mm, 2.56 cm^3/g, a) 96 m/min; b) 319 m/min

Curve fitting using the master creep equation.

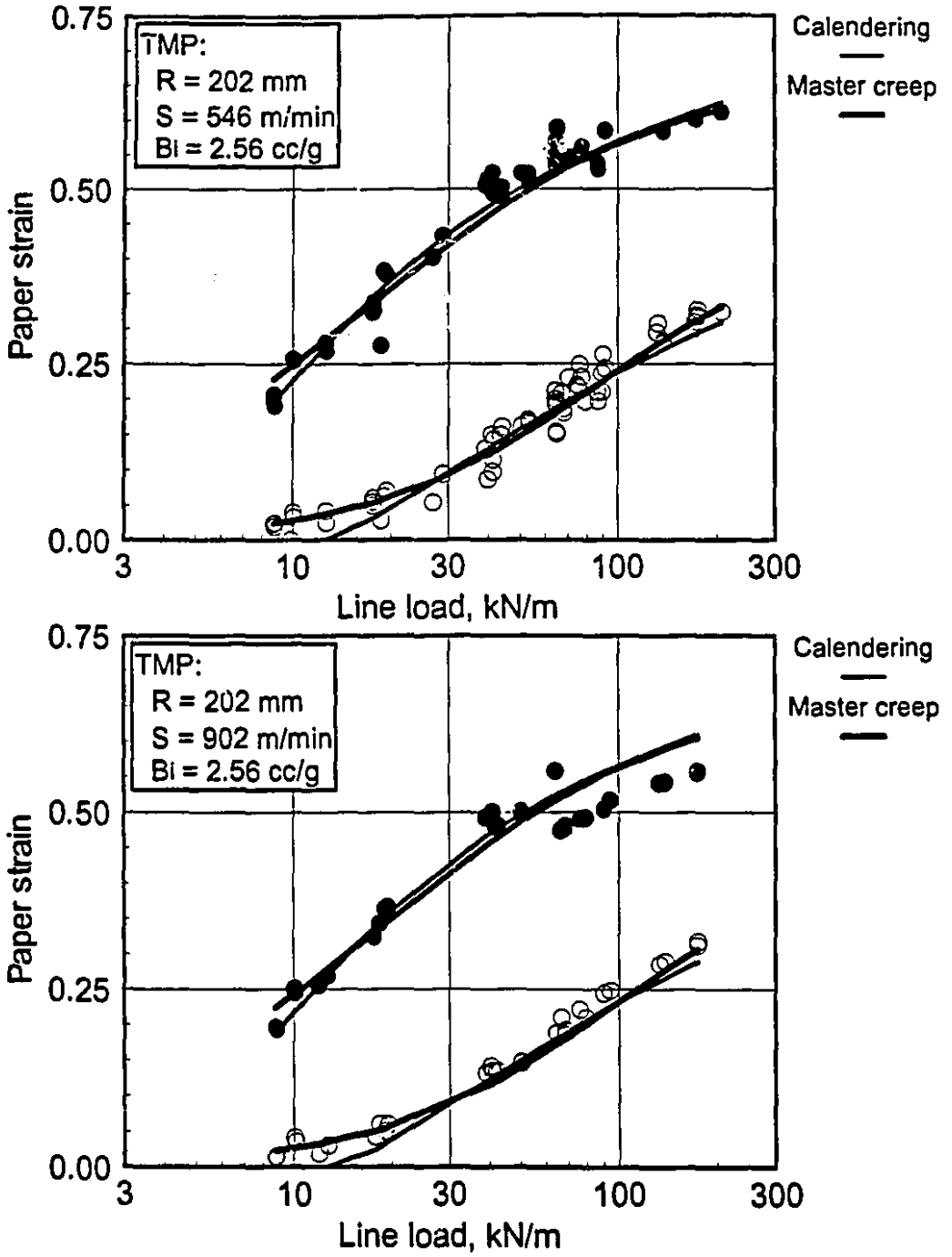

Figure 4.17 Strain vs. load, 202 mm, 2.56 cm^3/g: a) 546 m/min; b) 902 m/min.
Curve fitting using the master creep equation.

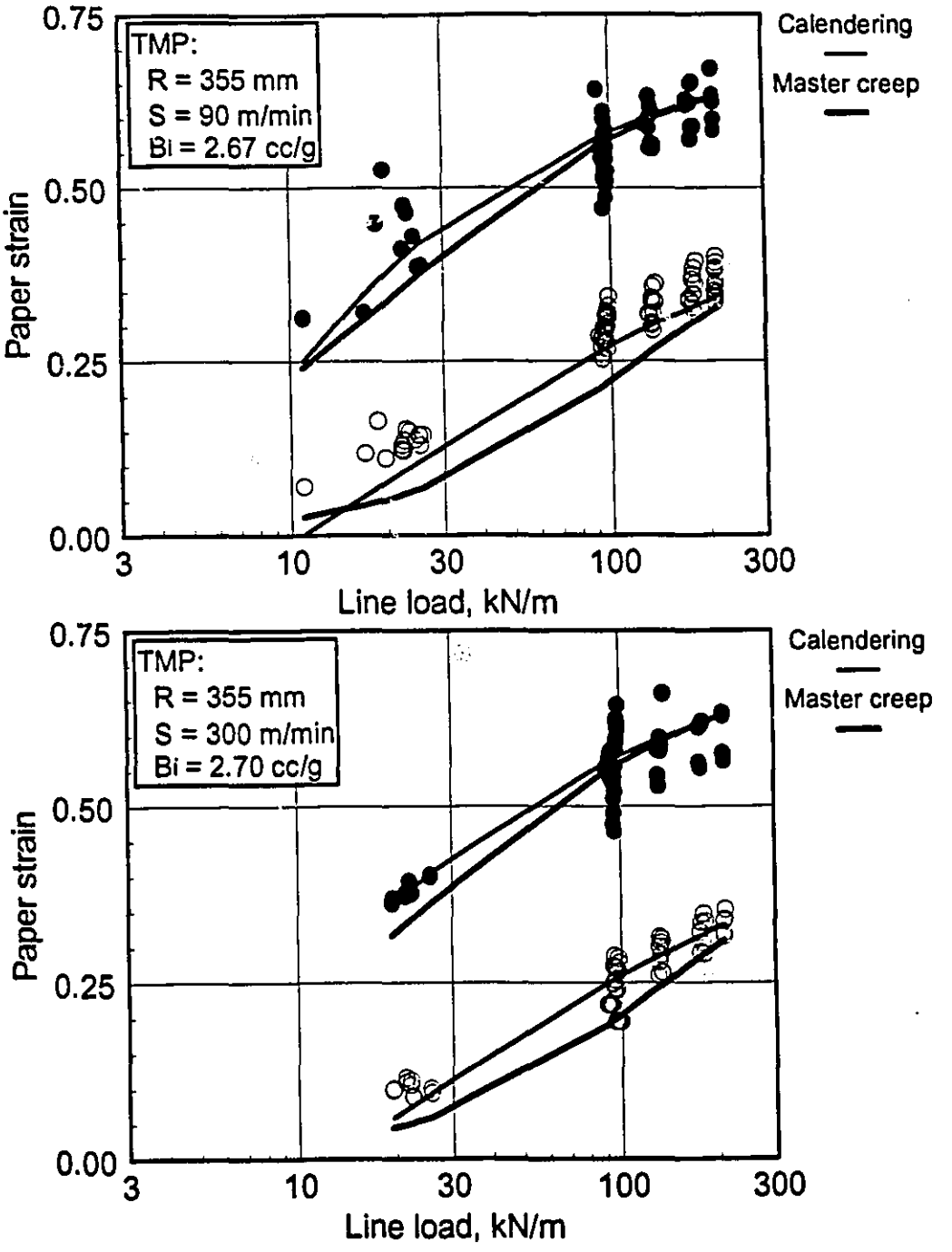

Figure 4.18 Strain vs. load, 355 mm, 2.68 cm^3/g, a) 90 m/min, b) 300 m/min

Curve fitting using the master creep equation.

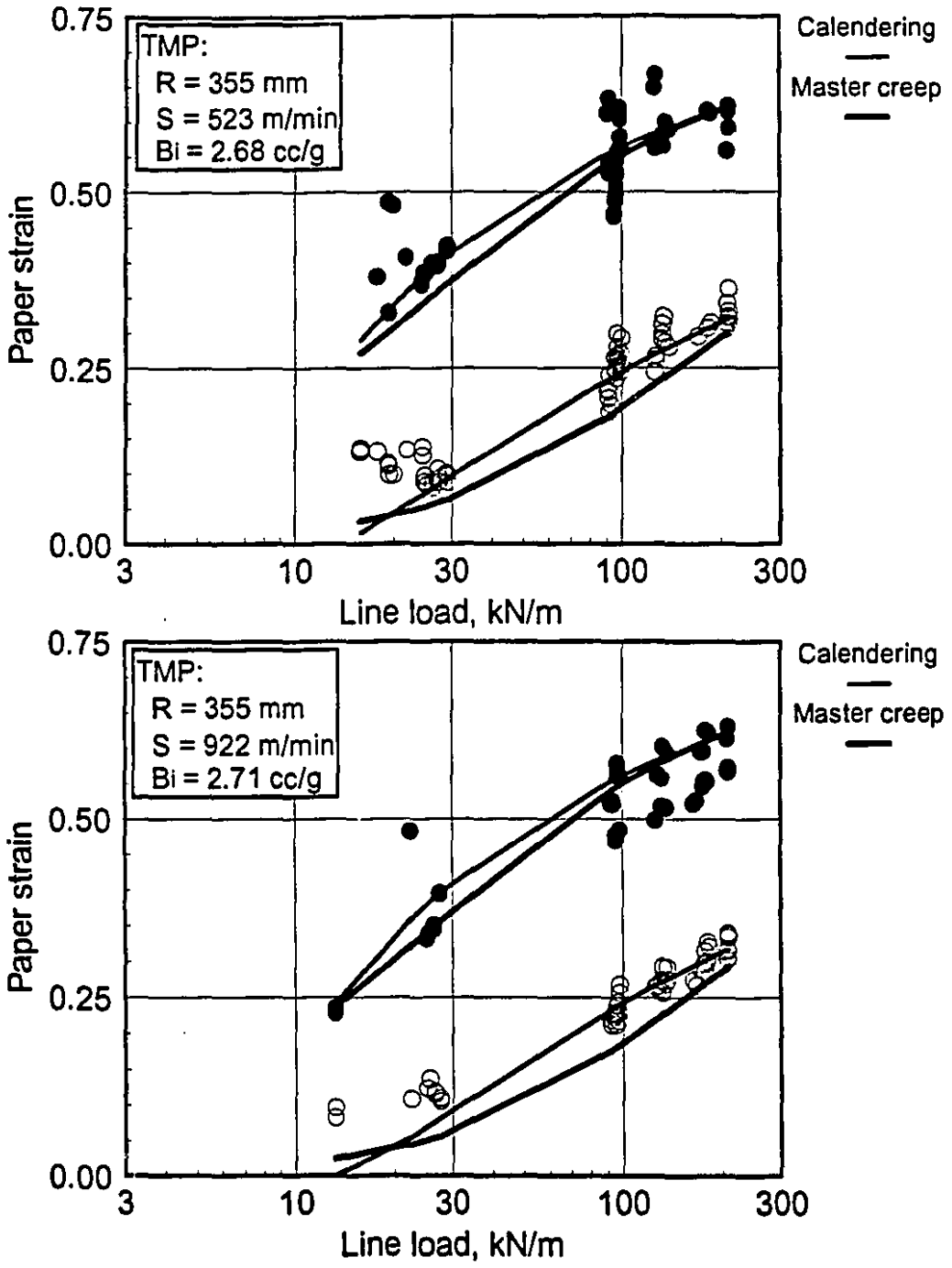

Figure 4.19 Strain vs. load, 355 mm, 2.69 cm^3/g: a) 523 m/min, b) 922 m/min
Curve fitting using the master creep equation.

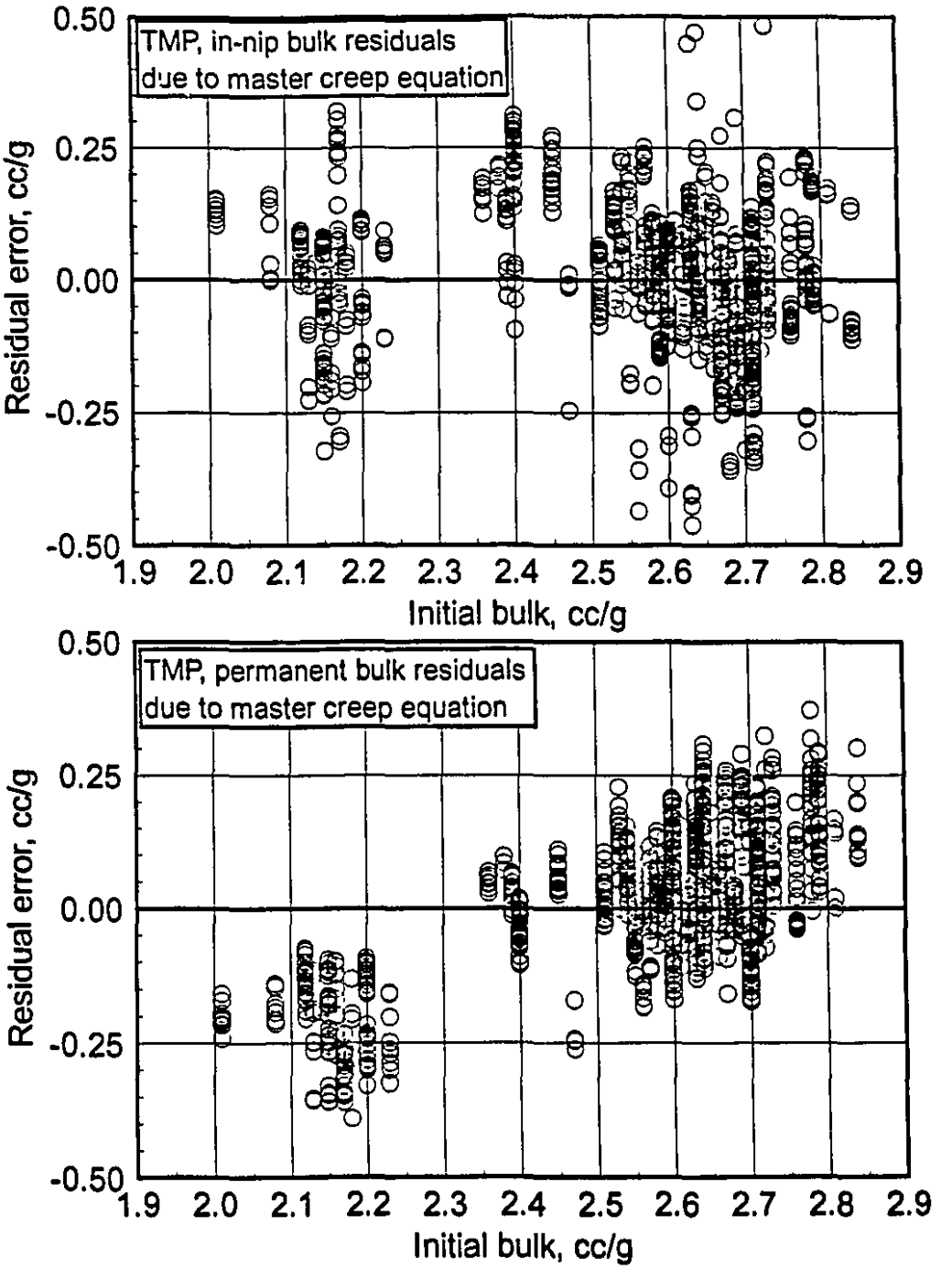

Figure 4.20 Bulk residuals vs. initial bulk, a) In-nip data,
b) Permanent data
Curve fitting using the master creep equation.

In the permanent case, the limiting density is 0.59 g/cm^3, corresponding to a minimum bulk of 1.70 cm^3/g. This is comfortably lower than the lowest bulk attained after two nips, which was 1.85 cm^3/g. After many more heavily loaded nips, a final bulk approaching 1.70 makes sense.

Residuals are plotted in Figure 4.20, where it can again be seen that the equation does not adequately predict the effect of initial bulk on permanent strain. Equation 4.18 predicts strain to be inversely proportional to the initial bulk where the calendering equation was linear with bulk; comparing with the permanent bulk residuals in Figure 4.8b it can be seen that where the calendering equation consistently predicts a lower permanent strain at low initial bulks, the master creep equation consistently predicts a higher strain.

Thus if strain is not a linear function of initial bulk, neither is it inversely proportional. There was insufficient data obtained in the present work to explore the relationship between initial bulk and strain any further.

Overall the fit of the master creep equation is similar to the calendering equation, with similar values of r^2 and RMS residuals. However, non-linear regression methods are necessary if a large range of nip intensities is to be investigated, and computational effort is greater than for the calendering equation. With these difficulties in mind, the continuous nature of the function, compared with the pieced-together nature of the calendering equation, make it an interesting alternative for industrial users wishing to investigate the effect of machine changes on paper caliper, especially at low nip intensities.

Comparing Table 4.14 with the in-nip data reported by Colley and Peel in Table 4.13, all coefficients are statistically similar. Comparing Equations 4.16 and 4.18, and using a typical initial bulk of 2.5 cm^3/g, the value of A can be estimated at 0.34, identical to Colley and Peel's.

In the permanent case, however, as illustrated in Table 4.15, there is no agreement between the current predictions and published work. This can be attributed to the value of A_p. Using Equations 4.16 and 4.18, with $B_i = 2.5$ as for the in-nip data,

TABLE 4.16: Permanent coefficients, master creep equation, $(\rho_p)_{max}$ = 1.28.

Parameter	Estimate	S.E.	Lower 95%	Upper 95%
(ρ_p)max (g/cm^3)	1.28	0.0 (fixed)	1.28	1.28
a_{op}	-2.4757	0.1461	-2.7631	-2.1883
a_{Lp}	1.0341	0.0440	0.9475	1.1207
a_{Rp}	-0.5395	0.1059	-0.7481	-0.3311
a_{Sp}	-0.1140	0.0315	-0.1759	-0.0518
r^2	0.76			
S.E., cm^3/g	0.137			

A_p is 0.16 compared in the current work compared with 0.33 previously; the low value of A_p here is then offset by higher values of the other coefficients. Effectively, previous work was based on the assumption that the limit is the same for both in-nip and permanent densities, at 1.20 to 1.30 g/cm^3. This implies that it is possible to press a sheet so hard that it doesn't recover at all. Further, the coefficients in Table 4.15 are not directly comparable to those in Table 4.13. In order to make a comparison, Equation 4.18 was fitted to the permanent data with $(\rho_p)_{max}$ fixed at 1.28 g/cm^3. The results are given in Table 4.16. Comparing these results with Table 4.13, it can be seen that the load coefficient is slightly higher, as it was for the calendering equation; the other coefficients are not different at the 95% level from Colley and Peel's data. Since the standard error and r^2 values are worse in Table 4.16, Table 4.15 contains the better fit, and the limiting density for permanent compression is substantially lower than the density of pure fibre.

4.2 Strain recovery after the nip

4.2.1 Strain recovery at short times after the nip

As mentioned in Section 3.1.1, the calender was equipped with modified industrial caliper gauges mounted 0.296 m and 1.050 m after the nip. Data from these gauges was frequently unuseable due to bounce of the floating head; however sufficient data was acquired at industrially relevant speeds to draw some useful conclusions.

Defining $\varepsilon_r(t)$ the partially recovered strain at a distance x after the nip, the recovery time t required for the sheet to cover a distance x is then x/V, where V is the sheet speed in m/s: V = S/60. Recovery times thus range from 20 to 200 ms for the first gauge at x = 0.296, and 60 to 600 ms for the second gauge at x = 1.050 m.

In general, the scatter in the strain data at x = 1.050 made it impossible to detect any statistically significant difference with those measured 24 hours after calendering. The first conclusion is therefore that within the accuracy of these online gauges, paper recovers from a calender pulse extremely quickly. As well, this was true even at higher speeds, when the recovery time was shorter. The recovery therefore occurs more quickly at higher speeds, implying the dwell time in the nip has an effect on the recovery time.

To quantify this statement, the strains measured in the nip, at x = 0.296 m and after 24 hours were used to estimate the recovery time constant τ for paper leaving a calender nip:

$$e^{-t/\tau} = \frac{\varepsilon_p - \varepsilon_r(t)}{\varepsilon_p - \varepsilon_e} \qquad [4.20]$$

where ε_e is the strain at the nip exit. This strain is unknown since it has not been measured, but must be in the range $\varepsilon_n < \varepsilon_e < \varepsilon_r(t=0.296/V)$. Since $\varepsilon_r(t=0.296/V)$ is still significantly greater than $\varepsilon_r(t=1.050/V)$, the time constant must be similar to 0.296/V, implying that ε_e is closer to ε_n than to $\varepsilon_r(t=0.296/V)$. Equation 4.20 was thus used to estimate τ using $\varepsilon_e = \varepsilon_n$.

The value of τ obtained using Equation 4.20 was not a constant for all conditions,

TABLE 4.17: Curve fitting constants for Equation 4.21.

m,	21.612
S.E.	1.655
n,	-1.100
S.E.	0.029
r^2	0.69

but was a strong function of sheet speed. Using the speed S in m/min, the time constant (in seconds) was found to fit Equation 4.21:

$$\tau = mS^n \qquad [4.21]$$

with values of m and n given in Table 4.17.

The possibility of a systematic error related to speed was considered and rejected. Errors occured when the floating gauge head, excited by small amplitude thickness changes in the moving sheet, ceased to contact the sheet due to bounce, or when paper dust or other material became lodged between the sheet and the head. The result of either of these errors was a false high thickness, causing a false low strain; the true strain $\varepsilon_r(t)$ (if either of these errors had occured) would thus be higher than the estimate used in Equations 4.20 and 4.21. Bounce did occur more frequently at higher speeds, but was immediately obvious from a plot of the sensor output signal versus time; these data points were discarded. Accumulated material in the gauge was also obvious since it caused a step change in the thickness reading from the sensor; compressed air was used to clean the head when this occured, and as a matter of routine after every few runs.

The time constant τ and the curve given by Equation 4.21 are plotted in Figure 4.21a, from which it can be seen that at industrially relevant speeds the time constant approaches a value in the vicinity of 10 ms.

It will be seen in Chapter 5 that the ingoing nip half-length a (the distance from the point of first contact between paper and roll to the nip centre line) depends on the in-nip strain ε_n, roll radius R and initial sheet half-thickness z_i:

$$a = \sqrt{2\varepsilon_n R z_i} \qquad [4.22]$$

The nip dwell time can thus characterized by the ingoing dwell time a/V, which

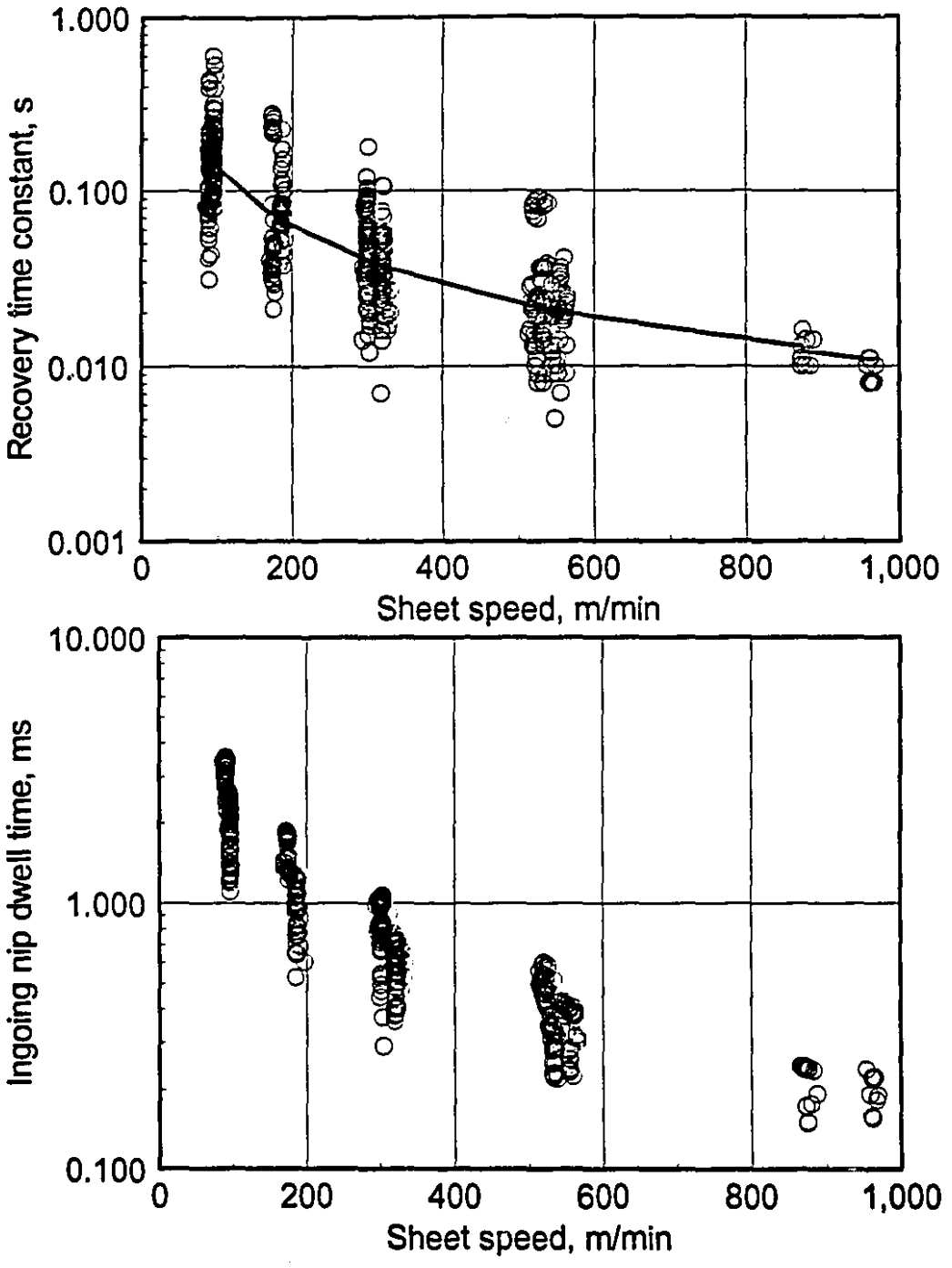

Figure 4.21 a) Strain recovery time constant τ, computed using Equation 4.21
b) Ingoing nip dwell time a/V, computed using Equation 4.22.

becomes a sensible choice for normalizing the strain recovery time t. While load does not appear explicitly in Equation 4.22, its effect is present in the form of the measured in-nip strain ε_n. As seen in Figure 4.21b, typical values of a/V at industrially relevant speeds are in the range 0.100 to 0.300 ms.

In Chapter 5 it will also be seen that if the ingoing sheet thickness is small compared to the roll radius, the strain while the paper is in contact with the roll surface is parabolic:

$$\varepsilon(t) = \varepsilon_n \left(\frac{Vt}{a}\right)\left(2 - \frac{Vt}{a}\right) \qquad [4.23]$$

Paper strain is thus zero when $Vt/a = 0$ at the nip entrance, and again (for an elastic material) when $Vt/a = 2$. Paper is not elastic, and so contact with the roll ends somewhere in the range $1 \leq Vt/a \leq 2$. Analogous to the ingoing half-length a is the outgoing half-length b, which is equal to a for an elastic material, and must be in the range 0 to b_{max} for paper:

$$\begin{aligned} b_{max} &= \sqrt{2Rz_i(\varepsilon_n - \varepsilon_p)} \\ &= a\sqrt{1 - \frac{\varepsilon_p}{\varepsilon_n}} \end{aligned} \qquad [4.24]$$

where b_{max} is the outgoing half-length if paper recovers immediately to its final thickness.

Figures 4.22 and 4.23 show the parabola defined by Equation 4.23, along with typical recovery strain data and strain recovery curves predicted using τ from Equation 4.21 substituted into Equation 4.20. The curves have been plotted in terms of normalized strain $\varepsilon/\varepsilon_n$ as a function of normalized time Vt/a.

Equation 4.20 with $\varepsilon_e = \varepsilon_n$ predicts the paper ceases to contact the roll surface almost immediately after passing the nip centerline; in effect, b tends to zero. This appears to be contradicted by at least two published articles.

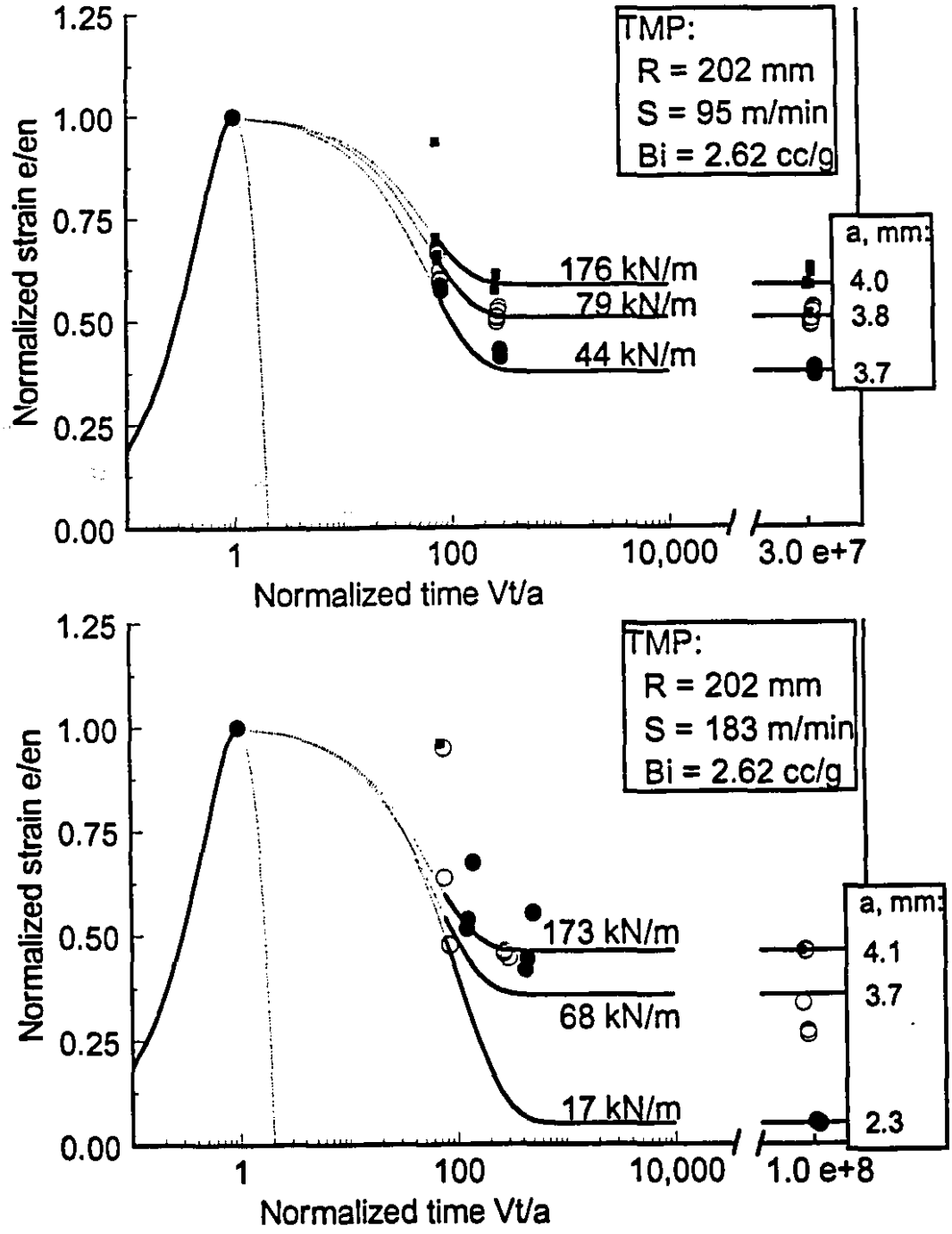

Figure 4.22 Strain recovery, 202 mm, 2.61 cm^3/g: a) 95 m/min (τ = 145 ms), b) 183 m/min (τ = 70 ms).

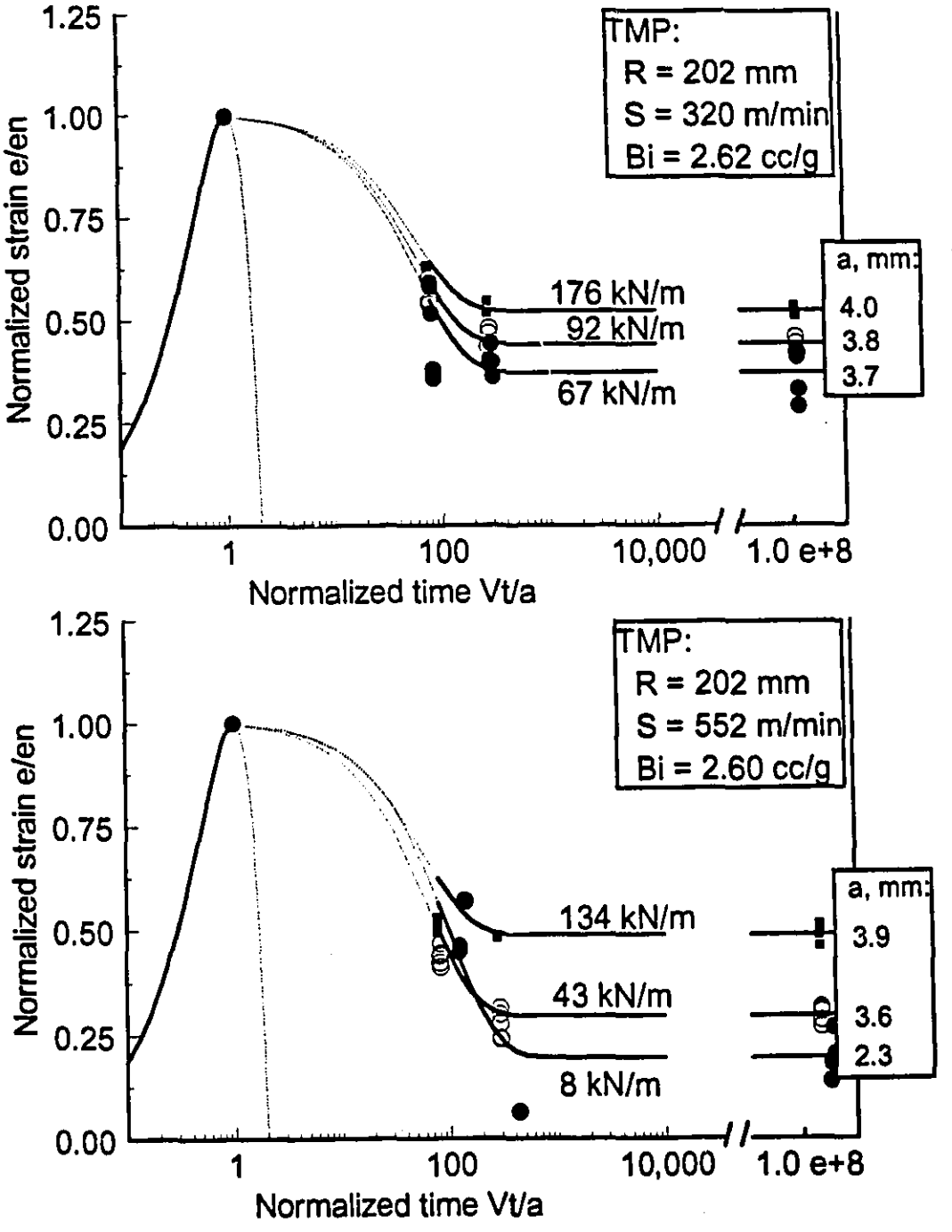

Figure 4.23 Strain recovery, 202 mm, 2.61 cm^3/g: a) 320 m/min (τ = 38 ms), b) 552 m/min (τ = 21 ms).

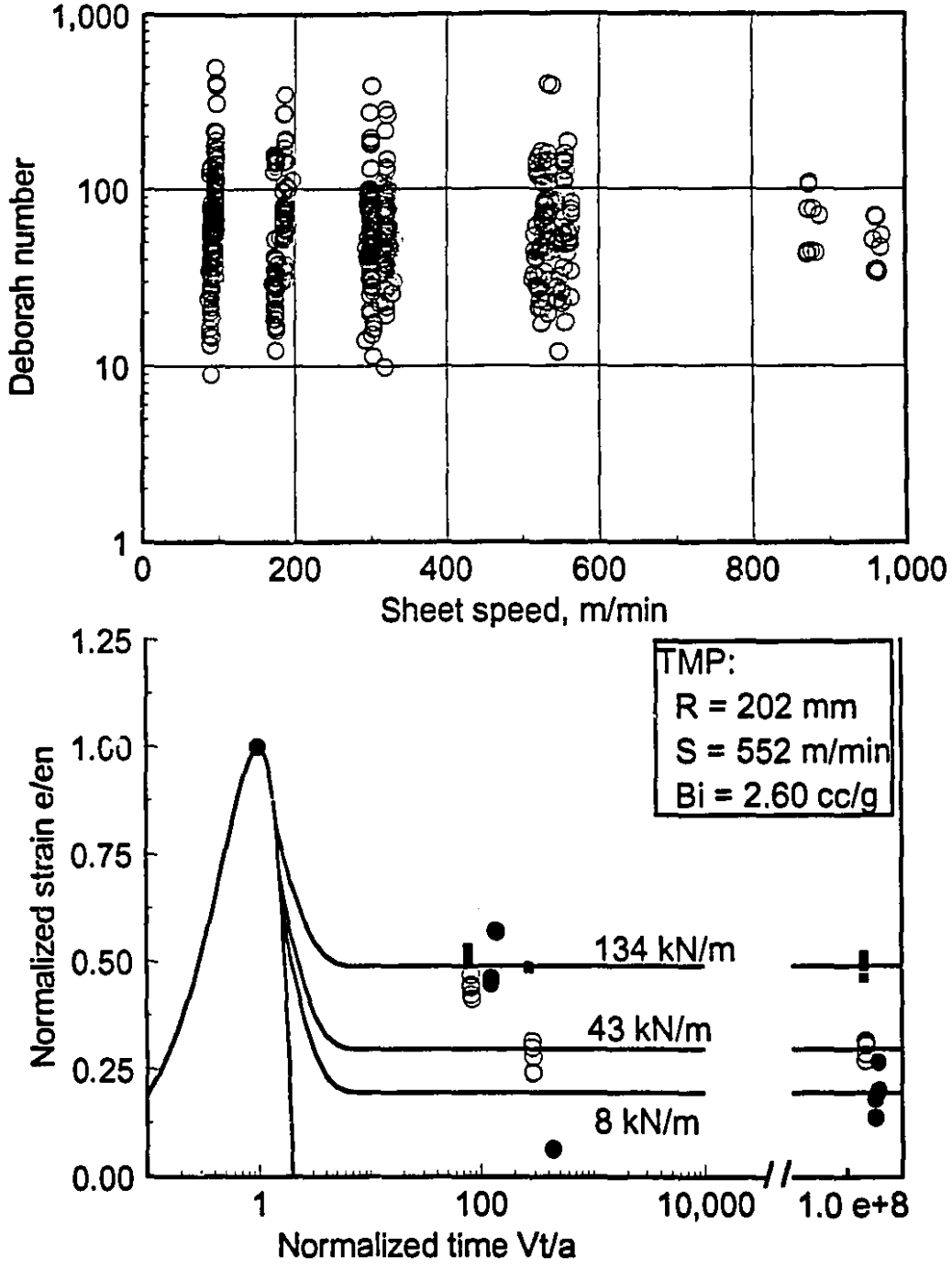

Figure 4.24 a) Deborah number $\xi = V\tau/a$;
b) Strain recovery for a material with $\xi = 1$.

Keller [43] has published graphs of pressure vs. MD distance in the nip which clearly show paper remaining in contact with the roll surface for a substantial portion of the range $1 \leq Vt/a \leq 2$; b is smaller than but of similar magnitude to a. The roll radius, sheet speed and nip load are all similar to the results presented here. However, one of the rolls in Keller's work was soft, with an elastic cover, which tends to keep the sheet in contact with the hard roll; the apparent large value of b is due to instantaneous elastic recovery of the roll surface, not viscoelastic recovery of the paper.

Watanabe et al. [80] measured paper strain at several points in the nip of a small bench scale printing tester; their results also show a significant b. However, reported nip dwell times are long, with $a/V \approx 5$ ms, and they estimate the recovery time τ at about 2.5 ms. From these numbers, the Deborah number for their conditions is about 0.5, compared with typical values of 30 to 100 found in the present work, cf. Figure 4.24a. As pointed out in Section 2.2, viscoelastic behaviour may be obtained with a sheet speed $V \approx a/\tau$, equivalent to a Deborah number of about 1. Under these conditions the strain recovery would appear as in Figure 4.24b, where it can be seen that the value of b is now significantly larger than zero. Thus the large values of b which can be deduced from their work are not inconsistent with the essentially negligible value reported here.

4.2.2 Recoverable strain at long times after the nip

Recoverable strain is defined as the difference between in-nip and permanent strain, and is the amount of strain which is recovered when a load is removed:

$$\varepsilon_R = \varepsilon_n - \varepsilon_p \qquad [4.25]$$

Figures 4.25 to 4.28 illustrate the recoverable strain ε_R computed from measured values of ε_n and ε_p (given by filled squares) and from the calendering equation estimates for ε_n and ε_p presented in Tables 4.5 and 4.6 (solid line). The calendering equation estimates were obtained using the full equations, including the limits as described by Equations 4.4, 4.5, 4.6 and 4.7. In-nip and permanent strains are also plotted for comparison.

At low loads behaviour is essentially elastic; the permanent strain becomes very small and virtually all the in-nip strain is recoverable. At moderate loads, the permanent strain begins to increase, but the recoverable strain remains essentially constant, possibly decreasing slightly at higher loads.

In order to quantify the possibility of a decreasing ε_R at high loads, the recoverable strain data was fitted to a pair of line segments. The first segment, at loads less than some limiting load L_{lim}, has a steep positive slope and a zero intercept; the second segment has a small, possibly negative slope and an intercept of about 0.35:

$$\begin{aligned} \varepsilon_R &= m_1 L \qquad \textit{when} \quad L < L_{lim} \\ &= m_2 L + \varepsilon_o \qquad \textit{when} \quad L \geq L_{lim} \end{aligned} \qquad [4.26]$$

Since iterative methods were necessary to locate the unknown intersection L_{lim}, and since the small magnitude of m_2 caused instability in the numerical methods, Equation 4.26 was rewritten in a more robust form, with the slope m_2 defined explicitly:

TABLE 4.18: Parameters for recoverable strain ε_R as given by Equation 4.26.

Parameter	Estimate	Lower 95%	Upper 95%
m_1, m/kN	0.0152	0.0140	0.0164
L_{lim}, kN/m	20.00	19.94	20.06
ε_o	0.3461	0.3320	0.3603
ε_∞	0.3007	0.2886	0.3129
$m_1 L_{lim}$	0.3040	0.2687	0.3290
m_2, m/kN	-0.000216	-0.000341	-0.000091
r^2	0.241		

$$m_2 = \frac{\varepsilon_\infty - \varepsilon_o}{L_\infty} \qquad [4.27]$$

where L_∞ = 210 kN/m is the largest load obtained and ε_∞, the recoverable strain at a load L_∞, is the parameter controlling the slope. The parameters are thus m_1, L_{lim}, ε_o and ε_∞, from which m_2 can be calculated; estimates of the parameters are given in Table 4.18.

While the value of r^2 is poor, due to the scatter inherent in subtracting two quantities which themselves are subject to substantial scatter, the 95% confidence intervals for all the parameters exclude the possibility of a value of zero. The root mean square of the residual strain error computed using Equations 4.26 and 4.27 is 0.060, compared with the value of 0.044 computed when the measured data is compared to the difference between the calendering equation predictions. Thus the value of Equation 4.26 is in the predictions of the slope m_1 and the maximum recoverable strain $m_1 L_{lim}$; the

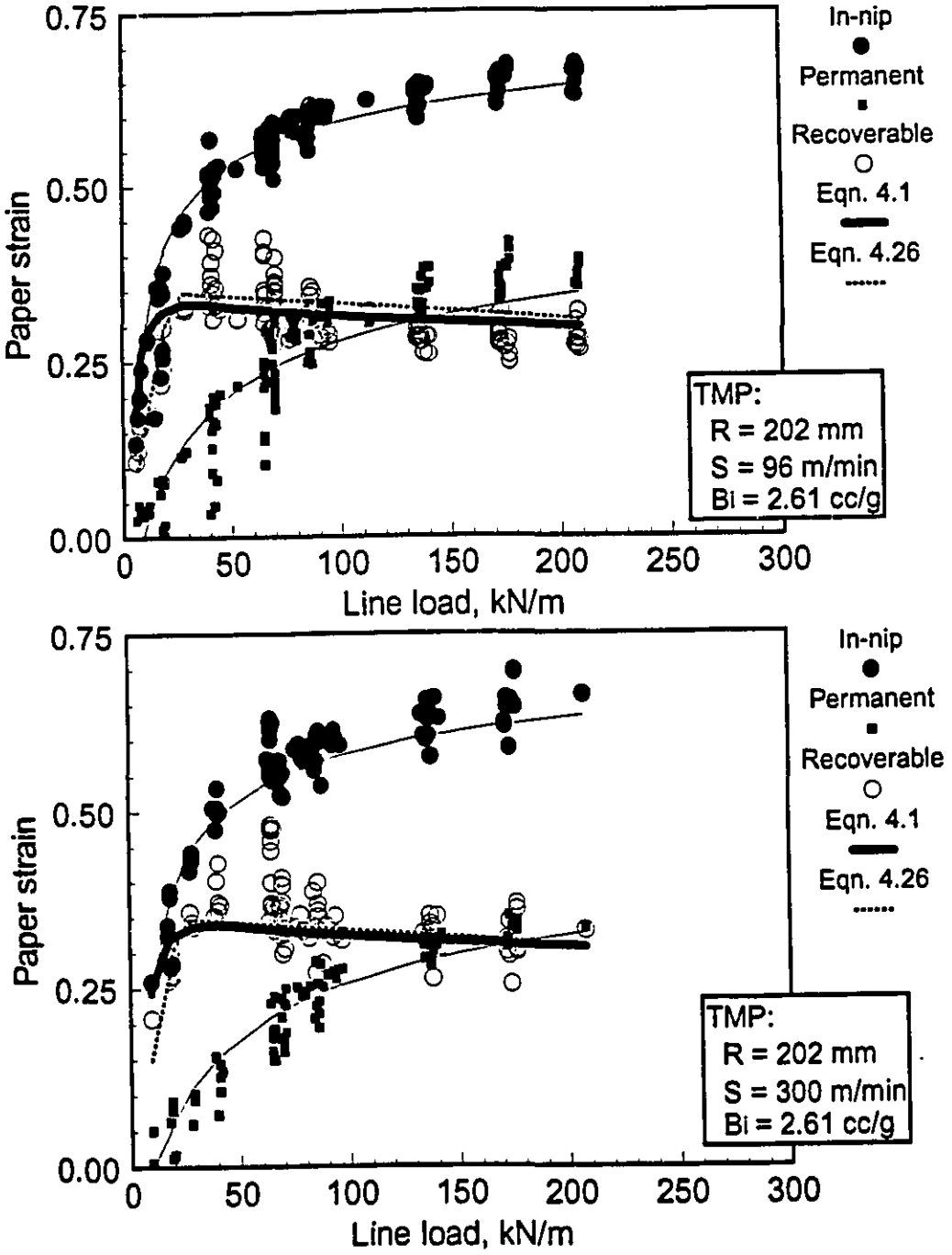

Figure 4.25 Recoverable strain ε_n-ε_p, 202 mm, 2.62 cm^3/g: a) 96 m/min, b) 316 m/min.

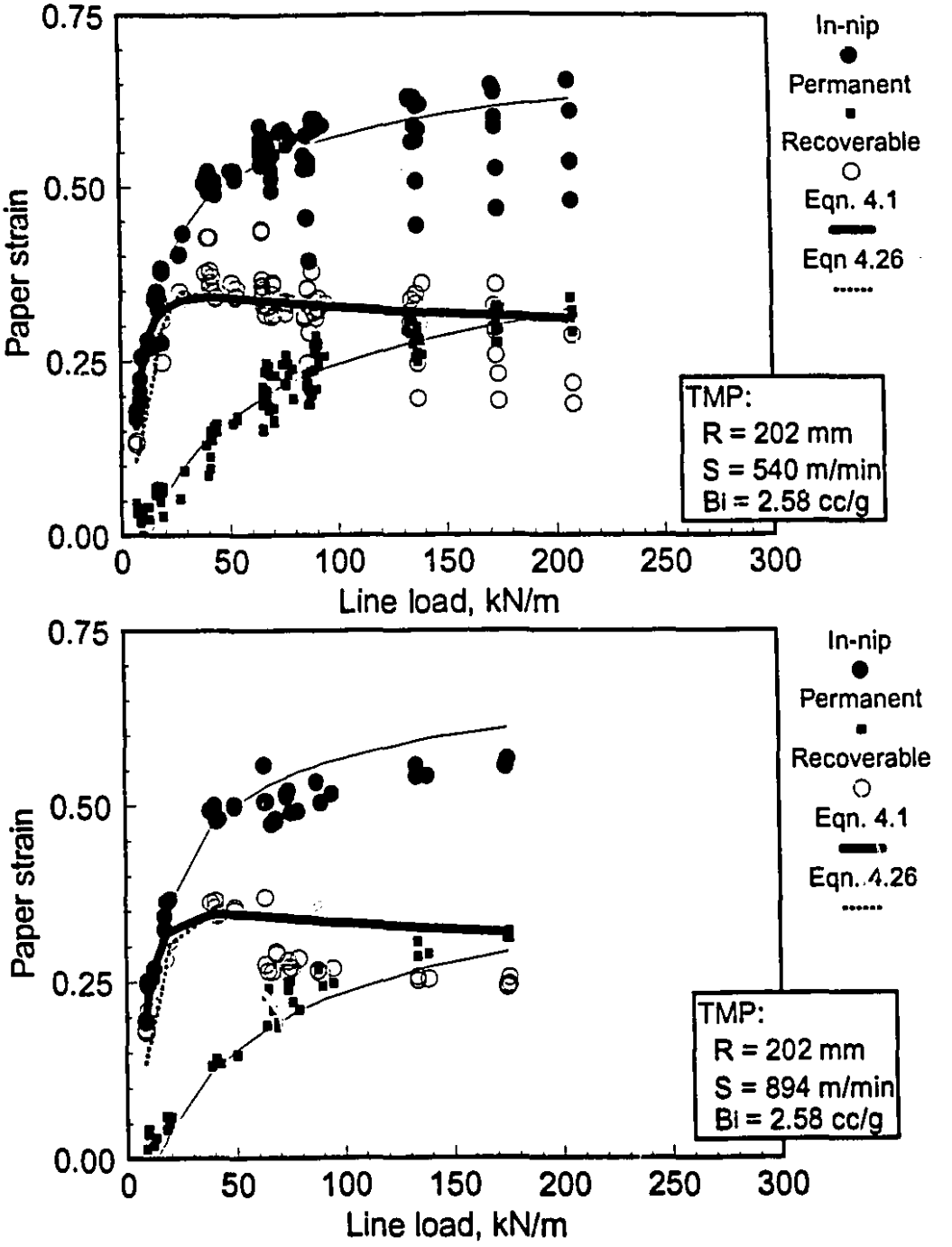

Figure 4.26 Recoverable strain ε_n-ε_p, 202 mm, 2.61 cm^3/g: a) 542 m/min, b) 881 m/min.

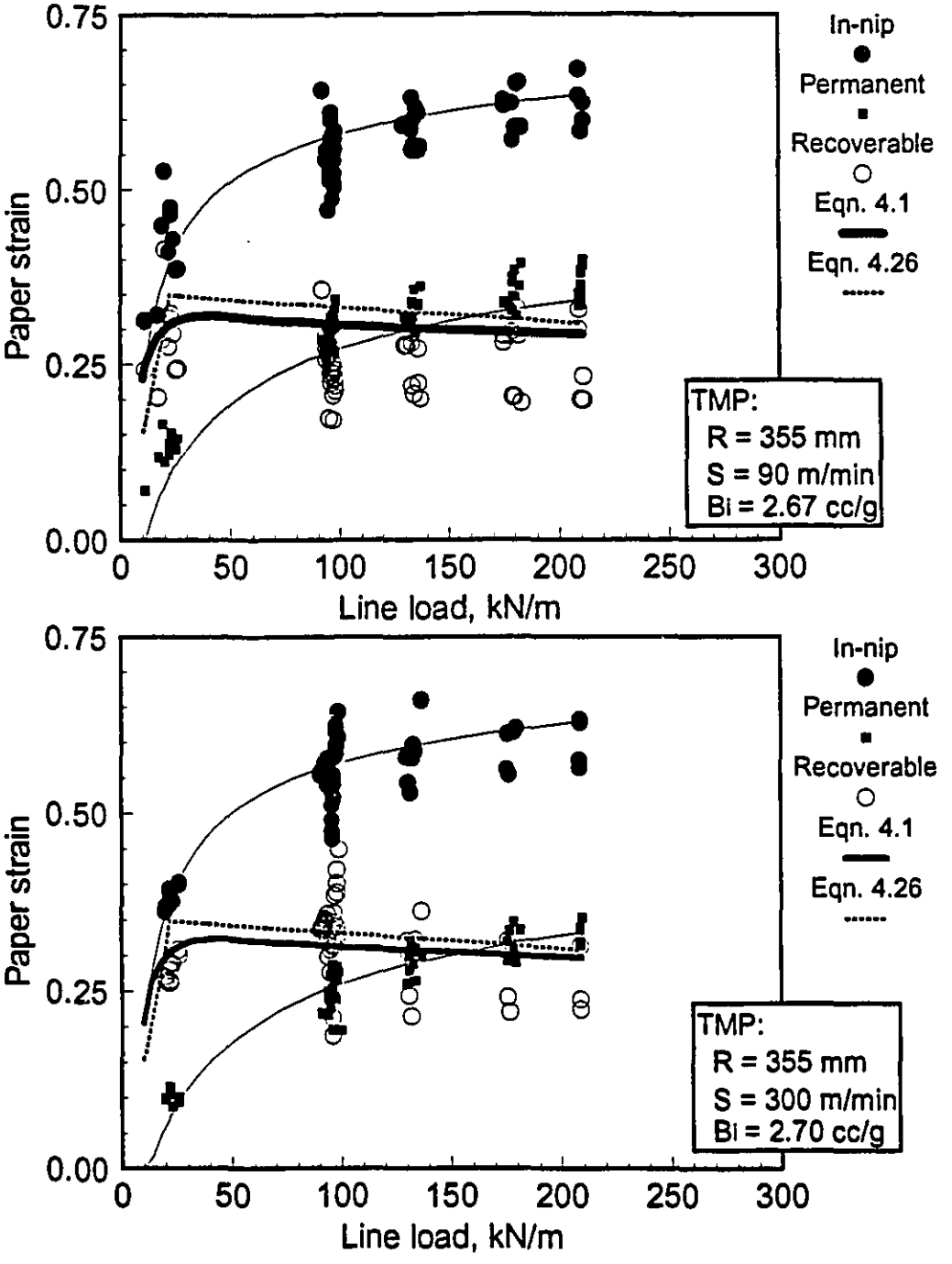

Figure 4.27 Recoverable strain ε_n-ε_p, 355 mm, 2.65 cm^3/g: a) 90 m/min, b) 301 m/min.

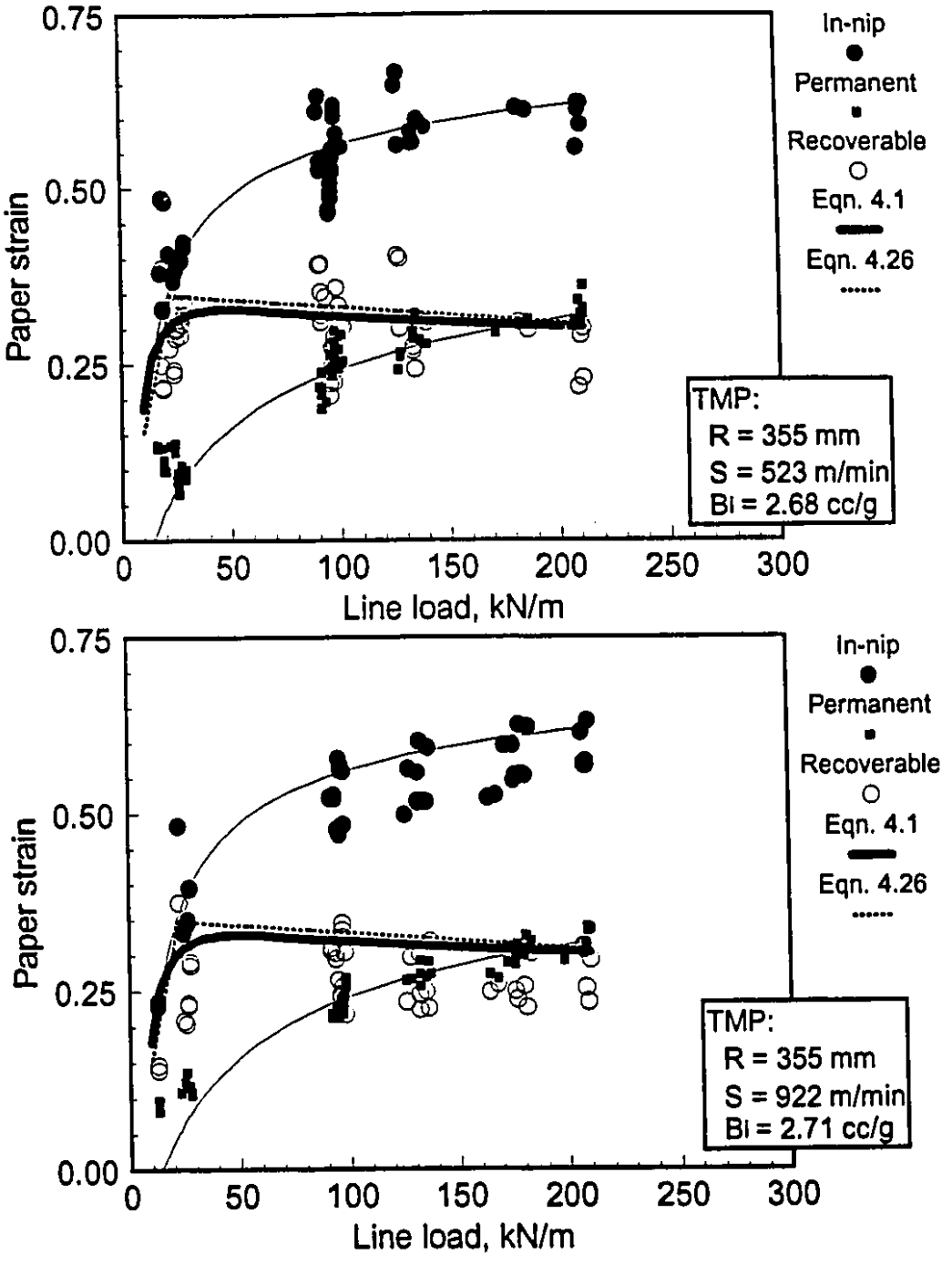

Figure 4.28 Recoverable strain ε_n-ε_p, 355 mm, 2.65 cm^3/g: a) 523 m/min, b) 923 m/min.

calendering equations provide an adequate description of recoverable strain as long as the calendering limits are respected.

The shape of the recoverable strain curves suggests that there are two stages to paper compression in a calender nip. At low loads, the strain is essentially elastic (whether instantaneous or time-delayed); an apparent modulus may be obtained from the slope m_1, which predicts 0.66 kN/m per 0.01 strain. Recalling $(a + b) \approx a$ from Section 4.3.1, an average nip length a for loads $L < L_{lim}$ was estimated at 3.121 mm. Converting line load to average nip pressure using this nip length gives an apparent elastic modulus of about 22 MPa for loads up to a few megapascals. This value is only approximate since it is based on four assumptions, first that the elastic recovery is instantaneous rather than time-delayed, that the parabolic stress profile in the nip can be approximated with a single average value L/a, that $b \approx 0$, and that the load vs. recoverable strain is indeed a straight line up to 20 kN/m. However, it is similar to the value of 39 MPa obtained by Mann et al. [54] for a different furnish; the similarity is improved when their statement that their methods tend to overestimate moduli by about 25%, and the probable curvature of the load vs. strain curve at very low loads are taken into account.

At higher loads, permanent deformation becomes substantial, but the recoverable strain remains essentially constant, ranging from $0.269 < m_1 L_{lim} < 0.329$ at 20 kN/m to $0.289 < \varepsilon_\infty < 0.313$ at 210 kN/m.

It can thus be suggested that the recoverable behaviour at very low loads is due to fibres which are stressed to some point well below the yield point, while permanent strain is due to irreversible fibre deformation; the yield point is 20 kN/m, or about 7 MPa when $a = 3.121$ mm. In other words, the results imply that fibres behave elastically up to a point (with either instantaneous or time-delayed full recovery), while all further strain beyond the yield point is permanent.

4.2.3 Relationship between in-nip and permanent strain

Ionides et al. [38] have suggested, in the course of an analysis of paper compression based on a statistical description of fibre distribution in the plane of a sheet, that a simple linear relation might exist between ε_n and ε_p. They suggest a relationship of the form

$$\varepsilon_n = c + m\varepsilon_p \qquad [4.28]$$

Using published data obtained with a platen press, they predict m = 0.75 for the approximate range $0.2 < \varepsilon_p < 0.4$.

Using all TMP data with initial bulk greater than 2.50 cm^3/g, data in the range $0.2 < \varepsilon_p < 0.4$ was fitted to Equation 4.28. Data for the entire range of permanent strains, also with $B_i > 2.50$ cm^3/g, was also fitted to Equation 4.28. The results of both fittings are given in Table 4.19, where it can be seen that all the coefficients are statistically non-zero. The subset $0.2 < \varepsilon_p < 0.4$ generated m = 0.67, statistically smaller than 0.75; however the full set generated m = 0.93, implying that moving the cutoff point from $\varepsilon_p = 0.2$ to $\varepsilon_p \approx 0.15$ would generate $m \approx 0.75$.

Both values of r^2 are poor, however, and in Figure 4.28 it can be seen that while it may be possible to fit a straight line to data in the range $0.2 < \varepsilon_p < 0.4$, a nonlinear relationship is necessary for the full range of strains investigated. Accordingly, a logarithmic fit was tried:

TABLE 4.19: Coefficients for Equation 4.28.

Range of ε_p:	m, S.E.	c, S.E.	r^2
$0.20 < \varepsilon_p < 0.40$	0.666, 0.032	0.392, 0.040	0.37 (712 data points)
$0.00 < \varepsilon_p < 0.45$	0.930, 0.020	0.319, 0.056	0.69 (1000 data points)

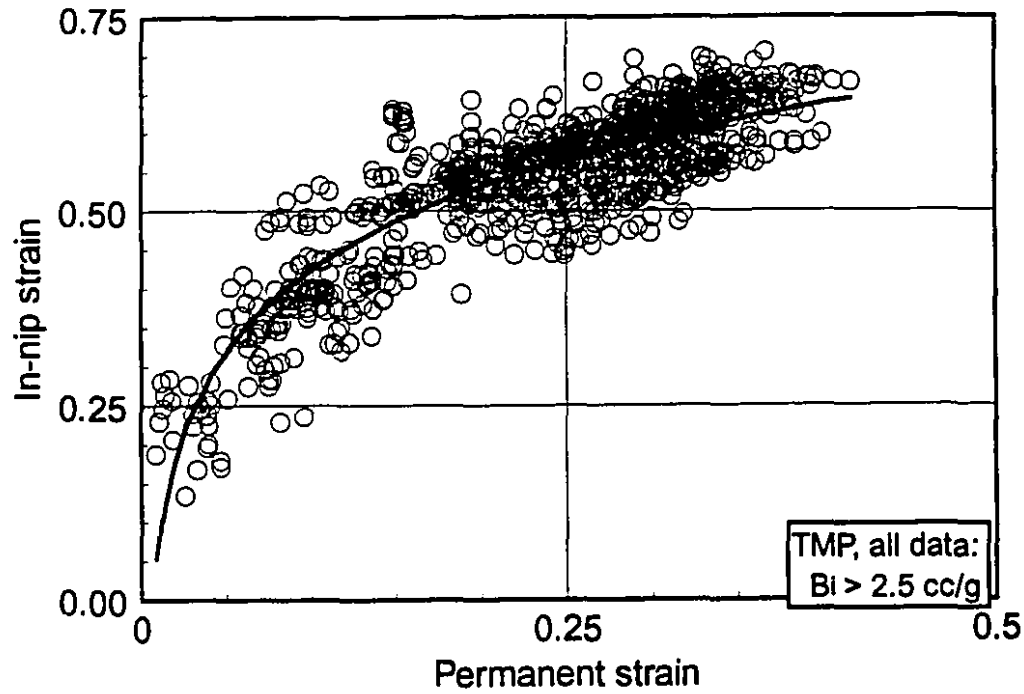

Figure 4.29 Relationship between ε_n and ε_p; curve fitting using Equation 4.29.

$$\varepsilon_n = c_0 + c_1 \log_{10} \varepsilon_p \qquad [4.29]$$

The coefficients defined in Equation 4.29 are given in Table 4.20 and the curve is plotted in Figure 4.29. The coefficients are all statistically non-zero, and the predicted curve passes (within 95% confidence limits) through the origin. If paper exhibits elastic behaviour at low loads (as suggested in Section 4.3.2), the in-nip strain at those low loads would be accompanied by a zero permanent strain, which the curve in Figure 4.29

TABLE 4.20: Coefficients for Equation 4.29.

c_0, S.E.	c_1, S.E.	r^2
0.778, 0.049	0.354, 0.007	0.74

predicts.

There is considerable scatter in the data, and the value of r^2 is low. The scatter is due in large measure to the effect of initial bulk. Strain data at low bulk fall below the curve in Figure 4.29; unfortunately there is insufficient data at low bulk to determine a statistically useful relationship. For the curve fitting, bulk ranged from 2.5 to 2.8 cm^3/g, a substantial variation. The coefficients are also likely to be furnish dependent.

Nonetheless, this relationship fulfills one of the goals of this research project, namely facilitating design of a complete cross-direction control system for paper strain leaving a calender. Once the bulk and furnish dependencies have been elucidated, the curve-fitting results or a graph similar to Figure 4.29 can be used to estimate the in-nip strain existing at a given CD position, from the permanent strain measured at that position. If a lower or higher permanent strain is required locally, the required new local in-nip strain can also be estimated. The difference between the current and required in-nip strains gives explicitly the local roll deformation which is required. With knowledge of the roll response to an actuator input, the energy required to effect the required change in permanent strain can be calculated.

4.3 Machine-direction extension of paper in a rolling nip

Extension of paper in a calender nip was measured as described in Section 3.1. Results are described next and plotted in Figure 4.30. Figure 4.30a shows the measured MD sheet speed increase, or tensile strain, in terms of the change in sheet tension before and after the nip. (Data acquired when the magnitude of the sheet tension change was greater than 20% were discarded). Average sheet tension for the data given here was 627 N/m on the unwind side, with a standard deviation of 65 N/m, and 566 N/m on the wind-up side with a standard deviation of 13 N/m. The lower variability in the wind-up tension was due to computer control on this side; unwind tension was under manual control. The average tension change through the nip was -9.7%.

Table 4.21: Curve fitting constants for Figure 4.30b.

Slope (% draw per 1000 kN/m) at 96 m/min	1.766
Standard error	0.335
Intercept	-0.025
Standard error	0.105
r^2	0.40

The speed increase was measured by counting pulses from two optical triggers over a set period of time. The resolution of the system corresponds to a strain of about 0.12%, which is the strain resulting from a difference of 1 in the number of pulses counted. An error of ± 1 count therefore results in a strain error of $\pm 0.24\%$, a large amount considering the small overall range of strains measured. Nonetheless, it can be seen that the MD strain does not exceed 0.5%, or 0.005 in absolute terms; average MD strain was 0.106%, with a standard deviation of 0.144%. Compared to *z*-direction permanent strains ranging up to 30%, these strains are extremely small.

Next, the effect of line load can be seen in Figure 4.30b, where data at constant speed, radius and bulk have been plotted in terms of line load. A straight line has been fitted to the data; the constants defining the line are given in Table 4.21. The slope is non-zero at the 95% confidence level, while the intercept is not significantly different

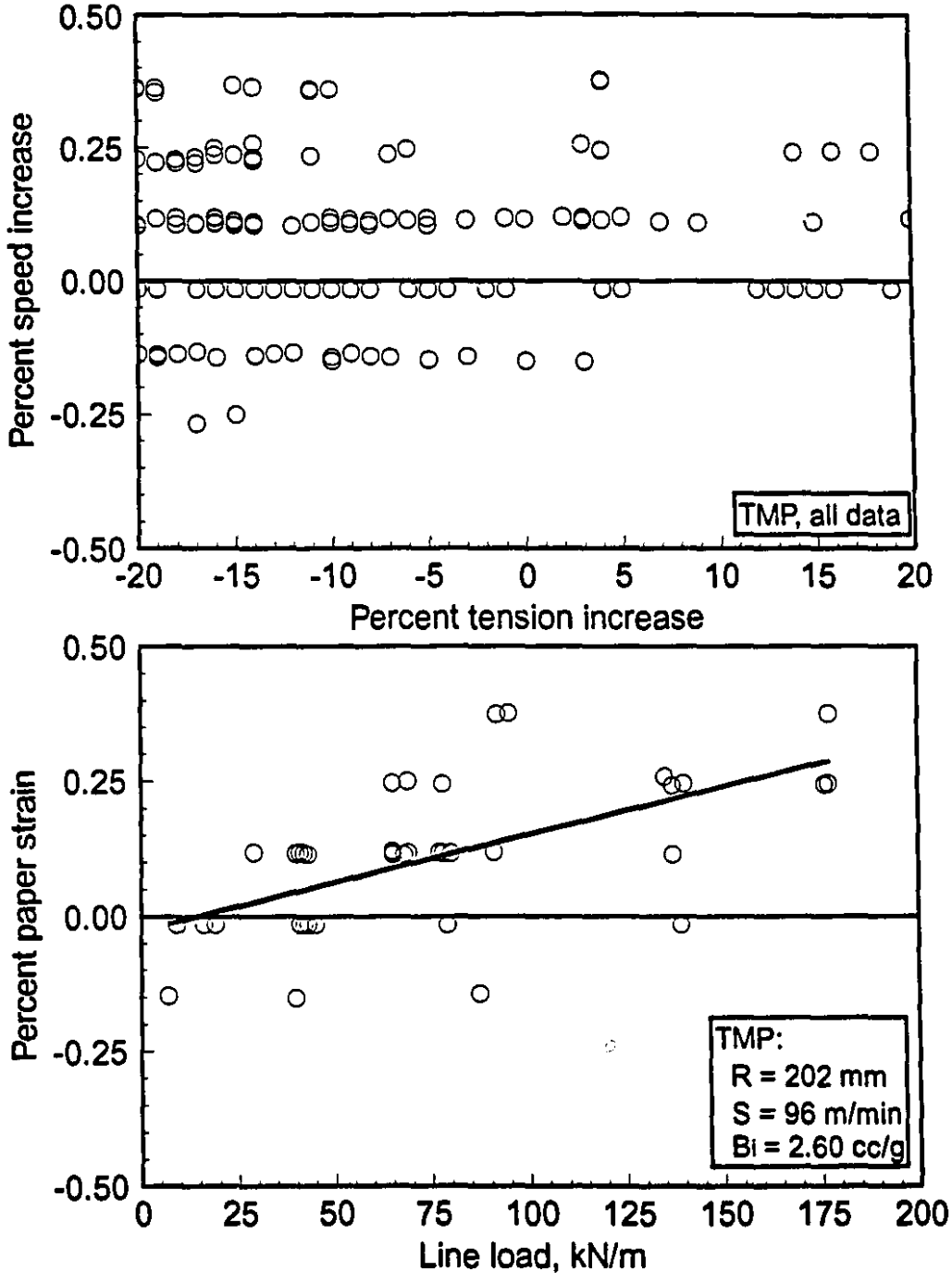

Figure 4.30 Machine direction strain, a) as a function of sheet tension change; b) as a function of line load.

from zero. The value of r^2 is low, reflecting large scatter in the data; however the zero intercept and positive slope are consistent with the expected behaviour of paper, i.e. that the strain vs. load curve should pass through the origin, and that paper will stretch as the compressive load is increased.

The small values of MD strains measured here are consistent with CD strain data published by Krenkel [47], Baumgarten [4], Gay et al. [29] and Mann et al. [54], and can be explained by considering the structured nature of paper. Since fibres are in contact at localized crossing points with large voids between them, there is ample space for the structure to deform in the *z*-direction before all the pores and gaps are filled. A typical fibre lying in the plane of the sheet may be a few millimetres long; as it enters the nip one end of that fibre is deflected downwards by only a few tens of microns. The fibre is bent more than it is stretched by this action, and there is very little in-plane stress imposed despite the large *z*-direction stresses. This is also confirmed by the Poisson's ratio measurements of Mann et al. [54]. Once the density of the sheet approaches that of individual fibres, further compression will result in greater MD and CD strains, as described by Gay et al. [29] and elaborated here.

Data at higher speed show smaller slopes with larger standard errors. This is partly due to the increasing scatter, and partly to the fact that at higher speed the paper is less highly stressed, leading to lower stretch. At industrial speeds, MD stretch becomes too small to measure using the equipment described here.

In conclusion, the quality of the MD strain measurements make it difficult to extract statistically meaningful results; however, it can be deduced that typical MD strains under industrial conditions are two orders of magnitude smaller than the corresponding *z*-direction strain, and that the MD strain increases with load and decreases with speed. This implies that compressive stresses applied at a point in a sheet dissipate quickly in the fibre network and are thus not felt by unstressed fibres at distances more than several fibre lengths away. Approximating paper compression with one-dimensional models ignoring shear stresses, as will be done in Chapter 5, is thus not unreasonable.

4.4 Conclusions

The experimental part of this research project leads to the following conclusions regarding calendering practice and theory:

The calendering equation still provides the best description of permanent paper deformation in a calender nip, except at low nip intensity where the master creep equation fits better. The dependency of both equations on bulk needs to be elucidated.

As in-nip paper deformation is generally above the upper limit of the calendering equation, describing deformation in terms of the density ratio ρ_n/ρ_i may be more useful in obtaining coefficients from laboratory in-nip measurements since that relationship fits as well as the calendering equation but only requires a multiple linear regression package rather than non-linear iterative methods.

Kerekes' prediction for the radius coefficient is verified.

A convenient relationship between in-nip and permanent strain can be found, and is probably a function (at least) of initial bulk and pulp properties. This relationship will permit estimating in-nip strain at a local CD position given local permanent strain.

Strain recovery immediately after an industrial nip is governed by a time constant whose magnitude is in the range 10 to 30 ms. At high speeds with small rolls, significant recoverable strain remains from the first nip at the entrance to the second nip. However, the effect is small.

Recoverable strain is essentially constant above a certain point, implying that fibres are essentially elastic (with time-dependent complete recovery) until some plastic limit is exceeded.

Machine direction stretch is two orders of magnitude less than compressive strain. Cross direction stretch was too small to measure by simple scaling, implying that it is less than 1 part in 70, or 1.5%. One-dimensional approximations ignoring shear stresses in the nip are therefore not unreasonable.

5. Modeling paper compression in a rolling nip

5.1 Introduction

The data presented in Chapter 4 show the viscoelastic behaviour of paper when compressed in a calender nip: there is partial, time-delayed strain recovery after the nip with very little instantaneous elastic recovery. The relationship between in-nip and permanent strains proposed in Section 4.2.3 and plotted in Figure 4.29 illustrates this behaviour. Data for a material exhibiting elastic recovery would fall on the ordinate since there would be no permanent strain regardless of in-nip strain; paper approaches this limit for loads at or below the lower limit attainable with the equipment described in Chapter 3. Similarly data for a viscous material which has no strain recovery ($\varepsilon_n = \varepsilon_p$) would fall on a line of slope 1; this is true of paper under moderate calendering conditions, although a portion of the total strain applied is not recoverable as it would be in a purely viscous material. Finally, under extreme conditions of high load and low speed in-nip paper strain levels off as sheet density in the nip approaches a limiting density constrained by the density of pure fibre. Paper thus exhibits viscoelastic behaviour when *z*-direction compressive stresses are in the range encountered in calendering.

The calendering equations fitted to the data in Chapter 4 describe this behaviour in purely empirical terms. The various coefficients, obtained by curve-fitting methods, were not related to more fundamental parameters describing fibre or paper properties. Several authors [45, 61, 62, 80] have used viscoelastic methods to provide more insight into the calendering process. These methods are now examined in the search for a relationship between the empirical results of Chapter 4 and the physical properties of fibres and paper.

Models for compression of a viscoelastic sheet due to an indenting object have been described by many authors [2, 27, 37, 45, 49, 50, 53, 57, 58, 76, 77, 78], either with or without rolling motion of the indenter. In the most general case, models must allow for significant shear stresses in the material as the indenting object (whether flat,

cylindrical, spherical or random) is pressed into it. In the case of paper in a calender nip, shear stresses may be neglected, as shown next.

As machine direction extension of paper in a calender nip was shown in Section 4.3 to be small, and others have shown the magnitude of cross-direction extension to be small [4, 29, 47, 54], paper compression can be approximated as a one-dimensional process. This can be demonstrated by considering a fibre lying in the MD on the surface of a sheet 120 μm thick, as illustrated in Figure 5.1. Typical fibre dimensions (exaggerated for clarity in Figure 5.1) are 2 mm long and 10 μm in diameter. As it enters the calender nip one end of the fibre is both flattened and displaced downward from the surface towards the sheet centerline 60 μm below. If the in-nip strain is 0.50, the downward displacement is about 30 μm. The new length of a fibre with one end at the nip centerline and one end just entering the nip, as deduced from geometry, is 2.0002 mm, which represents a negligibly small lengthwise strain of 0.01%. A fibre closer to the sheet midplane will see even less MD strain since the downward displacement goes to zero at the sheet centreline. The larger MD strains reported in Section 4.3 can be explained by fibre flattening, as described next.

The change in width of fibres lying in the CD is likely to contribute more to the MD strain than the lengthwise strain described above. When a fibre with diameter of 10 μm is compressed, the width of the fibre will increase to 12 to 14 μm in the nip depending on the wall thickness and how much open lumen remains. The increase in width corresponds to an in-plane strain on the scale of the fibre of 0.2 to 0.4, a large amount; however, the strain on the scale of the sheet is much smaller since fibres expand into inter-fibre voids as they compress and do not necessarily force adjacent fibres to displace. A change in the width of a fibre is likely to cause strain in the fibres crossing it; the extension of a fibre caused by 5 fibre crossings per mm of fibre length, each crossing extending 3 μm, is 15 μm, corresponding to a total lengthwise strain of 1.5%. This amount is consistent with measured MD and CD strains reported here and elswhere.

Overall, MD strain in a calender is due to the large deformation of CD oriented fibres being constrained by small deformations and by unkinking of the MD oriented

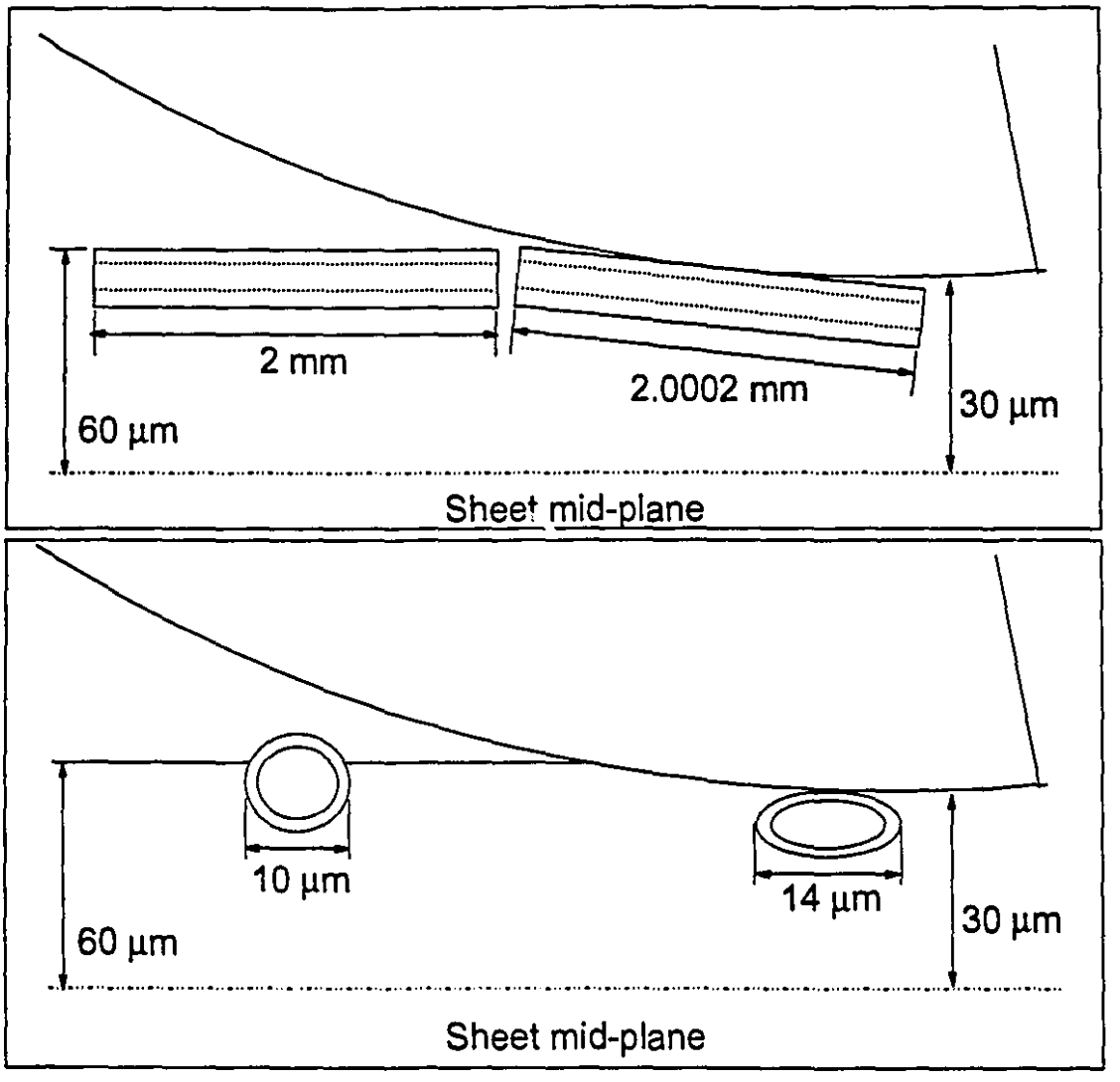

Figure 5.1 A typical fibre entering a calender nip. Fibre orientation: a) in the MD; b) in the CD.

fibres to which they are bonded. The three-dimensional structure of the sheet shifts and stretches, dissipating the large radial deformation of individual fibres. These conclusions are supported by experimental work of Mann et al. [54], as discussed in Sections 2.2 and 4.2.2. Their measurements of in-plane Poisson's ratios show that large z-direction strains result in very small CD or MD strains.

Thus modeling the viscoelastic behaviour of paper using one-dimensional models which neglect shear forces is reasonable. This approach will be taken in the discussion which follows. Quantitative results will then be compared with a qualitative description of fibre and paper structure.

5.2 Quantitative results: linear viscoelastic models

5.2.1 Geometry of a smooth, thin strip in a rolling nip

The analysis of May et al. [53] of the geometry of a thin strip in a rolling nip can be used to describe the strain history imposed on a sheet as it passes through the calender nip. Since strain history is a required element for viscoelastic modeling, the nip geometry is described next.

In the cartesian coordinate system shown in Figure 5.2, the origin is at the intersection of the plane of the undeformed sheet and the centreline joining the rolls. The x-axis is positive in the direction of sheet displacement, or machine direction, while the z-axis is positive downwards. The sheet mid-plane is assumed to be a plane of symmetry. Time is measured from the point of first contact between sheet and roll; thus t = 0 at the entrance to the nip when x = $-a$. Distances z_i, z_n and z_p are the initial, in-nip and permanent recovered sheet half-thicknesses, $z(t)$ is the downward deflection of a point P(x,z) on the surface of the paper from the plane defining the initial paper surface, $z_o = z_i - z_n$ is the maximum value of $z(t)$ at the point of minimum paper thickness, and z_e is the half-thickness at the nip exit. Distances a and b are the ingoing and outgoing nip lengths; b_{max} is the value of b if the material recovers to its final thickness immediately on leaving the nip. Calendering variables are the roll radius R, sheet velocity V and line load L. The symbol V is used for sheet velocity in meters per second in order to distinguish it from sheet speed S in meters per minute, as used in previous chapters.

The expression for $z(t)$, the deflection of a point with coordinates P(x,z) from the initial paper surface due to intrusion of the roll, is derived from the right-angle triangle with hypotenuse R and sides x and R-z_o. As the roll radius R is much larger than z_o-$z(t)$, terms in $[z_o-z(t)]^2$ can be ignored, and

$$z(t) = \frac{Vt}{2R}(2a - Vt) \qquad [5.1]$$

where

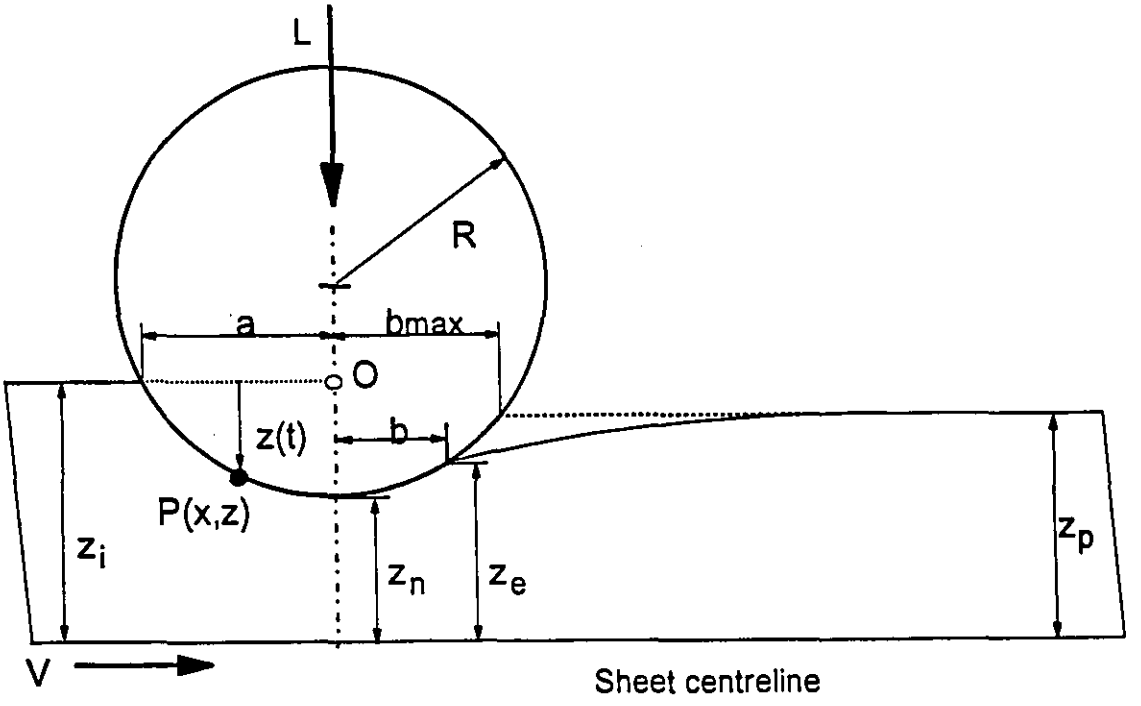

Figure 5.2 Geometry of a thin strip in a rolling nip.

$$a^2 = 2R(z_i - z_n) \qquad [5.2]$$

The deflection of a point in contact with the roll is therefore parabolic when second-order terms are neglected. By definition, strain is the change in thickness divided by the initial thickness:

$$\varepsilon_1(t) = \frac{Vt}{2Rz_i}(2a - Vt) \qquad [5.3]$$

In-nip and permanent strains are defined as follows:

$$\varepsilon_n = \frac{z_i - z_n}{z_i} \qquad [5.4]$$

$$\varepsilon_p = \frac{z_i - z_p}{z_i} \qquad [5.5]$$

The ingoing and maximum outgoing nip lengths a and b_{max} are then given by

$$a^2 = 2Rz_i\varepsilon_n \qquad [5.6]$$

$$b_{max}^2 = 2Rz_i\,(\varepsilon_n - \varepsilon_p) \qquad [5.7]$$

The strain and strain rate while paper remains in contact with the rolls are

$$\varepsilon_1(t) = \varepsilon_n \left(\frac{Vt}{a}\right)\left(2 - \frac{Vt}{a}\right) \qquad [5.8]$$

$$\frac{\partial\varepsilon_1(t)}{\partial t} = \frac{2\varepsilon_n V}{a}\left(1 - \frac{Vt}{a}\right) \qquad [5.9]$$

The largest strain rate is thus the initial strain rate at the nip entrance, when t=0:

$$\left(\frac{\partial\varepsilon_1(t)}{\partial t}\right)_{max} = \frac{2\varepsilon_n V}{a} \qquad [5.10]$$

In the experimental program described in Chapter 4, ingoing nip lengths, as computed using Equation 5.2, ranged from 2 to 5 mm, and so initial strain rates varied from 2000 to 6000 s^{-1}.

5.2.2 Constitutive equations for linear viscoelastic models

Mathematical descriptions of stress and strain for a thin, smooth continuous web in a rolling nip are derived next. The web is modeled using three linear viscoelastic models, each made up of ideal elastic elements with moduli G_i and ideal viscous elements with viscosities η_j. The models are the standard linear solid, the standard linear liquid, and Burger's model. In the derivations, the following assumptions are made.

1. The deformation of the rolls under the largest load applied is assumed to be small compared to the resulting deformation of the material in the nip.
2. Roughness of the strip is assumed small compared to z_i, and full contact between the sheet and roll is assumed to occur immediately upon entering the nip.
3. The material is assumed to be a continuum in the z-direction.
4. The material is assumed linear under typical calendering conditions, i.e. the moduli G_i and viscosities η_j are assumed to be material constants unaffected by applied stress, the resulting strain, or stress or strain rates.
5. A compressive pulse in the z-direction is assumed to result in negligible deformations in either the machine or cross directions, thus limiting the problem to one dimension. Another way of stating this assumption is to specify that Poisson's ratio is negligibly small. The tensor form of the constitutive equation can therefore be replaced with a scalar form.
6. The thickness of the web is assumed small compared to the roll radius.

Assumption #1 is valid when both calender rolls are steel, since the roll elastic modulus is then about 200 GPa compared to effective paper moduli of the order of 40 MPa (Mann et al. [54]). In the case of a soft nip, where the roll cover modulus may be 1 GPa, deformation of the soft roll is significant and the analysis presented here does not apply. Assumptions #2 and #3 do not apply for paper; the rough, structured nature of paper will be discussed in Section 5.3. The validity of assumption #4 has been questioned by Popil [70], and will be discussed in Section 5.3. Assumption #5 was discussed in

Section 5.1, and is consistent with published data (Mann et al. [54]). The validity of assumption #6 is confirmed when typical roll radii (0.1 to 0.5 m) are compared to typical paper thicknesses (80 to 150 μm).

The Deborah number ξ, the ratio of a typical material response time τ and a time characteristic of a process, occurs frequently in the derivation of pressure profiles caused by a given strain history. In a rolling nip, the Deborah number is the ratio of a time constant τ to the ingoing nip dwell time a/V:

$$\xi = \frac{\tau}{a/V} \qquad [5.11]$$

Depending on the type of time constant, there are two different interpretations of the Deborah number. First, the time constant may correspond to a stress relaxation time, in which case when τ is large compared to a/V, ξ is much larger than 1 and the material appears elastic since relaxation of the applied stress does not begin to occur in the short time the load is applied. If the stress relaxation time is very short compared to a/V, ξ is much smaller than 1 and the material appears viscous since there is little residual stress in material when the load is removed. Only when the relaxation and process times are similar does viscoelastic behaviour occur.

On the other hand the time constant may be a strain recovery time, as discussed in Section 2.2, in which case the situation is reversed: a long recovery time (corresponding to a large Deborah number) leads to behaviour which appears viscous since no apparent recovery occurs after removal of a load until many processing times have elapsed. Similarly, a short recovery time leads to apparently elastic behaviour since the strain recovery occurs immediately on removal of a load. As pointed out in Section 2.2, material behaviour in a rolling nip will be viscoelastic for a given material time τ, whether stress relaxation or strain recovery, if the sheet speed $V \approx a/\tau$.

A second non-dimensional number is the nip length ratio β, defined by

$$\beta = \frac{a + b}{a} \qquad [5.12]$$

When a material shows large permanent deformations (ε_p approaching ε_n), or recovers slowly due to a long strain recovery time, the outgoing nip length b approaches 0, and β approaches 1. On the other hand a material which recovers quickly due to a short recovery time will exhibit a longer nip length, with b approaching b_{max} and β approaching β_{max}:

$$\beta_{max} = 1 + \sqrt{1 - \frac{\varepsilon_p}{\varepsilon_n}} \qquad [5.13]$$

When a material recovers quickly and shows no permanent deformation, z_p approaches z_i, β_{max} and β both approach 2, ε_p approaches zero and b approaches a.

In linear viscoelastic behaviour, discussed in Section 2.2, the stress response to an arbitrary strain input is given by the Boltzmann integral:

$$\sigma(t) = - \int_0^t \psi(t-t') \frac{\partial \varepsilon_1(t')}{\partial t'} dt' \qquad [5.14]$$

For a rolling nip, the strain rate $\partial\varepsilon_1(t)/\partial t$ is given by Equation 5.9. The relaxation function $\psi(t)$ describes the material response to the imposed strain. In the case of a pure elastic material, Equation 5.14 reduces to Hooke's law. Once the stress history is known and can be differentiated for $0 \leq t \leq t_e$, where t_e is the elapsed time at the nip exit, the strain recovery for $t > t_e$ is given by

$$\varepsilon_2(t) = \int_0^{t_e} \phi(t-t') \frac{\partial \sigma(t')}{\partial t'} dt' \qquad [5.15]$$

Values of the various moduli and viscosities can be determined if strains or stresses are known at certain critical points. As knowledge of the maximum strain attained in the nip is crucial to solving Equations 5.14 and 5.15, the experimental measurements of Chapter 4 are essential in determining viscoelastic behaviour.

Two linear models, each made up of several springs and dampers and with specific relaxation and retardation functions, will be discussed in detail next. The standard linear solid, described briefly in Section 2.2, does not predict permanent deformation and is therefore a poor approximation for paper in a calender. Constitutive equations for this model in a rolling nip were derived by Kerekes [45], and are not repeated here.

The standard linear liquid

The standard linear liquid, illustrated in Figure 5.3, combines a single viscous element in series with a Kelvin model. The viscous element η_M models stress relaxation under load and permanent deformation once the load is removed, while the Kelvin model η_K, G_K reproduces creep under load and time-delayed strain recovery. There is no instantaneous elastic response, either under load or afterward. If the material remains in contact with the roll surface after the nip centerline, it is due to the recovery of the Kelvin element occuring faster than the rate of removal of the load. Application of a compressive stress for a long period results in the predicted strain becoming very large, eventually exceeding 1. As this result implies negative thicknesses, the model is limited to cases where the duration of the load is short compared to material response times. Dwell times in industrial papermachine calenders meet this requirement, as illustrated by Figures 4.22 and 4.23, Section 4.2.1.

The stress relaxation and strain recovery functions describe the model's behaviour:

$$\psi(t) = \eta \left[\frac{\eta_M}{\eta_K} \frac{e^{-t/\tau}}{\tau} + \delta(t) \right]$$

$$\phi(t) = \frac{t}{\eta_M} + \frac{1 - e^{-t/\tau_K}}{G_K} \qquad [5.16]$$

where $\delta(t)$ is the unit impulse function, and the equivalent viscosity η and overall time constant τ are given by

$$\eta = \frac{\eta_M \eta_K}{\eta_M + \eta_K} \qquad \tau = \frac{\eta_M + \eta_K}{G_K} \qquad [5.17]$$

The Kelvin time constant τ_K is equal to the ratio η_K/G_K. The unit impulse function arises because imposition of a step strain on the viscous element η_M requires an infinite stress of infinitely short duration. Substituting Equations 5.9 and 5.16 into the Boltzmannn

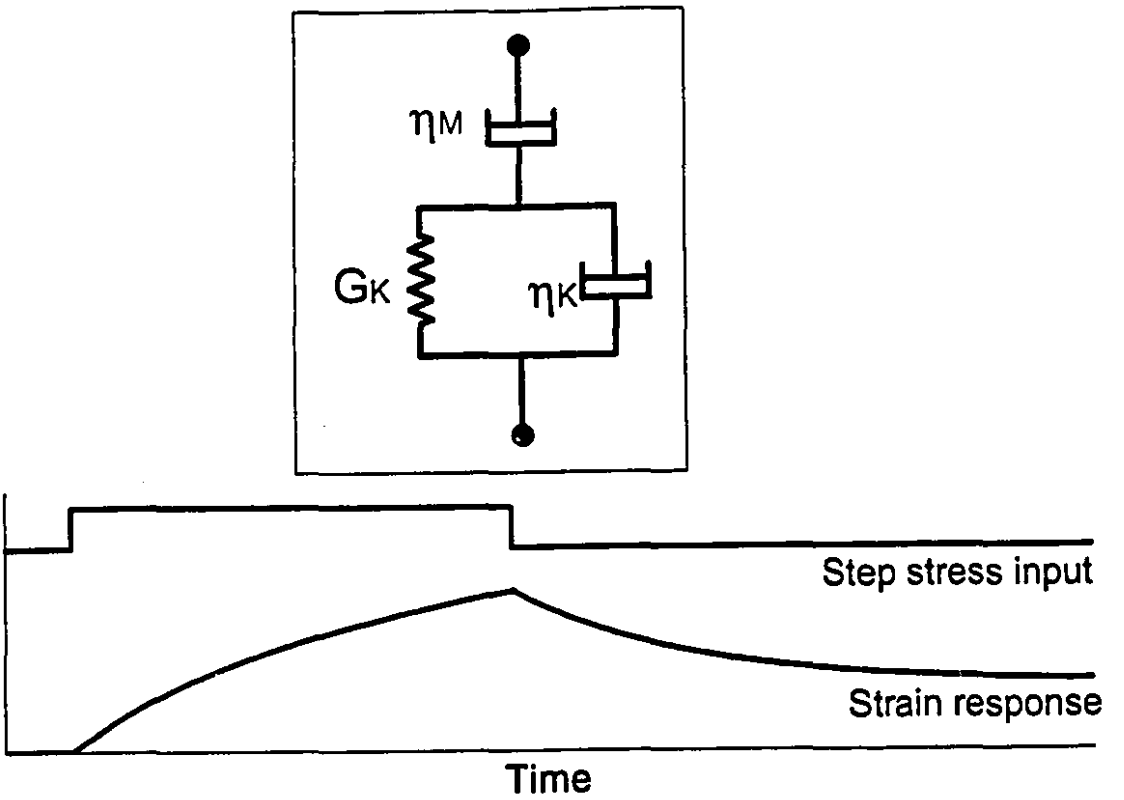

Figure 5.3 A linear liquid showing partial time-delayed recovery.

integral gives the stress profile in a rolling nip:

$$\sigma(t) = \frac{2\varepsilon_n V}{a} \frac{\eta_M^2}{\eta_M + \eta_K} \left[(1+\xi)(1-e^{-t/\tau}) - \frac{Vt}{a} \right] + \frac{2\varepsilon_n V}{a} \left(1 - \frac{Vt}{a}\right) \frac{\eta_M \eta_K}{\eta_M + \eta_K} \quad [5.18]$$

where ξ is the Devorah number associated with τ:

$$\xi = \frac{V\tau}{a} \quad [5.19]$$

The last term in Equation 5.18 is the strain rate times the apparent viscosity of the model. Equation 5.18 does not predict a zero stress when $t = 0^+$, as predicted by

Kerekes [45] and measured by Keller [43], but the pure Newtonian stress $\eta\dot{\varepsilon}$ which is non-zero since the initial strain rate is non-zero. The stress at the nip exit should also be zero. Equation 5.18 correctly predicts the stress at the nip exit when $t = t_e$ and when the nip length is a:

$$(1+\xi)(1-e^{-1/\xi}) - 1 = 0 \qquad [5.20]$$

When t_e is small compared to τ, as it is in a calender, ξ is large and Equation 5.20 reduces to the first two terms of the series expansion for e^{-x}, $x = 1/\xi$; when ξ is sufficiently large, as it is here, further terms in the expansion can be neglected, and Equation 5.20 reduces to an identity. Thus Equations 5.18 and 5.20 cannot be used to predict model parameters. The three unknowns in Equations 5.18 and 5.20 are the three model parameters implicit in the time constant τ. Three equations are necessary to solve for the unknowns: the first is obtained by integrating the stress over the length of the nip and equating to the line load L:

$$L = \int_0^{t_e} \sigma(t) V \, dt \qquad [5.21]$$

Two more equations can be obtained using the retardation function, the response to a step stress input, which is given by Findley et al. [27]:

$$\phi(t) = \frac{t}{\eta_M} + \frac{1 - e^{-t/\tau_k}}{G_K} \qquad [5.22]$$

where $\tau_K = \eta_K/G_K$ is the relaxation time for the Kelvin element. Differentiating Equation 5.18 with respect to time and substituting the resulting stress rate and the retardation function $\phi(t)$ into the Boltzmann integral for strain, Equation 5.15, gives an expression for the strain recovery curve after the nip. This expression consists of two terms, one constant and one an exponential decay. Equating the constant term to the permanent deformation gives a second relationship for the three unknowns. The decay term,

controlled by τ_K, gives a third relationship when τ_K is known, as it is here.

Equation 5.21, along with expressions for strain recovery and permanent strain, make up a set of three equations in three unknowns. In the absence of knowledge of the recovery time constant τ_K, a fourth equation may be obtained by comparing the strain at the nip exit computed using the strain recovery curve, $\varepsilon_2(t_e)$ in Equation 5.15, with the exit strain computed from geometry, $\varepsilon_1(t_e)$ in Equation 5.8. However, as the outgoing nip length b approaches 0, as it does for the standard linear liquid, this comparison yields the identity $\varepsilon_n = \varepsilon_n$, which provides no additional information.

Finally, strain rates at the nip exit may also be compared:

$$\frac{\partial \varepsilon_1(t)}{\partial t} = \frac{\partial \varepsilon_2(t)}{\partial t} \qquad [5.23]$$

As b approaches 0, however, Equation 5.23 predicts $\varepsilon_n = \varepsilon_p$. Thus knowledge of τ_k and ε_n is essential for a solution. An estimate of the time constant is available; numerical solutions will be discussed in Section 5.2.3.

Burger's 4-element model

The Burger's model, shown in Figure 5.4, is composed of a Maxwell model in series with a Kelvin model. The viscous element η_M models permanent deformation of the material, the elastic element G_M models initial instantaneous elastic compression and partial instantaneous elastic recovery once a load is removed, and the Kelvin model exhibits time-delayed thickness recovery controlled by the time constant η_K/G_K. This model is therefore the minimum required to describe viscoelastic solids which show instantaneous elasticity, time-dependent partial recovery and creep under load.

The relaxation function $\psi(t)$ is given by Findley et al. [27] for a Burger's model:

$$\psi(t) = K_1 e^{-t/\tau_1} - K_2 e^{-t/\tau_2} \qquad [5.24]$$

where K_1 and K_2, functions of the model parameters G_M, G_K, η_M, and η_K, have units of pressure. Similarly the time constants τ_1 and τ_2 also depend on the model parameters:

$$p_1 = \frac{\eta_M}{G_M} + \frac{\eta_K}{G_K} + \frac{\eta_M}{G_K} \qquad (r_1, r_2) = \frac{p_1 \pm A}{2p_2}$$

$$p_2 = \frac{\eta_M \eta_K}{G_M G_K} \qquad (\tau_1, \tau_2) = \left(\frac{1}{r_1}, \frac{1}{r_2}\right)$$

$$q_1 = \eta_M \qquad (\xi_1, \xi_2) = \left(\frac{V\tau_1}{a}, \frac{V\tau_2}{a}\right) \qquad [5.25]$$

$$q_2 = \frac{\eta_M \eta_K}{G_K} \qquad K_1 = \frac{q_1 - q_2 r_1}{A}$$

$$A = \sqrt{p_1^2 - 4p_2} \qquad K_2 = \frac{q_1 - q_2 r_2}{A}$$

The retardation function $\phi(t)$ is also given by Findley et al. [27]:

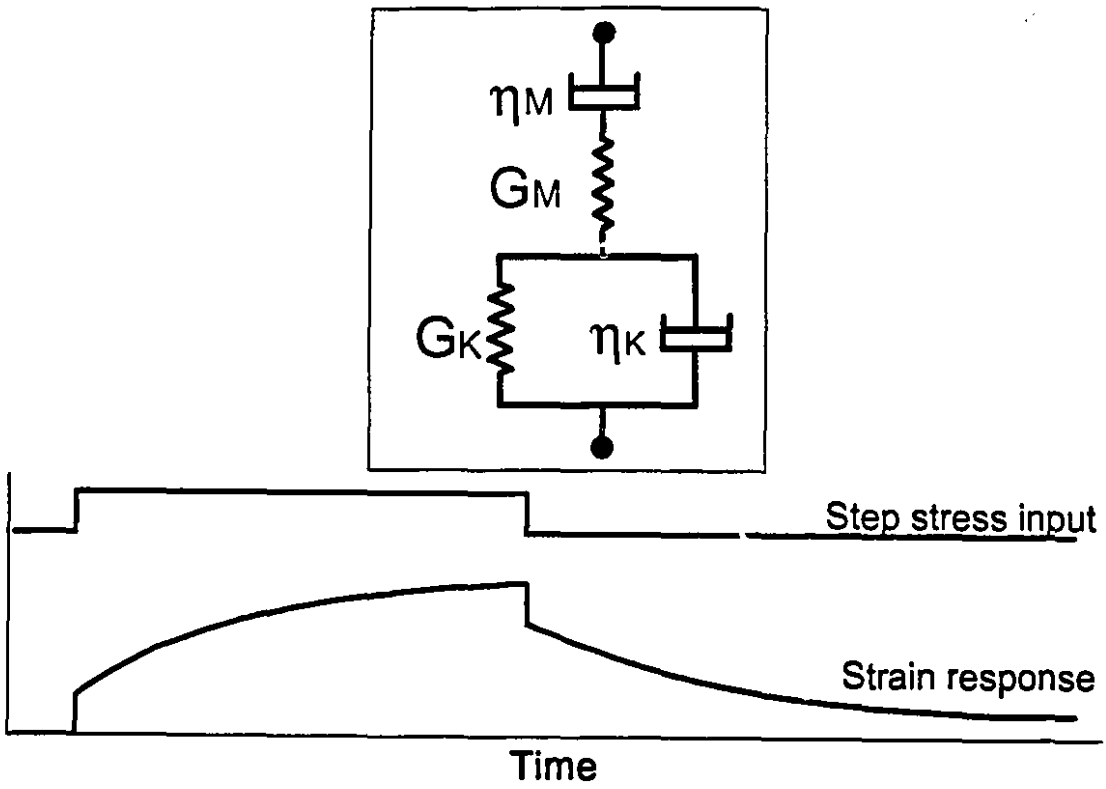

Figure 5.4 Burger's model showing instantaneous elasticity and delayed partial recovery.

$$\phi(t) = \frac{1}{G_M} + \frac{t}{\eta_M} + \frac{1 - e^{-t/\tau_K}}{G_K}$$
$$= \frac{1}{G_M}\left[1 + \frac{t}{\tau_M} + \frac{G_M}{G_K}\left(1 - e^{-t/\tau_K}\right)\right] \qquad [5.26]$$

where the Maxwell and Kelvin time constants τ_M and τ_K are given by

$$\tau_M = \frac{\eta_M}{G_M} \qquad \tau_K = \frac{\eta_K}{G_K} \qquad [5.27]$$

$\phi(t)$ is the sum of the responses of the Maxwell spring G_M, Maxwell damper η_M and the Kelvin element G_K, η_K, and has units of reciprocal pressure. Substituting

Equations 5.9 and 5.24 into Boltzmann's integral, Equation 5.14, gives an explicit expression for stress in the nip:

$$\sigma(t) = -\frac{2\varepsilon_n V}{a}\int_0^t \left(K_1 e^{-(t-t')/\tau_1} - K_2 e^{-(t-t')/\tau_2}\right)\left(1-\frac{Vt'}{a}\right) dt' \qquad [5.28]$$

$$= -2\varepsilon_n\left[K_1\xi_1(1+\xi_1)\left(1-e^{-t/\tau_1}\right) - K_2\xi_2(1+\xi_2)\left(1-e^{-t/\tau_2}\right) - (K_1\xi_1-K_2\xi_2)\frac{Vt}{a}\right] \qquad [5.29]$$

Unlike the standard linear liquid, $\sigma(0) = 0$. Evaluating $\sigma(t_e)$ and equating to zero gives

$$K_1\xi_1(1+\xi_1)(1-e^{-\beta/\xi_1}) - K_2\xi_2(1-\xi_2)(1-e^{-\beta/\xi_2}) - (K_1\xi_1 - K_2\xi_2) = 0 \qquad [5.30]$$

Equation 5.30 gives one relationship between the five unknowns G_M, η_M, G_K, η_K and b (implicitly in the variables K_1, K_2, ξ_1, ξ_2 and β) in terms of the processing parameters L, V and R and the in-nip strain ε_n.

Integrating the expression for $\sigma(t)$ from t=0 to $t=t_e$ gives a second relationship:

$$L = \int_0^{t_e} \sigma(t)\, V\, dt \qquad [5.31]$$

$$\frac{L}{2\varepsilon_n a} = K_1\xi_1^2(1+\xi_1)\left(1-e^{-\beta/\xi_1}\right) - K_2\xi_2^2(1+\xi_2)\left(1-e^{-\beta/\xi_2}\right) - \left(K_1\xi_1(1+\xi_1) - K_2\xi_2(1+\xi_2)\right)\beta + \left(K_1\xi_1-K_2\xi_2\right)\frac{\beta^2}{2} \qquad [5.32]$$

Strain $\varepsilon_2(t)$ at times $t \geq t_e$ is given by

$$\varepsilon_2(t) = \frac{1}{G_M}\int_0^{t_e}\left[1 + \frac{t-t'}{\tau_M} + \frac{G_M}{G_K}\left(1 - e^{-(t-t')/\tau_K}\right)\right]\frac{\partial\sigma(t')}{\partial t'}\,dt' \qquad [5.33]$$

After equating the sum of constant terms to the permanent strain ε_p, strain $\varepsilon_2(t)$ becomes

$$\varepsilon_2(t) = \varepsilon_p - \frac{2\varepsilon_n}{G_K}\left[\frac{K_1\xi_1(1+\xi_1)}{1-\xi_1/\xi_K}\left(e^{-\frac{\beta}{\xi_1}\left(1-\frac{\xi_1}{\xi_k}\right)}-1\right) - \frac{K_2\xi_2(1+\xi_2)}{1-\xi_2/\xi_K}\left(e^{-\frac{\beta}{\xi_2}\left(1-\frac{\xi_2}{\xi_k}\right)}-1\right)\right.$$
$$\left. - \xi_k\left(K_1\xi_1 - K_2\xi_2\right)\left(1-e^{\beta/\xi_k}\right)\right]e^{-t/\tau_k} \qquad [5.34]$$

The second term decays exponentially at a rate depending on the time constant τ_K of the Kelvin model.

The third of the five equations defining the Burger's model is obtained by equating ε_p to the constant terms obtained in the derivation of $\varepsilon_2(t)$:

$$\varepsilon_p = \lim_{t\to\infty}\varepsilon_2(t)$$
$$= \frac{2\varepsilon_n a}{V\eta_M}\left[K_2\xi_2(1+\xi_2)(\beta+\xi_2)e^{-\beta/\xi_2} - K_1\xi_1(1+\xi_1)(\beta+\xi_1)e^{-\beta/\xi_1}\right. \qquad [5.35]$$
$$\left. + \left(K_1\xi_1^2(1+\xi_1) - K_2\xi_2^2(1+\xi_2)\right) - \left(K_1\xi_1 - K_2\xi_2\right)\frac{\beta^2}{2}\right]$$

As for the standard linear liquid, two more equations for the five unknowns can be obtained by evaluating the two expressions for strain and their derivatives at $t=t_e$. These equations become progressively less useful as β approaches 1. Equating $\varepsilon_1(t_e)$ to $\varepsilon_2(t_e)$ gives

$$\beta(2-\beta)-\frac{\varepsilon_p}{\varepsilon_n}=\frac{2}{G_K}\left[\frac{K_1\xi_1(1+\xi_1)}{1-\xi_1/\xi_K}\left(e^{-\beta/\xi_1}-e^{-\beta/\xi_K}\right)\right.$$
$$-\frac{K_2\xi_2(1+\xi_2)}{1-\xi_2/\xi_K}\left(e^{-\beta/\xi_2}-e^{-\beta/\xi_K}\right) \qquad [5.36]$$
$$\left.-\xi_K(K_1\xi_1-K_2\xi_2)\left(1-e^{-\beta/\xi_K}\right)\right]$$

Equating the strain rates when $t=t_e$ gives a fifth equation:

$$\frac{2\varepsilon_n V(1-\beta)}{a}=\frac{\varepsilon_p-\varepsilon_n\beta(2-\beta)}{\tau_k} \qquad [5.37]$$

Equations 5.30, 5.32, 5.35, 5.36 and 5.37, along with the definitions of the various intermediate variables, make up a set of five equations in the five unknowns G_M, G_K, η_M, η_K and b. The required calendering parameters are the line load L, machine speed V, equivalent roll radius R, initial sheet half-thickness z_i, in-nip half-thickness z_n and fully-recovered half-thickness z_p. The number of unknowns and equations is reduced when estimates of τ_K and β are available; however two of these, Equations 5.36 and 5.37, are only useful when β is not too close to 1.

Estimates of the values of the parameters are made in the next section, using methods that do not require solving sets of non-linear equations.

5.2.3 Initial estimates of parameters

As shown in the previous section, there are sufficient equations to solve for the unknown model parameters and the outgoing nip length b when modeling either a standard linear liquid or a Burger's model. Since the sets of equations are highly non-linear for both models, numerical methods are necessary; the literature on iterative solutions for sets of non-linear equations is large [1, 28, 59, 60, 71]. However, a full numerical solution may not be possible since there are not enough equations when β approaches 1, which appears to be the case for paper. As well, the equations are extremely nonlinear, requiring a set of initial estimates for the parameters which is extremely close to the solution set. On the other hand, model parameters for the standard linear liquid and Burger's model can be estimated from the data presented in Chapter 4 without resorting to iterative methods.

As described in Section 4.2.1, the partially recovered strain ε_r can be used to estimate the strain recovery time τ_K, the Kelvin time constant. This value appears to be a fairly strong function of sheet speed, implying that the assumption of linearity (Assumption #4 , Section 5.2.2) is false. However, as much of the present data was obtained at speeds which are low compared to industrial practice, useful information may still be obtained when data at low speeds is ignored. Restricting the analysis in this fashion, Figure 4.21a gives $\tau_K \approx 15$ ms when V $\approx$ 17 m/s (S = 1000 m/min). From Figure 4.21b, a typical value of the dwell time a/V at these speeds is 0.2 ms. The Deborah number associated with the Kelvin element is therefore $\xi_K \approx 75$. Of the two components of the Kelvin element, G_K and η_K, only one need now be determined, the other being obtained from the definition of τ_K.

Both models predict that the permanent deformation is due to a single viscous element η_M. The value of this parameter can be obtained by integrating Equation 5.38, relating viscous stress to permanent strain in the viscous element:

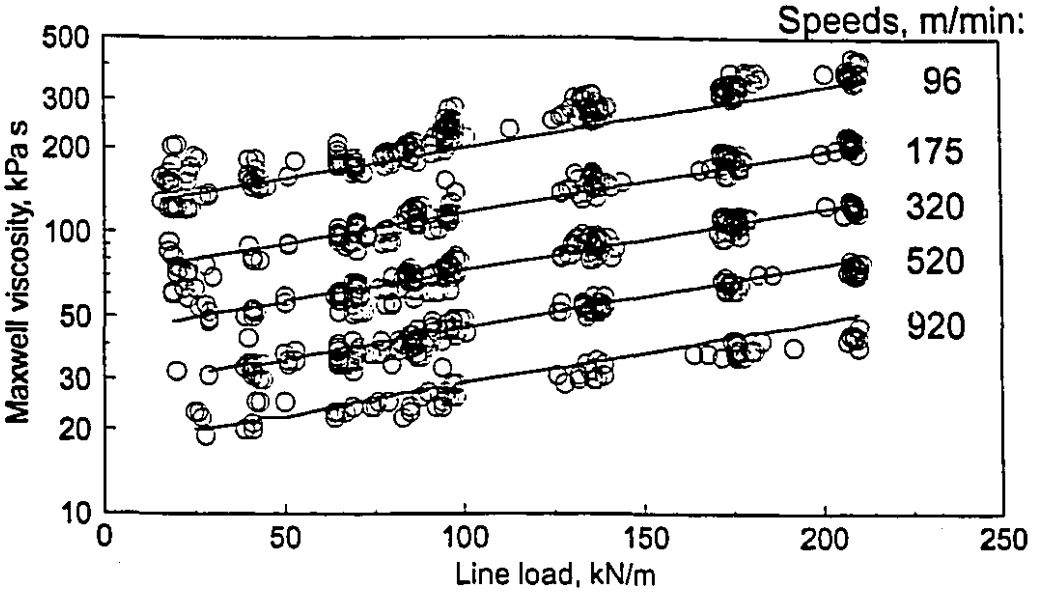

Figure 5.5 Maxwell viscosity η_M, for the standard linear liquid or the Burger's model.

$$\sigma_V(t) = \eta_M \frac{\partial \varepsilon_p}{\partial t} \qquad [5.38]$$

$$\int_0^{t_e} \sigma_V(t)\, dt = \eta_M\, \varepsilon_p \qquad [5.39]$$

By definition, the left hand side of Equation 5.39 is equal to the impulse L/V, as seen in Equation 5.31. Then Equation 5.39 gives

$$\eta_M = \frac{L}{V \varepsilon_p} \qquad [5.40]$$

Equation 5.40 (with ε_p computed using the calendering equation) is plotted in Figure 5.5, where it can be seen that η_M is a function of both load and speed. Nonlinear curve fitting methods were used to quantify this function; good agreement was obtained with Equation 5.41:

$$\eta_M = k_1 S^{k_2} e^{k_3 L} \qquad [5.41]$$

Values for the constants (with S in m/min and L in kN/m) are given in Table 5.1, and the curves are plotted with the data in Figure 5.5. Rearranging equation 5.40 gives

$$\frac{L}{a} = \frac{\varepsilon_p V}{a} \eta_M \qquad [5.42]$$

The ratio a/V is the time during which the average pressure L/a is applied, causing the deformation ε_p. The material property relating this average strain rate $\varepsilon_p V/a$ to the average pressure L/a is the viscosity η_M. This viscosity is not a constant, as seen in Figure 5.5, since the permanent strain ε_p is not proportional to the ratio L/V.

A similar analysis can be performed for the Kelvin element, where the strain imposed is all recovered:

$$\sigma_K(t) = \eta_K \frac{\partial \varepsilon_K}{\partial t} + G_K \varepsilon_K \qquad [5.43]$$

Substituting $G_K \tau_k$ for η_K, an expression for G_K can be obtained:

$$G_K = \frac{L}{V(\tau_K + t_e)\varepsilon_K} \qquad [5.44]$$

TABLE 5.1: Coefficients for Equation 5.41. Sheet speed in m/min, load in kN/m.

	Parameter	S.E.
k_1	5741	1.065
k_2	-0.852	0.035
k_3	0.00512	0.00057

Two terms must be defined: the total nip dwell time t_e, and the strain in the Kelvin unit ε_K. The nip dwell time depends on b, which is not known:

$$\frac{a}{V} \leq \left[t_e = \frac{a+b}{V} \right] \leq \frac{a+b_{max}}{V} \qquad [5.45]$$

A non-zero value of b occurs when there is contact after the nip centreline, which in turn occurs either when there is instantaneous elastic recovery, or when the load is removed slowly enough that the recovery of the Kelvin element can keep up with the rate of load removal. The time constant governing the recovery, estimated in Section 4.2.1 at 10 to 30 ms, is far too high compared to typical nip dwell times of 100 to 300 μs for the second case to apply in either model. Only the Burger's model can exhibit any instantaneous elastic recovery; for the standard linear liquid, therefore, the best estimate is $b = 0$, from which $t_e = a/V$.

For Burger's model, the length b depends on the unknown amount of instantaneous elastic recovery. As reported in Section 4.2, there was complete recovery of in-nip strain when $\varepsilon_n < 0.3$; most of this recovery was time delayed but a small portion may be elastic. In Figure 4.29 the elastic portion of the curve is very short, and an estimate for the instantaneous elastic recovery ε_{el} of 0.01 to 0.03 seems reasonable; Rodal [73] has proposed $\varepsilon_{el} < 0.05$. Using the estimated elastic modulus $G_M \approx 22$ MPa and an ingoing nip length of 3 mm, the elastic limit for ε_{el} of 0.01 to 0.03 occurs at nip loads of 0.67 to 2.0 kN/m, and the magnitude of b can be estimated:

$$b = \sqrt{2Rz_i\varepsilon_{el}} \qquad [5.46]$$

Using $z_i = 60$ μm and R of 202 to 355 mm, Equation 5.46 predicts b in the range 0.5 to 1.1 mm, which gives β in the range 1.17 to 1.37.

The maximum strain in the Kelvin element, ε_K, also needs to be defined. In the standard linear liquid, this is the total recoverable strain $\varepsilon_R = \varepsilon_n - \varepsilon_p$, since the Kelvin element is the only element predicting recovery after the nip. In Burger's model, the strain ε_K is the total recoverable strain ε_R less the instantaneous elastic recovery of the

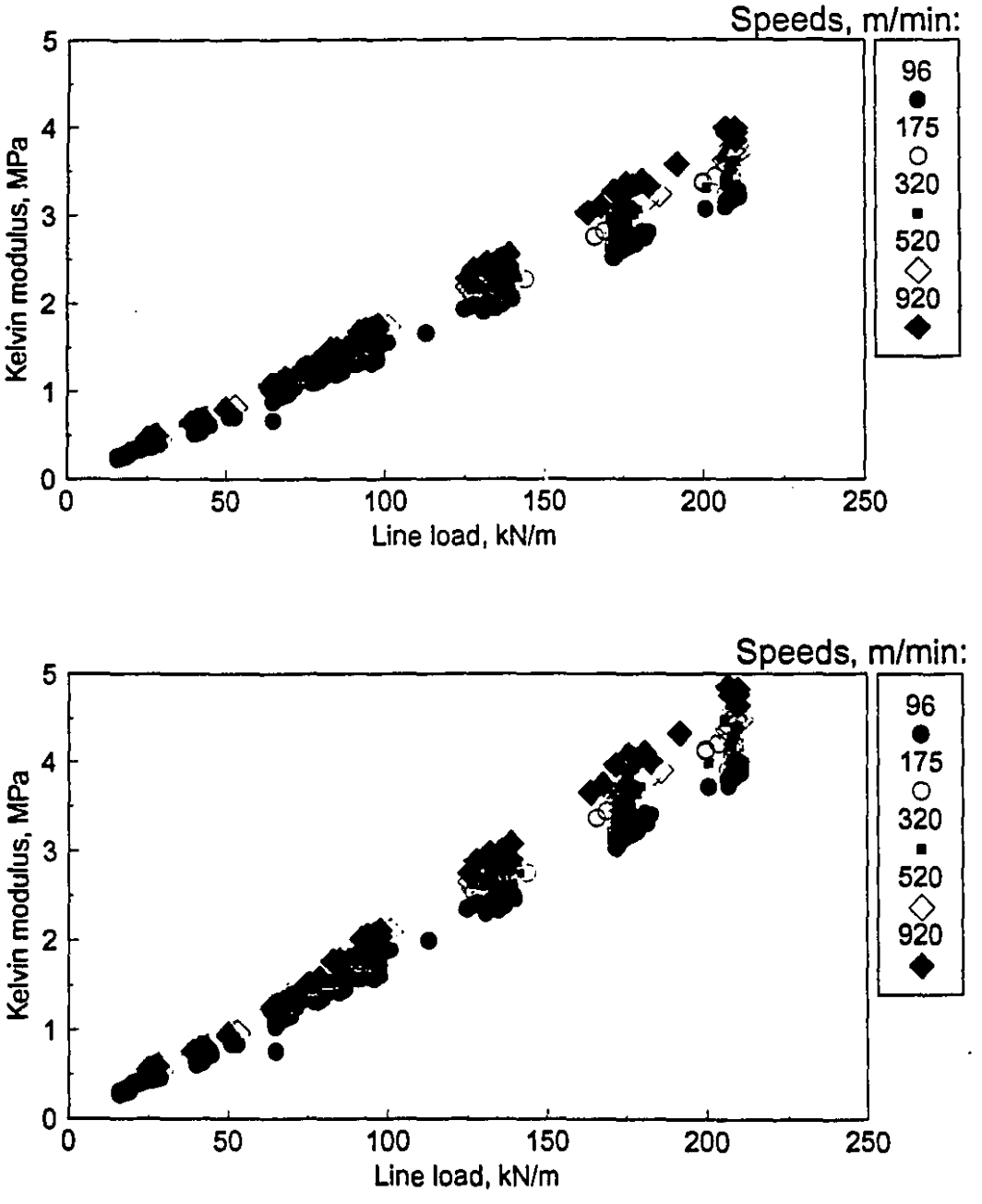

Figure 5.6 Kelvin modulus G_K: a) for the standard linear liquid;
b) for Burger's model.

Maxwell spring G_M, estimated above at $0.01 < \varepsilon_{el} < 0.03$. Results for G_K for both models are plotted in Figure 5.6; the values of in-nip and permanent strains were calculated using the calendering equations to avoid excessive scatter. The estimated elastic strain used to calculate data for the Burger's model in Figure 5.6b was $\varepsilon_{el} = 0.017$. For both models the modulus is a strong function of load, and a weak function of speed.

Finally, the viscous component of the Kelvin element is the product of G_K and τ_k; since τ_k is approximately proportional to 1/V and G_K is proportional to L, η_K, like η_M, is approximately proportional to L/V.

Thus the viscous and time-dependent components in both models are strong functions of either load alone, or of both load and velocity. Table 5.2 summarizes the results for industrially relevant conditions, i.e. a speed of 920 m/min and loads of 10 to 50 kN/m. The Deborah number describing stress relaxation in the nip, ξ_M, is in the range 2 to 10, while ξ_K, which describes strain recovery after the nip, is an order of magnitude larger at 50 to 100. The behaviour under load thus appears viscoelastic or mildly elastic, while the recovery after the nip appears strongly viscous.

Figure 5.7 gives the predicted pressure profiles for the two models at a load of 25 kN/m. The pressure profile for the Burger's model shows the expected parabolic shape with skew to the ingoing side of the nip. Pressure is zero at the nip entrance ($Vt/a = 0$) and again at a distance b after the nip centerline, $b < a$. For the standard linear liquid, however, the pressure profile starts off high due to the high strain rate at $t = 0^+$, and decreases essentially linearly until it reaches zero at the nip centreline, where the strain rate is also zero. The exponential component in Equation 5.18 is small when τ is much larger than the dwell time t_e, as it is here; when $(1-e^{-t/\tau})$ is exactly zero, the stress predicted by Equation 5.18 is exactly linear, decreasing to zero at time $t_e = a/V$. An estimate of the validity of this model can be obtained by considering the torque Γ required to pull the sheet through the nip against this pressure profile. Integrating the stress field over the nip length gives the drive torque required to compress the sheet in the nip:

TABLE 5.2: Summary of modeling results for L = 10 to 50 kN/m, S = 920 m/min.

	Standard linear liquid	Burger's model
τ_K, ms	15	15
ξ_K	75	75
G_K, kPa	19.3 kPa per kN/m	23.5 kPa per kN/m
η_K, Pa s	230 Pa s per kN/m	280 Pa s per kN/m
τ_M, ms	--	0.9
ξ_M	--	4.5
G_M, MPa	--	22
η_M, kPa s	25	25

$$\Gamma = \int_0^{t_e} W\sigma(t)(a - Vt)V\,dt \qquad [5.47]$$

where the product of machine width W and the pressure at a point in the nip $\sigma(t)$ is the portion of the total line load applied at the MD position defined by the elapsed time t; multiplied by an element dx = V dt, this becomes the force applied at that MD position. The distance (a - Vt) is the moment of that force about the roll axis. Summing the force times the moment arm gives the torque Γ required to impose a stress field on the ingoing nip while maintaining a steady speed. Using Equation 5.47 with typical values of S = 920 m/min, L = 20 kN/m, R = 202 mm, with the model parameters estimated as described above, and estimating ε_n using the calendering equation, the torque to pull a linear liquid through a single 70 mm wide calender nip at steady state is 4.8 Nm

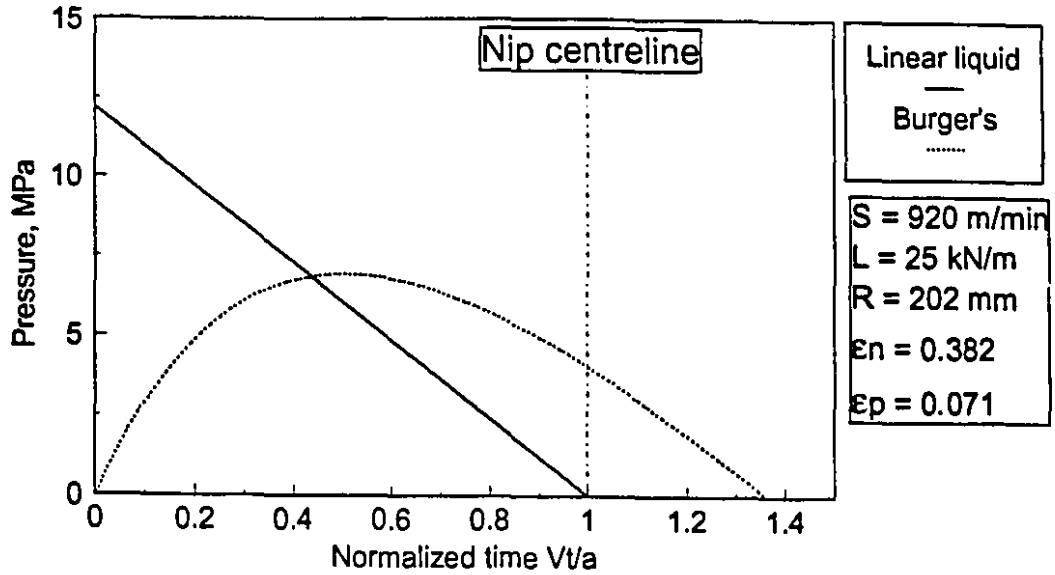

Figure 5.7 Predicted pressure profiles in a calender nip for two linear models. Conditions: S = 920 m/min, L = 25 kN/m, R = 202 mm.

(exclusive of bearing friction, web tension differential, etc.).

An empirical method for estimating the power requirements for a calender nip, Bentley and Derrick [6], predicts power requirements of 0.0009 HP per inch of machine width and per 100 fpm of machine speed to overcome bearing friction. Converting horsepower to torque using the angular velocity of the roll, this method produces a torque estimate of 0.75 Nm per bearing, or 3.0 Nm for a two roll stack, for the above machine conditions. They state that the nip work load due to compression of the sheet is "so small in magnitude in comparison to the major factors [governing drive requirements] that it may be neglected when selecting drive ratings". The authors caution that this assumption needs to be verified, especially for heavier grades. While it may therefore be accepted that the torque requirement to compress the light grade of newsprint tested here is much less than the torque to drive the bearings, Equation 5.47 predicts a substantially higher torque (4.8 Nm) for paper compression than to drive the bearings (3.0 Nm). Thus the linear liquid, while correctly predicting time-dependent

partial recovery and permanent deformation, does not adequately account for other aspects of nip mechanics.

The standard linear solid described by Kerekes [45] can be compared with the standard linear liquid and Burger's model. As shown in Figures 2.2 and 2.5, it predicts a skewed parabolic stress profile similar to the prediction of Burger's model. This is consistent with industrially realistic drive torques. Unlike Burger's model, however, the standard linear solid is unrealistic in predicting full recovery of initial thickness at a long enough time after removal of the load.

Of the three models, the Burger's model provides the best fit with observed behaviour. The standard linear solid is a poorer approximation, but is still superior to the standard linear liquid. Each standard model predicts just one aspect of paper response to a calender pulse, i.e. creep under load or permanent deformation, while Burger's model is the simplest linear model describing both. For all models, however, the parameters are not material properties but are strong functions of the processing parameters. The assumption of linearity does therefore not apply when considering paper in a calender nip. In light of the nonlinear results, the assumptions made at the beginning of this Section will be re-examined.

5.3 Qualitative results: paper as a rough, structured material

5.3.1 Introduction

Linear viscoelastic models were not successful in describing the strongly viscoelastic behaviour of paper in a calender nip since the modeling parameters turn out to be strong functions of processing parameters. Several reasons for the modeling difficulties can be proposed. Paper is a rough, heterogenous, structured material, contradicting Assumptions 2 and 3, Section 5.2.2. Furthermore, the linear modeling is based on the implicit assumption that there are no irreversible changes in paper or fibre response to a stress or strain input. As there is evidence of fibre fracture at high loads, this assumption may also be violated in calendering. The validity of these assumptions is now discussed qualitatively.

5.3.2 Surface roughness

The assumption of surface smoothness is examined first, with the structured nature of a sheet of paper considered subsequently.

A full description of the surface roughness of an anisotropic material such as paper is extremely complex [10, 30]. For an isotropic material, the probability distributions of three variables along a particular direction x_1 in the plane are necessary. These variables are the height z_r of the surface above a reference plane, the average slope of the surface dz_r/dx_1, and the average surface curvature d^2z_r/dx_1^2. For an anisotropic material, the variation of these distributions with the angle between the direction x_1 and some reference direction, such as the MD, is also necessary. As well, the problem of contact between smooth and rough surfaces is generally extremely difficult to solve analytically unless the distributions are assumed exponential, which is not necessarily the case with paper. Finally, there is an additional complication in the case of calendering, which is the parabolic nature of the imposed deformation. Thus no attempt was made to evaluate roll-to-paper contact on the scale of the roughness using formal mathematical methods. Rather, the contact area in the nip as described by the ingoing nip length a will be modified for a rough surface by using a common method of estimating roughness height for paper.

The roughness height of paper can be measured using an air-leak test instrument such as the one described by Parker [65]. The device measures the rate of air leakage at a constant supply pressure past a ring pressed into the sheet with a specified force. The average roughness height is then defined as the gap between two smooth plates giving the same volumetric flow rate for flow analogous to Hagen-Poiseuille flow in a cylinder; this gap is proportional to the cube root of the flow rate. The effect of in-plane permeability of the sheet, allowing additional leakage which is not due to roughness, is assumed small. This approximation is reasonable except in the extreme cases of a very smooth or very porous sheet. If the paper surface is modeled as a sinusoidal wave, the roughness obtained this way corresponds to the average amplitude.

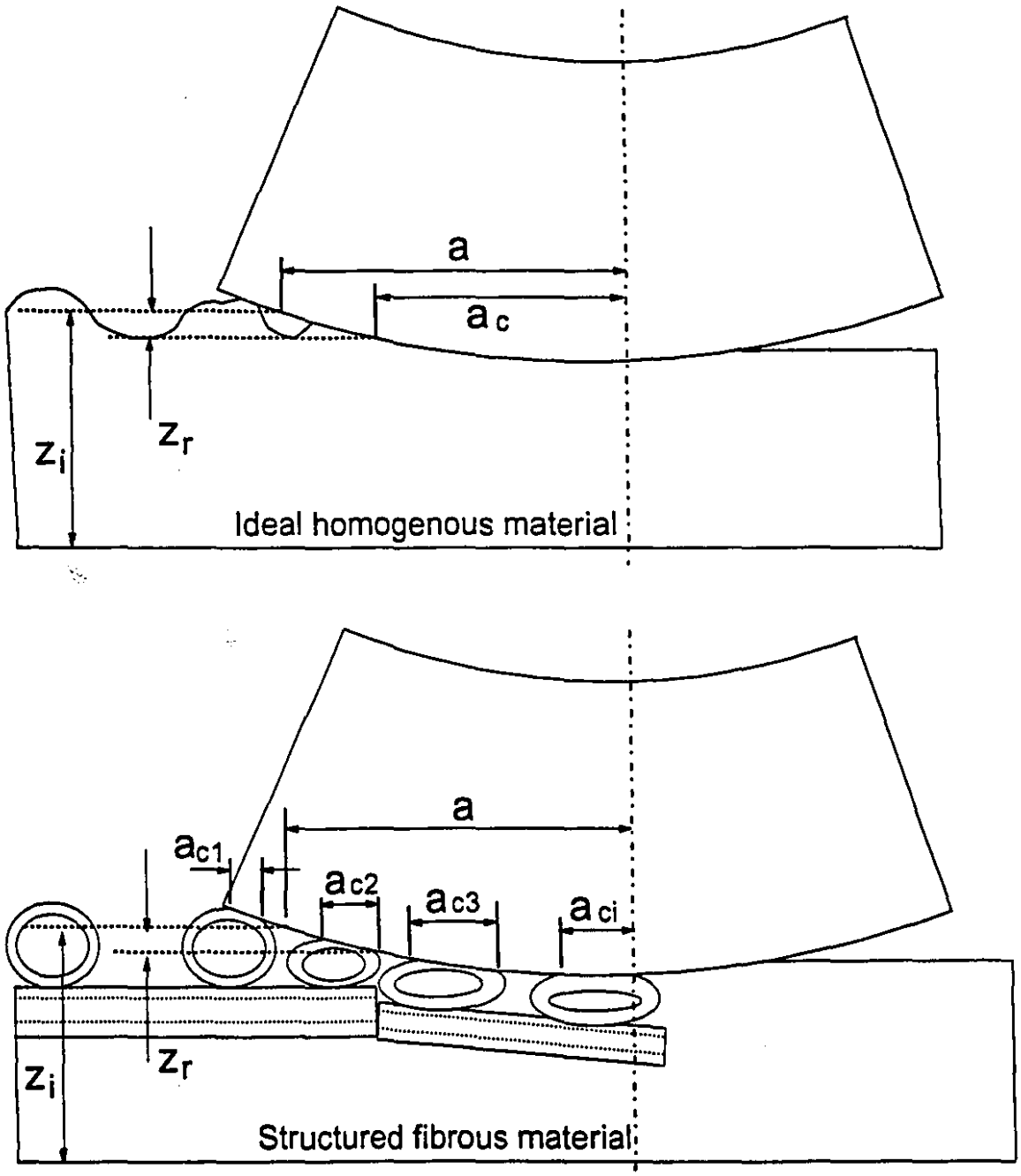

Figure 5.8 Geometry of a rough thin strip in a rolling nip:
a) for an ideal, homogenous material; b) for paper.

Typical roughness values for the paper used in this study were given in Section 4.1, Table 4.2, where it was seen that the roughness height ranged from 5 to 6.5 μm. These values are about 10% of the typical ingoing half-thickness z_i, which ranged from 55 to 65 μm. From the point of view of roughness alone, therefore, full contact between a calender roll and this particular type of paper cannot be expected until strain in the nip exceeds 0.1.

It is useful to consider what happens as a peak is pushed into the body of the sheet. In Figure 5.8a, peaks are shown being compressed by the calender roll while low spots remain unaffected until the depth of penetration of the roll exceeds the typical roughness height. In fact, when the structured nature of paper is considered in the next section it will be seen that the low spots are likely to be deflected early in the nip due to the fibre network spreading the load, as seen in Figure 5.8b. Some low spots may never contact the roll if there are sufficiently dense areas immediately adjacent. This has been investigated by Chapman [14], who pressed sheets against a transparent prism. Photographic methods were then used to estimate the percentage of the sheet contacting the prism at various compression pressures. At the largest average load of 5.5 MPa, the fraction of the total prism area contacting a newsprint sheet was only 18%. This load compares with typical values of the average nip pressure L/a, which ranged from 7.5 to 40 MPa in the present study. Fractional contact area in a calender is thus more than 18%, but certainly considerably less than 100%.

The "true" contact area is thus smaller than the contact area for a smooth material as defined by the ingoing nip length a. Leaving the effect of the structured nature of paper for consideration in the next section, the effect of roughness on contact area can be described quantitatively. The roughness-compensated nip length, a_c, is illustrated in Figure 5.8a, and can be determined for a given roughness height z_r:

$$a_c^2 = 2R\varepsilon_n(z_c - z_n) \qquad [5.48]$$

where $z_c = z_i - z_r$. Defining ε_c, the strain correponding to a contact length a_c, as

$$\varepsilon_c = \frac{z_r}{z_i} \qquad [5.49]$$

then the fractional contact area a_c/a comparing the estimates for rough and smooth ingoing nip lengths is

$$\frac{a_c}{a} = \sqrt{1 - \frac{\varepsilon_c}{\varepsilon_n}} \qquad [5.50]$$

Equation 5.50 is illustrated in Figure 5.9 for various values of ε_c ranging from 0.01 to 0.30. The length a_c defined by Equation 5.48 remains an approximation to the "true" contact length for two reasons. First, Equation 5.48 ignores contact of peaks at the nip entrance, as shown in Figure 5.8, thus underestimating a_c. On the other hand, in a structured material such as paper, as a peak is deflected downwards low spots will be deflected as well by the surrounding structure, causing Equation 5.48 to overestimate a_c. The "true" contact length is in fact the sum of the individual contact lengths Σa_{ci}, which is less than a. Overall, a_c thus remains a better estimate of the contact length than the smooth estimate a, while still overestimating the true contact length.

Figure 4.4 showed that permanent strains are small unless in-nip strains exceed 0.25, while permanent strains of 0.15 are not possible without imposing in-nip strains exceeding 0.50. At $\varepsilon_n = 0.25$, the roughness-compensated area a_c for a typical roughness value equal to 10% of z_i is about 75% of the theoretical contact area a, exceeding 90% only when ε_n exceeds 0.50. A similar argument applies to the outgoing area, with the smaller roughness after the nip reducing the difference between the smooth estimate b and the roughness compensated estimate b_c.

The assumption of full roll-to-paper contact immediately on entering the nip is thus not reasonable unless either the load exceeds industrially relevant values, or the sheet is already extremely smooth. The implication is that typical pressures encountered locally in the sheet must be higher than previously thought, since the line load is spread

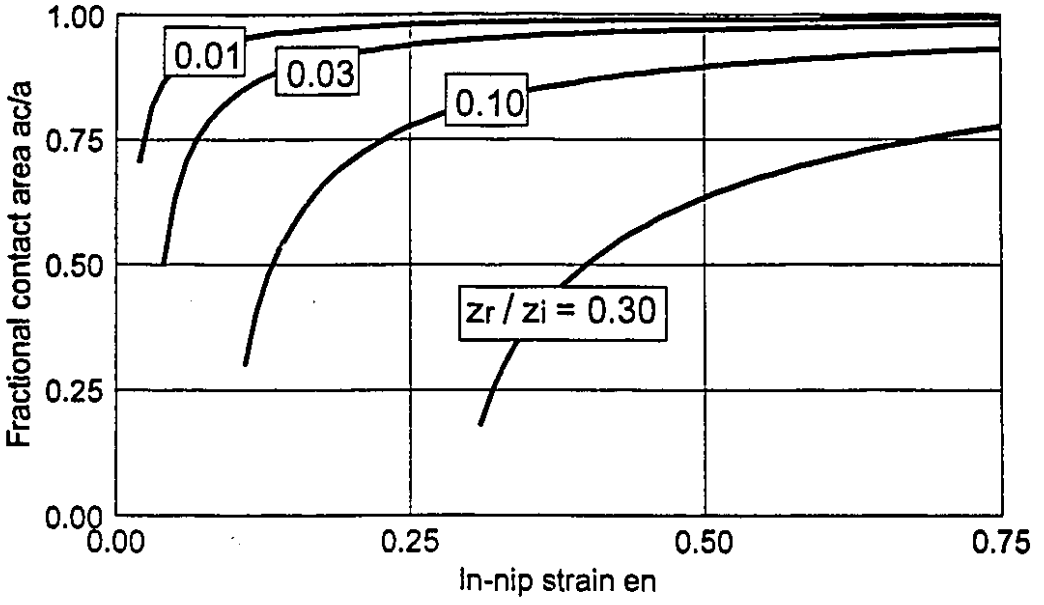

Figure 5.9 Fractional contact area in a calender nip for ε_c = 0.01, 0.03, 0.10, 0.30.

over a significantly smaller area. As well, as the strain is increased the contact area also increases. Since the contact area increases more quickly than the greater depth of indentation would imply, the pressure profile increases more slowly than predicted by the assumption of smoothness. The effect is particularly evident with rough sheets at low loads, where the actual maximum pressure encountered in the nip may be double the value predicted using the ratio L/*a* since the "true" value of the ingoing nip length *a* may be as little as half the value predicted by the assumption of minimal roughness. In Section 4.3.1 it was suggested that the outgoing nip length may be significantly shorter than the ingoing length; when these two effects are combined, peak pressures may easily reach values locally up to four times the estimates provided using Hertzian or other methods.

The effect of roughness is thus to distort the pressure profile predicted from the smooth model, which underestimates the maximum pressure by a significant amount; for a given ratio z_r/z_i the error is larger at lower in-nip strains. Any model for paper

compression in a calender nip must thus use an estimate of the ingoing nip length better than a. Since there exists no simple method for determining the true contact length Σa_{ci} at industrially relevant pressures, the roughness compensated length a_c is an obvious alternative.

Equation 5.42 defining η_M can be reconsidered in the light of the preceding discussion. The ratio a/V, the time from first contact to the nip centreline, remains unchanged even when the contact area is discontinuous. The average pressure L/a, on the other hand, is a poor estimate of the average nip pressure and should be replaced by L/a_c. A better estimate for η_M is thus the roughness compensated viscosity η_{Mc}:

$$\eta_{Mc} \approx \frac{L}{a_c}\frac{a/V}{\varepsilon_p} = \frac{a}{a_c}\eta_M \qquad [5.51]$$

where the ratio a/a_c is given by Equation 5.50.

From Table 3.1, the average roughness for the TMP newsprint is 5.74 μm; ε_c thus ranges from 0.09 to 0.10. At low loads in-nip strain is low, and $a/a_c \approx 1.2$, while at high loads $a/a_c \approx 1.1$. When the estimate of η_{Mc} obtained from Equation 5.51 is fitted to Equation 5.41, the coefficients in Table 5.3 are obtained. Comparing these

TABLE 5.3: Coefficients for Equation 5.41 after roughness compensation. Sheet speed in m/min, load in kN/m.

	Parameter	S.E.
k_1	6462	1.070
k_2	-0.853	0.038
k_3	0.00492	0.00056

results with those in Table 5.1, it can be seen that k_2 and k_3 are statistically unchanged at the 95% confidence level. Similar results are obtained when the estimates for η_K and G_K are revised using the same method; the correction does not account for the non-linearities but shifts the entire family of curves in Figure 5.5 upwards by about 12%.

An improved estimate for the true contact length Σa_{ci} might have a greater effect on the load dependency. The expression for strain rate could be modified using a statistical description of surface roughness. Paper could then be described using a large number of identical linear models in parallel, each with the same rheological behaviour but with different initial heights; as the sheet is compressed more of these elements would be activated and begin to contribute to carrying the applied load. Then the Burger's model could be modified to provide a stress-strain relationship consisting of a sum over all active elements. However, the pressure profile is also dependent on local density distributions in the plane of the sheet, as will be seen in the next section.

5.3.3 Paper and fibre structure

Paper is not a continuum, nor can it be described by a continuous density distribution function since it consists of two distinct phases, air and fibre; in effect paper could be considered fibre-reinforced air. Fibre and sheet properties are related by

$$\frac{\rho_p}{\rho_f} = \frac{v_f}{v_f + v_a} \qquad [5.52]$$

where ρ and v are density and volume, and the subscripts a,f,p indicate air, fibre and paper respectively. A typical initial bulk for uncalendered sheets in the present study was 2.70 cm^3/g, corresponding to an apparent sheet density ρ_p of 0.370 g/cm^3. The density of cellulose in wood fibres is ρ_f = 1.5 g/cm^3; the uncalendered sheet is thus at most 25% fibre by volume, increasing to 35% fibre by volume when ε_p = 0.30, and reaching a maximum of over 80% fibre in the nip when ε_n = 0.70.

As strain is increased, void fraction decreases. Illustrated in Figure 5.10, thin-walled, flexible fibres deform first; the apparent elastic modulus is defined by the resistance of a cellulose sheet to bending. As strain is increased beyond 0.50, flexible fibres collapse completely, thus becoming more difficult to deform. Stiffer fibres then begin to deform, requiring a higher load for more deformation; the apparent elastic modulus increases. As the strain increases towards 0.70, the void fraction approaches 0.15, and the material becomes increasingly difficult to compress. At a sheet average strain of 0.70, the highest measured in this study, the sheet average void fraction has fallen below 0.15. Under these conditions, areas of higher than average local thickness experience local strains higher than 0.70, and locally the void fraction of the sheet approaches zero. Similarly in areas of high local density the local void fraction is also lower than in surrounding areas. An area which is thicker or denser may thus be compressed to a void fraction approaching zero even though the sheet average void fraction is significant. In these thick or dense spots, the apparent elastic modulus at high average strains is defined by the compressive properties of solid cellulose rather than by

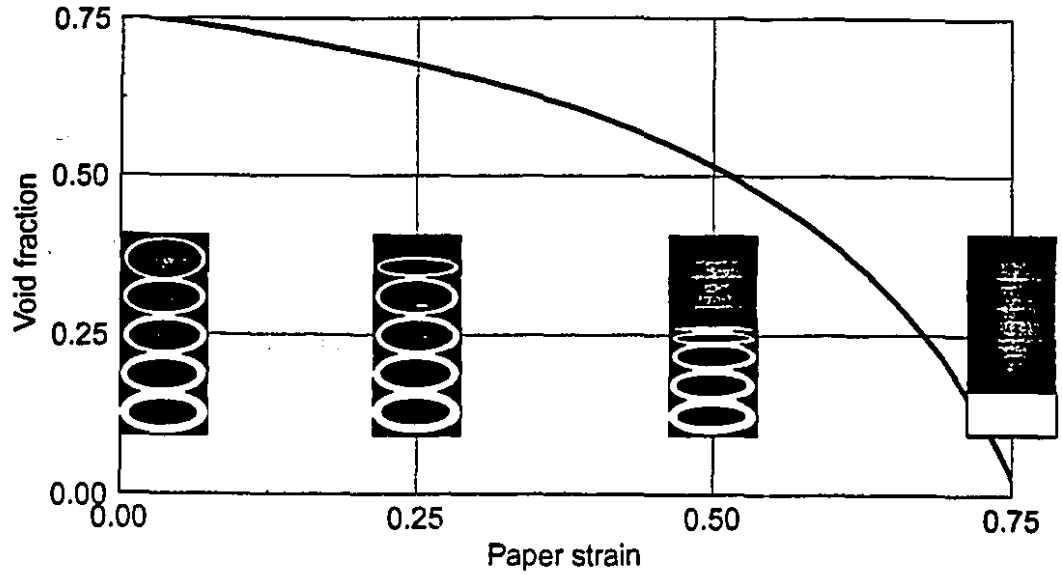

Figure 5.10 Void fraction as a function of average paper strain.

the open structure as before. The heterogenous, structured nature of paper thus results in large changes in the response to an applied stress for different levels of previously applied strain; the material behaviour is non-linear since the response function, whether stress relaxation or strain recovery, depends at the very least on the previous strain history. Furthermore, the non-linearities depend not only on the structure of paper, as defined by the initial apparent density and the spatial distribution of fibres of different flexibility, but on the structure of the fibre as it affects fibre compressibility.

The non-continuous nature of paper will now be examined using photo-micrographs of sheet cross-sections. The range of characteristic dimensions describing paper and machine geometry is large: roll radius may be 100 to 350 mm while nip lengths are about 2 to 5 mm; flocs are of the order of 1 cm in diameter while fibre dimensions are about 1 mm long and 0.01 mm in diameter. A 200 mm radius roll is shown reduced in Figure 5.11A, where the line width representing the paper web in the nip is not to scale. With the nip magnified by a factor of 50 in Figure 5.11B, roll curvature appears infinite and paper thickness is now apparent, but no details of paper

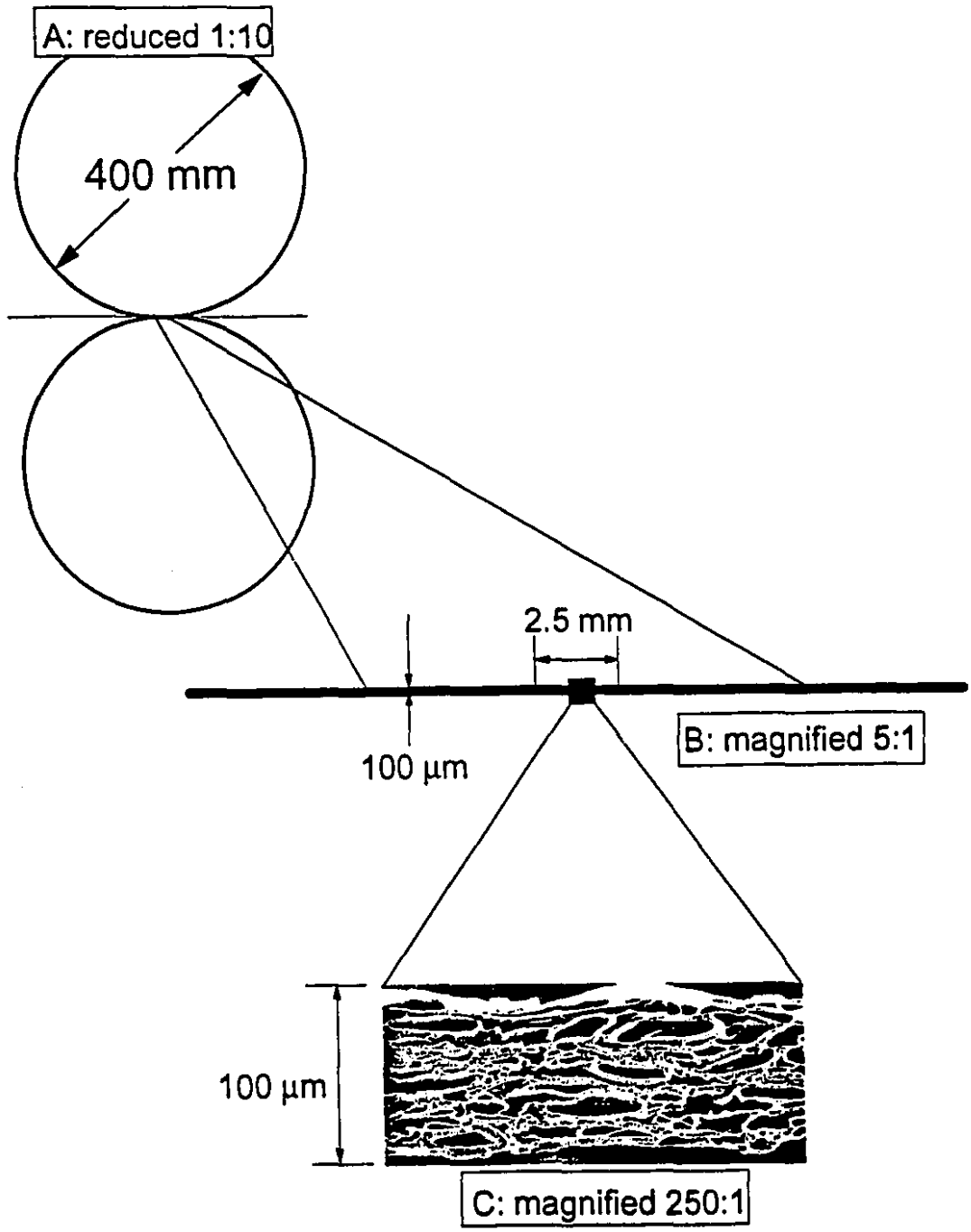

Figure 5.11 Relative dimensions of calender roll, nip, and paper.
A: calender stack; B: nip length of 2.5 mm; C: sheet section 250 μm long.

structure are visible. With an increase in magnification by a further factor of 50, Figure 5.11C, details of paper structure can be identified; there are large thickness and density variations on a scale of one-tenth the total nip length. From the point of view of a fibre, the radius of the roll is essentially infinite, and the contact length is similar to typical fibre lengths.

Cross-sections of TMP newsprint were prepared for microscopy by scanning electron microscope using methods developed by Williams et al. [81]. The section plane in the selected micrographs presented in Figures 5.12 to 5.20 is aligned with the cross-machine direction. As all sections were taken near the centre of the 70 mm wide web, they all come from the same CD position on the paper machine. All came from the same reel and were thus made within the space of a few minutes. An uncalendered sample was taken from the beginning of the reel; the remainder of the reel was calendered under a variety of conditions and samples were removed corresponding to two conditions. Each calendering condition is illustrated with a group of six micrographs taken from a series of ten spanning a continuous 2.8 mm wide CD section, a small distance compared to the machine CD width of 70 mm. After allowing for overlap between adjacent photographs, each covers a CD distance of 0.33 mm.

The micrographs illustrate several aspects of paper nonuniformities as they affect compression in a calender nip. On a large scale, of the order of a millimetre, significant variations are apparent from place to place in the sheet in both thickness and density, leading to non-uniformities in the CD and MD pressure profiles and thus in the local strain of the sheet. On the scale of the sheet thickness, about 100 μm,there are variations in typical fibre dimensions. Earlywood fibres, which come from the spring and summer growth of the tree, have large diameters and thin walls, while latewood fibres are smaller and coarser with thicker walls. Every position in the sheet is made up of a stack of fibres with different distribution of fibre coarseness, leading to local variations in compressibility with applied strain. Finally, on the scale of the fibre diameter, about 10 μm, the fibre wall is itself made up of fibrils wound in a spiral about the fibre axis; the fibril angle varies from the outside of the fibre to the inside, thus varying the strength properties as

the fibre is compressed.

Figures 5.12 to 5.17 show sections of uncalendered paper. The position of each micrograph in the continuous set of ten is shown schematically. The average thickness for these samples is 122 μm when measured using a standard caliper gauge. It may be recalled that the platen on this gauge has a diameter of 16 mm, almost 50 times larger than the area shown in the micrographs. Basis weight of the samples is 45 g/m^2, and the average fibre content by volume in the uncalendered sheet is about 25%.

There is a large variety of fibre coarsenesses visible in the uncalendered samples, ranging from large diameter, thick-walled latewood (5.12, bottom centre) to small diameter fibres which are either hardwood fibres or ray cells (5.12, center left) to large diameter thin-walled earlywood (5.13, top right). At the upper left in 5.12 there is a fibre which has been split open and which then curled back on itself.

Density variations in Figures 5.12 and 5.13 appear small, but they are much larger in Figures 5.14 and 5.15. The lower edge of 5.14 shows a shive made up of earlywood fibres and ray cells, while to the lower left in 5.15, there is another large shive. In both cases these consist of fibres which were not separated during pulping. Since the shives are mainly thin-wall earlywood, the density in this area, about 1 mm from Figure 5.12, is extremely low. In the calender nip, low density areas such as this will not be deformed appreciably since adjacent high density areas can be expected to carry a larger portion of the load through the nip. Finally, there are still a variety of fibre types, including an extremely coarse fibre to the right of 5.14. This area shows how density can vary on a millimetre scale while caliper remains essentially constant.

If Figures 5.13 and 5.14 showed regions of variable density and constant caliper, Figures 5.16 and 5.17 show an area immediately adjacent of constant density and variable caliper which is composed of smaller and coarser fibres. The density is higher than in Figure 5.13, while the thickness is lower and much more variable over the total CD distance of 660 μm illustrated. As well, there is another broken fibre to the upper left of 5.17.

These micrographs of uncalendered paper illustrate several aspects of the structure

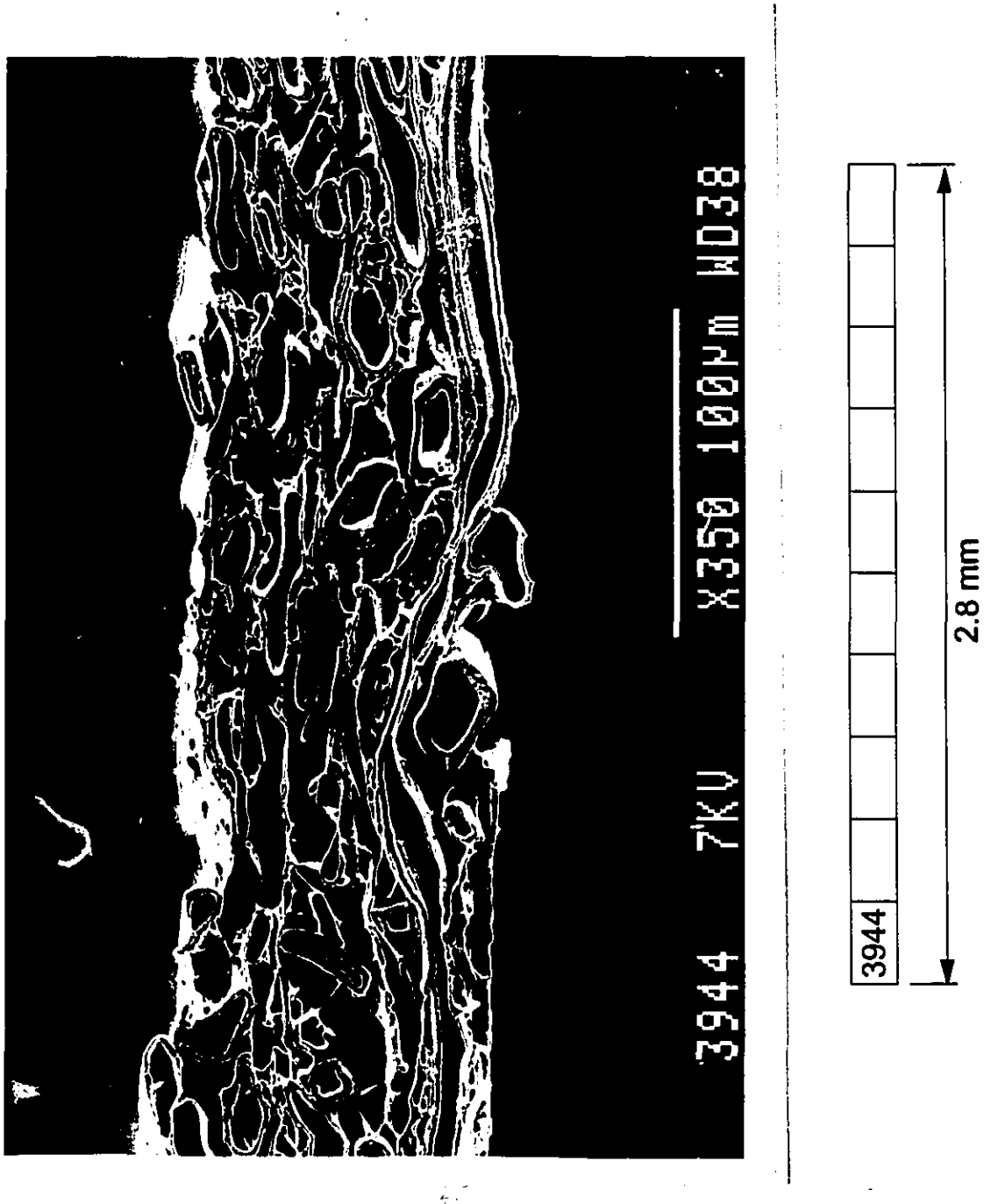

Figure 5.12 Uncalendered sheet. Section plane in CD; magnification 500X.

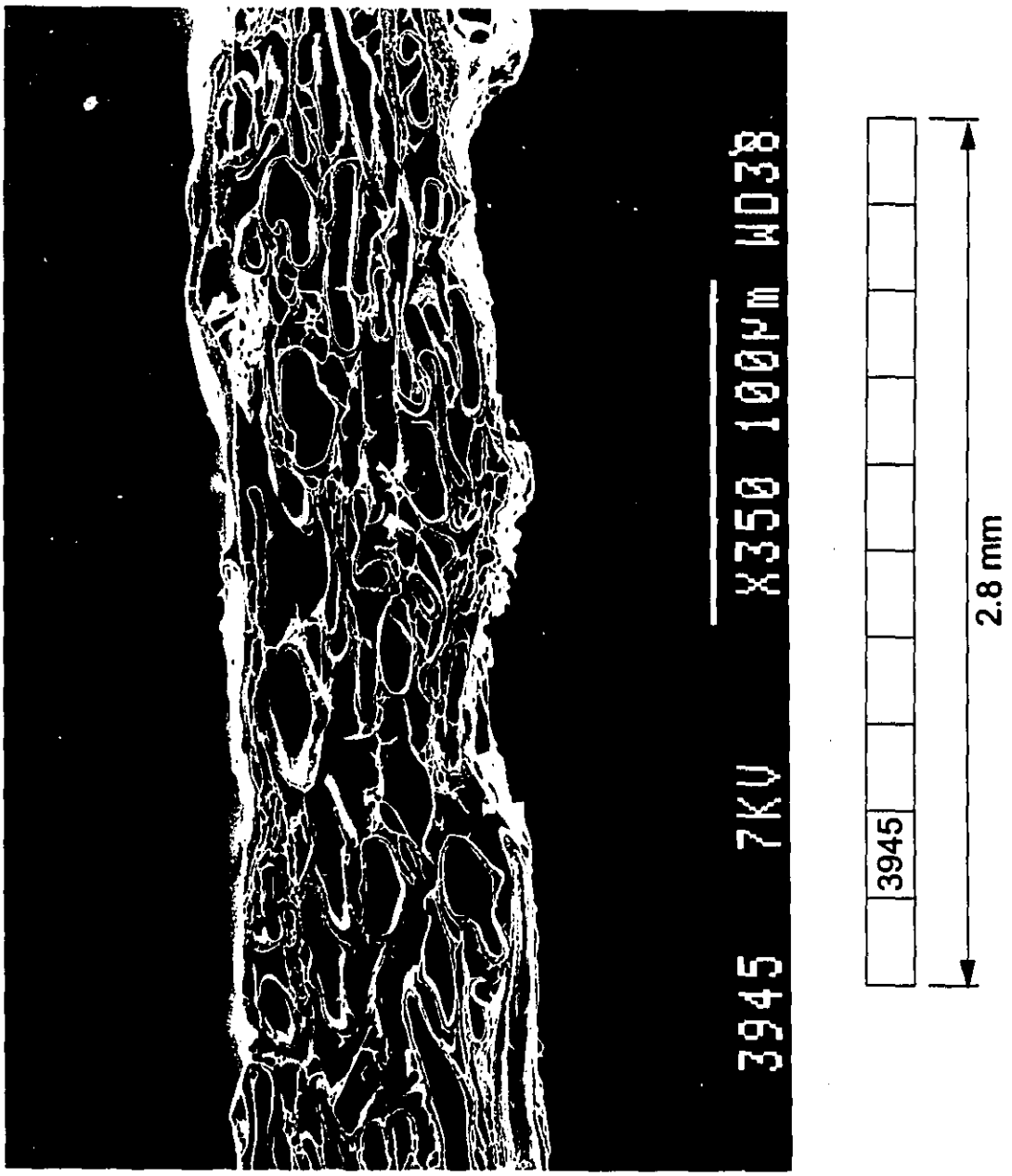

Figure 5.13 Uncalendered sheet. Section plane in CD; magnification 500X.

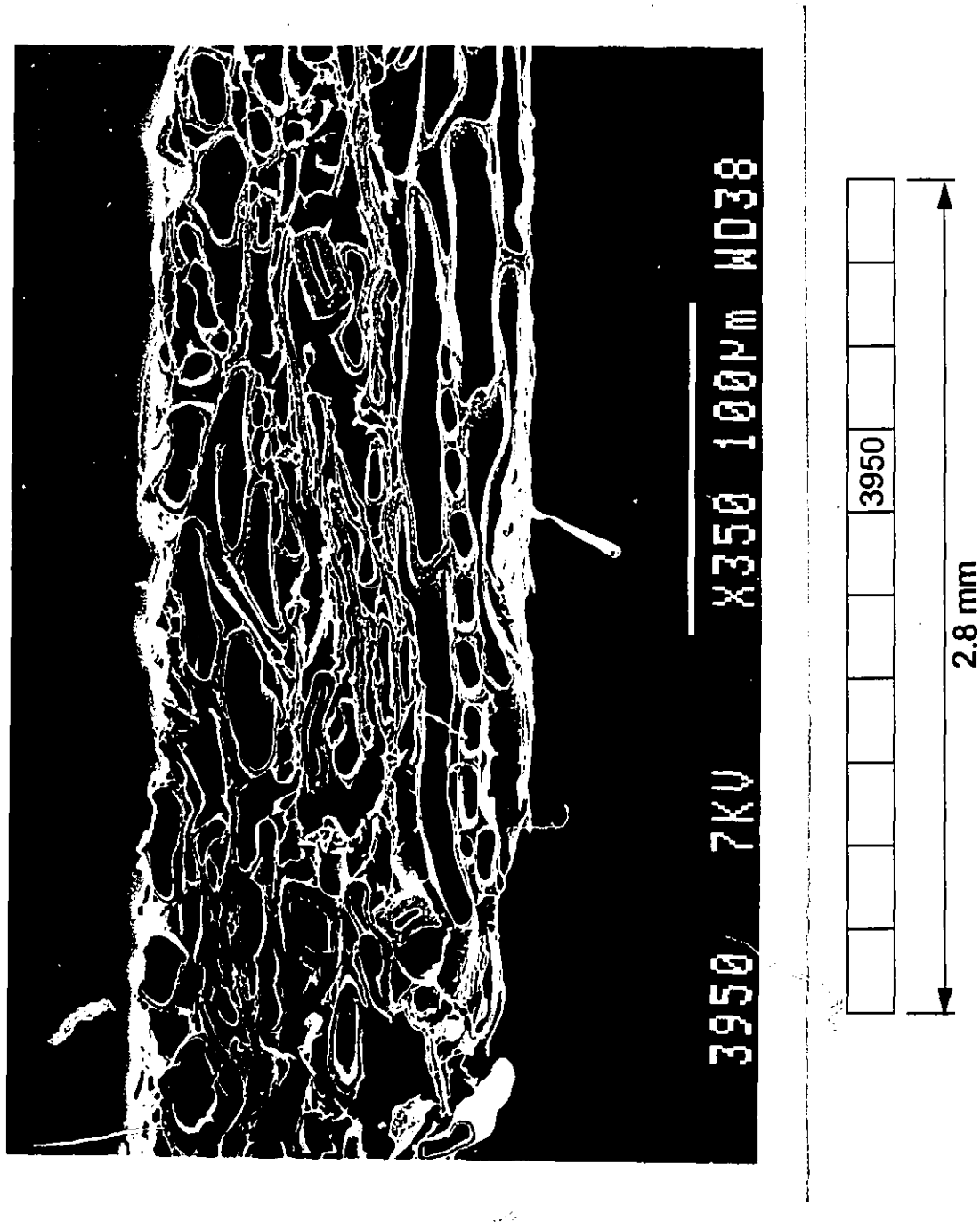

Figure 5.14 Uncalendered sheet. Section plane in CD; magnification 500X.

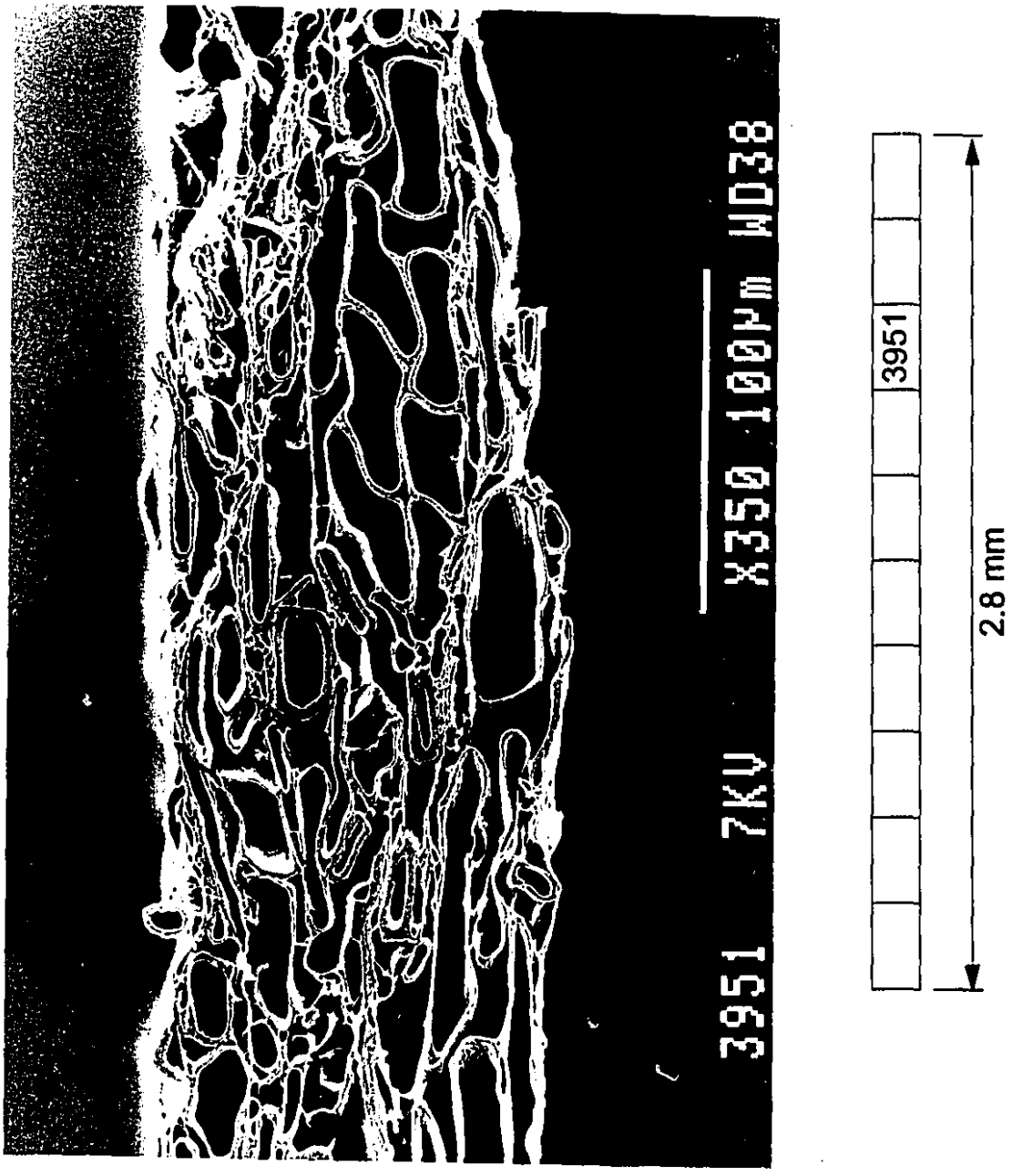

Figure 5.15 Uncalendered sheet. Section plane in CD; magnification 500X.

Figure 5.16 Uncalendered sheet. Section plane in CD; magnification 500X.

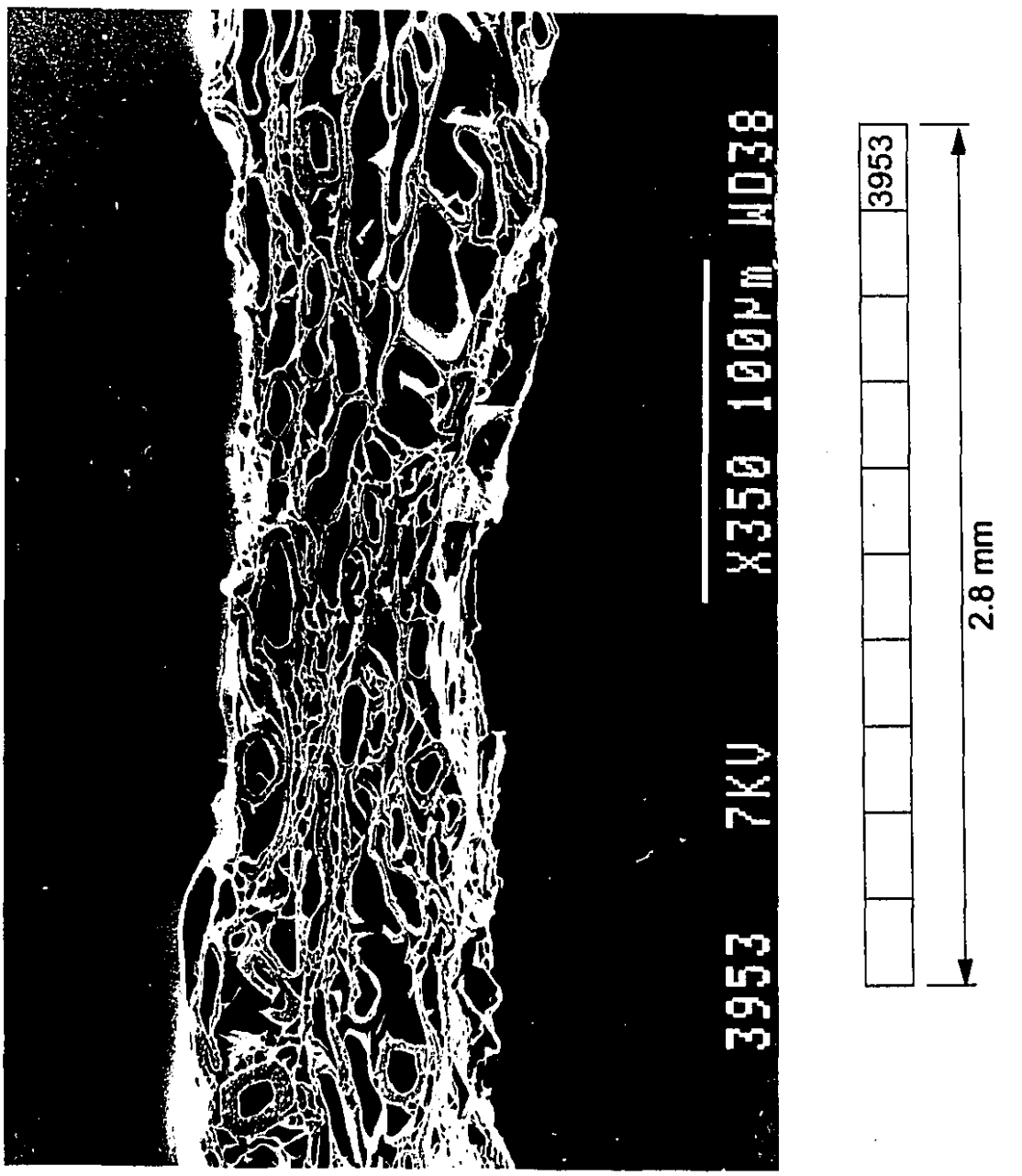

Figure 5.17 Uncalendered sheet. Section plane in CD; magnification 500X.

of a TMP sheet. First, both the thickness and density of the sheet vary significantly from place to place over distances which are much shorter than the nip length of 2 to 5 mm. Density variations, which are due to formation, will result in large local nonuniformity of pressure in the calender nip over small distances in both the machine and cross directions, with the scale of the pressure nonuniformities the same as those for density and thickness. There is also a wide range of fibre sizes and wall thicknesses which contribute to local small-scale variation in fibre density in all three directions. Finally, the sheet arriving in the calender contains a number of fibres damaged in the pulping process.

Some results of these large local pressure variations in the nip can be seen in Figures 5.18 to 5.23, which show sections of paper calendered at a sheet speed of 519 m/min and a line load of 28 kN/m. In the nip, average strain was about 0.35, average thickness was about 78 μm while the average fibre content by volume was about 40%. After calendering, the average strain is about 0.10, average thickness is about 110 μm, and average fibre content has increased slightly from 25% by volume in the uncalendered sheet to 27%.

The same small-scale nonuniformity in paper thickness and density seen in the uncalendered sheets are visible in these sections of moderately calendered samples. Fibres deformed by the action of the calender are not easily differentiated from those deformed earlier in the pulping process. However there is a new type of fibre damage, fracture of the fibre wall, which, if present, was not seen in any of the uncalendered samples. The first such fibre is to the left of Figure 5.18, at about the mid-plane of the sheet. This fibre has two internal cracks in the wall, located at the top and bottom of the fibre, and has a single external crack to the right. Another fibre with a single internal fracture may be seen in the centre of Figure 5.20. Numerous other fibres with smaller fractures are visible in these figures; this type of damage will be examined in the next section. There are also several broken fibres; an example may be seen lying on the surface of the sheet to the left in Figure 5.19. Finally, there is a fibre to the right of center in 5.23 which is delaminated: the inner wall has broken and separated from the

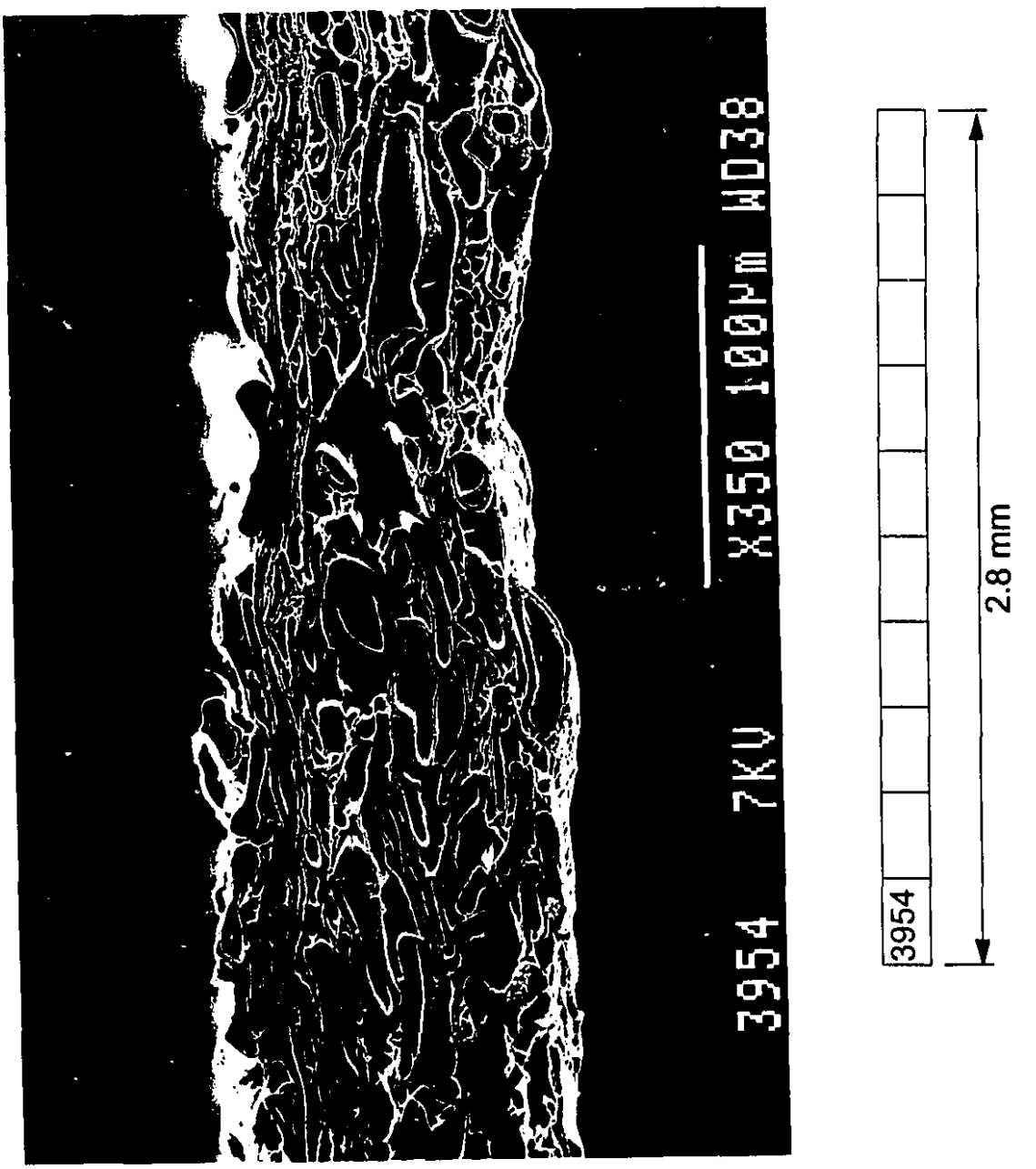

Figure 5.18 Lightly calendered sheet. Section plane in CD; magnification 500X.

Figure 5.19 Lightly calendered sheet. Section plane in CD; magnification 500X.

Figure 5.20 Lightly calendered sheet. Section plane in CD; magnification 500X.

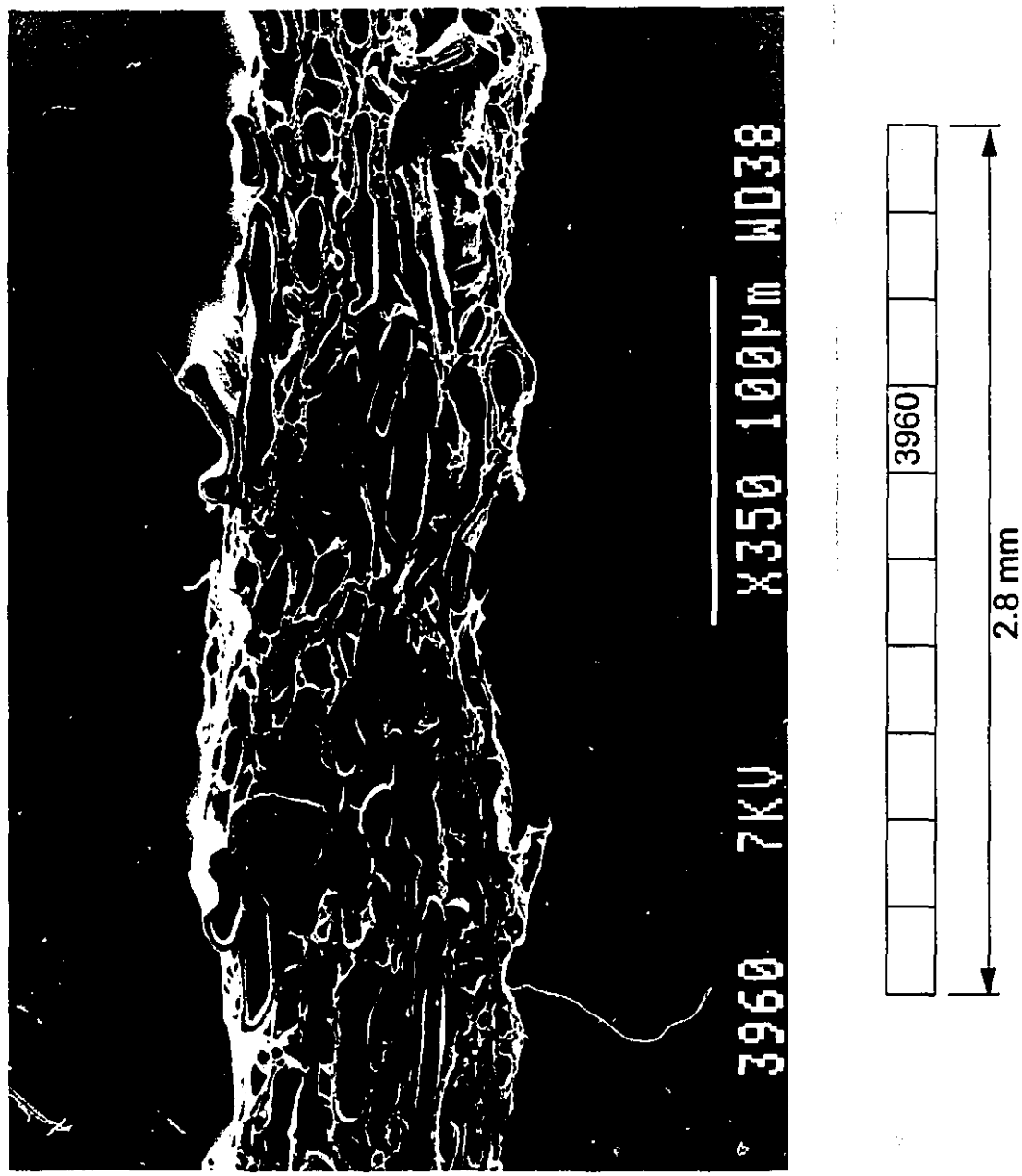

Figure 5.21 Lightly calendered sheet. Section plane in CD; magnification 500X.

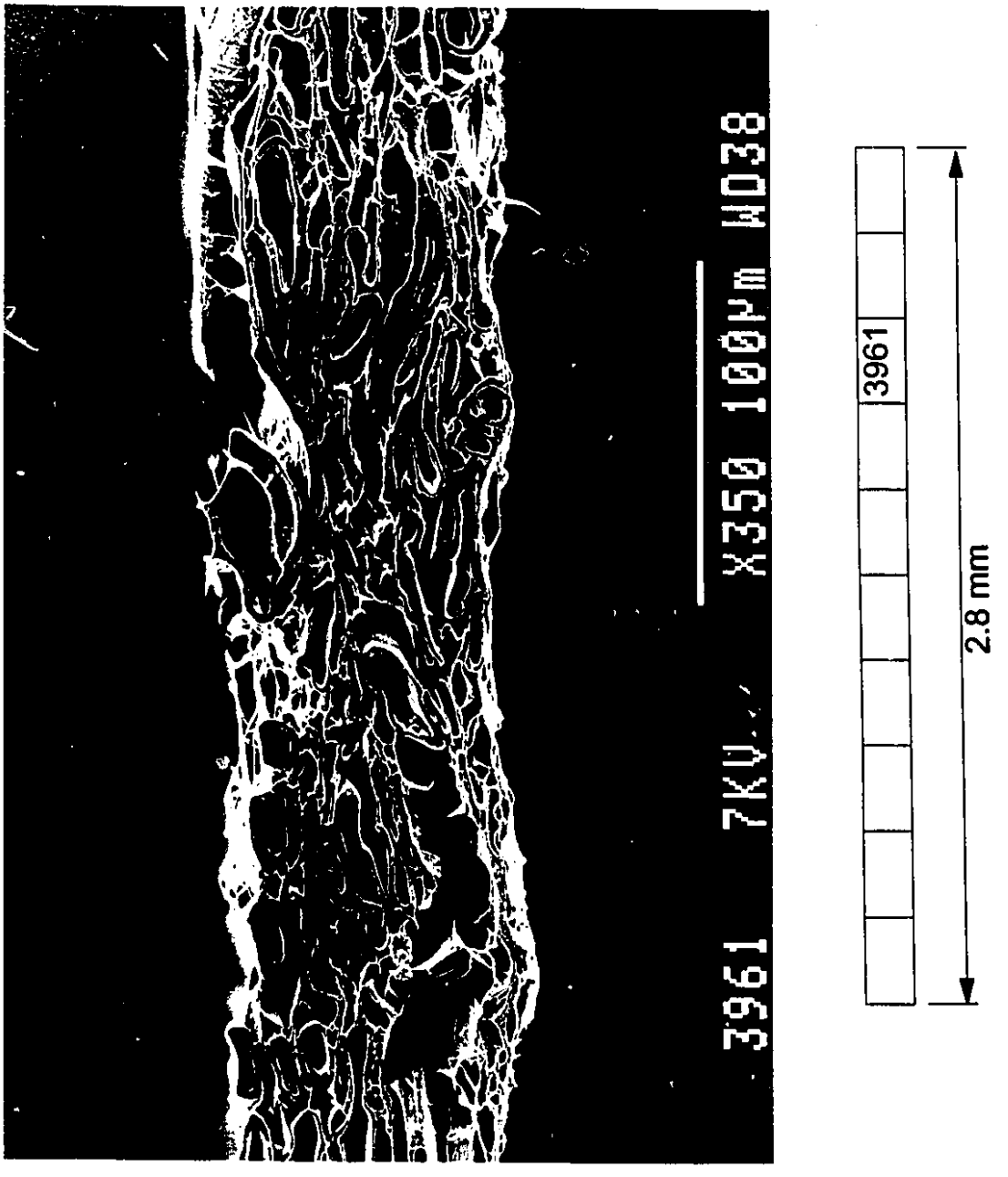

Figure 5.22 Lightly calendered sheet. Section plane in CD; magnification 500X.

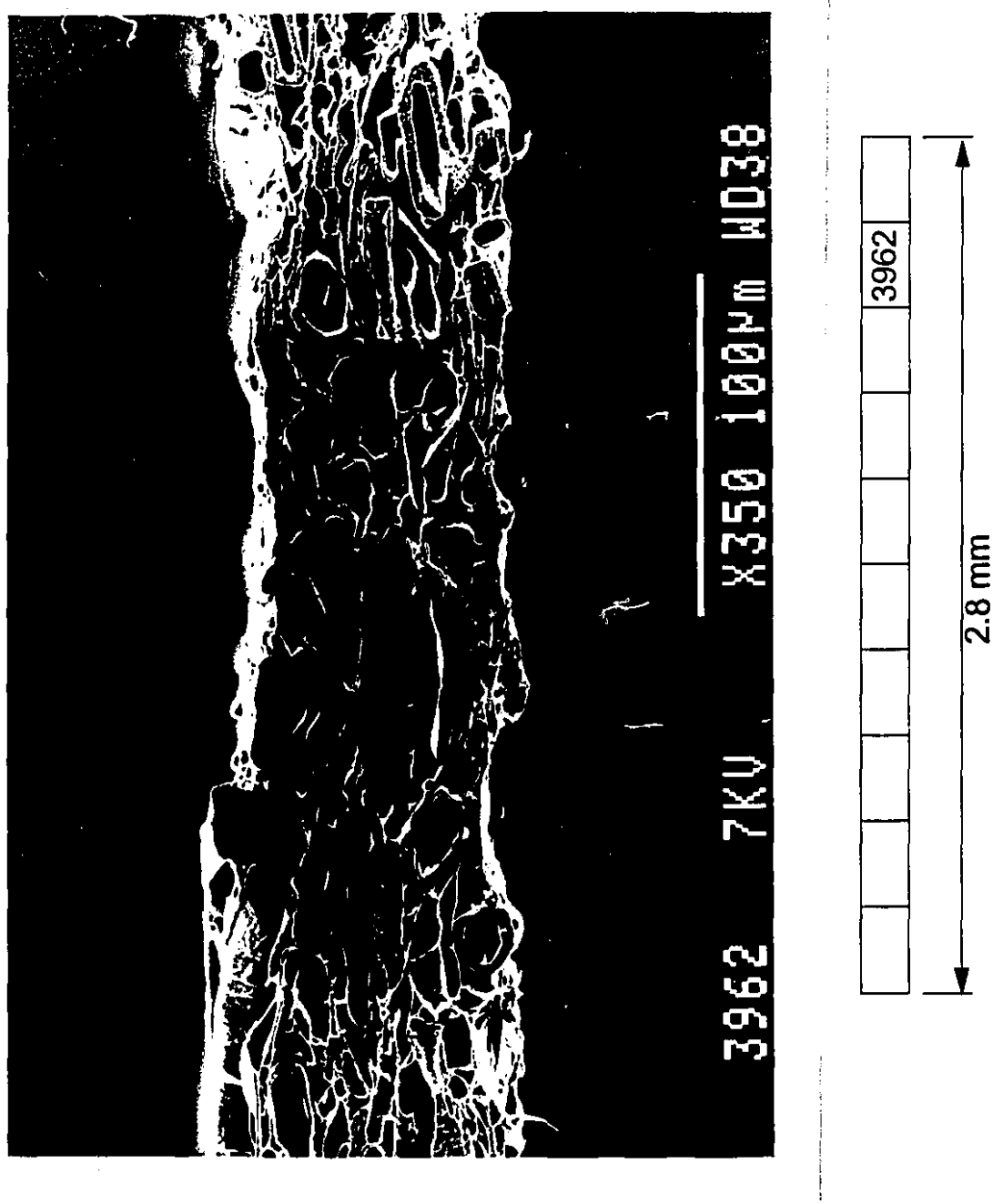

Figure 5.23 Lightly calendered sheet. Section plane in CD; magnification 500X.

outer wall. Taken to its extreme, this type of damage is similar to the broken fibres seen in Figures 5.12 and 5.19.

Results of local pressure variations are even more evident in Figures 5.24 to 5.29, which are sections of heavily calendered paper. Sheet speed was 304 m/min, and load was 206 kN/m. Average in-nip strain reached 0.65, at which point the average fibre content by volume was over 70% and the average thickness was 42 μm. At this high average strain, which far exceeds industrially relevant conditions, all but the pores which were originally the widest would have been collapsed in the nip. Locally thick or dense areas would have seen much higher pressures, and in places the fibre content may have approached 100% by volume. Average permanent strain in this case is 0.33, and the average fibre content after calendering is 37% by volume.

Figures 5.24 and 5.25 illustrate the large number of damaged fibres in this heavily calendered sheet. In Figure 5.24, there are two large fibres to the lower left which are damaged: one fractured internally and one broken. To the right there are several fibres with internal fractures or breaks in the fibre wall, in particular a round one at the lower right which has several fractures on the inner side of the wall at the top. There are several other internal fractures in these six micrographs, but only a few external fractures; one may be seen in Figure 5.26 at the sheet mid-plane and to the right. Another fibre showing both internal and external fractures along with delamination of the inner wall may be seen in Figure 5.27, lying on top of the sheet to the right of centre.

The variability in paper density is well illustrated in Figures 5.28 and 5.29. A large dense area to the right of 5.28, which is continued at the left of 5.29, has supported the calendering load in the nip and the fibres have been severely deformed, while large coarse fibres in adjacent low-density areas to the left of 5.28 and right of 5.29 have seen much less deformation and thus little damage. The locally low in-nip pressure occuring in these bulky areas must be offset by correspondingly high local pressure in dense areas, implying that some fibres will have experienced extremely high pressure in the nip even when the CD average line load is low.

The conclusion to be drawn from these micrographs is that substantial local

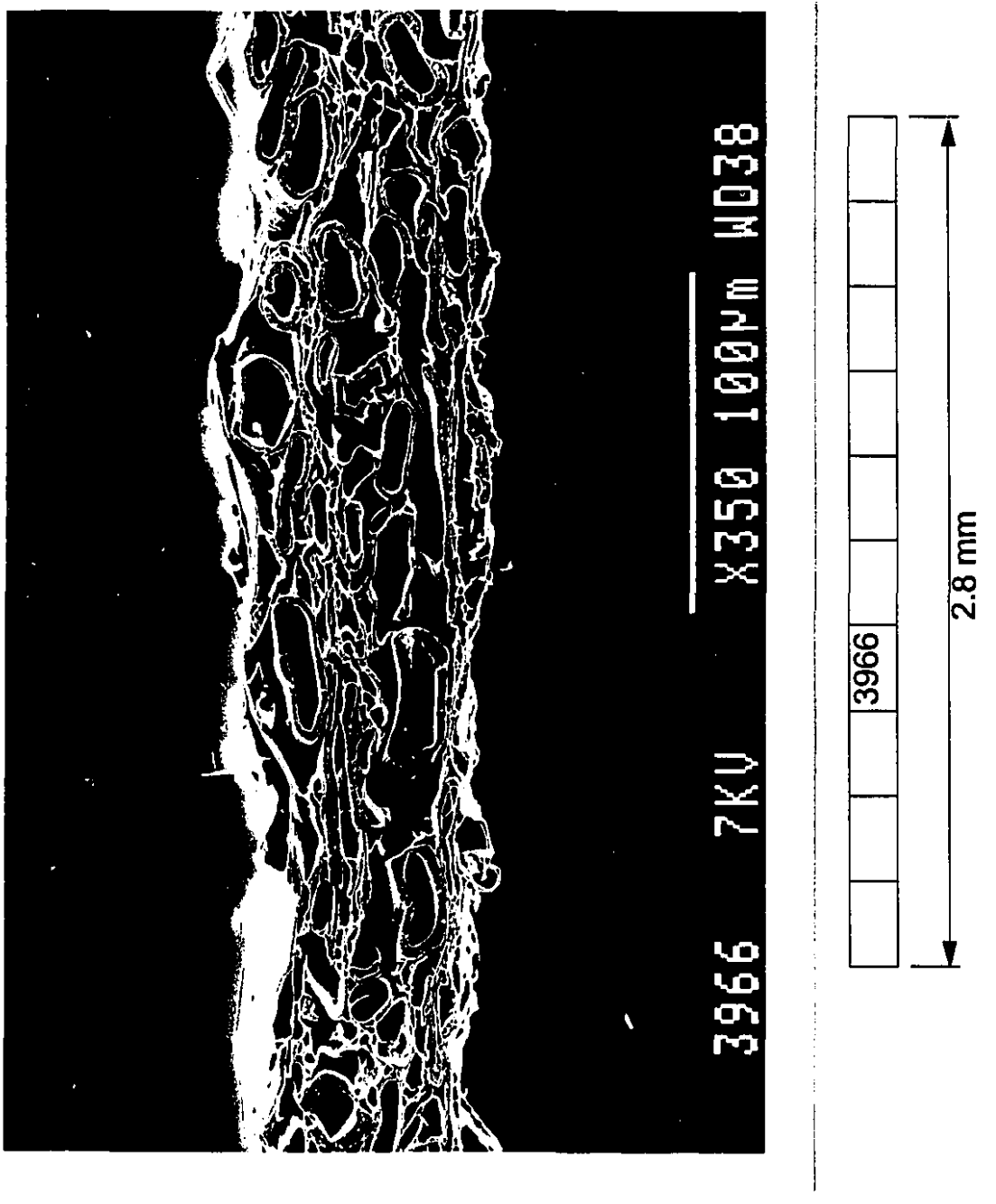

Figure 5.24 Heavily calendered sheet. Section plane in CD; magnification 500X.

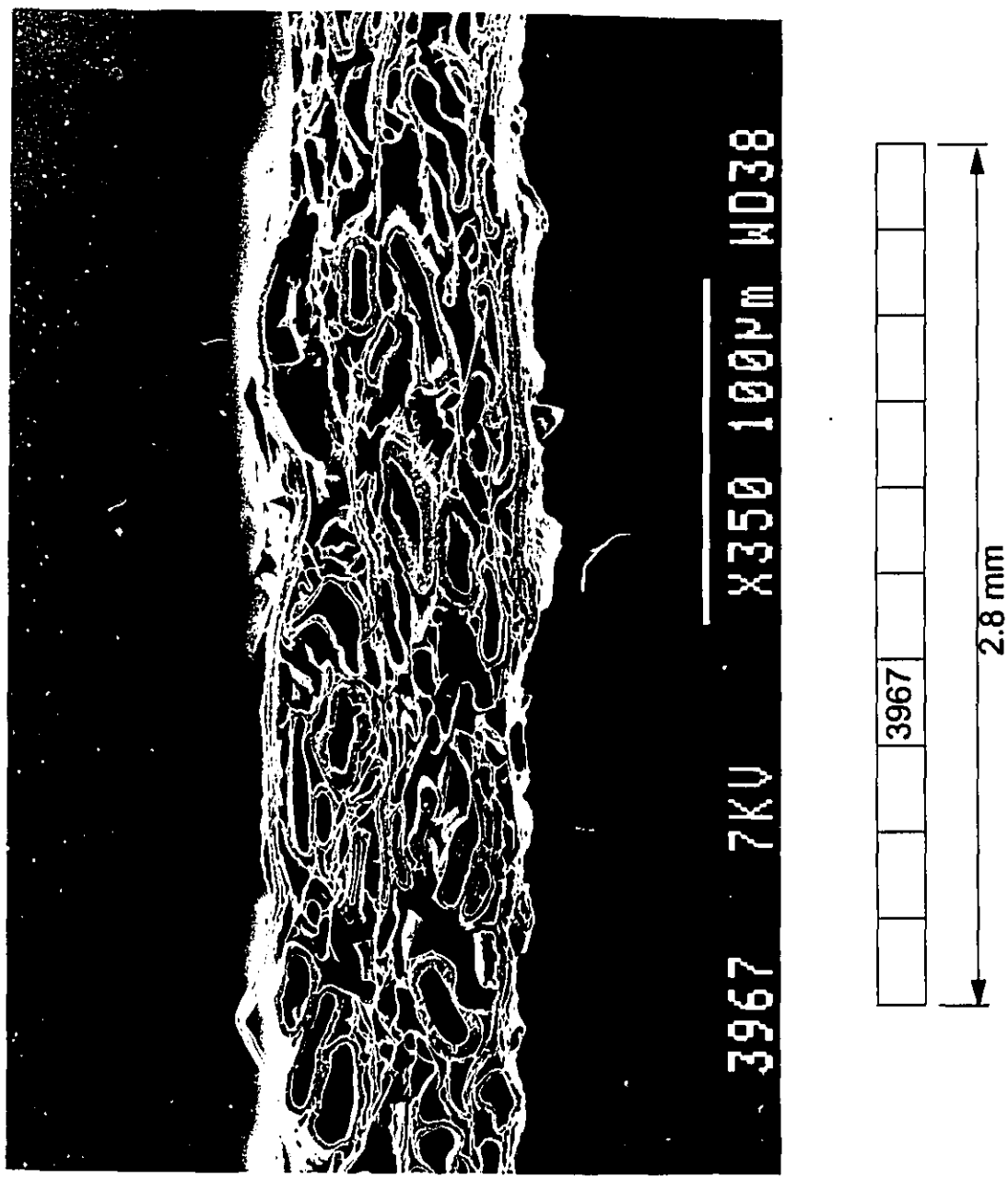

Figure 5.25 Heavily calendered sheet. Section plane in CD; magnification 500X.

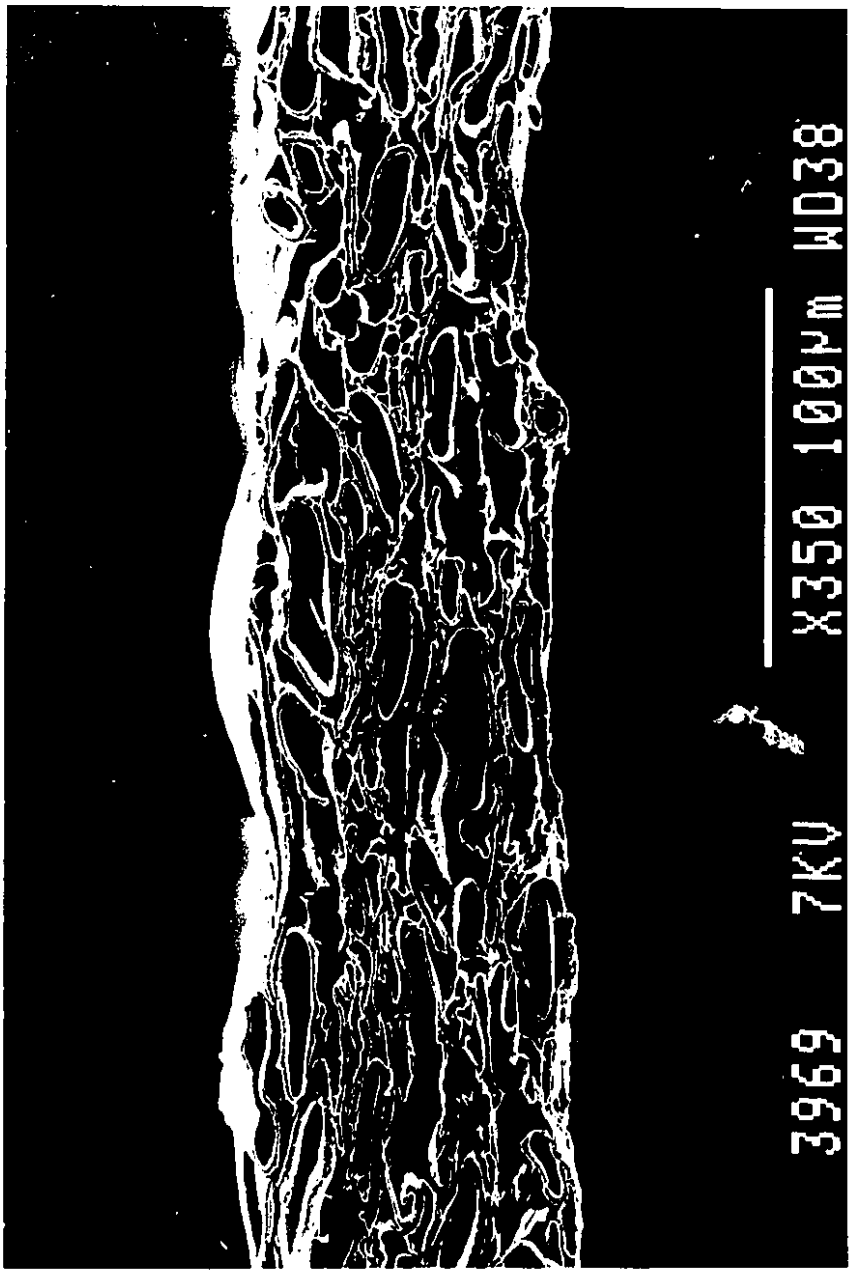

Figure 5.26 Heavily calendered sheet. Section plane in CD; magnification 500X.

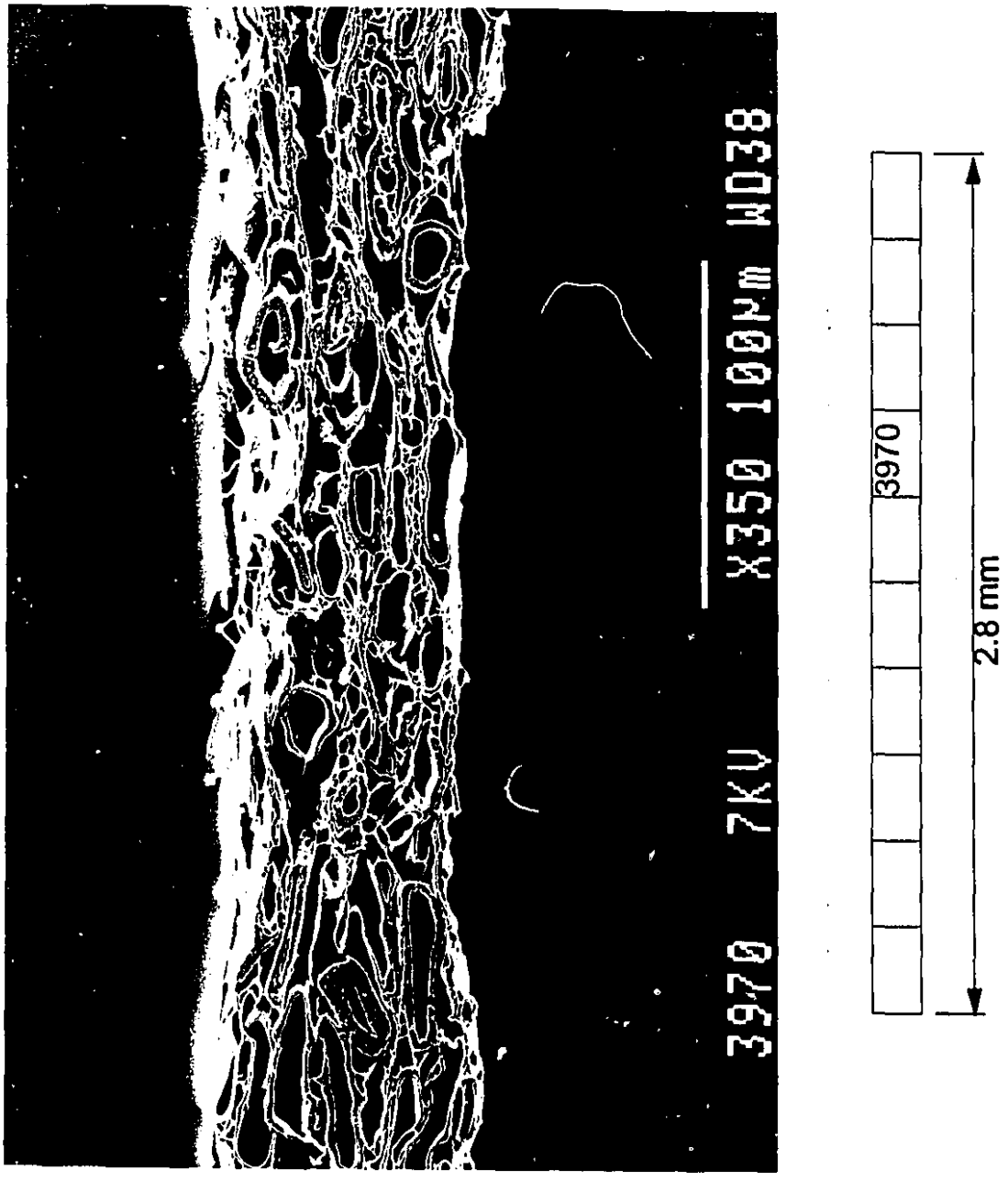

Figure 5.27 Heavily calendered sheet. Section plane in CD; magnification 500X.

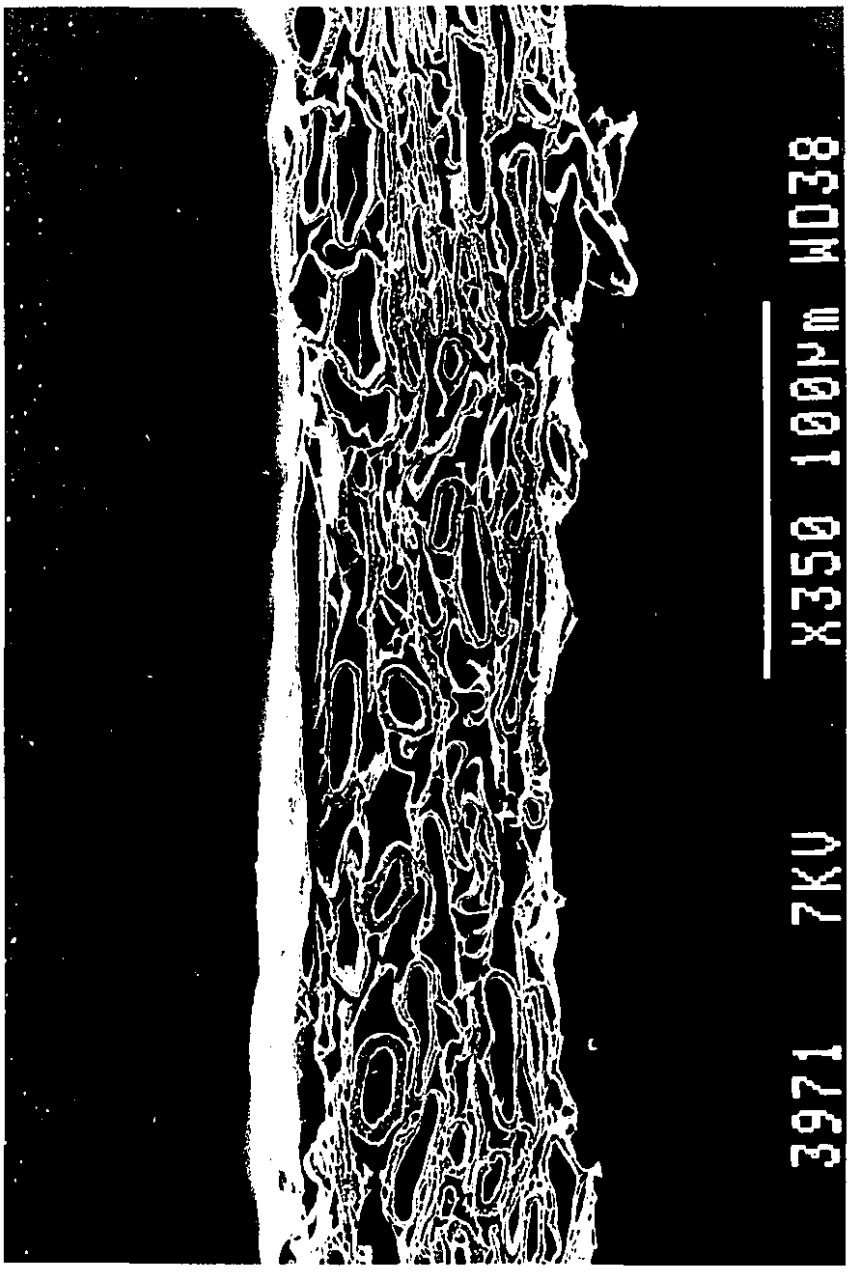

Figure 5.28 Heavily calendered sheet. Section plane in CD; magnification 500X.

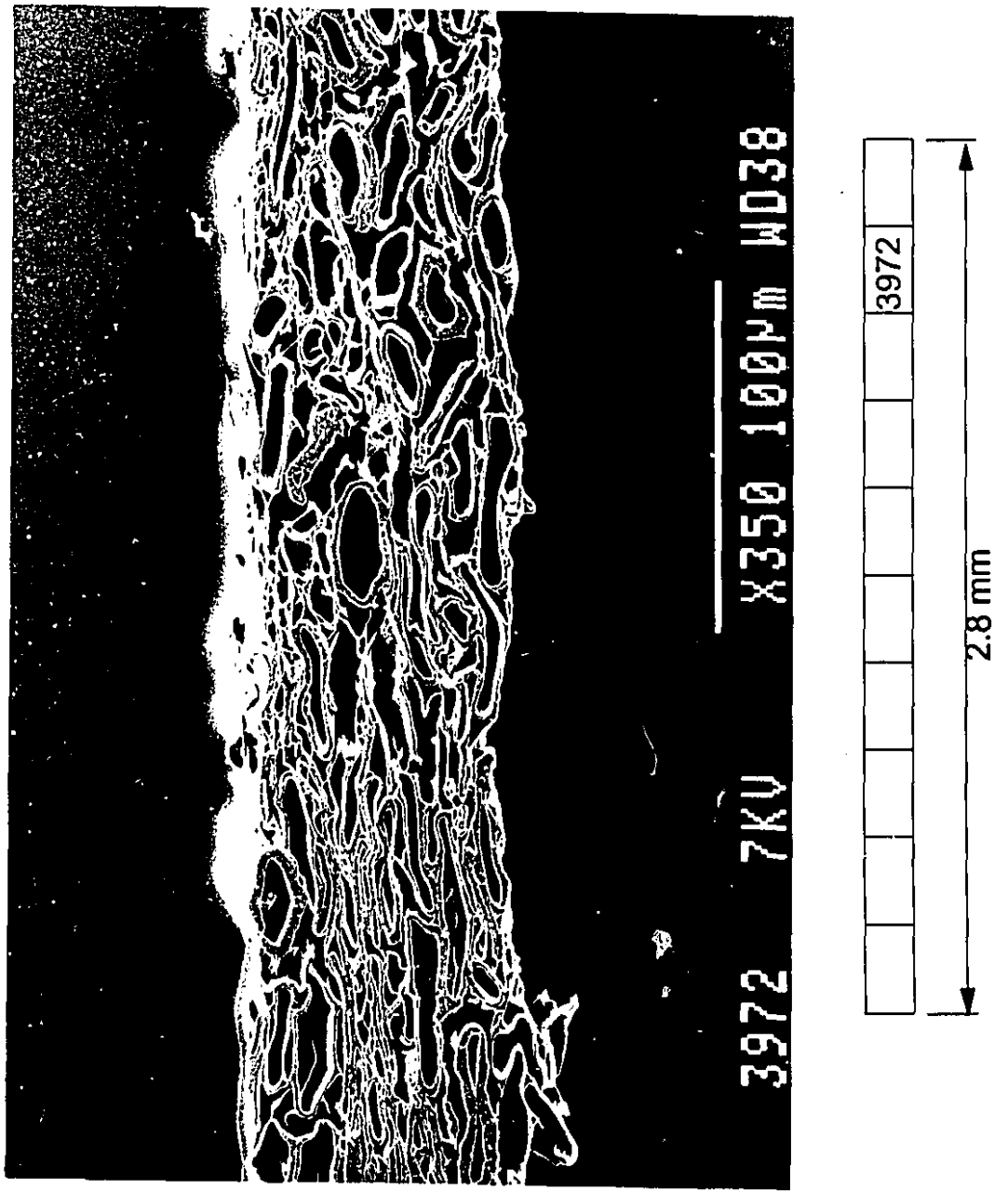

Figure 5.29 Heavily calendered sheet. Section plane in CD; magnification 500X.

nonuniformities in both thickness and density before calendering are a major factor in pressure distribution in both the MD and CD. Denser areas with in-plane dimensions in the range of a few fibre thicknesses will support the entire load through a hard nip, so that local in-nip pressure on the sheet varies substantially over distances as little as 100 μm even when the roughness level is small. Added to the effect of roughness discussed in Section 5.3.2, and of a substantially shorter nip as suggested in Chapter 4, the result is that peak pressures locally can far exceed average values estimated from nip lengths and line loads.

In order to investigate the effect of earlier processing steps on fibre flexibility and paper response to a calender pulse, similar micrographs were taken of a machine-formed fully bleached kraft paper containing a mix of soft and hardwood fibres. The paper also contained a significant amount of filler. One sample was pressed in a hand sheet press to about 7 MPa, while a second sample was pressed to about 40 MPa. Pressing times, about 0.5 s, were long compared to typical calendering dwell times, about 0.5 ms. A third sample was not pressed. All three samples came from the same 300 mm square sheet. Details of the physical properties are given in Table 5.4.

As with the TMP samples, Figures 5.30 to 5.35 show selected micrographs taken from three continuous strips of ten photos, one strip from each pressing condition. Each strip covers a total distance of about 2.8 mm. The sheet is initially much denser, with less local thickness and density nonuniformities than for the TMP paper. Most fibres have already collapsed and show little or no lumen. Very few obviously damaged fibres are seen in Figures 5.30 and 5.31. At higher pressures, Figures 5.32 to 5.35, the sheet becomes significantly more compacted as the more flexible kraft fibres deform more readily, but there is still little sign of fibre damage such as delamination or fracture. Fibre processing as it affects flexibility is thus an important factor in paper behaviour in a calender.

Qualitatively, the micrographs show that compression of TMP paper is a two-step process, as suggested by Rodal [73]: there is an initial settling of the network and deformation of slender, flexible earlywood fibres, followed by permanent deformation

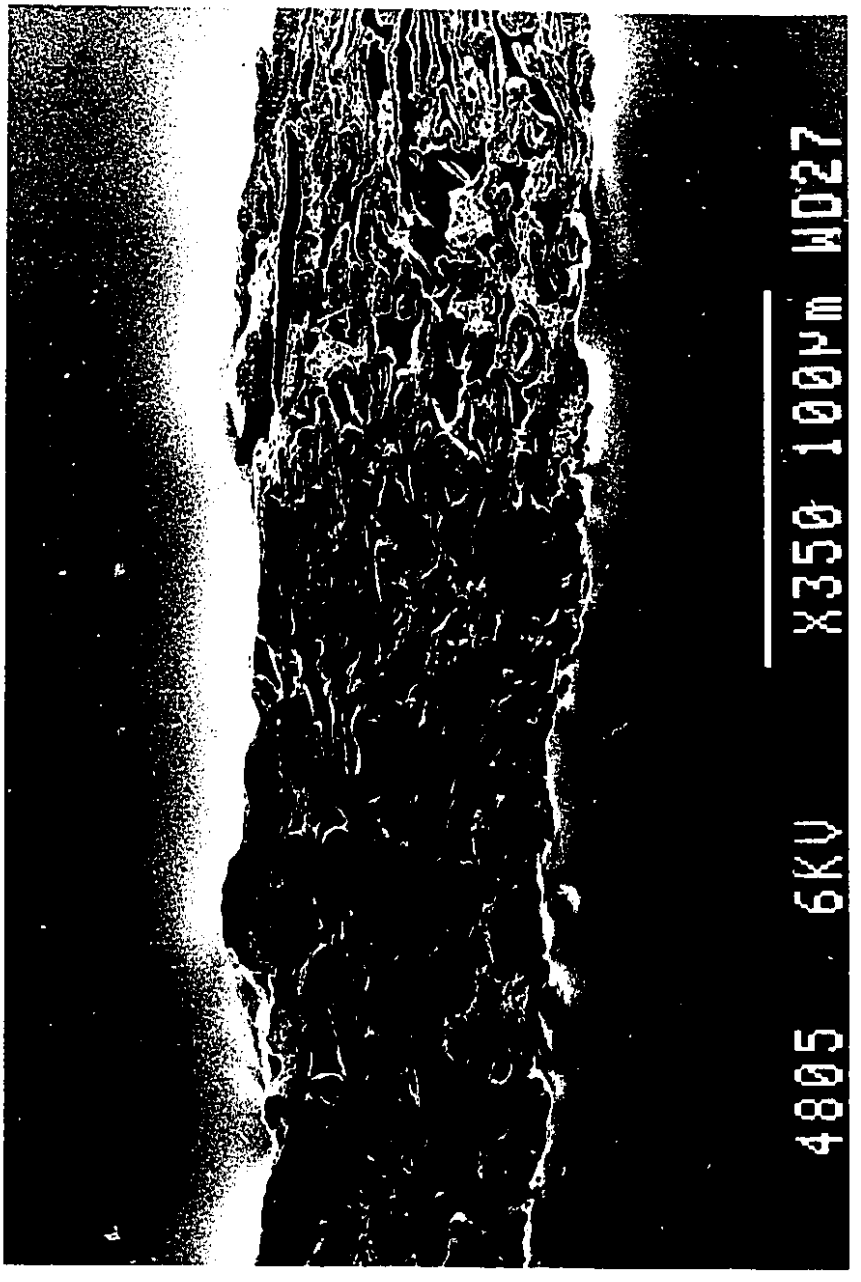

Figure 5.30 Kraft sheet, no pressing. Magnification 500X

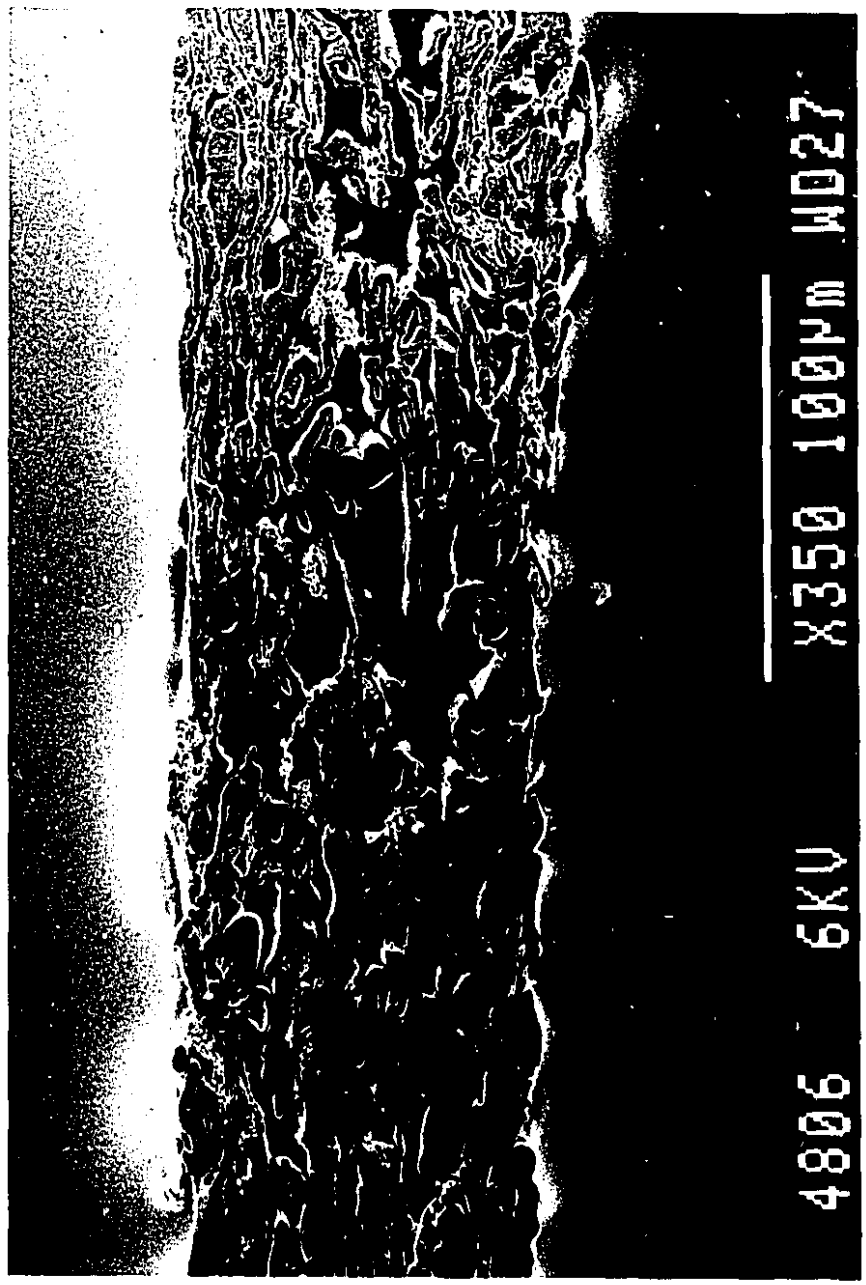

Figure 5.31 Kraft sheet, no pressing. Magnification 500X

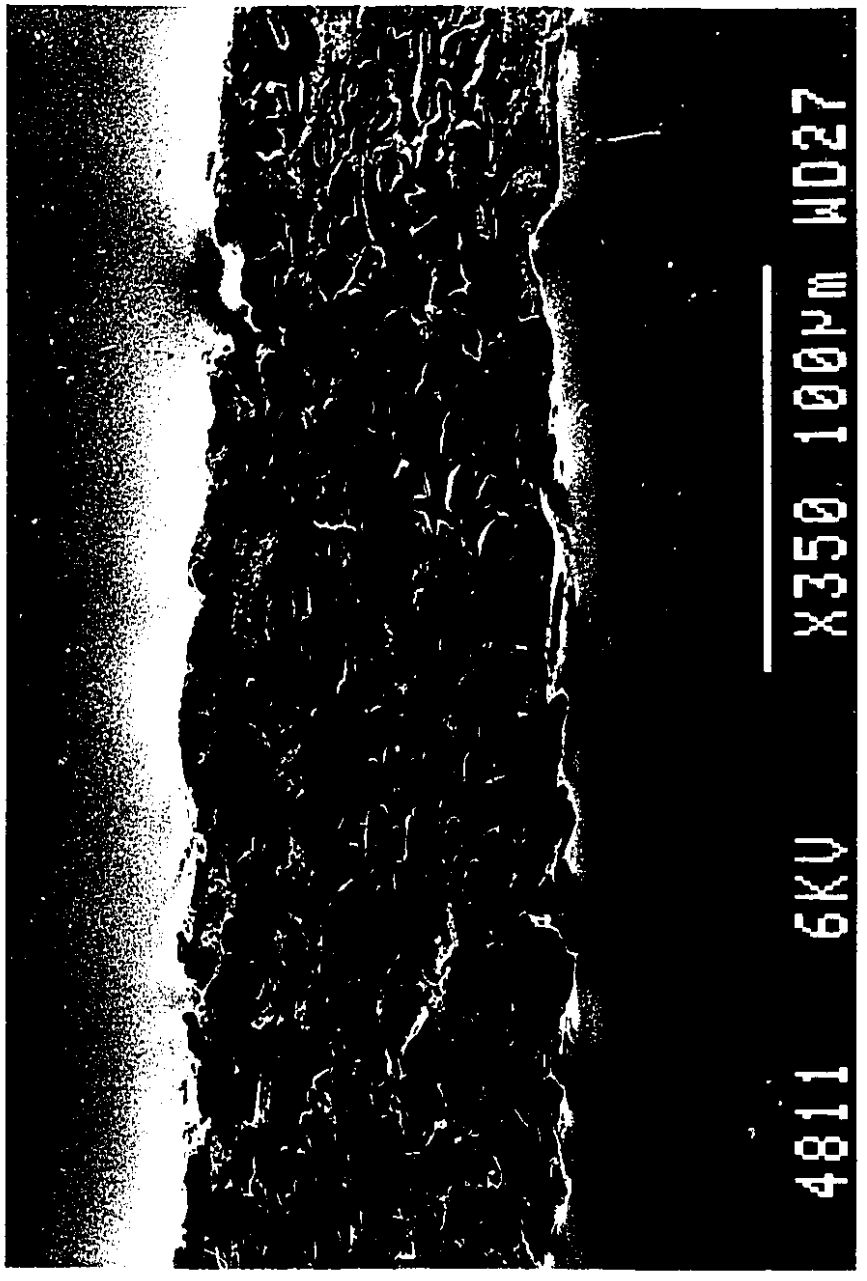

Figure 5.32 Kraft sheet, pressed at 7 MPa. Magnification 500X

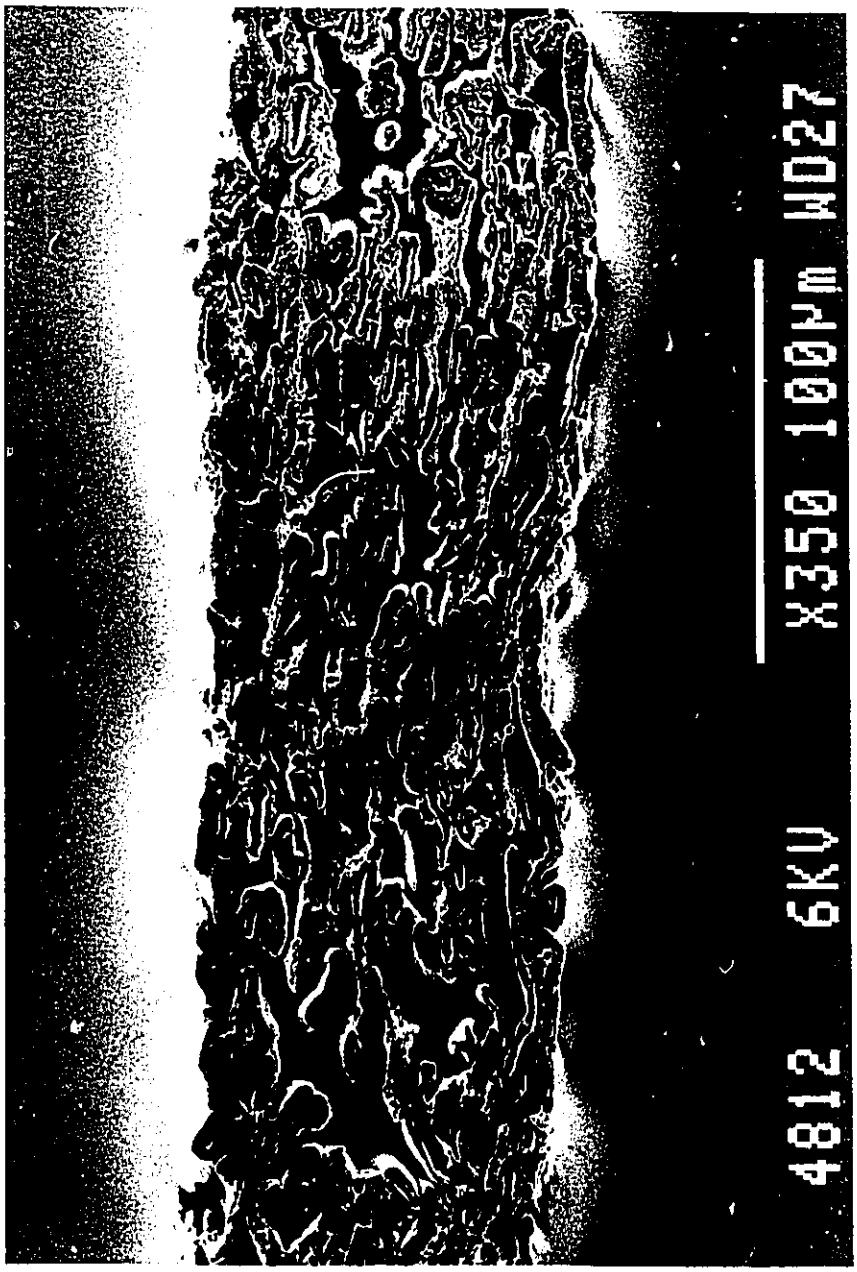

Figure 5.33 Kraft sheet, pressed at 7 MPa. Magnification 500X

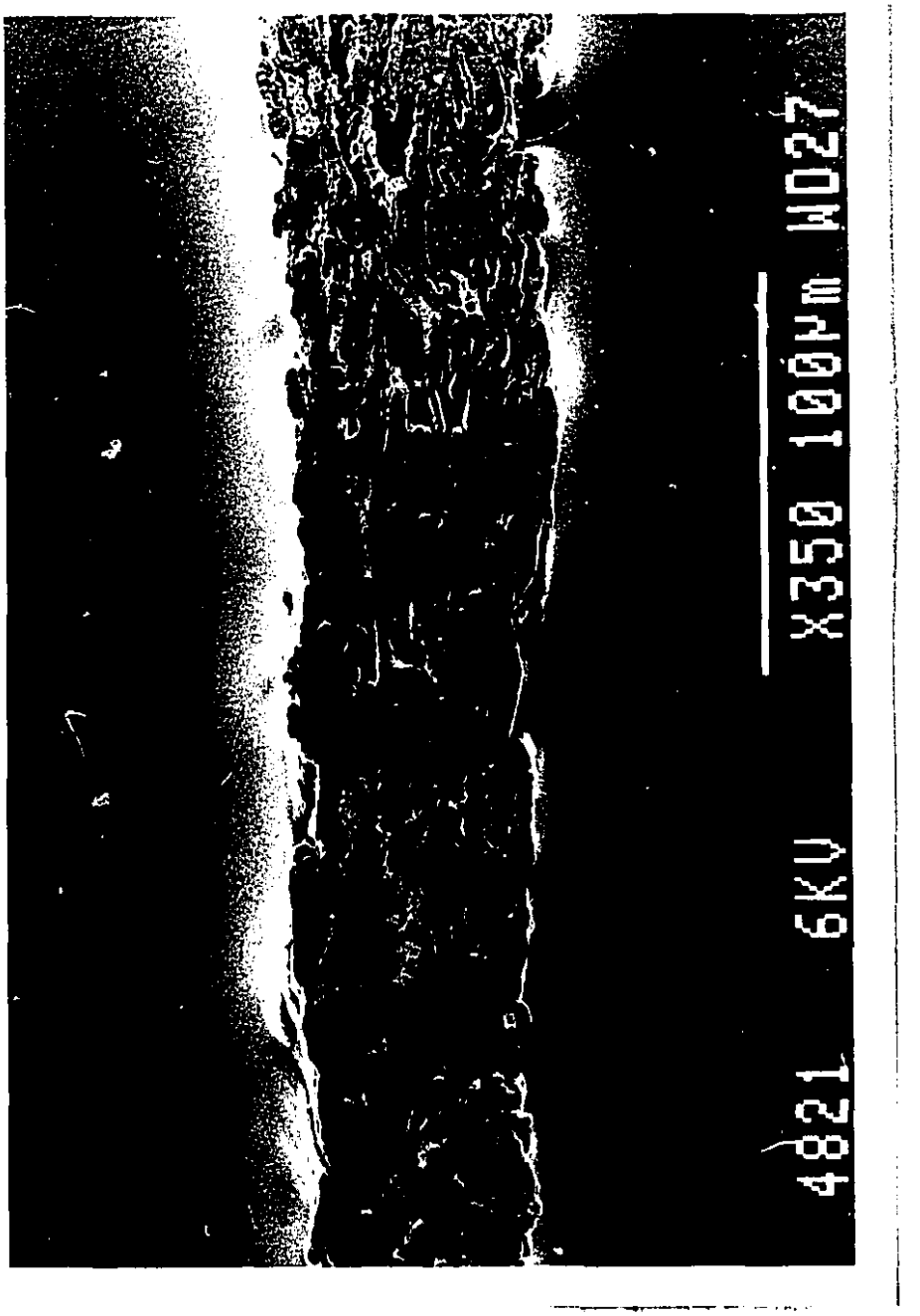

Figure 5.34 Kraft sheet, pressed at 40 MPa. Magnification 500X

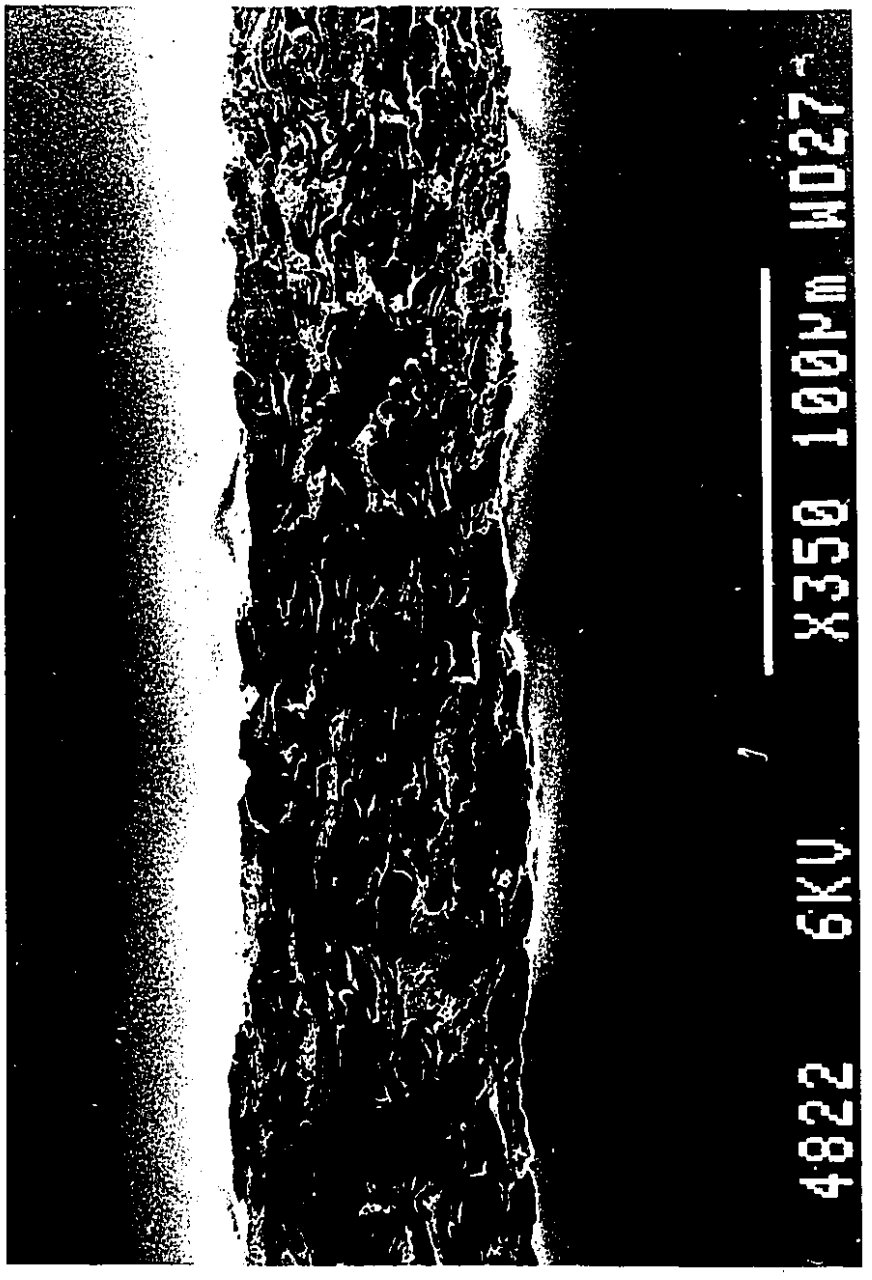

Figure 5.35 Kraft sheet, pressed at 40 MPa. Magnification 500X

of flexible fibres and crushing of stiffer latewood fibres. Kraft fibres are much more flexible and easily deformed, making the sheet easier to calender.

TABLE 5.4: Properties for kraft paper samples in Figures 5.30 to 5.35.

Basis weight	68.5 g/m^2
Bulk	1.5g/cm^3
Caliper	102 μm
Filler	13.5%

It was suggested in Section 5.3.2 that a linear viscoelastic model incorporating a statistical description of surface roughness might be adequate to describe paper behaviour in a calender nip. It has been shown in this section that while a method of incorporating the effect of surface roughness may be neccessary, this is not sufficient for modeling paper in a calender nip. Additional probability functions describing local nonuniformity of density and thickness are also necessary. Thicker areas will experience higher strains, and dense spots will be harder to compress; at the very least the elastic moduli G_i will thus be functions of density. In the limit, each individual fibre could be modelled using a single Burger's model. However, several problems arise with this approach. First is the large variation in fibre wall thickness and flexibility, implying that each model would have its own viscoelastic parameters. Second, the fracture behaviour seen in the more brittle fibres represents a sudden change in behaviour which is not easily modeled using simple linear models. Finally, assembling fibres in a three-dimensional pattern does not create a sheet unless the bonds joining the fibres are also modeled. While there exists (or will soon exist) sufficient computing power to accomplish this modeling task using iterative numerical methods, there appears insufficient justification at this time to expend the effort.

In conclusion, the assumptions of smoothness and homogeneity used in Section 5.2.2 are clearly invalid when the material is paper. The violation of these assumptions should be expected to cause non-linearities, as were indeed observed in the results of the linear viscoelastic modeling.

5.3.4 Fibre fracture and strength losses in calendering TMP

Calendering reduces the bulk, roughness and thickness variations in the sheet. These improvements are generally obtained at the expense of reduced strength properties. Charles and Waterhouse [16] measured the effect of supercalendering on strength properties such as breaking length and tear for several types of paper. They found that while densification by wet pressing improved these properties and reduced their anisotropic nature, densification by supercalendering had the reverse effect. They suggest that since wet pressing increases bonding, these results implicate bond failure as a major source of the observed strength loss. Similarly, Shallhorn [74] noted a reduction in effective fibre length when calendering kraft sheets. Effective fibre length is obtained by assuming the number of bonds per unit fibre length and the average strength of a bond are constants; since true fibre length is not decreased in calendering, the number or the quality of the bonds anchoring the fibre in the sheet must be reduced.

Gratton et al. [31] performed a series of strength measurements on food board made from a kraft pulp and calendered at various conditions. Their highest calender load was 100 kN/m, resulting in a permanent bulk reduction of about 0.26. At this loading condition, they reported decreases in MD and CD breaking strength, elastic modulus and in-plane compressive strength in the range of 10% to 15%. Stretch at break was increased by 10% in the CD and by 15% in the MD. Strength reductions when calendering recycled newsprint were also reported by Gratton [32]. Most strength properties were reduced slightly when permanent strains of up to about 0.25 were imposed, but dropped quickly at higher strains. For an uncalendered machine-made paper which was then recycled and made into handsheets, burst and tensile indices were reduced by only 3% and 5%, respectively, when the handsheet was calendered to ε_p = 0.25; however, the indices were reduced by 30% and 43%, respectively, at ε_p = 0.36. Similarly, tear index and specific Young's modulus were reduced by 15% and 33% at ε_p = 0.25, while both were reduced by 43% at ε_p = 0.36. Zero-span breaking length was unaffected by calendering when the paper entering the recycling stage was

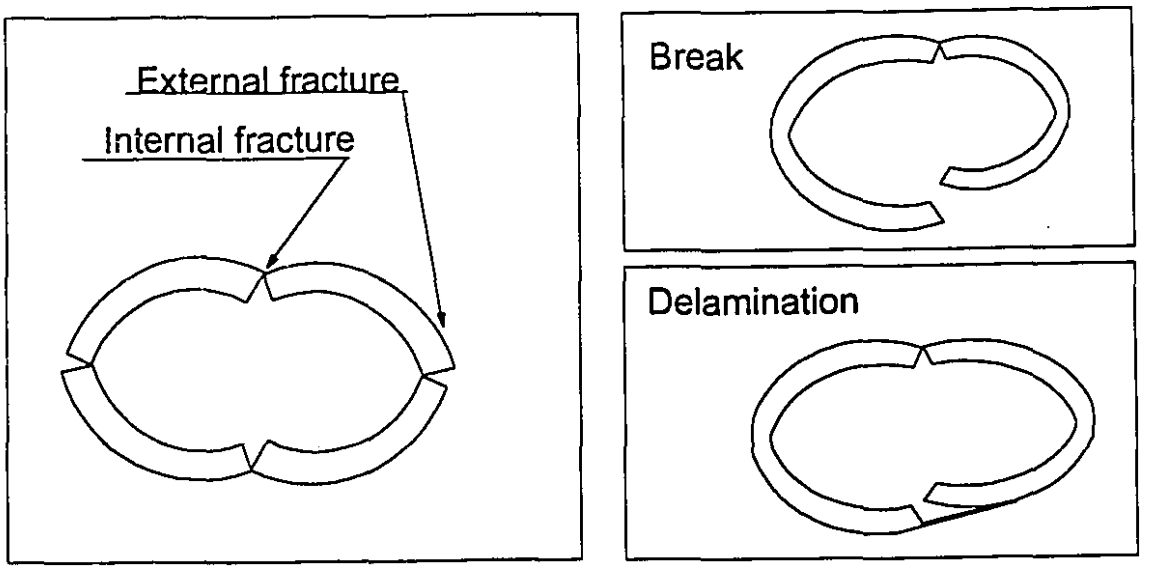

Figure 5.36 Types of fibre damage

uncalendered. Since zero-span is related to the axial tensile strength of an individual fibre, fibre fractures oriented along the axis of the fibre as seen in the micrographs of Figures 5.18 to 5.29 would not reduce the zero-span length unless the fibre were oriented at an angle to the direction of the applied stress.

Crotogino [21] published data showing conventionally calendered newsprint suffers strength losses of 20% to 25% when calendered to $\varepsilon_p = 0.23$, increasing to 30% to 48% at $\varepsilon_p = 0.34$. Strength losses for a given bulk reduction were lower when the newsprint was calendered using the temperature gradient technique, where the relatively cool sheet encounters a hot roll in the nip; the sheet is not wrapped around the roll and there is therefore no heat transfer to the sheet from the roll before the nip. The result is higher fibre flexibility and increased fibre deformation at the surface due to the elevated temperature, improving the smoothness and gloss with less bulk reduction. The cooler, stiffer, more brittle fibres in the centre of the sheet are not strained as highly since the more ductile surface fibres deform more readily, thus leading to less damage to the body of the sheet and increased strength properties.

The micrographs presented in the previous section illustrate two quite different

TABLE 5.5: Number of damaged fibres at different calendering conditions

	Uncalendered	Low intensity	High intensity
Internal fractures	7	7	12
External fractures	0	1	3
Delaminations	1	4	1
Breaks	4	1	6

deformation mechanisms: plastic, or ductile deformation of thinner-walled fibres, and fracture, or brittle deformation of coarser, stiffer fibres. Under more severe calendering conditions, the evidence of Figures 5.18 to 5.29 suggests that fracture is increasingly common. In order to quantify the fibre damage identified in Section 5.3.3, the complete set of micrographs was examined to obtain a count of fibres that had experienced different types of damage. Whole, damaged fibres (as opposed to small pieces of fibre) were subdivided into the four types illustrated in Figure 5.36, internal fracture, external fracture, delamination and breakage. The total number of micrographs taken for a given calendering condition covered a CD length of about 2.8 mm, or, given the initial thickness of about 120 μm, a sectional area before calendering of about 0.33 mm^2. Results are given in Table 5.5 and Figure 5.37. As the sample size is small, the results should be interpreted with caution. Nonetheless, the four types of damage appear to be due to two different processing steps, each imposing a different type of load on individual fibres.

Page [63], Page and De Grâce [64] and McIntosh [55], among others, have shown that delamination occurs in refining and beating processes, where the fibre encounters shearing forces. In extreme cases of delamination, the type of axial break illustrated in Figure 5.36 can occur. As seen in Figure 5.37, the number of delaminated fibres in the

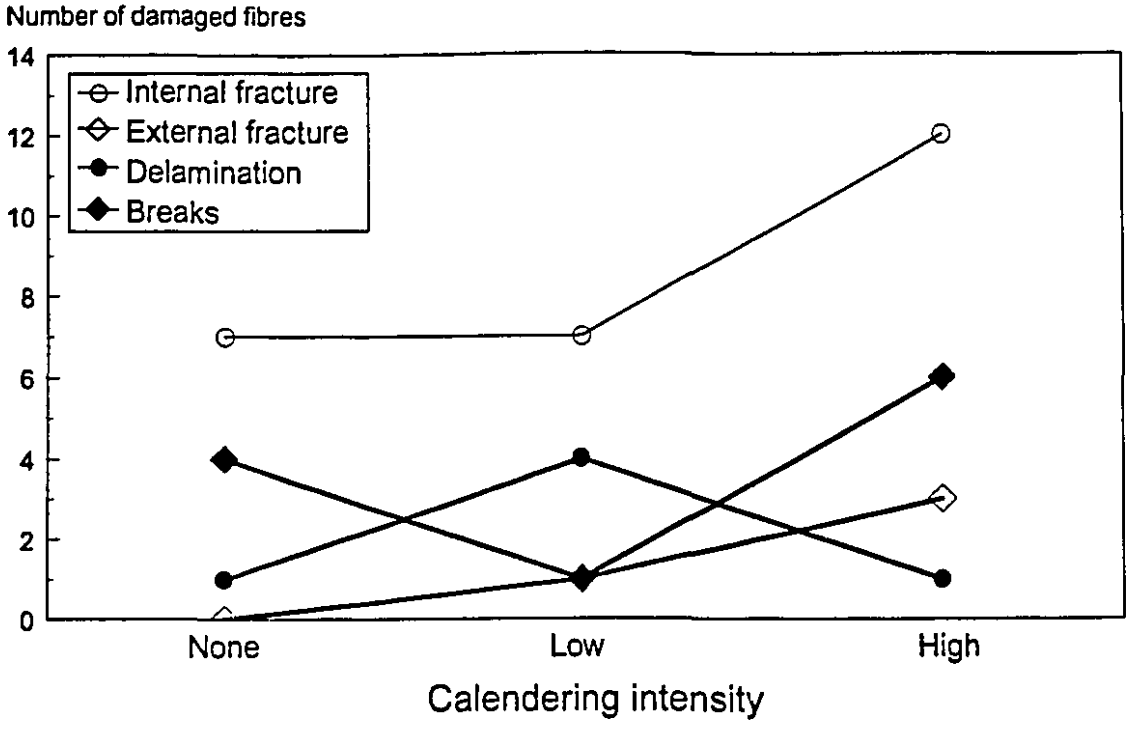

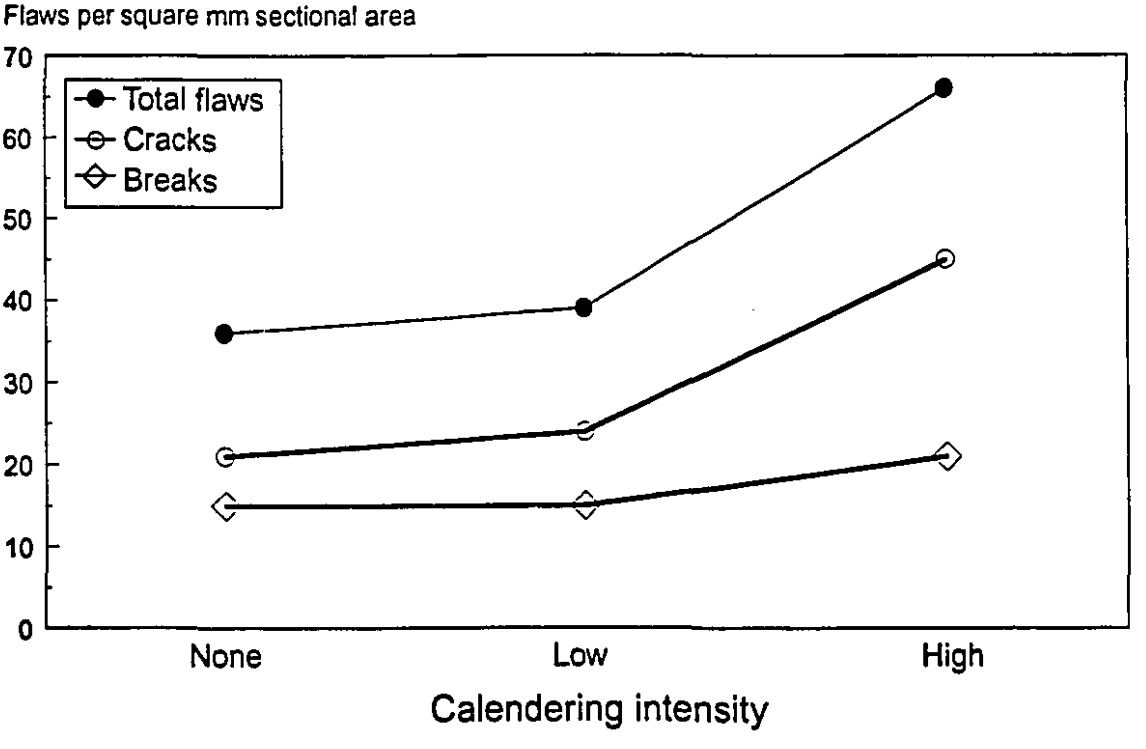

Figure 5.37 Damaged fibres as a function of calendering intensity.

TABLE 5.6: Effect of load condition on number of damaged fibres.

	Uncalendered	Low intensity	High intensity
Compression-damaged	7	8	15
Shear-damaged	5	5	7

samples obtained in this study increases from 1 to 4, then decreases to 1 as calendering intensity is increased. Similarly the number of broken fibres decreases at first from 4 to 1, then increases to 6. These values imply that the average number of fibres which are either delaminated or broken is essentially constant, at 2.0 and 3.7 per 0.33 mm^2 respectively, and that the standard deviations for these measurements are about 1.7 and 2.5. The sum of these shear-deformed fibres thus increases slightly from 5 to 7, as shown in Table 5.6. If this total is assumed unaffected by calendering then the micrographs display an average of 5.7 shear-deformed fibres with a standard deviation of 1.2. As the increase is not statistically significant, this type of damage is not attributable to the calendering process.

Fracture, on the other hand, can be attributed to tensile failure of the fibre wall caused by compressive loads. A wood fibre is itself a structure consisting of smaller fibrous strands called fibrils. The relatively low number of external fractures in all sheets can be explained by considering the fibril angle of a typical fibre. In the thicker, inner wall of the fibre, the fibrils are aligned at a small angle to the fibre centreline, while the thinner, external wall has the fibrils wound at a larger angle to the fibre centreline, as illustrated in Figure 5.38. A compressive stress on a cylindrical element, Figure 5.39, would be expected to generate tensile stresses perpendicular to the load at the inner wall at the top and bottom, and at the outer wall parallel to the load. An isotropic material would thus be as likely to fracture at the outer wall as at the inner. The data in Table 5.5 imply that this is not the case for paper, as the number of external fractures is con-

sistently smaller than the number of internal fractures. However, a tensile stress on the inside of the fibre tends to separate fibrils, while externally the stresses are much more closely aligned with the axis of the fibrils. Thus tensile stresses in the outer wall act to stretch individual fibrils, pulling with the grain of the outer wall, while internal fractures are caused by tensile stresses pulling at right angles to the grain of the inner wall. The result is a greater likelihood of internal fracture due to anisotropic strength properties. The positions of most of the fractures seen in the micrographs are consistent with this theory: most internal fractures are on the top or bottom of the fibre, as seen in both cases in Figure 5.39, while the few external fractures are in the plane of the sheet as seen in the anisotropic case. This effect is also seen in micro-photographs published by Williams et al. [81], where internal fibre fractures oriented in the plane of the sheet appear to be more frequent in TMP after calendering.

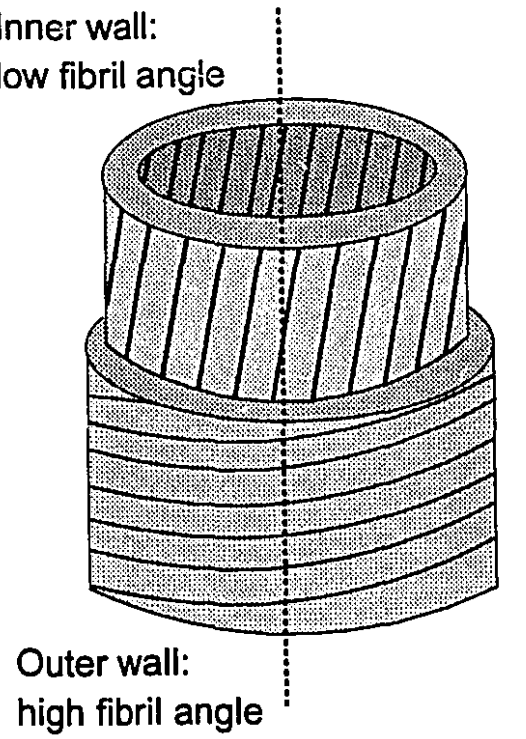

Figure 5.38 Typical fibril structure.

The standard deviation estimated for the total number of compression-damaged fibres may be assumed to be similar to that of the shear-damaged fibres, at 1.16. The total number of compression-damaged fibres increases from 7 to 15 as calendering intensity increases, a significant change given the estimated standard deviation. The type and frequency of the fractures is therefore consistent with the compressive loading experienced by the fibres. Compression fractures are much more numerous in a heavily calendered TMP paper than in an uncalendered sheet, and are extremely infrequent in kraft sheets due to the increased flexibility of the fibres.

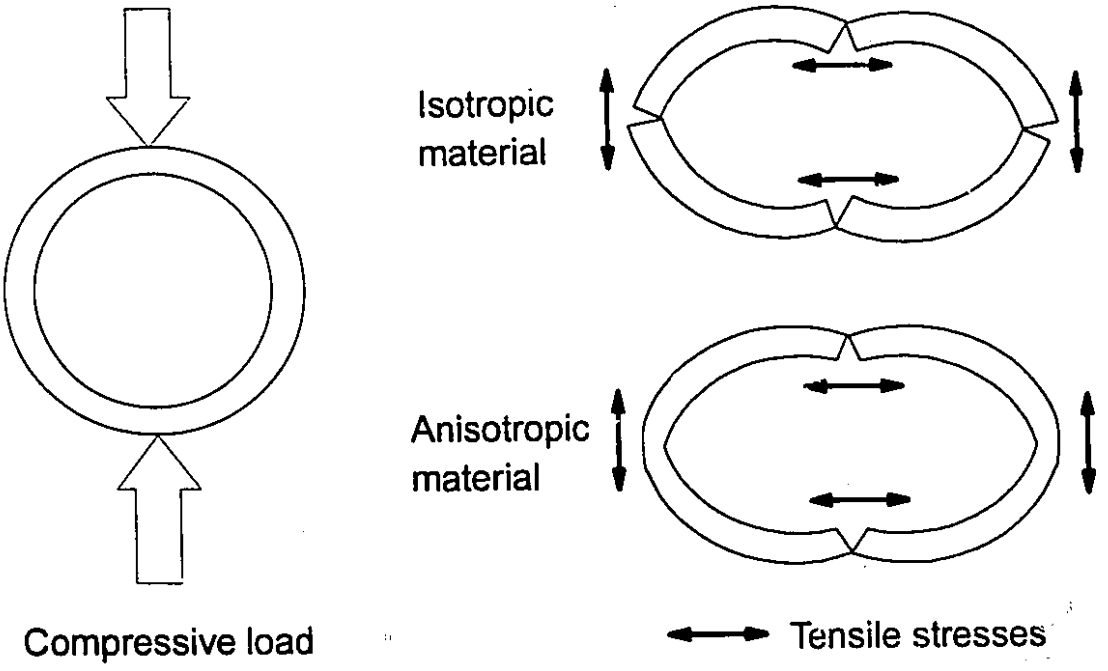

Figure 5.39 Tensile failure in isotropic and anisotropic cylinders loaded in compression.

The observed increase in fibre fracture in the calendered TMP paper is also consistent with observed strength losses. While internal fibre fracture contributes to a general weakening of the fibre network by providing a place for the initiation of a larger crack in the sheet, bond weakening or failure as a contributing factor is not eliminated. When a dense spot is compressed, fibres bordering a less dense area will tend to be displaced sideways in the plane of the sheet, putting shear forces on bonds. These forces in turn weaken or break bonds, creating further weak spots for the initiation of a crack when the sheet is loaded in tension. Unfortunately this type of failure is not visible in the photomicrographs presented here, and so the relative magnitude of the two effects cannot now be estimated. The fact that kraft sheets also lose strength but without the fibre damage seen in the TMP samples suggests that bond failure plays a significant part; nonetheless fibres damaged in the nip can only weaken the structure and must therefore play a part in the well-documented strength reduction in calendered paper.

5.4 Conclusions

Paper behaviour in a calender nip is far more complex than can be adequately described in a linear viscoelastic model. Paper exhibits significant local nonuniformities in structure and material properties over widely different scales. Sheet formation problems result in the presence of flocs with typical dimensions of a centimetre. At a resolution in the range of a millimetre, there are local nonuniformities in both thickness and density. On a smaller scale, of the order of 100 μm, there are variations in fibre coarseness which cause the effective compressive elastic modulus of the sheet to vary substantially as the sheet is stressed. Finally, at the micrometre level, the variation in fibril angle from the outside to the inside of the fibre, along with variations in fibre coarseness, cause different fibres to react differently to an applied stress: some will collapse and deform while others will fracture, mirroring the ductile vs. brittle failure of metals. All of these effects result in pressure profiles which are highly nonuniform over very small distances in a calender nip, resulting in material behaviour which also varies substantially over the same small distances.

Linear viscoelastic modeling is therefore inadequate for predicting the large deformations found in a calender nip. Paper behaviour in compression is related to fibre properties, which can vary substantially in mechanical pulps, and the distribution of the fibres within the sheet. As characteristic dimensions describing the fibre distribution may be similar to typical nip lengths, the objective of relating the coefficients of the empirical relations described in Chapter 4 to more fundamental parameters describing fibre properties and paper structure was not achieved.

The evidence obtained from photomicrographs of sheet cross-sections indicates that fibre fracture may play a significant role in the well-documented strength losses found in calendered papers. While it is likely that a large part of these strength losses are due to bond breakage, there is visual evidence that fibre fracture occurs more frequently as loads are increased, reaching a peak under extreme calendering conditions of several broken fibres every millimetre along the sheet. This damage to the fibres undoubtedly

contributes to the general strength losses noted in heavily calendered sheets, although the magnitude of the contribution is not known.

6. Conclusions

6.1 Summary

Paper is calendered to reduce its surface roughness, thus improving the printing properties, and to minimize thickness variations from place to place in the sheet, thus improving the printability of the sheet in modern high-speed printing presses: the process improves the quality of the finished product.

To reduce thickness variations in the cross-machine direction, improved control methods are necessary. One of the problems in CD calender control is the delay between the implemention of a control action and the material response. CD control is usually implemented using localized heating or cooling of the roll, altering the local roll radius and thus the local load; the delay is due to the large thermal inertia of a typical calender roll, resulting in a long response time. As a result of this response time, which may be as large as 10 to 20 minutes [41, 42], control systems using feedback methods may require excessively long times to settle if a reasonable estimate of paper response to a control action is not available. A typical 10 metre wide machine running at 1000 m/min will produce almost 30 tonnes per hour of 48 g/m^2 newsprint; if the control system requires 20 minutes to arrive at 95% of the target variation, almost 10 tonnes of substandard paper will have been made. To improve the response of the control system, there are two possibilities: reduce the response time by reducing roll thermal inertia, or improve the effectiveness of the control action by improving the estimate of the material response to a control input. Reducing the thermal inertia of a calender roll is limited by the necessity of maintaining roll resistance to bending and other mechanical considerations.

The present work shows that it is possible to improve the estimate of paper response to a control action. This improved estimate will allow the use of control algorithms using feedforward methods, thus eliminating the possibility of a control action overshooting the target. As described in Section 4.2.3, an empirical relationship between CD local permanent strain ε_p and CD local in-nip strain ε_n was obtained from the present

experimental data. This relationship will facilitate design of a complete cross-direction control system for paper strain leaving a calender. Once future work has elucidated the bulk and furnish dependencies, the in-nip strain existing at any CD position can be estimated given the permanent strain measured at that same position. Thick or thin streaks require higher or lower permanent strains; from this new permanent strain the required new local in-nip strain can be estimated. The difference between current and required in-nip strains gives explicitly the required local roll shape. With knowledge of the roll response to an actuator input, determined by a previous study in this laboratory, the thermal energy required to obtain the desired roll profile and thus effect the required change in permanent strain can be calculated.

The primary goal of this thesis, clarifying the material response to an actuator input, has thus been attained.

The relationship between load and strain has also been described qualitatively in terms of paper and fibre properties such as specific volume and fibre coarseness. This results in a better understanding of paper behaviour subjected to compressive loads. At very low loads the structure is deformed and thin-walled, flexible fibres collapse; if the load is removed there is very little permanent strain as most of the deformation is recovered. If the load is increased permanent deformation in both the structure and the more flexible fibres begins to occur, while coarser fibres tend to fracture. The limiting density in the nip, which was approached in this study, is close to the accepted value for fibre density while the limiting density after recovery is somewhat less, implying that within the range of loads examined here there is always some recoverable strain.

Thus the second goal of this project, an improved understanding of paper structure and properties, has also been attained.

Finally, viscoelastic modeling methods were used in an attempt to relate the coefficients of the empirical results to paper and fibre properties. Parameters for two linear viscoelastic models were estimated from the data and were found to be functions of the processing parameters. It is concluded that in calendering under typical industrial conditions, the stress-strain behaviour of paper cannot be described using linear

viscoelastic methods. The assumptions of continuum mechanics do not apply to paper, which is a rough, structured material made up of hollow fibres with a wide range of coarseness and flexibility. As well, irreversible damage to fibres and bonds occurs in calendering; modeling this type of behaviour is beyond the scope of simple stress-strain relationships. Thus linear viscoelastic methods are inadequate for describing paper compression in a calender nip, and no simple relationship exists between the coefficients of the various empirical results and more fundamental paper and fibre properties.

6.2 Contributions to knowledge

The present work made contributions in three distinct categories. In the experimental part of the work, empirical relationships describing unique in-nip strain measurements were presented which will be of use in the design of improved control systems. Secondly, the potential for the use of linear viscoelastic modeling methods to describe the behaviour of paper in a calender nip was determined. Finally, analysis of the microstructure of different types of paper subjected to different calendering conditions provided an improved understanding of the interaction between the calendering process and paper and fibre structure.

Contributions pertaining to improved control systems are:

1. Equations relating local CD paper strain in the nip of a calender to local CD load have been obtained from experimental measurements;

2. A relationship between in-nip and permanent strain which can be used to estimate local CD in-nip strain given local CD permanent strain has been obtained from experimental measurements; this relationship, describing the material response to an actuator input, is the missing link in a complete CD calender control model;

3. There is evidence that the outgoing nip length is small compared to the ingoing length, implying that average or peak pressures in the nip may be higher than current estimates;

4. The nip length corresponding to full contact is significantly shorter than the calculated length when paper roughness is as little as 5% of sheet thickness, again implying nip pressures are higher than current estimates;

5. The effects of points 3 and 4 being additive, current methods for estimating in-nip pressures appear to produce results which are unrealistically low;

6. Machine direction stretch is small compared to typical z-

direction strain, which can be understood by considering fibre bending and flattening as the sheet enters the nip;

7. Kerekes' prediction for a_R has been verified.

The viscoelastic modeling of the experimental measurements led to the following contributions:

8. Paper thickness recovers exponentially on leaving a calender nip; the recovery can be described for typical industrial speeds using a time constant of 10 to 30 ms;

9. The instantaneous elastic response to a calendering pulse is small, verifying previous experimental work;

10. The total recoverable strain approaches a constant at higher loads, implying the existence of two mechanisms in paper compression: delayed elasticity and partial permanent deformation;

11. As a result of points 8, 9 and 10, paper behaviour in a calender nip may be described as viscoelastic;

12. Constitutive equations for two linear viscoelastic models were derived for the strain history imposed in a calender. Both models were fitted to the data; the Burger's model described observed behaviour significantly better than did the standard linear liquid;

13. Initial estimates of parameters for the Burger's model reproduce predicted and measured pressure profiles, but are functions of calendering conditions;

14. As a result of points 11 and 13, paper behaviour may be concluded to be non-linear viscoelastic; the most likely reason for the non-linear behaviour is that the assumptions of continuum mechanics are not applicable to paper.

The analysis of the effect of fibre and paper structure on the calendering process,

and of the process on the properties, produces the following contributions:

15. Paper compressibility is a strong function of void fraction;

16. Local nonuniformity of thickness, density and fibre coarseness can be substantial, causing correspondingly large local nonuniformity in the pressure pulse applied to the sheet;

17. Internal and external fibre fracture is more common in calendered than uncalendered sheets, and is seen mainly in sheets made from TMP. Sheets made from a fully bleached kraft exhibit very little fracture;

18. Delaminated and broken fibres are no more common in calendered sheets than in uncalendered sheets, and do not appear in significant numbers in kraft sheets;

19. As a result of points 17 and 18, delamination and breakage is probably attributable to shear stresses in the refiner, and fracture to compressive stresses in the calender;

20. There appear to be two types of fibre fracture, with internal fracture more frequent than external fracture; this finding was related to the variation of fibril angle from layer to layer in the fibre wall;

21. As a result of points 17, 18, 19 and 20, it is concluded that fibre fracture plays a role in strength losses when calendering paper made from TMP, although the relative magnitude of the mechanisms of fibre fracture and bond breakage in strength losses cannot yet be estimated.

6.3 Suggestions for future study

The present work has also raised new questions.

The various empirical stress-strain relationships, whether in-nip or permanent, and whether based on the master creep equation of Colley and Peel or the calendering equation of Crotogino, are functions of paper bulk. Linear relationships between strain and initial bulk are poor approximations to reality. An improved description of the bulk dependency of paper strain in a calender would improve the predictive ability of the various relationships when used successively for multiple nips. Experimentally, difficulties arise due to the narrow range of bulk (1.5 to 3.0 cm^3/g) compared to the large range of load and roll radius commonly used in industry. In the case of the in-nip calendering equations, the dependency of strain on web temperature and moisture content also needs to be investigated.

Pulp type is another variable whose effect on in-nip strain has not been investigated. Kraft papers are more easily calendered than those from TMP, since kraft pulp fibres are more flexible; whether this effect will carry over to the in-nip case remains to be seen, although there is no obvious reason to suspect otherwise.

Fibre fracture and bond failure have both been suggested as causes for the strength reduction in calendered TMP paper. While the role of bond failure cannot be assessed from the data, the evidence presented here suggests that when TMP is calendered, fracture occurs frequently and is a likely cause of weaker tensile, tear and other strength measurements. However, the present evidence is based on a very small number of micrographs. The relationships between calendering intensity and number of fibre fractures, and number of fibre fractures and strength loss should be investigated in a systematic fashion.

Linear viscoelastic models are inadequate for describing paper compression in a calender nip. Alternative non-linear methods developped to describe shear in a polymer melt are not suited to the structured nature of paper. Other methods of describing paper strain in a calender might involve defining the pressure pulse in terms of an impulse

function, and representing paper and fibre structure using either statistical or fractal methods. The applicability of the modeling might be improved by developing methods for measuring the pressure pulse and nip length in a hard nip, much as Keller has done in a soft nip.

The development of better empirical or viscoelastic models for local CD strain both in the nip and after is of immediate use to industry only if these relationships are used to design better control systems. Development of a complete CD calender control algorithm using feedforward methods is the next step in improving the quality of newsprint made from TMP. In the longer term, a better understanding of paper structure and properties will have benefits which cannot presently be estimated.

References

1. ACTON, F.S., "Numerical methods that work", Harper and Row, New York (1970).
2. ALBLAS, J.B., and KUIPERS, M., "The contact problem of a rigid cylinder rolling on a thin viscoelastic layer", Int. J. Engng. Sci. 8(5):363-380 (1970).
3. BAUMGARTEN, H.L., KEREKES, R.J., and PEEL, J.D., "Calendering and supercalendering: an appraisal of current practice, understanding and needs", Symposium on Calendering and Supercalendering, University of Manchester Institute of Science and Technology (UMIST) (1975).
4. BAUMGARTEN, H.L., "Changes of web dimensions during calendering and supercalendering", Symposium on Calendering and Supercalendering, University of Manchester Institute of Science and Technology (UMIST) (1975).
5. BAUMGARTEN, H.L., and GÖTTSCHING, L., "The influence of calendering parameters on the properties of paper grades, Symposium on Calendering and Supercalendering, University of Manchester Institute of Science and Technology (UMIST) (1975).
6. BENTLEY, J.M., and DERRICK, R.P., "Drive power requirements for paper machine calenders and reels", TAPPI Preliminary Report CA #4487, 1982 TAPPI Engineering Conference.
7. BOND, J.-F., CROTOGINO, R.H., VAN HEININGEN, A.R.P., and DOUGLAS, W.J.M., "An experimental study of the falling rate period of superheated steam impingement drying of paper", Drying Technol. 10(4):961-977 (1992).
8. BROWNE, T.C., "Design and construction of an experimental paper calender", M.Eng thesis, McGill University, Montreal, 1991.
9. BROWNE, T.C., CROTOGINO, R.H., and DOUGLAS, W.J.M., "An experimental calender for in-nip paper caliper measurements", J. Pulp Paper Science 19(2):J92-96 (1992).
10. BUSH, A.W., "Contact mechanics", in "Rough surfaces", T.R. Thomas ed., Longman Group, Harlow, Essex, U.K. (1982).

11. CARINI, A., and De DONATO, O., "Fundamental solutions for linear viscoelastic continua", Int. J. Solids Struct. 29(23):2989-3009 (1992).

12. CASTAGNEDE, B., MARK, R.E., and SEO, Y.B., "New concepts and experimental implications in the description of the 3-D elasticity of paper. Part I: General considerations", J. Pulp Paper Science 15(5):J178-J182 (1989).

13. CASTAGNEDE, B., MARK, R.E., and SEO, Y.B., "New concepts and experimental implications in the description of the 3-D elasticity of paper. Part II: Experimental results", J. Pulp Paper Science 15(6):J201-J205 (1989).

14. CHAPMAN, S.M., "The measurement of printing smoothness", Pulp Paper Mag. Can. 48, 140 (1947).

15. CHAPMAN, D.L.T. and PEEL, J.D., "Calendering processes and the compressibility of paper (part 1)", Paper Technol. 10(2):T116-T124 (1969).

16. CHARLES, L.A. and WATERHOUSE, J., "The effect of supercalendering on the strength properties of paper", J. Pulp Paper Science 14(3):59-65 (1988).

17. COLLEY, J. and PEEL, J.D., "Calendering processes and the compressibility of paper (part 2)", Paper Technol. 13(5):T166-T173 (1972).

18. CROTOGINO, R.H., "Towards a comprehensive calendering equation", Trans. Tech. Sect. CPPA 6(4):TR89-TR94 (1980).

19. CROTOGINO, R.H., "Supercalendered and conventionally calendered newsprint - a comparison of surface and printing properties", TAPPI 63(11):101-105 (1980).

20. CROTOGINO, R.H., "Response of calendered newsprint to testing conditions", J. Pulp Paper Science 10(5):J126-J133 (1984).

21. CROTOGINO, R.H., "Temperature-gradient calendering of newsprint", TAPPI 65(10):97-101 (1982).

22. CROTOGINO, R.H., HUSSAIN, S.M. and McDONALD, J.D., "Mill application of the calendering equation", J. Pulp Paper Science 9(5):TR128-TR133 (1983).

23. CROTOGINO, R.H., GRATTON, M.F., and HAMEL, J., "A design procedure for machine calenders", presented at the 1988 TAPPI Finishing and Converting Conference, Richmond, Virginia (October 1988).

24. CROTOGINO, R.H., "Making a good impression", Pulp Paper Can. 90(7):T230-235 (July 1989).

25. CZYZ, J.A., and SZYSZKOWSKI, W., "An effective method for nonlinear viscoelastic structure analysis", Computers & Structures 37(5):637-646 (1990).

26. de MONTMORENCY, W.H., "The calendering of newsprint: a laboratory study of temperature and pressure effects", Pulp Paper Mag. Can. 68(7):T326-T345 (1967).

27. FINDLEY, W.N., LAI, J.L., and ONARAN, K., "Creep and relaxation of non-linear viscoelastic materials, with an introduction to linear viscoelastic behaviour", Dover Publications, New York (1976).

28. FLETCHER, R., "FORTRAN subroutines for minimization by Quasi-Newton methods", Report AERE R7125, Theoretical Physiscs Division, Atomic Energy Research Establishment, Harwell, Berkshire, England (1972).

29. GAY, J.P., RANTANEN, R., and NYKANEN, I., "A solution to calender sheet bubbling problems", Pulp Paper Can 94(2):T32-T35 (1993).

30. GIBSON, R.D., "The surface as a random process", in "Rough surfaces", T.R. Thomas ed., Longman Group, Harlow, Essex, U.K. (1982).

31. GRATTON, M.F., SETH, R.S., and CROTOGINO, R.H., "Temperature-gradient calendering of foodboard", TAPPI 71(1):81-86 (1988).

32. GRATTON, M.F., "The recycling potential of calendered newsprint fibres", J. Pulp Paper Science 18(6):J206-J215 (1992).

33. HAGLUND, L., "A profile model for a calender nip", Symposium on Calendering and Supercalendering, University of Manchester Institute of Science and Technology (UMIST) (1975).

34. HAGLUND, L. and ROBERTSON, G., "Local Thickness Reduction in a Calender Nip - An Experimental Study", Svensk Papperstidning 77(14):521-530 (1974).

35. HAMEL, J., CROTOGINO, R.H. and GRATTON, M.F., "Measurement of nip load distribution in calenders using uncalendered paper", J. Pulp Paper Science 18(1):17-23 (1992).

36. HUANG, N.C., and LEE, E.H., "Nonlinear viscoelasticity for short time ranges", J. Appl. Mech. Trans ASME 33(2): 313-321 (1966).

37. HUNTER, S.C., "The rolling contact of a rigid cylinder with a viscoelastic half-space", J. Appl. Mechanics Trans. ASME, 611-617 (1961).

38. IONIDES, G.N., MITCHELL, J.G, and CURZON, F.L., "A theoretical model of paper response to compression", Trans. Tech. Sect. CPPA 7(1):TR1-5 (1981).

39. JOHNSON, K.L., "Contact Mechanics", Cambridge University Press, Cambridge (1985).

40. JOHNSON, K.L., "One hundred years of Hertz contact", Proc. Instn. Mech. Engrs. 196, 363-378 (1982).

41. JOURNEAUX, I.A., "Impinging jet heat transfer and thermal deformation for rotating calender rolls", Ph.D. Thesis, McGill University (1990).

42. JOURNEAUX, I.A., CROTOGINO, R.H., and DOUGLAS, W.J.M., "Effect of actuator position on performance of a CD [Cross-machine Direction] calender control system: experimental study on a commercial calender", Pulp Paper Can. 93(1):42-46 (1992).

43. KELLER, S.F., "Measurement of the pressure-time profile in a rolling calender nip", J. Pulp Paper Science 18(1):J44-J48 (1992).

44. KEREKES, R.J., "Speed and loading effects in a calender nip", Trans. Tech. Sect. CPPA 2(3):TR88-TR91 (1976).

45. KEREKES, R.J., "Pressure distribution on a thin viscoelastic strip rolling between two rigid cylinders", Trans. CSME 4(1):27-32 (1976).

46. KEREKES, R.J. and PYE, I.T., "Newsprint calendering: an experimental comparison of temperature and loading effects", Pulp Paper Can 75(11):65-72 (1974).

47. KRENKEL, B., "Glätteerzeugung und Glättemessung", Wochenblatt fur Papierfabrikation 104(17):621-631 (1976).

48. LEE, E.H., "Stress analysis in visco-elastic bodies", Quart. Applied Math. 13:183-190 (1955).

49. LEE, E.H., and RADOK, J.R.M., "The contact problem for viscoelastic bodies",

J. Appl. Mech. Trans ASME 27(9): 438-444 (1960).

50. LO, C.C., "Elastic contact of rough cylinders", Int. J. Mech. Sci. 11, 105-115 (1969).

51. LUBLINER, J., "Short-time approximations in nonlinear viscoelasticity", Int. J. Solids Structures, 3, 513-520 (1967).

52. LYONS, A.V., and THUREN, A.R., "Scale-up procedure for relating pilot calendering to commercial reality", TAPPI 75(10):173-183 (1992).

53. MAY, W.D., MORRIS, E.L., and ATACK, D., "Rolling friction of a hard cylinder over a viscoelastic material", J. Appl. Phys. 30(11): 1713-1724 (1959).

54. MANN, R.W., BAUM, G.A., and HABERGER, C.C., "Determination of all nine orthotropic constants for machine-made paper", TAPPI 63(2): 163-166 (1980).

55. McINTOSH, D.H., "The effect of refining on the structure of the fiber wall", TAPPI 50(10):482-487 (1967).

56. MITCHELL, J.G., "Calendering alternatives for reducing the bulk of TMP newsprint", Pulp Paper Can 81(4):T102-T197 (1980).

57. MORLAND, L.W., "A plane problem of rolling contact in linear viscoelasticity theory", J. Appl. Mech. Trans ASME 29(6): 345-352 (1962).

58. MORLAND, L.W., "Exact solutions for rolling contact between viscolelastic cylinders", Quart. Journ. Mech. and Applied Math 20(1):73-106 (1967).

59. O'NEILL, R., "Function minimization using a simplex procedure", AS47, in Applied Statistics Algorithms (P. Griffiths and L.D. Hill, eds.), Ellis Horwood Limited for the Royal Statistical Society, London (1985).

60. ORTEGA, J.M., and RHEINBOLDT, W.C., "Iterative solutions of nonlinear equations in several variables", Academic Press, New York (1970).

61. OSAKI, S., and FUJII, Y., "Theory on compressive properties of paper", Report on Progress in Polymer Physics in Japan 23:375-378 (1980).

62. OSAKI, S., FUJII, Y. and KIICHI, T., "Z-direction compressive properties of paper", Report on Progress in Polymer Physics in Japan 25:413-416 (1982).

63. PAGE, D.H., "The collapse behaviour of pulp fibres", TAPPI 50(9):449-454 (1967).

64. PAGE, D.H., and De GRÂCE, J.H., "The delamination of fiber walls by beating and refining", TAPPI 50(10):489-495 (1969).

65. PARKER, J.R., "An air instrument to measure printing roughness of paper and board", Paper Technol. 6(2):T32-T36 (1965).

66. PEEL, J.D., "Recent developments in the technology and understanding of the calendering processes", in Fundamentals of Papermaking: Transactions of the Ninth Fundamental Research Symposium, Volume 2, edited by C.F. Baker, pp. 979-1025, Mechanical Engineering Publications Ltd., London (1989).

67. PEEL, J.D., "Developments in calendering technology: a literature review", PIRA, Leatherhead, Surrey, U.K. (1990).

68. PELLETIER, L., "Impingement heat transfer on a rotating cylinder - an experimental study of calender cooling", Master's thesis, McGill University (1984).

69. PELLETIER, L., DOUGLAS, W.J.M., and CROTOGINO, R.H., "CD calender control with air jets - an experimental study of impingement heat transfer", J. Pulp Paper Science 13(2):49-55 (1987).

70. POPIL, R.E., "The calendering creep equation - a physical model", Trans. 9th Fundamental Res. Symp., Cambridge 1989.

71. PRESS, W.H, FLANNERY, B.P., TEUKOLSKY, S.A., and VETTERLING, W.T., "Numerical recipes in C: The art of scientific computing, Second Edition", Cambridge University Press, Cambridge (1992).

72. RADOK, J.R.M., "Viscoelastic stress analysis", Q. Appl. Math. 15(2):198 (1957).

73. RODAL, J.A., "Soft-nip calendering of paper and paperboard", TAPPI 72(5):177-186 (1989).

74. SHALLHORN, P.M., "Fracture resistance: Theory and experiment", J. Pulp Paper Science 20(4):119-124 (1994).

75. ŠTOK, B., and KRANJEC, A., "Modelling of a rolling contact problem with the viscoelastic material response included", Computers & Structures 37(6):1037-1042 (1990).

76. TIMMS, D.G., "Laboratory calendering: a potential troubleshooting tool", Appita 46(2):127-130 (March 1993).

77. TING, T.C.T., "The contact stresses between a rigid indenter and a viscoelastic half-space", J. Appl. Mech. Trans ASME 33(12): 845-854 (1966).

78. TING, T.C.T., "Contact problems in the linear theory of viscoelasticity", J. Appl. Mech. Trans ASME 35(6): 248-254 (1968).

79. TSCHOEGL, N.W., "The phenomenological theory of linear viscoelastic behaviour", Springer-Verlag, Berlin, Heidelberg and New York (1989).

80. WATANABE, K., and AMARI, T., "Dynamic compressive modulus of paper", Report on Progress in Polymer Physics in Japan 25:409-412 (1982).

81. WILLIAMS, G.J., DRUMMOND, J.G. and CISNEROS, H.A., "A microscopical approach for examining fibre and paper structures", J. Pulp Paper Science 20(4):110-114 (1994).

Appendix A1: Raw data and non linear curve fitting results

TABLE A1.1: Summary of experimental conditions (Boise-Cascade)

Num	Rad	Vel	Load	Bin	Cal	en	ep
3258	0.202	96	40	2.00	104	0.405763	0.114020
3259	0.202	96	65	2.00	104	0.454856	0.146035
3260	0.202	96	42	2.00	104	0.408755	0.100358
3261	0.202	96	19	2.00	104	0.234250	0.058499
3262	0.202	96	16	2.00	104	0.198642	0.056037
3263	0.202	96	40	2.00	104	0.412289	0.088185
3264	0.202	96	65	2.00	104	0.457027	0.123691
3265	0.202	322	65	2.00	104	0.447458	0.110804
3266	0.202	324	41	2.00	104	0.394341	0.069169
3267	0.202	323	19	2.00	104	0.230015	0.044361
3268	0.202	321	19	1.94	101	0.204310	0.013059
3269	0.202	318	40	1.94	101	0.368864	0.035727
3270	0.202	320	65	1.94	101	0.428209	0.070488
3271	0.202	536	65	1.94	101	0.424955	0.061182
3272	0.202	542	41	1.94	101	0.364046	0.020493
3273	0.202	539	19	1.94	101	0.192796	-0.003
3274	0.202	534	19	1.94	101	0.191099	-0.003
3275	0.202	530	40	1.94	101	0.362231	0.032177
3276	0.202	529	65	1.94	101	0.422663	0.060913
3277	0.202	97	62	1.94	101	0.448408	0.084662
3278	0.202	97	95	1.94	101	0.499232	0.134630
3279	0.202	97	134	1.94	101	0.530177	0.165558
3280	0.202	97	175	1.94	101	0.550525	0.195458
3281	0.202	97	170	1.94	101	0.551347	0.191354
3282	0.202	97	135	1.94	101	0.538750	0.177048
3283	0.202	97	95	1.94	101	0.501250	0.127098
3284	0.202	97	64	1.94	101	0.445435	0.077731
3285	0.202	324	63	1.94	101	0.437326	0.065435
3286	0.202	320	95	1.97	103	0.496909	0.123938
3287	0.202	320	134	1.97	103	0.530040	0.157803
3288	0.202	318	174	1.97	103	0.555424	0.184834
3289	0.202	323	169	1.97	103	0.548043	0.181250
3290	0.202	323	134	1.97	103	0.528227	0.147561
3291	0.202	322	96	1.97	103	0.496416	0.134898
3292	0.202	544	87	1.97	103	0.485283	0.121119
3293	0.202	530	136	1.97	103	0.528419	0.143922
3294	0.202	530	164	1.97	103	0.545339	0.165230

TABLE A1.2: Command log input to SYSTAT (Boise-Cascade)

```
By
Select
Weight
Use 'c:\phd\calcs\systat\BCAL.SYS'
By
Select
Weight
Print Long
Format  4
Options

Nonlin

Model EN=(AA+B*(AL*log(L)+AV*log(V))),
    *(B<0.5*(1-AA)/(AL*log(L)+AV*log(V))),
    +(1-0.25*((1-AA)^2)/(B*(AL*log(L)+AV*log(V)))),
    *(B>=0.5*(1-AA)/(AL*log(L)+AV*log(V)))

Estimate /Iter=100 / Start = -.4,.1,-.02, Quasi, Print

By
Select
Weight
Use 'c:\phd\calcs\systat\BCAL.SYS'
By
Select
Weight
Print Long
Format  4
Options

Nonlin

Model EP=0+(AA+B*(AL*log(L)+AV*log(V))),
    *((B>=-AA/(AL*log(L)+AV*log(V))),
    AND (B<0.5*(1-AA)/(AL*log(L)+AV*log(V)))),
    +(1-0.25*((1-AA)^2)/(B*(AL*log(L)+AV*log(V)))),
    *(B>=0.5*(1-AA)/(AL*log(L)+AV*log(V)))

Estimate /Iter=100 / Start = -.4,.1,-.02, Quasi, Print
```

TABLE A1.3: SYSTAT output (Boise-Cascade)

DEPENDENT VARIABLE IS EN

SOURCE	SUM-OF-SQUARES	DF	MEAN-SQUARE
REGRESSION	7.2524	3	2.4175
RESIDUAL	0.0024	34	0.0001
TOTAL	7.2222	37	
CORRECTED	0.4588	36	

RAW R-SQUARED (1-RESIDUAL/TOTAL) = 0.9997
CORRECTED R-SQUARED (1-RESIDUAL/CORRECTED) = 0.9947

PARAMETER	ESTIMATE	A.S.E.	LOWER <95%>	UPPER
AA	-0.3874	0.0362	-0.4609	-0.3138
AL	0.1128	0.0051	0.1025	0.1232
AV	-0.0048	0.0010	-0.0068	-0.0028

DEPENDENT VARIABLE IS EP

SOURCE	SUM-OF-SQUARES	DF	MEAN-SQUARE
REGRESSION	0.4909	4	0.1227
RESIDUAL	0.0069	33	0.0002
TOTAL	0.5037	37	
CORRECTED	0.1178	36	

RAW R-SQUARED (1-RESIDUAL/TOTAL) = 0.9863
CORRECTED R-SQUARED (1-RESIDUAL/CORRECTED) = 0.9414

PARAMETER	ESTIMATE	A.S.E.	LOWER <95%>	UPPER
AA	-0.3874	0.0362	-0.4598	-0.3150
AL	0.0383	0.0042	0.0298	0.0468
AV	-0.0118	0.0020	-0.0159	-0.0077

TABLE A1.4: Summary of experimental conditions (F. Soucy)

Num	Rad	Vel	Load	Bin	Cal	ε_n	ε_p
638	0.202	96	70	2.60	128	0.563049	0.214025
639	0.202	96	86	2.60	128	0.593847	0.246898
640	0.202	96	137	2.60	128	0.630362	0.312001
641	0.202	96	173	2.60	128	0.644190	0.330506
642	0.202	96	208	2.60	128	0.656385	0.344223
643	0.202	169	71	2.60	128	0.542160	0.181364
644	0.202	169	87	2.60	128	0.568938	0.215326
645	0.202	169	136	2.60	128	0.606718	0.258005
646	0.202	169	173	2.60	128	0.620863	0.284779
656	0.202	299	70	2.60	128	0.555454	0.158935
657	0.202	297	70	2.60	128	0.543094	0.155887
658	0.202	301	84	2.60	128	0.577954	0.200738
660	0.202	97	70	2.60	128	0.570027	0.181796
661	0.202	299	70	2.60	128	0.541640	0.155887
662	0.202	301	86	2.60	128	0.579123	0.188763
667	0.202	173	70	2.59	127	0.555515	0.194344
668	0.202	172	87	2.59	127	0.585882	0.221966
669	0.202	173	136	2.59	127	0.608090	0.308999
670	0.202	173	172	2.59	127	0.627037	0.329606
671	0.202	301	70	2.59	127	0.527083	0.168914
672	0.202	301	86	2.59	127	0.548908	0.203551
673	0.202	301	137	2.59	127	0.581873	0.268004
674	0.202	301	172	2.59	127	0.599881	0.292557
683	0.202	99	70	2.62	128	0.563017	0.231203
685	0.202	98	135	2.62	128	0.634868	0.328927
686	0.202	98	172	2.62	128	0.650343	0.365330
687	0.202	98	209	2.62	128	0.661066	0.382232
690	0.202	170	88	2.57	126	0.585108	0.251791
691	0.202	170	136	2.57	126	0.618969	0.313110
692	0.202	169	172	2.57	126	0.638333	0.344874
693	0.202	170	208	2.57	126	0.653670	0.367815
694	0.202	298	70	2.57	126	0.518759	0.175248
695	0.202	292	85	2.57	126	0.555302	0.222679
696	0.202	296	135	2.57	126	0.600321	0.287970
697	0.202	296	172	2.57	126	0.614109	0.315985
698	0.202	97	70	2.57	126	0.528283	0.204368
699	0.202	97	85	2.57	126	0.561799	0.246502
700	0.202	96	135	2.57	126	0.601700	0.306718
701	0.202	96	172	2.57	126	0.617775	0.333407
702	0.202	97	207	2.57	126	0.625020	0.355023
703	0.202	171	208	2.57	126	0.615648	0.334734
704	0.202	174	70	2.57	126	0.551132	0.190916
705	0.202	171	86	2.57	126	0.585286	0.236354
706	0.202	171	136	2.57	126	0.633274	0.306496
707	0.202	173	172	2.57	126	0.642876	0.337156
708	0.202	171	208	2.57	126	0.654114	0.353037
709	0.202	171	207	2.57	126	0.648544	0.336719
712	0.202	97	70	2.62	128	0.553816	0.195492
713	0.202	97	87	2.62	128	0.587768	0.243606
714	0.202	96	137	2.62	128	0.631038	0.310360
715	0.202	97	172	2.62	128	0.645194	0.331383
716	0.202	96	207	2.62	128	0.655435	0.353273
717	0.202	171	70	2.62	128	0.536223	0.182705
718	0.202	169	87	2.62	128	0.566758	0.228652
719	0.202	171	135	2.62	128	0.607111	0.285219
720	0.202	171	174	2.62	128	0.622991	0.312094
721	0.202	169	209	2.62	128	0.627212	0.331383
722	0.202	524	70	2.62	128	0.488312	0.178370
723	0.202	500	85	2.62	128	0.519865	0.211964
724	0.202	528	135	2.62	128	0.558498	0.270264
725	0.202	500	173	2.62	128	0.582433	0.289120
727	0.202	500	70	2.62	128	0.534726	0.179454
728	0.202	528	86	2.62	128	0.567763	0.217382

TABLE A1.4: Summary of experimental conditions (F. Soucy), continued

Num	Rad	Vel	Load	Bin	Cal	ε_n	ε_p
729	0.202	528	136	2.62	128	0.621094	0.278717
730	0.202	500	172	2.62	128	0.639931	0.314261
731	0.202	528	207	2.62	128	0.647189	0.336368
749	0.202	97	70	2.64	129	0.560995	0.216158
750	0.202	96	86	2.64	129	0.590962	0.252901
751	0.202	96	113	2.64	129	0.612769	0.297593
752	0.202	96	172	2.64	129	0.639536	0.350021
753	0.202	97	208	2.64	129	0.651359	0.365277
754	0.202	173	90	2.64	129	0.574967	0.247959
755	0.202	171	70	2.64	129	0.532736	0.186936
756	0.202	169	87	2.64	129	0.565497	0.242372
757	0.202	169	136	2.64	129	0.603881	0.297808
758	0.202	169	173	2.64	129	0.621645	0.334766
759	0.202	169	208	2.64	129	0.633040	0.355823
760	0.202	298	71	2.64	129	0.512394	0.183713
761	0.202	97	70	2.63	118	0.559317	0.188502
767	0.202	173	70	2.64	119	0.558479	0.202098
768	0.202	173	69	2.64	119	0.551407	0.195922
769	0.202	173	86	2.64	119	0.577620	0.241118
770	0.202	173	86	2.64	119	0.574753	0.236449
771	0.202	99	70	2.64	119	0.553924	0.211443
772	0.202	99	86	2.64	119	0.584932	0.263551
773	0.202	98	136	2.64	119	0.623497	0.321731
774	0.202	98	173	2.64	119	0.640319	0.350464
775	0.202	98	208	2.64	119	0.648387	0.367287
776	0.202	173	70	2.64	119	0.540978	0.180607
777	0.202	100	70	2.64	119	0.568294	0.218458
778	0.202	304	69	2.64	119	0.550039	0.181305
779	0.202	99	70	2.64	119	0.546150	0.183879
780	0.202	304	70	2.64	119	0.529769	0.230604
781	0.202	301	85	2.64	119	0.560793	0.288549
782	0.202	301	136	2.64	119	0.603550	0.311915
783	0.202	99	70	2.64	119	0.513029	0.207010
784	0.202	98	86	2.64	119	0.554572	0.253735
785	0.202	98	136	2.64	119	0.599624	0.315423
786	0.202	98	172	2.64	119	0.619100	0.342987
787	0.202	98	208	2.64	119	0.631240	0.360280
788	0.202	500	70	2.64	119	0.527156	0.163313
789	0.202	535	70	2.64	119	0.513579	0.166585
790	0.202	539	86	2.64	119	0.544298	0.189018
791	0.202	535	136	2.64	119	0.591878	0.257705
797	0.202	535	69	2.70	122	0.538860	0.132620
798	0.202	528	87	2.70	122	0.560903	0.171192
800	0.202	171	70	2.70	122	0.550509	0.182606
801	0.202	171	86	2.70	122	0.574741	0.225516
802	0.202	171	136	2.70	122	0.616066	0.274368
803	0.202	171	172	2.70	122	0.630581	0.300393
804	0.202	171	208	2.70	122	0.641189	0.312259
805	0.202	323	70	2.70	122	0.516023	0.168685
806	0.202	323	86	2.70	122	0.544499	0.197898
807	0.202	321	136	2.70	122	0.581121	0.245608
808	0.202	323	173	2.70	122	0.602672	0.286464
809	0.202	173	70	2.70	122	0.508567	0.166401
810	0.202	171	87	2.70	122	0.538076	0.201095
811	0.202	171	136	2.70	122	0.577099	0.254967
812	0.202	170	173	2.70	122	0.595233	0.285092
813	0.202	169	208	2.70	122	0.604640	0.295142
816	0.202	95	69	2.66	120	0.559722	0.239080
817	0.202	94	86	2.66	120	0.583629	0.279406
818	0.202	94	136	2.66	120	0.622318	0.337814
819	0.202	94	173	2.66	120	0.637761	0.370030
820	0.202	94	209	2.66	120	0.643639	0.383013
825	0.202	173	137	2.68	121	0.617463	0.332797

TABLE A1.4: Summary of experimental conditions (F. Soucy), continued

Num	Rad	Vel	Load	Bin	Cal	ε_n	ε_p
827	0.202	173	137	2.68	121	0.601262	0.317847
828	0.202	175	69	2.68	121	0.572799	0.226311
829	0.202	304	69	2.68	121	0.560561	0.205152
831	0.202	500	87	2.58	126	0.534181	0.198679
832	0.202	95	86	2.58	126	0.574351	0.255916
833	0.202	95	137	2.58	126	0.619357	0.333187
834	0.202	95	173	2.58	126	0.637882	0.358943
835	0.202	171	87	2.58	126	0.566930	0.255036
836	0.202	171	136	2.58	126	0.609316	0.313374
837	0.202	170	174	2.58	126	0.620074	0.342653
838	0.202	500	87	2.58	126	0.543544	0.211888
839	0.202	535	138	2.58	126	0.588458	0.282554
840	0.202	500	173	2.58	126	0.607044	0.312713
841	0.202	500	208	2.58	126	0.615471	0.326582
846	0.202	528	86	2.63	129	0.470818	0.217053
847	0.202	520	137	2.63	129	0.525262	0.272099
848	0.202	500	174	2.63	129	0.543784	0.306422
849	0.202	528	208	2.63	129	0.554969	0.331678
850	0.202	524	87	2.63	129	0.406009	0.196330
851	0.202	517	137	2.63	129	0.459531	0.258931
852	0.202	513	174	2.63	129	0.483829	0.286778
853	0.202	500	208	2.63	129	0.496051	0.303832
854	0.202	94	69	2.71	122	0.522703	0.221489
855	0.202	94	87	2.71	122	0.545979	0.270658
856	0.202	94	135	2.71	122	0.588904	0.334851
857	0.202	93	173	2.71	122	0.605262	0.361484
858	0.202	528	87	2.71	122	0.522927	0.220578
861	0.202	543	87	2.71	122	0.595282	0.221489
865	0.202	543	88	2.71	122	0.623192	0.235622
872	0.202	306	86	2.69	121	0.520412	0.235397
873	0.202	301	136	2.69	121	0.557415	0.307826
874	0.202	304	173	2.69	121	0.565349	0.325698
876	0.202	309	87	2.69	121	0.512955	0.245480
877	0.202	309	139	2.69	121	0.548759	0.299113
878	0.202	306	175	2.69	121	0.556713	0.334865
879	0.202	304	210	2.69	121	0.566888	0.349998
880	0.202	174	86	2.69	121	0.546060	0.265192
881	0.202	174	136	2.69	121	0.578949	0.327076
883	0.202	177	87	2.69	121	0.512103	0.255563
884	0.202	177	136	2.69	121	0.550649	0.321573
885	0.202	178	173	2.69	121	0.561666	0.333949
886	0.202	177	88	2.69	121	0.509438	0.242733
887	0.202	178	137	2.69	121	0.548014	0.294987
888	0.202	101	87	2.69	121	0.513951	0.255563
898	0.202	299	69	2.62	129	0.572599	0.209251
899	0.202	301	86	2.62	129	0.605947	0.255725
900	0.202	299	136	2.62	129	0.639628	0.318791
901	0.202	280	173	2.62	129	0.646453	0.351626
902	0.202	543	85	2.62	129	0.547154	0.231971
903	0.202	500	137	2.62	129	0.618054	0.301086
904	0.202	535	173	2.62	129	0.641915	0.330026
905	0.202	531	87	2.62	129	0.527793	0.235859
906	0.202	500	137	2.62	129	0.569124	0.295900
907	0.202	539	173	2.62	129	0.588211	0.330026
908	0.202	299	88	2.62	129	0.537408	0.252700
909	0.202	294	138	2.62	129	0.577325	0.314903
910	0.202	294	174	2.62	129	0.589419	0.335205
917	0.202	304	86	2.61	118	0.602903	0.232776
918	0.202	297	137	2.61	118	0.647662	0.294152
919	0.202	299	173	2.61	118	0.662862	0.319172
920	0.202	299	208	2.61	118	0.668074	0.335702
921	0.202	528	88	2.61	118	0.583924	0.203974
922	0.202	535	139	2.61	118	0.624092	0.260625

TABLE A1.4: Summary of experimental conditions (F. Soucy), continued

Num	Rad	Vel	Load	Bin	Cal	ε_n	ε_p
923	0.202	528	173	2.61	118	0.641815	0.279518
937	0.254	97	85	2.63	126	0.634045	0.223812
938	0.254	97	136	2.63	126	0.660661	0.296216
939	0.254	97	176	2.63	126	0.674926	0.335171
940	0.254	97	210	2.63	126	0.688444	0.344195
974	0.254	550	85	2.67	128	0.504274	0.214235
975	0.254	547	138	2.67	128	0.573662	0.278367
976	0.254	174	87	2.67	128	0.498936	0.232438
977	0.254	173	137	2.67	128	0.559132	0.294176
978	0.254	174	175	2.67	128	0.592821	0.308909
979	0.254	173	209	2.67	128	0.620738	0.334256
980	0.254	305	86	2.67	128	0.487170	0.217269
981	0.254	303	137	2.67	128	0.547623	0.281612
982	0.254	305	177	2.67	128	0.581061	0.305875
983	0.254	303	209	2.67	128	0.604757	0.326247
984	0.254	500	87	2.67	128	0.469111	0.199073
985	0.254	535	138	2.67	128	0.534103	0.269266
986	0.254	538	176	2.67	128	0.568570	0.296563
987	0.254	541	209	2.67	128	0.592429	0.322129
1000	0.254	101	85	2.71	130	0.583661	0.256709
1001	0.254	100	136	2.71	130	0.644055	0.328132
1002	0.254	100	175	2.71	130	0.678713	0.351650
1003	0.254	100	209	2.71	130	0.705831	0.368116
1004	0.254	177	87	2.71	130	0.583360	0.241952
1005	0.254	176	137	2.71	130	0.639193	0.309310
1006	0.254	175	176	2.71	130	0.671779	0.343313
1007	0.254	176	209	2.71	130	0.694471	0.362127
1008	0.254	307	84	2.71	130	0.569361	0.219927
1009	0.254	313	135	2.71	130	0.631880	0.285361
1010	0.254	311	177	2.71	130	0.664227	0.319579
1011	0.254	305	209	2.71	130	0.687604	0.332620
1016	0.254	99	85	2.71	130	0.548868	0.237464
1017	0.254	99	136	2.71	130	0.604691	0.308887
1018	0.254	98	175	2.71	130	0.637685	0.328771
1019	0.254	99	210	2.71	130	0.666477	0.345237
1020	0.254	172	87	2.71	130	0.544670	0.226771
1021	0.254	172	138	2.71	130	0.600645	0.289426
1022	0.254	171	175	2.71	130	0.629857	0.318509
1023	0.254	172	209	2.71	130	0.654120	0.334760
1034	0.254	500	86	2.66	128	0.526988	0.190877
1035	0.254	529	137	2.66	128	0.609286	0.285826
1036	0.254	500	175	2.66	128	0.640704	0.314939
1037	0.254	532	209	2.66	128	0.667568	0.336887
1038	0.254	303	87	2.66	128	0.524683	0.205652
1039	0.254	297	138	2.66	128	0.601445	0.294078
1040	0.254	297	175	2.66	128	0.631080	0.320586
1041	0.254	299	209	2.66	128	0.653036	0.342965
1058	0.254	96	82	2.66	128	0.510331	0.194569
1059	0.254	96	135	2.66	128	0.583599	0.287562
1060	0.254	96	174	2.66	128	0.618183	0.319937
1061	0.254	96	209	2.66	128	0.646688	0.335143
1091	0.254	95	83	2.68	121	0.526842	0.232491
1092	0.254	90	138	2.68	121	0.613445	0.319225
1093	0.254	90	177	2.68	121	0.645004	0.350285
1094	0.254	94	211	2.68	121	0.664401	0.365931
1098	0.254	500	82	2.68	121	0.513445	0.203502
1099	0.254	515	83	2.68	121	0.507713	0.200048
1100	0.254	512	139	2.68	121	0.598905	0.276430
1101	0.254	500	175	2.68	121	0.625577	0.305418
1107	0.254	160	85	2.68	121	0.542708	0.237783
1108	0.254	164	136	2.68	121	0.617079	0.302428
1109	0.254	165	175	2.68	121	0.646445	0.337861
1110	0.254	165	208	2.68	121	0.664593	0.349821

TABLE A1.4: Summary of experimental conditions (F. Soucy), continued

Num	Rad	Vel	Load	Bin	Cal	ε_n	ε_p
1111	0.254	280	208	2.68	121	0.665821	0.340619
1112	0.254	287	179	2.68	121	0.646387	0.318306
1113	0.254	287	137	2.68	121	0.614808	0.279420
1114	0.254	284	84	2.68	121	0.529503	0.205572
1115	0.254	93	83	2.68	121	0.532950	0.233866
1116	0.254	93	137	2.68	121	0.615529	0.297136
1117	0.254	94	84	2.68	121	0.533211	0.222138
1118	0.254	93	138	2.68	121	0.616436	0.297832
1119	0.254	94	174	2.68	121	0.644002	0.320832
1120	0.254	94	211	2.68	121	0.665592	0.342002
1133	0.254	520	82	2.70	122	0.441306	0.173595
1134	0.254	500	137	2.70	122	0.531948	0.254911
1136	0.254	95	132	2.71	122	0.618573	0.302408
1137	0.254	95	177	2.71	122	0.655572	0.342886
1138	0.254	95	209	2.71	122	0.673287	0.360395
1143	0.254	520	85	2.71	122	0.524550	0.198730
1144	0.254	512	138	2.71	122	0.606312	0.280127
1145	0.254	520	175	2.71	122	0.632099	0.306730
1146	0.254	518	209	2.71	122	0.654609	0.333563
1151	0.254	280	84	2.71	122	0.553988	0.224416
1152	0.254	169	84	2.71	122	0.560751	0.227600
1153	0.254	166	138	2.71	122	0.633500	0.294910
1154	0.254	166	176	2.71	122	0.664192	0.324239
1155	0.254	166	209	2.71	122	0.685752	0.341748
1160	0.254	167	84	2.71	122	0.534715	0.216009
1161	0.254	166	137	2.71	122	0.612608	0.295360
1162	0.254	166	175	2.71	122	0.640592	0.322872
1163	0.254	165	210	2.71	122	0.661588	0.337195
1164	0.254	296	210	2.71	122	0.662822	0.316049
1165	0.254	296	177	2.71	122	0.639024	0.293766
1166	0.254	290	139	2.71	122	0.610314	0.273529
1167	0.254	293	86	2.71	122	0.537078	0.192356
1172	0.254	93	84	2.70	121	0.543637	0.207146
1173	0.254	94	138	2.70	121	0.606652	0.287762
1174	0.254	92	178	2.70	121	0.631697	0.310658
1177	0.254	921	85	2.69	121	0.474726	0.202433
1178	0.254	939	137	2.69	121	0.544649	0.265283
1179	0.254	912	192	2.69	121	0.581205	0.298546
1180	0.254	900	210	2.69	121	0.591471	0.307035
1185	0.254	900	85	2.69	121	0.520225	0.190731
1186	0.254	948	136	2.69	121	0.589493	0.258859
1187	0.254	900	176	2.69	121	0.623109	0.287538
1188	0.254	900	209	2.69	121	0.647047	0.299231
1189	0.254	285	84	2.69	121	0.518517	0.196702
1190	0.254	288	137	2.69	121	0.586675	0.273087
1191	0.254	280	176	2.69	121	0.615848	0.306341
1192	0.254	285	208	2.69	121	0.578028	0.329975
1201	0.254	500	139	2.72	122	0.618030	0.292649
1202	0.254	500	177	2.72	122	0.651851	0.326746
1203	0.254	500	210	2.72	122	0.674169	0.339241
1204	0.254	958	210	2.72	122	0.680664	0.316060
1205	0.254	930	178	2.72	122	0.652952	0.292649
1206	0.254	921	139	2.72	122	0.617590	0.254010
1207	0.254	939	83	2.72	122	0.540347	0.186043
1208	0.254	529	85	2.72	122	0.522746	0.196043
1209	0.254	500	138	2.72	122	0.593010	0.269917
1210	0.254	500	177	2.72	122	0.631877	0.302648
1211	0.254	515	210	2.72	122	0.645499	0.310831
1212	0.254	300	176	2.67	128	0.697998	0.291167
1213	0.254	300	177	2.67	128	0.675063	0.291167
1214	0.254	300	176	2.67	128	0.648307	0.291167
1215	0.254	300	176	2.67	128	0.632793	0.291167
1216	0.254	300	176	2.67	128	0.625055	0.291167

TABLE A1.4: Summary of experimental conditions (F. Soucy), continued

Num	Rad	Vel	Load	Bin	Cal	ε_n	ε_p
1217	0.254	300	176	2.67	128	0.621695	0.291167
1236	0.254	96	84	2.39	115	0.571391	0.229932
1237	0.254	95	137	2.39	115	0.616862	0.298598
1238	0.254	96	175	2.39	115	0.639116	0.329304
1239	0.254	95	209	2.39	115	0.645940	0.346954
1240	0.254	523	87	2.39	115	0.555697	0.197534
1241	0.254	500	139	2.39	115	0.604606	0.264990
1242	0.254	515	175	2.39	115	0.625982	0.294971
1243	0.254	520	209	2.39	115	0.640874	0.310203
1244	0.254	939	86	2.39	115	0.488595	0.172389
1245	0.254	900	138	2.39	115	0.542354	0.253385
1246	0.254	900	176	2.39	115	0.569594	0.269101
1247	0.254	900	209	2.39	115	0.586214	0.296180
1256	0.254	167	85	2.38	114	0.589156	0.232824
1257	0.254	204	137	2.38	114	0.635158	0.302015
1258	0.254	160	176	2.38	114	0.659698	0.329692
1259	0.254	167	208	2.38	114	0.670996	0.347414
1268	0.254	292	87	2.36	113	0.561626	0.207256
1269	0.254	289	138	2.36	113	0.612348	0.274421
1270	0.254	290	176	2.36	113	0.638569	0.308739
1271	0.254	290	209	2.36	113	0.653418	0.331045
1272	0.254	518	210	2.36	113	0.645985	0.310945
1273	0.254	513	179	2.36	113	0.633210	0.300650
1274	0.254	518	139	2.36	113	0.605925	0.265841
1279	0.254	288	84	2.45	118	0.612257	0.231546
1280	0.254	290	137	2.45	118	0.669947	0.295917
1281	0.254	280	176	2.45	118	0.693668	0.330343
1282	0.254	292	210	2.45	118	0.706861	0.356988
1283	0.254	515	86	2.45	118	0.617212	0.238148
1284	0.254	500	138	2.45	118	0.663836	0.298275
1285	0.254	520	177	2.45	118	0.680778	0.307000
1290	0.254	95	85	2.45	118	0.589739	0.241920
1291	0.254	95	136	2.45	118	0.641342	0.312659
1292	0.254	95	175	2.45	118	0.662502	0.331522
1293	0.254	95	209	2.45	118	0.678536	0.344255
1294	0.254	169	209	2.45	118	0.680078	0.345199
1295	0.254	167	179	2.45	118	0.665475	0.318554
1296	0.254	168	139	2.45	118	0.648007	0.287900
1297	0.254	167	85	2.45	118	0.592413	0.219992
1390	0.254	921	85	2.40	115	0.515527	0.174741
1391	0.254	900	137	2.40	115	0.558038	0.239817
1392	0.254	900	176	2.40	115	0.572891	0.264401
1393	0.254	900	210	2.40	115	0.581239	0.289467
1394	0.254	900	179	2.40	115	0.562187	0.272114
1395	0.254	900	140	2.40	115	0.532023	0.236443
1396	0.254	900	87	2.40	115	0.466175	0.174982
1404	0.254	939	87	2.40	115	0.573567	0.184382
1405	0.254	900	137	2.40	115	0.634432	0.248012
1410	0.254	520	85	2.40	115	0.598622	0.183659
1411	0.254	500	134	2.40	115	0.664985	0.254519
1412	0.254	512	176	2.40	115	0.695885	0.289226
1413	0.254	509	210	2.40	115	0.711991	0.307785
1414	0.254	500	178	2.40	115	0.697608	0.284647
1415	0.254	500	140	2.40	115	0.674074	0.260063
1416	0.254	939	136	2.40	115	0.649671	0.218848
1417	0.254	948	175	2.40	115	0.676997	0.249217
1418	0.254	939	208	2.40	115	0.696433	0.265124
1419	0.254	900	177	2.40	115	0.670445	0.235478
1420	0.254	930	139	2.40	115	0.641709	0.204387
1421	0.254	939	88	2.40	115	0.571575	0.137383
1426	0.254	93	86	2.40	115	0.585942	0.193059
1427	0.254	93	136	2.40	115	0.641293	0.255001
1428	0.254	93	175	2.40	115	0.673869	0.298385

TABLE A1.4: Summary of experimental conditions (F. Soucy), continued

Num	Rad	Vel	Load	Bin	Cal	ε_n	ε_p
1429	0.254	93	209	2.40	115	0.691715	0.321282
1430	0.254	93	178	2.40	115	0.675511	0.294047
1431	0.254	94	86	2.40	115	0.592737	0.183659
1432	0.254	93	137	2.40	115	0.653490	0.247289
1433	0.254	93	175	2.40	115	0.682284	0.276211
1434	0.254	93	209	2.40	115	0.702277	0.306339
1435	0.254	166	86	2.40	115	0.609147	0.161726
1436	0.254	163	136	2.40	115	0.670991	0.243673
1437	0.254	164	175	2.40	115	0.695293	0.276211
1438	0.254	163	209	2.40	115	0.709458	0.291396
1439	0.254	164	179	2.40	115	0.695749	0.279103
1440	0.254	165	140	2.40	115	0.670816	0.239576
1441	0.254	165	87	2.40	115	0.612584	0.164859
1482	0.254	308	50	2.59	124	0.515541	0.192804
1483	0.254	308	69	2.59	124	0.544752	0.220060
1484	0.254	307	84	2.59	124	0.564423	0.250445
1485	0.254	307	135	2.59	124	0.605956	0.311660
1486	0.254	306	177	2.59	124	0.621431	0.331991
1487	0.254	307	201	2.59	124	0.627937	0.343832
1488	0.254	513	50	2.59	124	0.530765	0.162866
1489	0.254	514	69	2.59	124	0.571759	0.207549
1499	0.254	93	70	2.65	127	0.514496	0.250574
1500	0.254	93	85	2.65	127	0.530876	0.256699
1501	0.254	172	84	2.65	127	0.527919	0.259324
1502	0.254	170	70	2.65	127	0.515399	0.234168
1503	0.254	172	51	2.65	127	0.480771	0.188888
1508	0.254	173	51	2.65	127	0.546543	0.191075
1509	0.254	170	85	2.65	127	0.602416	0.255824
1510	0.254	171	85	2.65	127	0.599835	0.242699
1511	0.254	290	70	2.65	127	0.585210	0.209450
1512	0.254	291	50	2.65	127	0.548075	0.179700
1513	0.254	288	84	2.65	127	0.595175	0.236137
1514	0.254	290	84	2.65	127	0.595407	0.236356
1515	0.254	518	84	2.65	127	0.593113	0.209231
1516	0.254	510	71	2.65	127	0.578870	0.196544
1517	0.254	514	51	2.65	127	0.538341	0.154107
1518	0.254	93	51	2.65	127	0.524781	0.192169
1519	0.254	93	69	2.65	127	0.558011	0.224543
1520	0.254	93	84	2.65	127	0.576480	0.248824
1521	0.254	93	135	2.65	127	0.619733	0.298698
1522	0.254	94	177	2.65	127	0.646655	0.326479
1523	0.254	93	201	2.65	127	0.655822	0.335448
1539	0.254	298	83	2.66	128	0.616160	0.232110
1540	0.254	296	84	2.66	128	0.594595	0.257815
1546	0.254	169	50	2.01	96	0.455902	0.016149
1547	0.254	165	69	2.01	96	0.484854	0.042981
1548	0.254	168	85	2.01	96	0.497059	0.047886
1549	0.254	167	135	2.01	96	0.538999	0.111649
1550	0.254	167	177	2.01	96	0.557528	0.142520
1551	0.254	167	201	2.01	96	0.564948	0.157523
1552	0.254	170	179	2.01	96	0.558484	0.144252
1553	0.254	171	136	2.01	96	0.530588	0.112803
1554	0.254	170	85	2.01	96	0.487280	0.066640
1555	0.254	169	70	2.01	96	0.476676	0.068371
1556	0.254	169	51	2.01	96	0.446929	0.029421
2004	0.355	301	98	2.65	122	0.621444	0.282683
2005	0.355	299	134	2.65	122		0.310062
2006	0.355	302	179	2.65	122		0.345426
2007	0.355	301	210	2.65	122		0.352042
2008	0.355	303	182	2.65	122		0.335159
2009	0.355	303	137	2.65	122	0.658340	0.297513
2010	0.355	303	99	2.65	122	0.604707	0.275838
2011	0.355	309	22	2.65	122	0.371293	0.108145

TABLE A1.4: Summary of experimental conditions (F. Soucy), continued

Num	Rad	Vel	Load	Bin	Cal	ε_n	ε_p
2012	0.355	299	22	2.65	122	0.374781	0.114990
2013	0.355	292	98	2.65	122	0.586077	0.264203
2022	0.355	89	96	2.64	121	0.600237	0.296085
2023	0.355	90	133	2.64	121	0.634001	0.337532
2024	0.355	89	179	2.64	121		0.376002
2025	0.355	89	210	2.64	121		0.382872
2026	0.355	90	182	2.64	121	0.654769	0.363179
2027	0.355	89	136	2.64	121	0.611470	0.338906
2028	0.355	91	96	2.64	121	0.574173	0.304328
2029	0.355	90	24	2.64	121	0.431259	0.137394
2030	0.355	86	95	2.64	121	0.561206	0.296771
2043	0.355	90	97	2.67	123	0.537569	0.300430
2044	0.355	89	133	2.67	123	0.558911	0.339370
2045	0.355	89	179	2.67	123	0.571860	0.368123
2046	0.355	89	210	2.67	123	0.584333	0.385103
2048	0.355	91	97	2.67	123	0.518945	0.313335
2049	0.355	88	23	2.67	123	0.465220	0.149875
2050	0.355	312	96	2.67	123	0.512181	0.272357
2051	0.355	295	132	2.67	123	0.530107	0.315372
2052	0.355	301	177	2.67	123	0.556300	0.335748
2053	0.355	301	209	2.67	123	0.565139	0.340276
2054	0.355	516	209	2.67	123	0.559776	0.342087
2055	0.355	532	96	2.67	123	0.496168	0.246547
2065	0.355	522	99	2.64	121	0.561625	0.235739
2066	0.355	519	136	2.64	121	0.580376	0.275830
2067	0.355	520	182	2.64	121	0.597563	0.295304
2068	0.355	521	211	2.64	121	0.604124	0.310195
2069	0.355	526	186	2.64	121	0.594542	0.302864
2070	0.355	527	139	2.64	121	0.571043	0.269874
2071	0.355	526	100	2.64	121	0.544337	0.243070
2072	0.355	534	20	2.64	121	0.467069	0.094387
2088	0.355	928	96	2.63	121	0.568740	
2089	0.355	924	133	2.63	121	0.592173	
2090	0.355	913	179	2.63	121	0.614280	
2091	0.355	919	210	2.63	121	0.619485	0.329963
2092	0.355	931	183	2.63	121	0.611922	0.313649
2093	0.355	924	137	2.63	121	0.583016	0.268612
2094	0.355	930	98	2.63	121	0.550875	0.251149
2095	0.355	937	23	2.63	121	0.474533	0.106158
2096	0.355	912	97	2.63	121	0.558804	0.238741
2097	0.355	921	97	2.63	121	0.555189	0.225414
2098	0.355	926	97	2.63	121	0.551735	0.213006
2114	0.355	533	97	2.69	120	0.549402	0.274901
2115	0.355	515	133	2.69	120	0.573854	0.307407
2117	0.355	89	98	2.69	120	0.534426	0.323891
2118	0.355	88	134	2.69	120	0.557009	0.351985
2119	0.355	87	180	2.69	120	0.579720	0.378686
2120	0.355	88	211	2.69	120	0.590434	0.393778
2121	0.355	91	183	2.69	120	0.581011	0.388670
2122	0.355	91	137	2.69	120	0.553723	0.355700
2123	0.355	90	98	2.69	120	0.516488	0.299512
2124	0.355	92	23	2.69	120	0.468261	0.149756
2125	0.355	174	97	2.69	120	0.517003	0.289296
2126	0.355	175	132	2.69	120	0.540810	0.311818
2127	0.355	173	177	2.69	120	0.564463	0.345020
2128	0.355	173	209	2.69	120	0.576481	0.357093
2129	0.355	306	97	2.69	120	0.514459	0.266543
2130	0.355	295	131	2.69	120	0.536197	0.295798
2131	0.355	298	176	2.69	120	0.555444	0.316229
2132	0.355	299	209	2.69	120	0.567811	0.332250
2133	0.355	89	96	2.69	120	0.512871	0.282331
2134	0.355	89	96	2.69	120	0.510453	0.273973
2135	0.355	533	96	2.69	120	0.501552	0.230323

TABLE A1.4: Summary of experimental conditions (F. Soucy), continued

Num	Rad	Vel	Load	Bin	Cal	ε_n	ε_p
2137	0.355	294	100	2.76	123		0.193841
2138	0.355	301	99	2.76	123		0.193841
2139	0.355	302	99	2.76	123	0.641061	0.193841
2140	0.355	301	98	2.76	123	0.612961	0.193841
2141	0.355	302	98	2.76	123	0.593902	0.193841
2142	0.355	304	98	2.76	123	0.580532	0.193841
2143	0.355	301	97	2.76	123	0.576255	0.193841
2145	0.355	300	97	2.76	123	0.551357	0.193841
2146	0.355	301	97	2.76	123	0.539003	0.193841
2147	0.355	300	96	2.76	123	0.529394	0.193841
2159	0.355	297	97	2.17	96	0.474783	0.014973
2160	0.355	302	97	2.17	96	0.481610	0.016124
2161	0.355	302	133	2.17	96	0.501241	0.045206
2162	0.355	300	178	2.17	96	0.525286	0.064498
2163	0.355	301	209	2.17	96	0.536999	0.087532
2164	0.355	302	209	2.17	96	0.547087	0.089548
2165	0.355	301	180	2.17	96	0.533075	0.073999
2166	0.355	306	135	2.17	96	0.495661	0.038871
2167	0.355	303	98	2.17	96	0.477179	0.016124
2168	0.355	519	94	2.17	96	0.503981	0.041463
2169	0.355	516	130	2.17	96	0.558898	0.060466
2170	0.355	523	174	2.17	96	0.635660	0.096458
2171	0.355	519	208	2.17	96	0.639587	0.105672
2172	0.355	525	178	2.17	96	0.616627	0.080910
2173	0.355	523	133	2.17	96	0.592665	0.066513
2174	0.355	525	96	2.17	96	0.561182	0.031385
2175	0.355	517	129	2.17	96	0.578472	0.061330
2176	0.355	518	173	2.17	96	0.595387	0.088684
2177	0.355	519	207	2.17	96	0.609772	0.109128
2229	0.355	90	94	2.73	123	0.547055	0.278388
2230	0.355	89	130	2.73	123	0.584141	0.310901
2231	0.355	89	175	2.73	123	0.617271	0.329867
2232	0.355	88	209	2.73	123		0.344995
2233	0.355	90	178	2.73	123	0.612676	0.326254
2234	0.355	92	133	2.73	123	0.575895	0.298934
2235	0.355	92	95	2.73	123	0.538586	0.270937
2236	0.355	95	22	2.73	123	0.404307	0.133659
2237	0.355	86	94	2.73	123	0.533366	0.280194
2238	0.355	935	94	2.73	123	0.512871	0.222844
2244	0.355	90	92	2.73	123	0.631007	0.279955
2245	0.355	532	91	2.73	123	0.621968	0.234202
2246	0.355	514	127	2.73	123	0.656164	0.260702
2247	0.355	519	171	2.73	123		0.289015
2248	0.355	519	207	2.73	123		0.307135
2249	0.355	522	207	2.73	123		0.298528
2255	0.355	527	90	2.73	123	0.601242	0.215176
2256	0.355	517	126	2.73	123	0.637901	0.238279
2263	0.355	538	98	2.73	123	0.588782	0.240682
2264	0.355	507	211	2.73	123		0.316094
2265	0.355	526	101	2.73	123	0.538581	0.244068
2266	0.355	541	19	2.73	123	0.467233	0.093469
2267	0.355	505	99	2.73	123	0.542753	0.242262
2268	0.355	505	210	2.73	123	0.599456	0.298709
2273	0.355	537	100	2.73	123		0.279743
2274	0.355	534	16	2.73	123		0.129595
2275	0.355	524	16	2.73	123		0.125305
2276	0.355	503	99	2.73	123		0.259873
2277	0.355	543	98	2.73	123	0.581312	
2278	0.355	537	98	2.73	123	0.597676	
2279	0.355	526	98	2.73	123	0.585496	
2280	0.355	518	98	2.73	123	0.586365	
2286	0.355	89	97	2.63	117	0.557967	0.268044
2287	0.355	90	134	2.63	117	0.579609	0.288699

TABLE A1.4: Summary of experimental conditions (F. Soucy), continued

Num	Rad	Vel	Load	Bin	Cal	ε_n	ε_p
2288	0.355	89	179	2.63	117	0.599346	0.312441
2289	0.355	89	209	2.63	117	0.610612	0.318851
2290	0.355	89	97	2.63	117	0.551505	0.255698
2291	0.355	88	20	2.63	117	0.506713	0.106600
2297	0.355	89	97	2.64	116	0.541181	0.304659
2298	0.355	90	211	2.64	116	0.596074	0.371565
2299	0.355	89	98	2.64	116	0.533526	0.299403
2300	0.355	89	19	2.64	116	0.429163	0.155556
2301	0.355	517	97	2.64	116	0.520063	0.253524
2302	0.355	519	97	2.64	116	0.525649	0.247312
2303	0.355	521	210	2.64	116	0.586296	0.305854
2304	0.355	515	97	2.64	116	0.501278	0.283393
2305	0.355	522	211	2.64	116	0.565889	0.343369
2306	0.355	513	18	2.64	116	0.363834	0.124253
2307	0.355	520	22	2.64	116	0.389270	0.127599
2308	0.355	89	96	2.64	116		0.296057
2309	0.355	90	96	2.64	116		0.299881
2310	0.355	89	133	2.64	116		0.323297
2311	0.355	89	179	2.64	116		0.329032
2312	0.355	89	210	2.64	116		0.345520
2313	0.355	89	210	2.64	116		0.338590
2314	0.355	89	180	2.64	116		0.328315
2315	0.355	89	134	2.64	116		0.302031
2316	0.355	89	95	2.64	116		0.265233
2317	0.355	88	25	2.64	116		0.136679
2318	0.355	89	22	2.64	116		0.117085
2319	0.355	89	22	2.64	116		0.122103
2320	0.355	89	25	2.64	116		0.122820
2321	0.355	90	94	2.64	116		0.245639
2322	0.355	177	94	2.64	116		0.223417
2324	0.355	174	174	2.64	116		0.299164
2325	0.355	174	208	2.64	116		0.301075
2326	0.355	174	208	2.64	116		0.304421
2327	0.355	172	94	2.64	116		0.219833
2328	0.355	171	23	2.64	116		0.098447
2329	0.355	174	23	2.64	116		0.094385
2330	0.355	176	94	2.64	116		0.213859
2331	0.355	89	93	2.64	116		0.255436
2332	0.355	89	210	2.64	116		0.329988
2333	0.355	89	22	2.64	116		0.117085
2334	0.355	89	22	2.64	116		0.114695
2335	0.355	88	210	2.64	116		0.322581
2336	0.355	89	210	2.64	116		0.318041
2340	0.355	89	97	2.73	120	0.551538	0.298914
2343	0.355	90	97	2.73	120	0.551351	
2344	0.355	296	97	2.73	120	0.551157	
2346	0.355	89	96	2.67	120	0.530217	
2347	0.355	89	96	2.67	120	0.609068	0.313698
2348	0.355	89	97	2.67	120	0.485690	0.315546
2349	0.355	174	97	2.67	120	0.480320	
2350	0.355	298	96	2.67	120	0.473453	0.286902
2351	0.355	515	95	2.67	120	0.468698	0.264264
2352	0.355	89	95	2.67	120	0.470426	0.298683
2353	0.355	533	95	2.67	120	0.465275	0.242550
2354	0.355	301	96	2.67	120	0.463740	0.252021
2356	0.355	90	96	2.70	121	0.512365	0.289902
2357	0.355	175	96	2.70	121	0.498379	0.267003
2358	0.355	297	96	2.70	121	0.489984	0.254179
2359	0.355	518	96	2.70	121	0.485866	0.247309
2360	0.355	926	96	2.70	121	0.470014	0.225784
2361	0.355	918	126	2.70	121	0.497834	0.264026
2362	0.355	915	164	2.70	121	0.521782	0.274330
2363	0.355	916	198	2.70	121		0.291962

TABLE A1.4: Summary of experimental conditions (F. Soucy), continued

Num	Rad	Vel	Load	Bin	Cal	ε_n	ε_p
2364	0.355	924	168	2.70	121	0.525715	0.266545
2367	0.355	89	98	2.72	122	0.566008	0.338182
2368	0.355	89	97	2.72	122	0.562777	0.313864
2373	0.355	90	97	2.78	122	0.600273	0.343864
2374	0.355	175	97	2.78	122	0.589295	0.313409
2375	0.355	175	127	2.78	122	0.616129	0.329773
2376	0.355	175	166	2.78	122	0.633215	0.348864
2377	0.355	175	200	2.78	122	0.644544	0.352955
2378	0.355	175	200	2.78	122	0.642865	0.348409
2379	0.355	175	169	2.78	122	0.619694	0.329318
2380	0.355	174	130	2.78	122	0.589109	0.299773
2381	0.355	174	97	2.78	122	0.565517	0.277500
2382	0.355	176	23	2.78	122	0.425684	0.142955
2383	0.355	175	20	2.78	122	0.401973	0.127273
2384	0.355	175	20	2.78	122	0.400869	0.123864
2385	0.355	174	23	2.78	122	0.423879	0.150227
2386	0.355	174	95	2.78	122	0.553740	0.266818
2387	0.355	173	204	2.78	122	0.631912	0.333636
2388	0.355	173	96	2.78	122	0.555355	0.247955
2389	0.355	173	21	2.78	122	0.401214	0.105455
2390	0.355	176	95	2.78	122	0.553609	0.237273
2392	0.355	301	97	2.71	119	0.540321	0.232851
2393	0.355	302	97	2.71	119	0.538150	0.234484
2394	0.355	300	134	2.71	119	0.571614	0.256416
2395	0.355	301	180	2.71	119	0.604609	0.281148
2396	0.355	89	96	2.71	119	0.538641	0.268782
2397	0.355	301	95	2.71	119	0.532725	0.231218
2398	0.355	89	95	2.71	119	0.539639	0.267615
2399	0.355	300	94	2.71	119	0.532885	0.241717
2400	0.355	301	131	2.71	119	0.567763	0.270649
2401	0.355	89	94	2.71	119	0.529975	0.245684
2402	0.355	301	130	2.71	119	0.564977	0.252217
2403	0.355	297	176	2.71	119	0.596766	0.283248
2404	0.355	299	209	2.71	119	0.616061	0.310079
2405	0.355	300	209	2.71	119	0.612218	0.305413
2406	0.355	301	179	2.71	119	0.599203	0.297014
2407	0.355	301	133	2.71	119	0.563569	0.255716
2408	0.355	299	95	2.71	119	0.526036	0.217919
2409	0.355	298	26	2.71	119	0.390103	0.097060
2410	0.355	300	23	2.71	119	0.366795	0.084928
2411	0.355	299	23	2.71	119	0.366941	0.085628
2412	0.355	299	26	2.71	119	0.391990	0.091227
2413	0.355	303	94	2.71	119	0.526752	0.209986
2419	0.355	90	96	2.84	125	0.545353	0.323699
2420	0.355	174	96	2.84	125	0.542257	0.289684
2421	0.355	176	132	2.84	125	0.575806	0.325033
2422	0.355	175	177	2.84	125	0.601215	0.344153
2423	0.355	176	210	2.84	125	0.616869	0.358604
2424	0.355	175	210	2.84	125	0.617926	0.353713
2425	0.355	175	178	2.84	125	0.598162	0.333482
2426	0.355	174	134	2.84	125	0.568847	0.303246
2427	0.355	175	96	2.84	125	0.541224	0.255892
2428	0.355	174	25	2.84	125	0.417548	0.141618
2429	0.355	174	22	2.84	125	0.397186	0.120053
2430	0.355	302	95	2.76	124	0.535020	0.264969
2431	0.355	90	95	2.76	124	0.542516	0.286193
2432	0.355	175	129	2.76	124	0.561773	0.296693
2433	0.355	931	128	2.76	124	0.548031	0.257819
2434	0.355	915	172	2.76	124	0.580001	0.279714
2435	0.355	917	207	2.76	124	0.597855	0.295353
2436	0.355	923	207	2.76	124	0.597855	0.292449
2437	0.355	923	176	2.76	124	0.580480	0.278374
2438	0.355	923	132	2.76	124	0.543327	0.248883

TABLE A1.4: Summary of experimental conditions (F. Soucy), continued

Num	Rad	Vel	Load	Bin	Cal	ε_n	ε_p
2439	0.355	923	94	2.76	124	0.512191	0.216488
2440	0.355	919	94	2.76	124	0.507368	
2441	0.355	927	28	2.76	124	0.384178	0.105228
2442	0.355	919	28	2.76	124	0.384605	0.102100
2443	0.355	910	92	2.76	124	0.509260	0.211573
2444	0.355	923	92	2.76	124	0.508374	0.205764
2447	0.355	90	98	2.79	126	0.562613	0.296444
2448	0.355	90	22	2.79	126	0.412962	0.142699
2449	0.355	89	19	2.79	126	0.393838	0.138723
2450	0.355	90	20	2.79	126	0.395493	0.150210
2451	0.355	90	23	2.79	126	0.420627	0.159267
2452	0.355	176	23	2.79	126	0.409976	0.138502
2453	0.355	175	20	2.79	126	0.389774	0.127457
2454	0.355	175	20	2.79	126	0.393925	0.130108
2455	0.355	175	23	2.79	126	0.414624	0.142258
2456	0.355	176	96	2.79	126	0.556605	0.253590
2457	0.355	90	97	2.79	126	0.554757	0.272366
2458	0.355	175	131	2.63	118	0.558953	0.293290
2459	0.355	175	23	2.63	118	0.385525	0.103238
2460	0.355	174	20	2.63	118	0.363413	0.101361
2461	0.355	175	20	2.63	118	0.361386	0.094322
2462	0.355	175	23	2.63	118	0.385024	0.095260
2463	0.355	301	133	2.63	118	0.575137	0.293290
2464	0.355	298	22	2.63	118	0.376444	0.106757
2465	0.355	301	20	2.63	118	0.349605	0.093853
2466	0.355	300	20	2.63	118	0.356387	0.095260
2467	0.355	300	22	2.63	118	0.378824	0.100422
2468	0.355	300	133	2.63	118	0.570959	0.276161
2469	0.355	90	131	2.63	118	0.570718	0.301736
2470	0.355	89	175	2.63	118	0.597294	0.325434
2473	0.355	527	127	2.63	118	0.542236	0.250117
2474	0.355	519	28	2.63	118	0.384827	0.088691
2475	0.355	524	25	2.63	118	0.372732	0.084702
2476	0.355	519	25	2.63	118	0.369227	0.091976
2477	0.355	520	27	2.63	118	0.383194	0.102065
2478	0.355	521	91	2.63	118	0.507345	0.207180
2479	0.355	521	27	2.63	118	0.386992	0.084702
2480	0.355	520	25	2.63	118	0.371037	0.080009
2481	0.355	520	25	2.63	118	0.371042	0.080948
2482	0.355	520	27	2.63	118	0.381516	0.084233
2483	0.355	521	91	2.63	118	0.508743	0.198498
2485	0.355	90	101	2.81	126	0.555232	0.225594
2486	0.355	90	18	2.81	126	0.380533	0.103342
2487	0.355	90	16	2.81	126	0.358827	
2488	0.355	89	16	2.81	126	0.359838	0.088391
2489	0.355	90	19	2.81	126	0.383580	0.098065
2490	0.355	90	98	2.81	126	0.551464	0.227573
2491	0.355	90	97	2.79	126	0.552529	0.266150
2492	0.355	89	23	2.79	126	0.426889	0.142257
2493	0.355	90	20	2.79	126	0.403859	0.120354
2494	0.355	90	20	2.79	126	0.405175	0.128540
2495	0.355	90	24	2.79	126	0.425200	0.131858
2496	0.355	89	95	2.79	126	0.553242	0.242920
2497	0.355	90	133	2.79	126	0.604033	
2498	0.355	300	130	2.79	126	0.599415	0.286726
2499	0.355	90	127	2.79	126	0.602531	0.323230
2500	0.355	173	127	2.79	126	0.595270	0.309735
2501	0.355	300	127	2.79	126	0.596010	0.293805
2503	0.355	89	128	2.79	126	0.606981	0.314381
2504	0.355	175	127	2.79	126	0.601122	0.292035
2505	0.355	305	127	2.79	126	0.603418	0.279204
2506	0.355	305	171	2.79	126	0.632177	0.298451
2507	0.355	304	206	2.79	126	0.652136	0.328761

TABLE A1.4: Summary of experimental conditions (F. Soucy), continued

Num	Rad	Vel	Load	Bin	Cal	ε_n	ε_p
2508	0.355	303	206	2.79	126	0.647633	0.333850
2509	0.355	304	173	2.79	126	0.628747	0.303319
2510	0.355	303	129	2.79	126	0.597016	0.280973
2511	0.355	92	125	2.79	126	0.598219	0.292920
2512	0.355	93	129	2.66	120	0.585237	
2513	0.355	536	93	2.66	120	0.537991	0.194799
2514	0.355	526	29	2.66	120	0.418857	0.086139
2515	0.355	522	26	2.66	120	0.396315	0.065707
2516	0.355	524	26	2.66	120	0.395005	0.078245
2517	0.355	523	29	2.66	120	0.416125	0.098444
2518	0.355	526	26	2.66	120	0.395779	0.085674
2519	0.355	522	29	2.66	120	0.412649	0.095194
2520	0.355	516	91	2.66	120	0.534281	0.184583
2522	0.355	92	136	2.60	117	0.547506	0.328199
2523	0.355	92	26	2.60	117	0.381205	0.140995
2524	0.355	90	17	2.60	117	0.315467	0.116351
2525	0.355	91	25	2.60	117	0.379246	0.140521
2526	0.355	177	98	2.60	117	0.509253	0.267299
2527	0.355	175	25	2.60	117	0.367641	0.122275
2528	0.355	176	18	2.60	117	0.305883	0.088389
2529	0.355	177	25	2.60	117	0.366055	0.114929
2530	0.355	529	134	2.69	121	0.557153	0.316648
2531	0.355	534	24	2.69	121	0.367712	0.134788
2532	0.355	521	19	2.69	121	0.324311	0.111825
2533	0.355	525	19	2.69	121	0.322795	0.108840
2534	0.355	523	24	2.69	121	0.361971	0.123077
2535	0.355	514	97	2.69	121	0.519659	0.247072
2536	0.355	531	133	2.69	121	0.558175	0.292767
2537	0.355	523	133	2.69	121	0.555860	0.284271
2574	0.355	302	94	2.73	123	0.570715	0.216486
2575	0.355	302	94	2.73	123	0.570227	0.216486
2576	0.355	302	93	2.73	123	0.563916	0.216486
2577	0.355	301	93	2.73	123	0.561766	0.216486
2578	0.355	301	93	2.73	123	0.558052	0.216486
2579	0.355	301	92	2.73	123	0.554893	0.216486
2580	0.355	301	92	2.73	123	0.551323	0.216486
2581	0.355	301	91	2.73	123	0.550974	0.216486
2582	0.355	301	91	2.73	123	0.548583	0.216486
2583	0.355	301	91	2.73	123	0.548332	0.216486
2586	0.355	91	97	2.14	96	0.462947	0.084104
2587	0.355	303	97	2.14	96	0.453850	0.071098
2588	0.355	301	137	2.08	94	0.497812	0.102047
2589	0.355	303	185	2.08	94	0.532756	0.137051
2590	0.355	302	211	2.08	94	0.549263	0.135865
2591	0.355	303	210	2.08	94	0.546534	0.132898
2592	0.355	300	135	2.08	94	0.460261	0.095817
2593	0.355	304	97	2.08	94	0.420572	0.082171
2594	0.355	302	97	2.08	94	0.422185	0.084545
2599	0.355	297	135	2.12	96	0.460578	0.122455
2600	0.355	296	98	2.12	96	0.420144	0.091041
2601	0.355	304	99	2.12	96	0.423679	0.093950
2602	0.355	301	134	2.12	96	0.458333	0.109075
2603	0.355	300	181	2.12	96	0.497436	0.140780
2604	0.355	302	135	2.12	96	0.458376	0.120419
2605	0.355	302	181	2.12	96	0.496403	0.132344
2606	0.355	313	135	2.12	96	0.461745	0.123037
2607	0.355	303	210	2.12	96	0.518575	0.156486
2608	0.355	302	210	2.12	96	0.516283	0.140780
2609	0.355	302	185	2.12	96	0.501147	0.148633
2610	0.355	91	132	2.12	96	0.461520	0.160849
2611	0.355	530	131	2.12	96	0.452165	0.142234
2612	0.355	516	177	2.12	96	0.484331	0.148924
2613	0.355	522	209	2.12	96	0.509850	0.171902

TABLE A1.4: Summary of experimental conditions (F. Soucy), continued

Num	Rad	Vel	Load	Bin	Cal	ε_n	ε_p
2614	0.355	522	208	2.12	96	0.511418	0.172484
2615	0.355	523	181	2.12	96	0.492280	0.160268
2616	0.355	524	135	2.12	96	0.450217	0.143106
2617	0.355	519	135	2.12	96	0.450974	0.133799
2618	0.355	514	208	2.12	96	0.512806	0.165212
2619	0.355	521	208	2.12	96	0.506935	0.155323
2622	0.355	91	98	2.71	122	0.504045	
2623	0.355	91	98	2.71	122	0.497271	
2624	0.355	928	132	2.71	122	0.508639	0.287927
2625	0.355	920	177	2.71	122	0.545805	0.310706
2626	0.355	918	209	2.71	122	0.565571	0.334169
2627	0.355	923	209	2.71	122	0.559973	0.329157
2628	0.355	927	181	2.71	122	0.546367	0.322551
2629	0.355	925	136	2.71	122	0.509285	0.286788
2630	0.355	926	98	2.71	122	0.478187	0.263326
2631	0.355	924	26	2.71	122	0.335076	0.133713
2632	0.355	922	13	2.71	122	0.231659	0.094305
2633	0.355	920	13	2.71	122	0.224900	0.080410
2634	0.355	921	25	2.71	122	0.326790	0.121185
2635	0.355	916	96	2.71	122	0.472584	0.234396
2636	0.355	922	132	2.71	122	0.510497	0.269021
2637	0.355	918	176	2.71	122	0.539755	0.293166
2638	0.355	921	208	2.71	122	0.562689	0.312073
2639	0.355	922	208	2.71	122	0.560902	0.310251
2640	0.355	926	160	2.71	122	0.547778	0.294533
2641	0.355	926	135	2.71	122	0.510636	0.264692
2642	0.355	927	97	2.71	122	0.476187	0.224146
2643	0.355	927	27	2.71	122	0.341094	0.113895
2644	0.355	921	27	2.71	122	0.345664	0.116629
2645	0.355	914	95	2.71	122	0.471335	0.209339
2647	0.355	92	98	2.73	123	0.565264	0.256793
2648	0.355	91	135	2.73	123	0.596192	0.283062
2649	0.355	91	181	2.73	123	0.629765	0.307745
2650	0.355	92	209	2.73	123	0.649963	0.330163
2651	0.355	91	11	2.73	123	0.301786	0.067482
2653	0.355	91	98	2.53	114	0.536672	0.268620
2654	0.355	91	11	2.53	114	0.271546	0.074237
2655	0.355	91	11	2.53	114	0.279820	0.073993
2656	0.355	92	24	2.53	114	0.390901	0.125763
2657	0.355	91	24	2.53	114	0.397934	0.147253
2658	0.355	303	25	2.53	114	0.385370	0.100611
2659	0.355	302	12	2.53	114	0.279421	0.076190
2660	0.355	301	13	2.53	114	0.270914	0.062515
2661	0.355	301	25	2.53	114	0.382488	0.087912
2663	0.355	92	96	2.53	114	0.533737	0.276190
2664	0.355	174	95	2.53	114	0.527848	0.250305
2665	0.355	927	94	2.53	114	0.508046	0.218803
2666	0.355	922	28	2.53	114	0.388264	0.112332
2667	0.355	921	16	2.53	114	0.292477	0.072039
2668	0.355	921	16	2.53	114	0.297111	0.076679
2669	0.355	919	28	2.53	114	0.391806	0.097680
2670	0.355	923	28	2.53	114	0.396568	
2673	0.202	176	95	2.67	119	0.622866	0.308538
2674	0.202	175	140	2.67	119	0.635665	0.355088
2675	0.202	174	178	2.67	119	0.639193	0.372865
2676	0.202	171	178	2.67	119	0.638790	0.376842
2677	0.202	177	144	2.67	119	0.634163	0.356491
2678	0.202	178	98	2.67	119	0.622207	0.311579
2679	0.202	174	82	2.67	119	0.616804	0.283275
2680	0.202	179	73	2.67	119	0.604484	0.259415
2681	0.202	174	73	2.67	119	0.606028	0.250760
2682	0.202	177	140	2.54	113		0.344311
2683	0.202	176	178	2.54	113		0.370853

TABLE A1.4: Summary of experimental conditions (F. Soucy), continued

Num	Rad	Vel	Load	Bin	Cal	ε_n	ε_p
2684	0.202	176	143	2.54	113		0.349963
2685	0.202	176	98	2.54	113		0.307201
2686	0.202	177	82	2.54	113		0.293930
2687	0.202	177	74	2.54	113		0.249845
2688	0.202	321	137	2.54	113	0.662029	0.319980
2689	0.202	320	177	2.54	113	0.704563	0.333743
2690	0.202	319	177	2.54	113	0.701325	0.337921
2691	0.202	321	140	2.54	113	0.665303	0.312362
2692	0.202	319	95	2.54	113	0.607628	0.278693
2693	0.202	320	80	2.54	113	0.577915	0.244532
2694	0.202	319	71	2.54	113	0.560784	0.252642
2695	0.202	563	71	2.54	113	0.551750	0.232735
2696	0.202	552	77	2.54	113	0.566507	0.233473
2697	0.202	552	91	2.54	113	0.589772	0.246498
2700	0.202	96	137	2.71	121	0.646607	0.376295
2701	0.202	96	176	2.71	121	0.673189	0.397468
2702	0.202	96	176	2.71	121	0.669974	0.396548
2703	0.202	96	139	2.71	121	0.623301	0.371231
2704	0.202	95	95	2.71	121	0.572018	0.334407
2705	0.202	95	80	2.71	121	0.546100	0.32[illegible]3
2706	0.202	96	72	2.71	121	0.529092	0.307020
2707	0.202	96	72	2.71	121	0.524091	0.303567
2708	0.202	95	78	2.71	121	0.534026	0.314154
2709	0.202	95	91	2.71	121	0.552605	0.326122
2710	0.202	186	91	2.71	121	0.537360	0.310242
2711	0.202	187	133	2.71	121	0.591589	0.348216
2712	0.202	187	174	2.71	121	0.632235	0.379747
2713	0.202	187	173	2.71	121	0.631459	0.385040
2714	0.202	188	137	2.71	121	0.595461	0.359033
2715	0.202	186	93	2.71	121	0.540886	0.313003
2716	0.202	187	79	2.71	121	0.519503	0.293671
2717	0.202	187	70	2.71	121	0.503927	0.284235
2718	0.202	186	70	2.71	121	0.500698	0.277330
2719	0.202	186	77	2.71	121	0.513249	0.288147
2720	0.202	317	90	2.71	121	0.521460	0.290909
2721	0.202	320	173	2.71	121	0.607299	0.338780
2722	0.202	320	69	2.71	121	0.479619	0.238205
2723	0.202	320	69	2.71	121	0.481496	0.249022
2724	0.202	320	172	2.71	121	0.607962	0.330495
2725	0.202	95	93	2.71	121	0.497093	0.319678
2726	0.202	324	93	2.71	121	0.491981	0.301036
2727	0.202	313	137	2.71	121	0.548752	0.342232
2728	0.202	318	177	2.71	121	0.588453	0.375604
2729	0.202	320	177	2.71	121	0.585459	0.350978
2730	0.202	321	141	2.71	121	0.548280	0.322900
2731	0.202	324	96	2.71	121	0.488426	0.271577
2732	0.202	321	80	2.71	121	0.465116	0.258918
2733	0.202	320	72	2.71	121	0.448771	0.249482
2734	0.202	319	71	2.71	121	0.445759	0.242808
2735	0.202	318	78	2.71	121	0.458546	0.245109
2736	0.202	317	92	2.71	121	0.482763	0.255696
2737	0.202	317	135	2.71	121	0.545316	0.312773
2740	0.202	95	87	2.58	115	0.616958	0.308045
2741	0.202	186	87	2.58	115	0.613592	0.293066
2742	0.202	324	87	2.58	115	0.613484	0.283402
2747	0.202	96	138	2.63	117	0.649899	0.386730
2748	0.202	96	177	2.63	117	0.674007	0.413507
2749	0.202	96	177	2.63	117	0.673938	0.423697
2750	0.202	96	140	2.63	117	0.648891	0.387678
2751	0.202	96	95	2.63	117	0.619107	0.339573
2752	0.202	96	80	2.63	117	0.607856	0.319668
2753	0.202	96	70	2.63	117	0.596901	0.309479
2754	0.202	95	70	2.63	117	0.599260	0.320379

TABLE A1.4: Summary of experimental conditions (F. Soucy), continued

Num	Rad	Vel	Load	Bin	Cal	ε_n	ε_p
2755	0.202	96	77	2.63	117	0.604513	0.319668
2756	0.202	96	91	2.63	117	0.617498	0.337204
2757	0.202	562	90	2.63	117	0.605881	0.290758
2758	0.202	548	134	2.63	117	0.634597	0.326066
2759	0.202	566	66	2.60	116	0.571502	0.238187
2760	0.202	550	74	2.60	116	0.586937	0.248981
2761	0.202	552	89	2.60	116	0.600785	0.277285
2762	0.202	555	89	2.60	116	0.605285	0.266011
2763	0.202	556	76	2.60	116	0.590524	0.251379
2764	0.202	555	68	2.60	116	0.577779	0.236508
2767	0.202	884	64	2.60	116	0.511876	0.234828
2768	0.202	874	74	2.60	116	0.518519	0.253538
2769	0.202	868	88	2.60	116	0.539478	0.270808
2770	0.202	871	88	2.60	116	0.539214	0.272487
2771	0.202	878	75	2.60	116	0.527891	0.255217
2772	0.202	876	65	2.60	116	0.512419	0.244903
2773	0.202	870	74	2.60	116	0.523109	0.241545
2774	0.202	867	88	2.60	116	0.539741	0.271768
2775	0.202	862	134	2.60	116	0.564087	0.310386
2776	0.202	861	176	2.60	116	0.573560	0.325498
2777	0.202	870	176	2.60	116	0.572602	0.315423
2782	0.202	95	68	2.61	117	0.590433	0.296191
2783	0.202	95	78	2.61	117	0.606478	0.314644
2784	0.202	95	92	2.61	117	0.621809	0.336645
2785	0.202	95	137	2.61	117	0.653806	0.373788
2786	0.202	95	177	2.61	117	0.680455	0.398155
2787	0.202	95	177	2.61	117	0.679784	0.397918
2788	0.202	95	140	2.61	117	0.652459	0.365507
2789	0.202	95	95	2.61	117	0.621183	0.330968
2790	0.202	95	79	2.61	117	0.607773	0.305891
2791	0.202	95	68	2.61	117	0.589639	0.290750
2792	0.202	564	68	2.61	117	0.578472	0.246984
2793	0.202	555	77	2.61	117	0.586547	0.248876
2794	0.202	550	91	2.61	117	0.605707	0.277265
2795	0.202	543	135	2.61	117	0.637614	0.312042
2796	0.202	189	67	2.64	119	0.586890	0.288349
2797	0.202	185	77	2.64	119	0.601103	0.304226
2798	0.202	183	92	2.64	119	0.619091	0.318702
2799	0.202	183	138	2.64	119	0.652432	0.353958
2800	0.202	185	177	2.64	119	0.684734	0.386411
2801	0.202	185	177	2.64	119	0.682870	0.388980
2802	0.202	186	141	2.64	119	0.658348	0.353724
2803	0.202	186	95	2.64	119	0.624268	0.317067
2804	0.202	186	80	2.64	119	0.610004	0.296521
2805	0.202	186	68	2.64	119	0.595984	0.276442
2806	0.202	185	30	2.64	119	0.496855	0.190754
2807	0.202	185	68	2.64	119	0.585328	0.265351
2815	0.202	563	67	2.60	117	0.569043	0.250119
2816	0.202	553	76	2.60	117	0.583245	0.261984
2817	0.202	552	91	2.60	117	0.605657	0.280256
2818	0.202	545	134	2.60	117	0.638655	0.314665
2819	0.202	556	67	2.60	117	0.571851	0.238728
2820	0.202	551	77	2.60	117	0.586348	0.249881
2821	0.202	552	91	2.60	117	0.602288	0.260085
2822	0.202	545	134	2.60	117	0.635720	0.294020
2823	0.202	328	66	2.60	117	0.574449	0.240437
2824	0.202	317	76	2.60	117	0.593724	0.254455
2825	0.202	316	90	2.60	117	0.612282	0.272036
2826	0.202	311	134	2.60	117	0.643496	0.314326
2827	0.202	311	175	2.60	117	0.663284	0.342837
2828	0.202	317	175	2.60	117	0.662601	0.340223
2829	0.202	324	138	2.60	117	0.642623	0.305298
2830	0.202	324	94	2.60	117	0.620543	0.265859

TABLE A1.4: Summary of experimental conditions (F. Soucy), continued

Num	Rad	Vel	Load	Bin	Cal	ε_n	ε_p
2831	0.202	318	78	2.60	117	0.600662	0.243763
2834	0.202	882	67	2.59	117	0.479315	0.212467
2835	0.202	875	76	2.59	117	0.496304	0.224364
2836	0.202	867	90	2.59	117	0.510136	0.247680
2837	0.202	860	134	2.59	117	0.547277	0.288603
2838	0.202	858	175	2.59	117	0.562591	0.315965
2839	0.202	866	175	2.59	117	0.565044	0.321199
2840	0.202	883	139	2.59	117	0.548871	0.293362
2841	0.202	889	95	2.59	117	0.521918	0.251487
2842	0.202	881	79	2.59	117	0.498262	0.213419
2843	0.202	877	69	2.59	117	0.486469	0.194385
2844	0.202	873	69	2.59	117	0.482652	0.188199
2845	0.202	563	76	2.57	116		0.251441
2846	0.202	550	90	2.57	116		0.266330
2847	0.202	542	133	2.57	116		0.311720
2848	0.202	543	175	2.57	116		0.330932
2849	0.202	565	76	2.55	115		0.219022
2850	0.202	559	67	2.55	115		0.210794
2851	0.202	555	67	2.55	115		0.197725
2852	0.202	551	75	2.55	115		0.222168
2853	0.202	550	89	2.55	115		0.239835
2854	0.202	542	132	2.55	115		0.298403
2855	0.202	541	175	2.55	115		0.322362
2856	0.202	549	175	2.55	115		0.320426
2857	0.202	563	138	2.55	115		0.285818
2858	0.202	569	94	2.55	115		
2859	0.202	560	79	2.55	115		0.198693
2860	0.202	557	68	2.55	115		0.181994
2861	0.202	554	68	2.55	115		0.188529
2862	0.202	546	90	2.55	115		0.213214
2863	0.202	95	80	2.68	121	0.461489	0.269319
2864	0.202	194	80	2.68	121	0.457093	0.253680
2865	0.202	333	80	2.68	121	0.454665	0.235511
2866	0.202	562	80	2.68	121	0.449016	0.223551
2871	0.202	564	69	2.60	128	0.566403	0.233616
2872	0.202	552	79	2.60	128	0.577217	0.242108
2873	0.202	551	94	2.60	128	0.596029	0.261049
2874	0.202	323	69	2.60	128	0.566379	0.238842
2875	0.202	322	79	2.60	128	0.581571	0.247986
2876	0.202	319	93	2.60	128	0.600174	0.276072
2877	0.202	318	137	2.60	128	0.636218	0.315698
2878	0.202	317	177	2.60	128	0.653032	0.350316
2879	0.202	320	177	2.60	128	0.654733	0.349445
2880	0.202	325	142	2.60	128	0.637412	0.329632
2881	0.202	328	97	2.60	128	0.599873	0.279991
2882	0.202	324	82	2.60	128	0.579153	0.256042
2883	0.202	323	71	2.60	128	0.560581	0.230351
2884	0.202	188	68	2.63	129	0.570069	0.263101
2885	0.202	184	79	2.63	129	0.591843	0.292646
2886	0.202	185	92	2.63	129	0.605833	0.297606
2887	0.202	180	136	2.63	129	0.638684	0.347854
2888	0.202	189	68	2.63	129	0.574371	0.263964
2889	0.202	185	78	2.63	129	0.589539	0.283157
2890	0.202	95	78	2.63	129	0.591912	0.296528
2891	0.202	96	69	2.63	129	0.575300	0.280354
2892	0.202	95	69	2.63	129	0.574054	0.273237
2893	0.202	95	77	2.63	129	0.588964	0.289196
2894	0.202	94	91	2.63	129	0.606579	0.316800
2895	0.202	93	135	2.63	129	0.640651	0.355834
2896	0.202	90	176	2.63	129	0.662454	0.386888
2897	0.202	92	175	2.63	129	0.661213	0.390554
2898	0.202	97	139	2.63	129	0.644249	0.357343
2899	0.202	95	94	2.63	129	0.605201	0.308820

TABLE A1.4: Summary of experimental conditions (F. Soucy), continued

Num	Rad	Vel	Load	Bin	Cal	ε_n	ε_p
2900	0.202	94	80	2.63	129	0.587515	0.294587
2901	0.202	94	80	2.63	129	0.584897	0.284667
2915	0.202	96	42	2.51	123	0.503062	0.163505
2916	0.202	96	17	2.51	123	0.346396	0.064137
2917	0.202	96	12	2.51	123	0.284430	0.047200
2918	0.202	96	12	2.51	123	0.287193	0.035230
2919	0.202	96	65	2.51	123	0.561742	0.252258
2920	0.202	96	65	2.51	123	0.560783	0.237805
2921	0.202	97	53	2.51	123	0.534151	0.219512
2922	0.202	564	53	2.51	123	0.517453	0.169603
2923	0.202	553	65	2.51	123	0.540043	0.195122
2924	0.202	555	65	2.51	123	0.544083	0.195122
2925	0.202	559	53	2.51	123	0.519445	0.173442
2926	0.202	559	44	2.51	123	0.496740	0.151536
2927	0.202	565	18	2.51	123	0.329673	0.055104
2928	0.202	556	13	2.51	123	0.272479	0.024616
2929	0.202	555	9	2.51	123	0.194350	0.024842
2930	0.202	556	9	2.51	123	0.200546	0.023261
2931	0.202	884	42	2.51	123	0.487232	0.137534
2932	0.202	873	50	2.51	123	0.509300	0.148600
2933	0.202	872	50	2.51	123	0.506271	0.149503
2934	0.202	878	43	2.51	123	0.490258	0.137760
2935	0.202	888	18	2.51	123	0.329236	0.042683
2936	0.202	880	13	2.51	123	0.273196	0.030714
2937	0.202	875	9	2.51	123	0.196122	0.014228
2938	0.202	875	9	2.51	123	0.198965	0.014228
2939	0.202	873	12	2.51	123	0.259186	0.018970
2947	0.202	97	42	2.54	125	0.518747	0.204059
2948	0.202	563	42	2.54	125	0.501800	0.144960
2949	0.202	553	51	2.54	125	0.531398	0.163916
2950	0.202	551	65	2.54	125	0.556608	0.203390
2951	0.202	554	65	2.54	125	0.555275	0.198037
2952	0.202	562	53	2.54	125	0.531075	0.171053
2953	0.202	562	44	2.54	125	0.510408	0.163470
2954	0.202	565	18	2.54	125	0.343136	0.060437
2955	0.202	557	13	2.54	125	0.284443	0.041704
2956	0.202	555	9	2.54	125	0.209629	0.019402
2960	0.202	96	43	2.60	127	0.528014	0.193548
2961	0.202	95	65	2.60	127	0.577442	0.244987
2962	0.202	96	65	2.60	127	0.580651	0.253705
2963	0.202	96	45	2.60	127	0.537054	0.207280
2964	0.202	96	16	2.60	127	0.360687	0.082607
2965	0.202	96	7	2.60	127	0.173813	0.048169
2966	0.202	95	43	2.60	127	0.533827	0.200305
2967	0.202	561	43	2.60	127	0.513577	0.158675
2968	0.202	552	65	2.60	127	0.569251	0.207280
2969	0.202	557	65	2.60	127	0.569528	0.209024
2970	0.202	559	44	2.60	127	0.517495	0.162816
2971	0.202	564	16	2.60	127	0.343291	0.069529
2972	0.202	560	7	2.60	127	0.170461	0.034002
2973	0.202	556	7	2.60	127	0.181406	0.048169
2974	0.202	552	16	2.60	127	0.348473	0.059939
2975	0.202	547	42	2.60	127	0.514922	0.138622
2976	0.202	96	65	2.60	127	0.583937	0.251526
2977	0.202	559	65	2.60	127	0.568729	0.216652
2978	0.202	562	43	2.60	127	0.510399	0.155841
2979	0.202	565	17	2.60	127	0.353180	0.071927
2980	0.202	557	9	2.60	127	0.226308	0.031168
2981	0.202	555	9	2.60	127	0.226940	0.040759
2982	0.202	551	17	2.60	127	0.353851	0.072581
2983	0.202	544	41	2.60	127	0.505744	0.143636
2984	0.202	544	65	2.60	127	0.564273	0.191805
2985	0.202	96	40	2.55	125	0.520198	0.188444

TABLE A1.4: Summary of experimental conditions (F. Soucy), continued

Num	Rad	Vel	Load	Bin	Cal	ε_n	ε_p
2986	0.202	964	41	2.55	125	0.500652	0.142444
2987	0.202	967	18	2.55	125	0.346193	0.061111
2988	0.202	96	40	2.53	124	0.523060	0.176629
2989	0.202	96	65	2.53	124	0.581478	0.247817
2990	0.202	98	19	2.53	124	0.379494	0.078128
2991	0.202	96	9	2.53	124	0.241254	0.031789
2992	0.202	187	40	2.53	124	0.516499	0.158943
2993	0.202	187	65	2.53	124	0.574193	0.221849
2994	0.202	190	19	2.53	124	0.380930	0.086411
2995	0.202	188	9	2.53	124	0.239656	0.039624
2996	0.202	325	39	2.58	126	0.510849	0.155604
2997	0.202	320	64	2.58	126	0.579034	0.232308
2998	0.202	328	19	2.58	126	0.383449	0.079560
2999	0.202	322	10	2.58	126	0.261457	0.051868
3000	0.202	319	19	2.58	126	0.390867	0.092527
3001	0.202	541	65	2.58	126	0.575390	0.213626
3002	0.202	543	41	2.58	126	0.516334	0.150989
3003	0.202	545	19	2.58	126	0.381283	0.070110
3004	0.202	538	10	2.58	126	0.256860	0.033187
3005	0.202	535	10	2.58	126	0.258591	0.039560
3006	0.202	531	19	2.58	126	0.385853	0.063077
3007	0.202	528	39	2.58	126	0.510667	0.130769
3008	0.202	961	39	2.58	126	0.498288	0.132527
3009	0.202	954	64	2.58	126	0.563467	0.190769
3010	0.202	965	41	2.58	126	0.505228	0.136264
3011	0.202	969	20	2.58	126	0.370167	0.059560
3012	0.202	963	10	2.58	126	0.247499	0.034945
3013	0.202	961	10	2.58	126	0.253213	0.041978
3014	0.202	958	19	2.58	126	0.367332	0.050330
3023	0.202	97	41	2.59	127	0.522343	0.156137
3024	0.202	96	66	2.59	127	0.578038	0.225765
3025	0.202	100	43	2.59	127	0.526328	0.164676
3026	0.202	97	29	2.59	127	0.458456	0.125702
3027	0.202	97	18	2.59	127	0.354428	0.078626
3028	0.202	97	8	2.59	127	0.199508	0.039870
3029	0.202	96	8	2.59	127	0.204014	0.041184
3030	0.202	96	17	2.59	127	0.359453	0.082348
3031	0.202	96	27	2.59	127	0.448479	0.118038
3032	0.202	187	28	2.59	127	0.443593	0.108185
3033	0.202	188	28	2.59	127	0.445318	0.110813
3034	0.202	189	18	2.59	127	0.349528	0.070743
3035	0.202	184	41	2.59	127	0.518977	0.151758
3036	0.202	326	29	2.59	127	0.449423	0.099865
3037	0.202	321	29	2.59	127	0.446781	0.104244
3038	0.202	322	18	2.59	127	0.344293	0.064393
3039	0.202	317	41	2.59	127	0.514384	0.147816
3040	0.202	547	29	2.59	127	0.440195	0.095267
3041	0.202	535	18	2.59	127	0.334889	0.049942
3042	0.202	524	41	2.59	127	0.501970	0.116068
3043	0.202	523	66	2.59	127	0.563030	
3048	0.202	97	41	2.56	114	0.508575	0.130092
3049	0.202	327	41	2.56	114	0.507033	0.128874
3050	0.202	318	66	2.56	114	0.558610	0.196334
3051	0.202	320	66	2.56	114	0.554536	0.192194
3052	0.202	326	42	2.56	114	0.509533	0.135937
3053	0.202	324	29	2.56	114	0.438808	0.096241
3054	0.202	325	18	2.56	114	0.330682	0.064581
3055	0.202	322	66	2.56	114	0.554991	0.184400
3056	0.202	96	65	2.58	115	0.569439	0.219091
3057	0.202	96	42	2.58	115	0.521611	0.168757
3058	0.202	96	29	2.58	115	0.453692	0.124714
3059	0.202	96	19	2.58	115	0.353222	0.083091
3060	0.202	96	6	2.58	115	0.137108	0.026949

TABLE A1.4: Summary of experimental conditions (F. Soucy), continued

Num	Rad	Vel	Load	Bin	Cal	ε_n	ε_p
3061	0.202	95	18	2.58	115	0.361594	0.084543
3062	0.202	96	65	2.58	115	0.576106	0.219091
3063	0.202	330	65	2.58	115	0.566159	0.193924
3064	0.202	546	40	2.55	113	0.522844	0.087993
3065	0.202	526	65	2.55	113	0.598552	0.156166
3066	0.202	534	65	2.55	113	0.599675	0.153959
3067	0.202	547	41	2.55	113	0.533046	0.097802
3068	0.202	533	27	2.55	113	0.410066	0.054642
3069	0.202	536	19	2.55	113	0.281421	0.028892
3070	0.202	534	10	2.55	113		0.000201
3072	0.202	327	65	2.55	113	0.612048	0.160581
3073	0.202	328	41	2.55	113	0.543239	0.108347
3074	0.202	327	20	2.55	113	0.289515	0.016876
3075	0.202	320	28	2.55	113	0.425329	0.061508
3076	0.202	321	19	2.55	113	0.284936	0.012462
3077	0.202	323	10	2.55	113		0.005841
3078	0.202	331	65	2.55	113	0.625616	0.159109
3079	0.202	182	65	2.55	113	0.623241	
3080	0.202	187	41	2.57	118	0.572054	
3081	0.202	97	41	2.57	118	0.579590	
3082	0.202	322	66	2.57	118	0.636406	0.152194
3083	0.202	321	65	2.57	118	0.638487	0.152194
3084	0.202	321	65	2.57	118	0.636567	0.152194
3085	0.202	321	65	2.57	118	0.635114	0.152194
3086	0.202	323	65	2.57	118	0.637127	0.152194
3087	0.202	320	65	2.57	118	0.637376	0.152194
3088	0.202	321	65	2.57	118	0.642703	0.152194
3089	0.202	321	65	2.57	118	0.635960	0.152194
3090	0.202	188	65	2.57	118	0.641262	0.158625
3091	0.202	186	65	2.57	118	0.634000	0.158625
3092	0.202	189	66	2.57	118	0.627162	0.158625
3093	0.202	186	65	2.57	118	0.634061	0.158625
3094	0.202	186	65	2.57	118	0.627657	0.158625
3095	0.202	189	65	2.57	118	0.629650	0.158625
3096	0.202	183	65	2.57	118	0.626481	0.158625
3101	0.202	96	41	2.16	99	0.411972	0.000000
3102	0.202	97	29	2.16	99	0.328274	0.000000
3103	0.202	96	18	2.16	99	0.195950	0.000000
3104	0.202	320	18	2.16	99	0.205550	0.000000
3105	0.202	321	28	2.16	99	0.313059	0.000000
3106	0.202	321	41	2.16	99	0.408202	0.000000
3107	0.202	536	41	2.16	99	0.405575	0.000000
3108	0.202	538	18	2.16	99	0.212347	0.000000
3109	0.202	533	27	2.16	99	0.314115	0.000000
3110	0.202	534	18	2.16	99	0.203441	0.000000
3111	0.202	98	42	2.13	98	0.420530	0.000000
3112	0.202	96	29	2.13	98	0.328531	0.000000
3113	0.202	96	18	2.13	98	0.218781	0.000000
3114	0.202	95	28	2.13	98	0.321760	0.000000
3115	0.202	97	42	2.13	98	0.410386	0.000000
3116	0.202	192	42	2.13	98	0.413767	0.000000
3117	0.202	187	66	2.13	98	0.464916	0.000000
3118	0.202	187	66	2.13	98	0.464599	0.000000
3119	0.202	197	19	2.13	98	0.201164	0.000000
3120	0.202	185	28	2.13	98	0.320529	0.000000
3121	0.202	185	42	2.13	98	0.409848	0.000000
3122	0.202	185	66	2.13	98	0.462965	0.000000
3123	0.202	95	41	2.18	100	0.437968	0.000000
3124	0.202	95	66	2.18	100	0.494399	0.000000
3125	0.202	95	66	2.18	100	0.491293	0.000000
3126	0.202	96	42	2.18	100	0.436466	0.000000
3127	0.202	95	30	2.18	100	0.344990	0.000000
3128	0.202	95	19	2.18	100	0.228599	0.000000

TABLE A1.4: Summary of experimental conditions (F. Soucy), continued

Num	Rad	Vel	Load	Bin	Cal	ε_n	ε_p
3129	0.202	95	19	2.18	100	0.233956	0.000000
3130	0.202	95	28	2.18	100	0.344209	0.000000
3131	0.202	93	41	2.18	100	0.439213	0.000000
3132	0.202	95	41	2.15	98	0.436309	0.000000
3133	0.202	186	41	2.15	98	0.432681	0.000000
3134	0.202	186	66	2.15	98	0.492220	0.000000
3135	0.202	186	66	2.15	98	0.490328	0.000000
3136	0.202	187	42	2.15	98	0.442647	0.000000
3137	0.202	186	29	2.15	98	0.337891	0.000000
3138	0.202	186	18	2.15	98	0.206397	0.000000
3139	0.202	185	18	2.15	98	0.205866	0.000000
3140	0.202	185	16	2.15	98	0.134814	0.000000
3141	0.202	186	27	2.15	98	0.323205	0.000000
3142	0.202	544	41	2.15	98	0.422085	0.000000
3143	0.202	528	66	2.15	98	0.486125	0.000000
3144	0.202	533	66	2.15	98	0.484706	0.000000
3145	0.202	534	30	2.15	98	0.359144	0.000000
3146	0.202	533	30	2.15	98	0.340437	0.000000
3147	0.202	532	30	2.15	98	0.344577	0.000000
3148	0.202	531	41	2.15	98	0.430948	0.000000
3149	0.202	534	19	2.15	98	0.204259	0.000000
3150	0.202	533	19	2.15	98	0.210205	0.000000
3151	0.202	332	41	2.15	99	0.434311	0.000000
3152	0.202	320	66	2.15	99	0.491548	0.000000
3153	0.202	322	66	2.15	99	0.492202	0.000000
3154	0.202	325	42	2.15	99	0.441172	0.000000
3155	0.202	323	30	2.15	99	0.372607	0.000000
3156	0.202	325	20	2.15	99	0.246788	0.000000
3157	0.202	321	20	2.15	99	0.242044	0.000000
3158	0.202	320	29	2.15	99	0.341485	0.000000
3159	0.202	322	20	2.15	99	0.234830	0.000000
3160	0.202	319	41	2.15	99	0.435270	0.000000
3161	0.202	97	41	2.15	99	0.444946	0.000000
3162	0.202	98	29	2.15	99	0.355349	0.000000
3163	0.202	99	20	2.15	99	0.251160	0.000000
3164	0.202	192	20	2.15	99	0.246408	0.000000
3165	0.202	187	28	2.15	99	0.338011	0.000000
3166	0.202	188	28	2.15	99	0.341573	0.000000
3167	0.202	187	20	2.15	99	0.244433	0.000000
3168	0.202	185	41	2.15	99	0.435070	0.000000
3169	0.202	185	66	2.15	99	0.491694	0.000000
3170	0.202	326	65	2.15	99	0.488846	0.000000
3171	0.202	324	41	2.15	99	0.435952	0.000000
3172	0.202	323	20	2.15	99	0.237000	0.000000
3173	0.202	319	20	2.15	99	0.233076	0.000000
3174	0.202	314	41	2.15	99	0.427621	0.000000
3179	0.202	321	40	2.78	118	0.508706	
3180	0.202	320	20	2.78	118	0.295643	
3181	0.202	322	65	2.78	118	0.583589	
3182	0.202	324	41	2.78	118	0.513482	
3183	0.202	96	41	2.78	118	0.530872	
3184	0.202	96	39	2.78	118	0.528489	
3185	0.202	321	39	2.78	118	0.515444	
3186	0.202	322	20	2.78	118	0.311095	0.070383
3187	0.202	320	20	2.78	118	0.313010	0.084254
3188	0.202	97	65	2.67	113	0.576928	
3189	0.202	321	65	2.67	113	0.574345	0.166533
3190	0.202	320	65	2.67	113	0.563559	0.186581
3191	0.202	326	40	2.67	113	0.486993	0.075114
3192	0.202	96	40	2.47	105	0.474492	0.035381
3193	0.202	96	65	2.47	105	0.538926	0.105588
3194	0.202	96	42	2.47	105	0.481086	0.046243
3195	0.202	96	19	2.47	105	0.274308	0.001734

TABLE A1.4: Summary of experimental conditions (F. Soucy), continued

Num	Rad	Vel	Load	Bin	Cal	ε_n	ε_p
3196	0.202	187	40	2.17	92	0.391275	
3197	0.202	187	65	2.17	92	0.461257	
3198	0.202	187	65	2.17	92	0.469558	
3199	0.202	188	42	2.17	92	0.405748	
3200	0.202	187	20	2.17	92	0.178933	
3201	0.202	325	20	2.17	92	0.175618	
3202	0.202	319	40	2.17	92	0.389139	
3203	0.202	320	65	2.17	92	0.464888	
3204	0.202	321	41	2.23	94	0.450509	-0.006628
3205	0.202	538	41	2.23	94	0.437478	-0.021034
3206	0.202	533	41	2.23	94	0.440422	-0.003394
3207	0.202	527	65	2.23	94	0.490530	0.011599
3208	0.202	532	65	2.23	94	0.494033	0.022771
3209	0.202	539	41	2.23	94	0.443958	-0.008980
3210	0.202	536	20	2.23	94	0.267414	-0.019270
3211	0.202	533	20	2.23	94	0.266562	-0.018388
3212	0.202	529	40	2.23	94	0.452631	0.014539
3213	0.202	96	39	2.20	93	0.476105	0.007019
3214	0.202	96	65	2.20	93	0.522470	0.045176
3215	0.202	96	65	2.20	93	0.521359	0.051138
3216	0.202	96	41	2.20	93	0.479721	0.020732
3217	0.202	96	20	2.20	93	0.305539	-0.000136
3218	0.202	96	15	2.20	93	0.218725	-0.006098
3219	0.202	96	14	2.20	93	0.199041	-0.005799
3220	0.202	95	20	2.20	93	0.305896	-0.006396
3221	0.202	187	20	2.20	93	0.299639	-0.012954
3222	0.202	186	39	2.20	93	0.467665	0.016558
3223	0.202	186	65	2.20	93	0.516403	0.033848
3224	0.202	187	65	2.20	93	0.511299	0.020136
3225	0.202	188	41	2.20	93	0.461815	-0.004011
3226	0.202	188	20	2.20	93	0.307312	0.001653
3227	0.202	186	14	2.20	93	0.219480	-0.000732
3228	0.202	187	14	2.20	93	0.217681	-0.005799
3229	0.202	186	20	2.20	93	0.303488	0.002846
3230	0.202	322	20	2.20	93	0.304665	0.010894
3231	0.202	319	39	2.20	93	0.456589	-0.001626
3232	0.202	317	65	2.20	93	0.514245	0.029377
3233	0.202	320	65	2.20	93	0.510232	0.029377
3234	0.202	324	41	2.20	93	0.462081	0.003144
3235	0.202	321	20	2.20	93	0.301777	-0.005799
3236	0.202	320	15	2.20	93	0.199160	-0.013848
3238	0.202	96	41	2.56	108	0.498585	
3239	0.202	95	65	2.56	108	0.555536	0.141959
3240	0.202	95	65	2.56	108	0.557403	0.148130
3241	0.202	96	43	2.56	108	0.502062	0.084619
3242	0.202	95	18	2.56	108	0.234615	0.011337
3243	0.202	95	15	2.56	108	0.175301	-0.003062
3244	0.202	95	19	2.56	108	0.262478	0.018280
3245	0.202	96	41	2.56	108	0.495394	0.095675
3246	0.202	186	41	2.60	110	0.496347	0.077761
3247	0.202	188	65	2.60	110	0.557319	0.146910
3248	0.202	187	65	2.60	110	0.558265	0.150709
3249	0.202	187	43	2.60	110	0.503077	0.100811
3250	0.202	187	18	2.60	110	0.251976	0.012918
3251	0.202	187	15	2.60	110	0.191348	0.009119
3252	0.202	186	19	2.60	110	0.269652	0.014184
3253	0.202	185	41	2.60	110	0.497699	0.084093

TABLE A1.5: Command log input to SYSTAT (F. Soucy)

```
By
Select
Weight
Use 'c:\systat\data\SUM2REPL.SYS'
By
Select
Weight
Print Long
Format  4
Options

Nonlin

Model EW=(Aa+B*(ao+al*log(L)+ar*log(R)+av*log(V))),
  *(B<0.5*(1-Aa)/(ao+al*log(L)+ar*log(R)+av*log(V))),
  +(1-0.25*((1-Aa)^2)/(B*(ao+al*log(L)+ar*log(R)+av*log(V)))),
  *(B>=0.5*(1-Aa)/(ao+al*log(L)+ar*log(R)+av*log(V)))

Estimate /Iter=100 / Start = -.4,.1,0.1,-.02,-.02, Quasi, Print

By
Select
Weight
Use 'c:\systat\data\SUM2REPL.SYS'
By
Select
Weight
Print Long
Format  4
Options

Nonlin

Model EP=0+(Aa+B*(ao+al*log(L)+ar*log(R)+av*log(V))),
  *((B>=-Aa/(ao+al*log(L)+ar*log(R)+av*log(V))),
  AND (B<0.5*(1-Aa)/(ao+al*log(L)+ar*log(R)+av*log(V)))),
  +(1-0.25*((1-Aa)^2)/(B*(ao+al*log(L)+ar*log(R)+av*log(V)))),
  *(B>=0.5*(1-Aa)/(ao+al*log(L)+ar*log(R)+av*log(V)))

Estimate /Iter=100 / Start = -.4,.1,.1,-.02,-.02, Quasi, Print
```

TABLE A1.6: SYSTAT output (F. Soucy)

```
  FILE IN USE IS  c:\systat\data\SUM2REPL.SYS

 NONLIN VERSION 5.03

ITER   LOSS   PARAMETER VALUES
 0  .8591756D+00 -.4000D+00 .1000D+00 .1000D+00-.2000D-01-.2000D-01
 1  .6855326D+00 -.4003D+00 .9958D-01 .9827D-01-.1943D-01-.2223D-01
 2  .6016547D+00 -.4020D+00 .9933D-01 .8614D-01-.2032D-01-.1458D-01
 3  .5857486D+00 -.4172D+00 .5363D-01 .8939D-01-.3923D-01-.1183D-01
 4  .5843321D+00 -.4192D+00 .4868D-01 .9015D-01-.3631D-01-.1053D-01
 5  .5819153D+00 -.4446D+00 .5707D-01 .9336D-01-.3612D-01-.1127D-01
 6  .5812192D+00 -.4098D+00 .4198D-01 .8942D-01-.3690D-01-.9479D-02
 7  .5807190D+00 -.3823D+00 .4354D-01 .8617D-01-.3461D-01-.9695D-02
 8  .5806028D+00 -.3737D+00 .4434D-01 .8529D-01-.3374D-01-.9796D-02
 9  .5805716D+00 -.3608D+00 .4178D-01 .8387D-01-.3332D-01-.9494D-02
10  .5805642D+00 -.3636D+00 .4181D-01 .8422D-01-.3352D-01-.9508D-02
*1  .5805638D+00 -.3630D+00 .4183D-01 .8415D-01-.3348D-01-.9514D-02
12  .5805638D+00 -.3629D+00 .4182D-01 .8414D-01-.3347D-01-.9512D-02
13  .5805638D+00 -.3629D+00 .4182D-01 .8414D-01-.3347D-01-.9512D-02

 DEPENDENT VARIABLE IS   EN

  SOURCE SUM-OF-SQUARES  DF  MEAN-SQUARE

  REGRESSION   101.5741   5  20.3148
  RESIDUAL   0.5806 347   0.0017
   TOTAL   101.0736 352
 CORRECTED   4.4770 351

   RAW R-SQUARED (1-RESIDUAL/TOTAL)   =   0.9943
 CORRECTED R-SQUARED (1-RESIDUAL/CORRECTED) =   0.8703

 PARAMETER    ESTIMATE   A.S.E.    LOWER  <95%> UPPER
    AA    -0.3629   0.0764  -0.5131  -0.2127
    AO     0.0418   0.0202   0.0021   0.0815
    AL     0.0841   0.0084   0.0676   0.1007
    AR    -0.0335   0.0075  -0.0483  -0.0187
    AV    -0.0095   0.0025  -0.0144  -0.0047

 ASYMPTOTIC CORRELATION MATRIX OF PARAMETERS

      AA    AO    AL    AR    AV

AA    1.0000
AO     -0.5649  1.0000
AL     -0.9779  0.4885  1.0000
AR    0.4576  0.1806   -0.4536  1.0000
AV    0.5095   -0.7936   -0.5077  0.2097  1.0000
```

TABLE A1.6: SYSTAT output (F. Saucy), continued

```
  FILE IN USE IS  c:\systat\data\SUM2REPL.SYS

 ITER  LOSS   PARAMETER VALUES
 0  .4345868D+02 -.4000D+00 .1000D+00 .1000D+00-.2000D-01-.2000D-01
 1  .2281793D+02 -.4010D+00 .9841D-01 .9350D-01-.1776D-01-.2889D-01
 2  .4662654D+01 -.3883D+00 .9770D-01 .5046D-01-.1705D-01-.2752D-01
 3  .4366966D+01 -.4275D+00 .7858D-01 .3985D-01 .2282D-01-.2566D-02
 4  .4175684D+01 -.4925D+00 .7870D-01 .2074D-01-.1612D-01 .8733D-02
 5  .2251565D+01 -.5347D+00 .2037D+00 .1298D-01 .1969D-01 .8033D-02
 6  .7164177D+00 -.4487D+00-.4068D-01 .5096D-01-.2042D-01 .7996D-02
 7  .4448281D+00 -.4654D+00 .9113D-01 .4406D-01-.1148D-01-.6317D-02
 8  .4406292D+00 -.4743D+00 .1012D+00 .4189D-01-.8077D-02-.4806D-02
 9  .4397790D+00 -.4799D+00 .1167D+00 .4050D-01-.5226D-02-.5315D-02
10  .4385163D+00 -.4769D+00 .1095D+00 .4156D-01-.8149D-02-.5833D-02
11  .4376064D+00 -.4807D+00 .1158D+00 .4103D-01-.6379D-02-.5822D-02
12  .4338900D+00 -.4923D+00 .1237D+00 .4148D-01-.3344D-02-.6020D-02
13  .4165416D+00 -.5803D+00 .1677D+00 .4255D-01 .1353D-02-.7219D-02
14  .4037120D+00 -.6556D+00 .1770D+00 .4564D-01-.3147D-02-.6885D-02
15  .3980607D+00 -.6679D+00 .1628D+00 .4803D-01-.8782D-02-.6592D-02
16  .3977092D+00 -.6875D+00 .1684D+00 .4875D-01-.8773D-02-.6676D-02
17  .3974635D+00 -.7026D+00 .1752D+00 .4919D-01-.8040D-02-.6813D-02
18  .3974367D+00 -.7017D+00 .1742D+00 .4929D-01-.8197D-02-.6826D-02
19  .3974355D+00 -.7017D+00 .1743D+00 .4930D-01-.8151D-02-.6846D-02
20  .3974355D+00 -.7016D+00 .1743D+00 .4931D-01-.8134D-02-.6852D-02
21  .3974355D+00 -.7017D+00 .1743D+00 .4931D-01-.8133D-02-.6852D-02
22  .3974355D+00 -.7017D+00 .1743D+00 .4931D-01-.8133D-02-.6852D-02

 DEPENDENT VARIABLE IS   EP

 MISSING DATA OR ESTIMATES REDUCED DEGREES OF FREEDOM

  SOURCE SUM-OF-SQUARES  DF  MEAN-SQUARE

  REGRESSION    19.9625   5   3.9925
  RESIDUAL   0.3974 354   0.0011
   TOTAL    20.3392 359
 CORRECTED   4.6293 358

   RAW R-SQUARED (1-RESIDUAL/TOTAL)   =   0.9805
 CORRECTED R-SQUARED (1-RESIDUAL/CORRECTED) =   0.9141

 PARAMETER    ESTIMATE   A.S.E.    LOWER  <95%> UPPER
    AA   -0.7017   0.0625  -0.8246  -0.5788
    AO    0.1743   0.0176   0.1398   0.2089
    AL    0.0493   0.0034   0.0426   0.0560
    AR   -0.0081   0.0040  -0.0160  -0.0002
    AV   -0.0069   0.0009  -0.0087  -0.0050

 ASYMPTOTIC CORRELATION MATRIX OF PARAMETERS

      AA    AO    AL    AR    AV

AA    1.0000
AO     -0.8871  1.0000
AL     -0.9008  0.6678  1.0000
AR    0.0800  0.2359   -0.1528  1.0000
AV    0.4154   -0.3796   -0.5525  0.2912  1.0000
```

TABLE A1.7: SYSTAT output, converted to $\log_{10}$ (Boise-Cascade)

DEPENDENT VARIABLE IS EN

PARAMETER	ESTIMATE	A.S.E.	LOWER <95%>	UPPER
AA	-0.3874	0.0362	-0.4609	-0.3138
AL	0.2597	0.0117	0.2360	0.2837
AV	-0.0111	0.0023	-0.0157	-0.0064

DEPENDENT VARIABLE IS EP

PARAMETER	ESTIMATE	A.S.E.	LOWER <95%>	UPPER
AA	-0.3874	0.0362	-0.4598	-0.3150
AL	0.0882	0.0097	0.0686	0.1078
AV	-0.0272	0.0046	-0.0366	-0.0177

TABLE A1.8: SYSTAT output, converted to $\log_{10}$ (F. Soucy)

DEPENDENT VARIABLE IS EN

PARAMETER	ESTIMATE	A.S.E.	LOWER <95%>	UPPER
AA	-0.3629	0.0764	-0.5131	-0.2127
AO	0.0418	0.0202	0.0021	0.0815
AL	0.1937	0.0193	0.1557	0.2319
AR	-0.0771	0.0173	-0.1112	-0.0431
AV	-0.0219	0.0058	-0.0332	-0.0108

DEPENDENT VARIABLE IS EP

PARAMETER	ESTIMATE	A.S.E.	LOWER <95%>	UPPER
AA	-0.7017	0.0625	-0.8246	-0.5788
AO	0.1743	0.0176	0.1398	0.2089
AL	0.1135	0.0078	0.0981	0.1289
AR	-0.0187	0.0092	-0.0368	-0.0005
AV	-0.0158	0.0021	-0.0200	-0.0115

TABLE A1.9: Experimental results

(Sort order: Radius, Bulk, Velocity, Load, serial number)

Ser. Num.	Cal μm	B.W. g/m²	B_v cm³/g	Vel m/m	Load kN/m	Rad m	In-nip strain	Rec1 strain	Rec2 strain	Perm. strain
3103	99	45.8	2.16	96	18	0.202	0.196	0.052	0.040	0.000
3113	98	45.8	2.13	96	18	0.202	0.219	0.058	0.035	0.000
3128	100	45.8	2.18	95	19	0.202	0.229	0.054	0.038	0.000
3129	100	45.8	2.18	95	19	0.202	0.234	0.057	0.040	0.000
3163	99	45.8	2.15	99	20	0.202	0.251	0.076	0.053	0.000
3102	99	45.8	2.16	97	29	0.202	0.328	0.066	0.051	0.000
3112	98	45.8	2.13	96	29	0.202	0.329	0.069	0.040	0.000
3114	98	45.8	2.13	95	28	0.202	0.322	0.067	0.045	0.000
3127	100	45.8	2.18	95	30	0.202	0.345	0.064	0.044	0.000
3130	100	45.8	2.18	95	28	0.202	0.344	0.071	0.053	0.000
3162	99	45.8	2.15	98	29	0.202	0.355	0.091	0.062	0.000
3101	99	45.8	2.16	96	41	0.202	0.412	0.073	0.050	0.000
3111	98	45.8	2.13	98	42	0.202	0.421	0.090	0.056	0.000
3115	98	45.8	2.13	97	42	0.202	0.410	0.084	0.061	0.000
3123	100	45.8	2.18	95	41	0.202	0.438	0.074	0.049	0.000
3126	100	45.8	2.18	96	42	0.202	0.436	0.077	0.056	0.000
3131	100	45.8	2.18	93	41	0.202	0.439	0.091	0.071	0.000
3132	98	45.8	2.15	95	41	0.202	0.436	0.082	0.061	0.000
3161	99	45.8	2.15	97	41	0.202	0.445	0.104	0.068	0.000
3124	100	45.8	2.18	95	66	0.202	0.494	0.122	0.098	0.000
3125	100	45.8	2.18	95	66	0.202	0.491	0.120	0.100	0.000
3119	98	45.8	2.13	197	19	0.202	0.201	0.053	0.032	0.000
3138	98	45.8	2.15	186	18	0.202	0.206	0.045	0.025	0.000
3139	98	45.8	2.15	185	18	0.202	0.206	0.045	0.027	0.000
3140	98	45.8	2.15	185	16	0.202	0.135	0.038	0.026	0.000
3164	99	45.8	2.15	192	20	0.202	0.246	0.065	0.041	0.000
3167	99	45.8	2.15	187	20	0.202	0.244	0.070	0.046	0.000
3120	98	45.8	2.13	185	28	0.202	0.321	0.065	0.042	0.000
3137	98	45.8	2.15	186	29	0.202	0.338	0.054	0.029	0.000
3141	98	45.8	2.15	186	27	0.202	0.323	0.050	0.028	0.000
3165	99	45.8	2.15	187	28	0.202	0.338	0.075	0.049	0.000
3166	99	45.8	2.15	188	28	0.202	0.342	0.077	0.050	0.000
3116	98	45.8	2.13	192	42	0.202	0.414	0.074	0.044	0.000
3121	98	45.8	2.13	185	42	0.202	0.410	0.078	0.055	0.000
3133	98	45.8	2.15	186	41	0.202	0.433	0.069	0.048	0.000
3136	98	45.8	2.15	187	42	0.202	0.443	0.080	0.056	0.000
3168	99	45.8	2.15	185	41	0.202	0.435	0.088	0.065	0.000
3117	98	45.8	2.13	187	66	0.202	0.465	0.107	0.075	0.000
3118	98	45.8	2.13	187	66	0.202	0.465	0.110	0.081	0.000
3122	98	45.8	2.13	185	66	0.202	0.463	0.109	0.084	0.000
3134	98	45.8	2.15	186	66	0.202	0.492	0.109	0.087	0.000
3135	98	45.8	2.15	186	66	0.202	0.490	0.112	0.088	0.000
3169	99	45.8	2.15	185	66	0.202	0.492	0.115	0.089	0.000
3104	99	45.8	2.16	320	18	0.202	0.206	0.039	0.038	0.000
3156	99	45.8	2.15	325	20	0.202	0.247	0.045	0.045	0.000
3157	99	45.8	2.15	321	20	0.202	0.242	0.039	0.040	0.000
3159	99	45.8	2.15	322	20	0.202	0.235	0.042	0.043	0.000
3172	99	45.8	2.15	323	20	0.202	0.237	0.053	0.047	0.000
3173	99	45.8	2.15	319	20	0.202	0.233	0.052	0.045	0.000
3105	99	45.8	2.16	321	28	0.202	0.313	0.041	0.040	0.000
3155	99	45.8	2.15	323	30	0.202	0.373	0.047	0.042	0.000
3158	99	45.8	2.15	320	29	0.202	0.341	0.050	0.047	0.000
3106	99	45.8	2.16	321	41	0.202	0.408	0.056	0.050	0.000
3151	99	45.8	2.15	332	41	0.202	0.434	0.060	0.043	0.000
3154	99	45.8	2.15	325	42	0.202	0.441	0.064	0.057	0.000
3160	99	45.8	2.15	319	41	0.202	0.435	0.066	0.061	0.000
3171	99	45.8	2.15	324	41	0.202	0.436	0.075	0.061	0.000
3174	99	45.8	2.15	314	41	0.202	0.428	0.076	0.068	0.000
3152	99	45.8	2.15	320	66	0.202	0.492	0.092	0.083	0.000
3153	99	45.8	2.15	322	66	0.202	0.492	0.093	0.084	0.000
3170	99	45.8	2.15	326	65	0.202	0.489	0.103	0.086	0.000
3108	99	45.8	2.16	538	18	0.202	0.212	0.040	0.032	0.000
3110	99	45.8	2.16	534	18	0.202	0.203	0.036	0.029	0.000
3149	98	45.8	2.15	534	19	0.202	0.204	0.018	0.007	0.000
3150	98	45.8	2.15	533	19	0.202	0.210	0.025	0.015	0.000
3109	99	45.8	2.16	533	27	0.202	0.314	0.042	0.033	0.000
3145	98	45.8	2.15	534	30	0.202	0.359	0.028	0.014	0.000
3146	98	45.8	2.15	533	30	0.202	0.340	0.031	0.018	0.000
3147	98	45.8	2.15	532	30	0.202	0.345	0.035	0.024	0.000
3107	99	45.8	2.16	536	41	0.202	0.406	0.051	0.042	0.000
3142	98	45.8	2.15	544	41	0.202	0.422	0.053	0.039	0.000
3148	98	45.8	2.15	531	41	0.202	0.431	0.048	0.036	0.000
3143	98	45.8	2.15	528	66	0.202	0.486	0.084	0.067	0.000
3144	98	45.8	2.15	533	66	0.202	0.485	0.079	0.063	0.000
3219	93	42.4	2.20	96	14	0.202	0.199	0.132	0.117	-0.006
3217	93	42.4	2.20	96	20	0.202	0.306	0.138	0.123	-0.000
3218	93	42.4	2.20	96	15	0.202	0.219	0.133	0.119	-0.006
3220	93	42.4	2.20	95	20	0.202	0.306	0.140	0.124	-0.006
3213	93	42.4	2.20	96	39	0.202	0.476	0.162	0.128	0.007
3216	93	42.4	2.20	96	41	0.202	0.480	0.163	0.140	0.021
3214	93	42.4	2.20	96	65	0.202	0.522	0.194	0.165	0.045
3215	93	42.4	2.20	96	65	0.202	0.521	0.196	0.171	0.051
3227	93	42.4	2.20	186	14	0.202	0.219	0.127	0.121	-0.001
3228	93	42.4	2.20	187	14	0.202	0.218	0.124	0.120	-0.006
3200	92	42.4	2.17	187	20	0.202	0.179	-0.005		
3221	93	42.4	2.20	187	20	0.202	0.300	0.124	0.114	-0.013
3226	93	42.4	2.20	188	20	0.202	0.307	0.130	0.117	0.002
3229	93	42.4	2.20	186	20	0.202	0.303	0.127	0.123	0.003
3196	92	42.4	2.17	187	40	0.202	0.391	0.035	0.002	
3199	92	42.4	2.17	188	42	0.202	0.406	0.042	0.012	
3222	93	42.4	2.20	186	39	0.202	0.468	0.141	0.129	0.017
3225	93	42.4	2.20	188	41	0.202	0.462	0.132	0.116	-0.004
3197	92	42.4	2.17	187	65	0.202	0.461	0.091	0.066	

Ser. Num.	Cal μm	B.W. g/m²	B_L cm³/g	Vel m/m	Load kN/m	Rad m	In-nip strain	Rec1 strain	Rec2 strain	Perm. strain
3198	92	42.4	2.17	187	65	0.202	0.470	0.095	0.072	
3223	93	42.4	2.20	186	65	0.202	0.516	0.172	0.156	0.034
3224	93	42.4	2.20	187	65	0.202	0.511	0.166	0.149	0.020
3201	92	42.4	2.17	325	20	0.202	0.176			
3230	93	42.4	2.20	322	20	0.202	0.305	0.122	0.119	0.011
3235	93	42.4	2.20	321	20	0.202	0.302	0.114	0.120	-0.006
3236	93	42.4	2.20	320	15	0.202	0.199	0.089	0.097	-0.014
3202	92	42.4	2.17	319	40	0.202	0.389	0.011		
3204	94	42.4	2.23	321	41	0.202	0.451	0.104	0.091	-0.007
3231	93	42.4	2.20	319	39	0.202	0.457	0.123	0.119	-0.002
3234	93	42.4	2.20	324	41	0.202	0.462	0.124	0.124	0.003
3203	92	42.4	2.17	320	65	0.202	0.465	0.066	0.053	
3232	93	42.4	2.20	317	65	0.202	0.514	0.155	0.155	0.029
3233	93	42.4	2.20	320	65	0.202	0.510	0.149	0.150	0.029
3210	94	42.4	2.23	536	20	0.202	0.267	0.094	0.075	-0.019
3211	94	42.4	2.23	533	20	0.202	0.267	0.096	0.076	-0.018
3205	94	42.4	2.23	538	41	0.202	0.437	0.094	0.076	-0.021
3206	94	42.4	2.23	533	41	0.202	0.440	0.099	0.081	-0.003
3209	94	42.4	2.23	539	41	0.202	0.444	0.102	0.081	-0.009
3212	94	42.4	2.23	529	40	0.202	0.453	0.122	0.103	0.015
3207	94	42.4	2.23	527	65	0.202	0.491	0.122	0.104	0.012
3208	94	42.4	2.23	532	65	0.202	0.494	0.125	0.108	0.023
3060	115	44.5	2.58	96	6	0.202	0.137	0.068	0.054	0.027
3195	105	42.4	2.47	96	19	0.202	0.274	0.121		0.002
3242	108	42.2	2.56	95	18	0.202	0.235	0.132	0.110	0.011
3243	108	42.2	2.56	95	15	0.202	0.175	0.128	0.105	-0.003
3244	108	42.2	2.56	95	19	0.202	0.262	0.139	0.119	0.018
3059	115	44.5	2.58	96	19	0.202	0.353	0.136	0.120	0.083
3061	115	44.5	2.58	95	18	0.202	0.362	0.128	0.108	0.085
3058	115	44.5	2.58	96	29	0.202	0.454	0.181	0.155	0.125
3048	114	44.5	2.56	97	41	0.202	0.509	0.210	0.149	0.130
3057	115	44.5	2.58	96	42	0.202	0.522	0.221	0.193	0.169
3081	118	45.8	2.57	97	41	0.202	0.580	0.192	0.125	
3192	105	42.4	2.47	96	40	0.202	0.474	0.160		0.035
3194	105	42.4	2.47	96	42	0.202	0.481	0.167		0.046
3238	108	42.2	2.56	96	41	0.202	0.499	0.226	0.197	
3241	108	42.2	2.56	96	43	0.202	0.502	0.233	0.208	0.085
3245	108	42.2	2.56	96	41	0.202	0.495	0.225	0.200	0.096
3056	115	44.5	2.58	96	65	0.202	0.569	0.309	0.243	0.219
3062	115	44.5	2.58	96	65	0.202	0.576	0.255	0.251	0.219
3193	105	42.4	2.47	96	65	0.202	0.539	0.220		0.106
3239	108	42.2	2.56	95	65	0.202	0.556	0.283	0.266	0.142
3240	108	42.2	2.56	95	65	0.202	0.557	0.282	0.261	0.148
3028	127	49.0	2.59	97	8	0.202	0.200	0.125	0.049	0.040
3029	127	49.0	2.59	96	8	0.202	0.204	0.122	0.048	0.041
3027	127	49.0	2.59	97	18	0.202	0.354	0.176	0.096	0.079
3030	127	49.0	2.59	96	17	0.202	0.359	0.173	0.095	0.082
3026	127	49.0	2.59	97	29	0.202	0.458	0.220	0.142	0.126
3031	127	49.0	2.59	96	27	0.202	0.448	0.208	0.134	0.118
3023	127	49.0	2.59	97	41	0.202	0.522	0.260	0.175	0.156
3025	127	49.0	2.59	100	43	0.202	0.526	0.262	0.188	0.165
3024	127	49.0	2.59	96	66	0.202	0.578	0.311	0.240	0.226
3034	127	49.0	2.59	189	18	0.202	0.350	0.146	0.081	0.071
3032	127	49.0	2.59	187	28	0.202	0.444	0.184	0.119	0.108
3033	127	49.0	2.59	188	28	0.202	0.445	0.186	0.120	0.111
3035	127	49.0	2.59	184	41	0.202	0.519	0.228	0.170	0.152
3080	118	45.8	2.57	187	41	0.202	0.572	0.171	0.110	
3079	113	44.5	2.55	182	65	0.202	0.623	0.201	0.180	
3090	118	45.8	2.57	188	65	0.202	0.641	0.220	0.186	0.159
3091	118	45.8	2.57	186	65	0.202	0.634	0.214	0.180	0.159
3092	118	45.8	2.57	189	66	0.202	0.627	0.207	0.174	0.159
3093	118	45.8	2.57	186	65	0.202	0.634	0.210	0.175	0.159
3094	118	45.8	2.57	186	65	0.202	0.628	0.198	0.171	0.159
3095	118	45.8	2.57	189	65	0.202	0.630	0.196	0.169	0.159
3096	118	45.8	2.57	183	65	0.202	0.626	0.193	0.170	0.159
3077	113	44.5	2.55	323	10	0.202				0.006
3038	127	49.0	2.59	322	18	0.202	0.344	0.134	0.070	0.064
3054	114	44.5	2.56	325	18	0.202	0.331	0.110	0.068	0.065
3074	113	44.5	2.55	327	20	0.202	0.290	0.037	-0.003	0.017
3076	113	44.5	2.55	321	19	0.202	0.285	0.033	0.001	0.012
3036	127	49.0	2.59	326	29	0.202	0.449	0.173	0.116	0.100
3037	127	49.0	2.59	321	29	0.202	0.447	0.173	0.111	0.104
3053	114	44.5	2.56	324	29	0.202	0.439	0.153	0.113	0.096
3075	113	44.5	2.55	320	28	0.202	0.425	0.073		0.062
3039	127	49.0	2.59	317	41	0.202	0.514	0.205	0.152	0.148
3049	114	44.5	2.56	327	41	0.202	0.507	0.172	0.137	0.129
3052	114	44.5	2.56	326	42	0.202	0.510	0.192	0.158	0.136
3073	113	44.5	2.55	328	41	0.202	0.543	0.124		0.108
3050	114	44.5	2.56	318	66	0.202	0.559	0.230	0.198	0.196
3051	114	44.5	2.56	320	66	0.202	0.555	0.233	0.199	0.192
3055	114	44.5	2.56	322	66	0.202	0.555	0.237	0.207	0.184
3063	115	44.5	2.58	330	65	0.202	0.566	0.209	0.216	0.194
3072	113	44.5	2.55	327	65	0.202	0.612	0.188	0.149	0.161
3078	113	44.5	2.55	331	65	0.202	0.626	0.192	0.165	0.159
3082	118	45.8	2.57	322	66	0.202	0.636	0.220	0.169	0.152
3083	118	45.8	2.57	321	65	0.202	0.638	0.217	0.166	0.152
3084	118	45.8	2.57	321	65	0.202	0.637	0.215	0.170	0.152
3085	118	45.8	2.57	321	65	0.202	0.635	0.213	0.169	0.152
3086	118	45.8	2.57	323	65	0.202	0.637	0.209	0.168	0.152
3087	118	45.8	2.57	320	65	0.202	0.637	0.204	0.164	0.152
3088	118	45.8	2.57	321	65	0.202	0.643	0.208	0.173	0.152
3089	118	45.8	2.57	321	65	0.202	0.636	0.200	0.164	0.152
3070	113	44.5	2.55	534	10	0.202				0.000
3041	127	49.0	2.59	535	18	0.202	0.335	0.120	0.059	0.050
3069	113	44.5	2.55	536	19	0.202	0.281	0.034	0.011	0.029
3040	127	49.0	2.59	547	29	0.202	0.440	0.156	0.106	0.095
3068	113	44.5	2.55	533	27	0.202	0.410	0.060	0.043	0.055

Ser. Num.	Cal μm	B.W. g/m²	B_L cm³/g	Vel m/m	Load kN/m	Rad m	In-nip strain	Rec1 strain	Rec2 strain	Perm. strain
3042	127	49.0	2.59	524	41	0.202	0.502	0.179	0.127	0.116
3064	113	44.5	2.55	546	40	0.202	0.523	0.108	0.098	0.088
3067	113	44.5	2.55	547	41	0.202	0.533	0.109	0.101	0.098
3043	127	49.0	2.59	523	66	0.202	0.563	0.218	0.180	
3065	113	44.5	2.55	526	65	0.202	0.599	0.166	0.157	0.156
3066	113	44.5	2.55	534	65	0.202	0.600	0.161	0.158	0.154
2917	123	48.5	2.51	96	12	0.202	0.284	0.146	0.050	0.047
2918	123	48.5	2.51	96	12	0.202	0.287	0.148	0.057	0.035
2991	124	48.5	2.53	96	9	0.202	0.241	0.149	0.061	0.032
2916	123	48.5	2.51	96	17	0.202	0.346	0.175	0.077	0.064
2990	124	48.5	2.53	98	19	0.202	0.379	0.203	0.105	0.078
2915	123	48.5	2.51	96	42	0.202	0.503	0.285	0.192	0.164
2947	125	48.5	2.54	97	42	0.202	0.519	0.292	0.194	0.204
2985	125	48.5	2.55	96	40	0.202	0.520	0.298	0.207	0.188
2988	124	48.5	2.53	96	40	0.202	0.523	0.294	0.198	0.177
2921	123	48.5	2.51	97	53	0.202	0.534	0.317	0.234	0.220
698	126	49.0	2.57	97	70	0.202	0.528			0.204
2919	123	48.5	2.51	96	65	0.202	0.562	0.344	0.265	0.252
2920	123	48.5	2.51	96	65	0.202	0.561	0.342	0.261	0.238
2989	124	48.5	2.53	96	65	0.202	0.581	0.355	0.267	0.248
699	126	49.0	2.57	97	85	0.202	0.562			0.247
832	126	49.0	2.58	95	86	0.202	0.574			0.256
2740	115	44.5	2.58	95	87	0.202	0.617		0.373	0.308
700	126	49.0	2.57	96	135	0.202	0.602			0.307
833	126	49.0	2.58	95	137	0.202	0.619			0.333
701	126	49.0	2.57	96	172	0.202	0.618			0.333
834	126	49.0	2.58	95	173	0.202	0.638			0.359
702	126	49.0	2.57	97	207	0.202	0.625			0.355
2995	124	48.5	2.53	188	9	0.202	0.240	0.146	0.059	0.040
2994	124	48.5	2.53	190	19	0.202	0.381	0.203	0.115	0.086
2992	124	48.5	2.53	187	40	0.202	0.516	0.289	0.199	0.159
667	127	49.0	2.59	173	70	0.202	0.556			0.194
704	126	49.0	2.57	174	70	0.202	0.551			0.191
2993	124	48.5	2.53	187	65	0.202	0.574	0.343	0.260	0.222
2686	113	44.5	2.54	177	82	0.202		0.338	0.307	0.294
2687	113	44.5	2.54	177	74	0.202		0.326	0.292	0.270
668	127	49.0	2.59	172	87	0.202	0.586			0.222
690	126	49.0	2.57	170	88	0.202	0.585			0.252
705	126	49.0	2.57	171	86	0.202	0.585			0.236
835	126	49.0	2.58	171	87	0.202	0.567			0.255
2741	115	44.5	2.58	186	87	0.202	0.614		0.363	0.293
2685	113	44.5	2.54	176	98	0.202		0.349	0.307	0.307
669	127	49.0	2.59	173	136	0.202	0.608			0.309
691	126	49.0	2.57	170	136	0.202	0.619			0.313
706	126	49.0	2.57	171	136	0.202	0.633			0.306
836	126	49.0	2.58	171	136	0.202	0.609			0.313
2682	113	44.5	2.54	177	140	0.202		0.380	0.350	0.344
2684	113	44.5	2.54	176	143	0.202			0.387	0.342	0.350
670	127	49.0	2.59	173	172	0.202	0.627				0.330
692	126	49.0	2.57	169	172	0.202	0.638				0.345
707	126	49.0	2.57	173	172	0.202	0.643				0.337
837	126	49.0	2.58	170	174	0.202	0.620				0.343
2683	113	44.5	2.54	176	178	0.202			0.405	0.374	0.371
693	126	49.0	2.57	170	208	0.202	0.654				0.368
703	126	49.0	2.57	171	208	0.202	0.616				0.335
708	126	49.0	2.57	171	208	0.202	0.654				0.353
709	126	49.0	2.57	171	207	0.202	0.649				0.337
2999	126	48.5	2.58	322	10	0.202	0.261	0.148	0.065	0.052
2998	126	48.5	2.58	328	19	0.202	0.383	0.192	0.105	0.080
3000	126	48.5	2.58	319	19	0.202	0.391	0.202	0.116	0.093
2996	126	48.5	2.58	325	39	0.202	0.511	0.273	0.189	0.156
671	127	49.0	2.59	301	70	0.202	0.527			0.169
694	126	49.0	2.57	298	70	0.202	0.519			0.175
2694	113	44.5	2.54	319	71	0.202	0.561		0.261	0.253
2997	126	48.5	2.58	320	64	0.202	0.579	0.329	0.257	0.232
2693	113	44.5	2.54	320	80	0.202	0.578	0.254	0.270	0.245
672	127	49.0	2.59	301	86	0.202	0.549			0.204
695	126	49.0	2.57	292	85	0.202	0.555			0.223
2742	115	44.5	2.58	324	87	0.202	0.613		0.351	0.283
2692	113	44.5	2.54	319	95	0.202	0.608	0.278	0.286	0.279
673	127	49.0	2.59	301	137	0.202	0.582			0.268
696	126	49.0	2.57	296	135	0.202	0.600			0.288
2688	113	44.5	2.54	321	137	0.202	0.662	0.329	0.341	0.320
2691	113	44.5	2.54	321	140	0.202	0.665	0.319	0.329	0.312
674	127	49.0	2.59	301	172	0.202	0.600			0.293
697	126	49.0	2.57	296	172	0.202	0.614			0.316
2689	113	44.5	2.54	320	177	0.202	0.705		0.376	0.334
2690	113	44.5	2.54	319	177	0.202	0.701		0.365	0.338
2928	123	48.5	2.51	556	13	0.202	0.272	0.114	0.009	0.025
2929	123	48.5	2.51	555	9	0.202	0.194	0.091		0.025
2930	123	48.5	2.51	556	9	0.202	0.201	0.093		0.023
2955	125	48.5	2.54	557	13	0.202	0.284	0.115	0.021	0.042
2956	125	48.5	2.54	555	9	0.202	0.210	0.095		0.019
3004	126	48.5	2.58	538	10	0.202	0.257	0.127	0.035	0.033
3005	126	48.5	2.58	535	10	0.202	0.259	0.127	0.033	0.040
2927	123	48.5	2.51	565	18	0.202	0.330	0.133		0.055
2954	125	48.5	2.54	565	18	0.202	0.343	0.135	0.047	0.060
3003	126	48.5	2.58	545	19	0.202	0.381	0.172	0.084	0.070
3006	126	48.5	2.58	531	19	0.202	0.386	0.170	0.074	0.063
2926	123	48.5	2.51	559	44	0.202	0.497	0.228	0.138	0.152
2948	125	48.5	2.54	563	42	0.202	0.502	0.226	0.145	0.145
2953	125	48.5	2.54	562	44	0.202	0.510	0.225	0.147	0.163
3002	126	48.5	2.58	543	41	0.202	0.516	0.245	0.164	0.151
3007	126	48.5	2.58	528	39	0.202	0.511	0.232	0.138	0.131
2922	123	48.5	2.51	564	53	0.202	0.517	0.255	0.166	0.170
2925	123	48.5	2.51	559	53	0.202	0.519	0.249	0.161	0.173
2949	125	48.5	2.54	553	51	0.202	0.531	0.249	0.169	0.164

Ser. Num.	Cal μm	B.W. g/m²	B_i cm³/g	Vel m/m	Load kN/m	Rad m	In-nip strain	Rec1 strain	Rec2 strain	Perm. strain
2952	125	48.5	2.54	562	53	0.202	0.531	0.247	0.170	0.171
2695	113	44.5	2.54	563	71	0.202	0.552		0.259	0.233
2850	115	45.0	2.55	559	67	0.202			0.213	0.211
2851	115	45.0	2.55	555	67	0.202			0.204	0.198
2860	115	45.0	2.55	557	68	0.202		0.167	0.204	0.182
2861	115	45.0	2.55	554	68	0.202			0.203	0.189
2923	123	48.5	2.51	553	65	0.202	0.540	0.272	0.184	0.195
2924	123	48.5	2.51	555	65	0.202	0.544	0.273	0.186	0.195
2950	125	48.5	2.54	551	65	0.202	0.557	0.272	0.197	0.203
2951	125	48.5	2.54	554	65	0.202	0.555	0.268	0.193	0.198
3001	126	48.5	2.58	541	65	0.202	0.575	0.296	0.222	0.214
2696	113	44.5	2.54	552	77	0.202	0.567		0.285	0.233
2845	116	45.0	2.57	563	76	0.202				0.251
2849	115	45.0	2.55	565	76	0.202			0.242	0.219
2852	115	45.0	2.55	551	75	0.202			0.227	0.222
2859	115	45.0	2.55	560	79	0.202		0.180	0.224	0.199
831	126	49.0	2.58	500	87	0.202	0.534			0.199
838	126	49.0	2.58	500	87	0.202	0.544			0.212
2846	116	45.0	2.57	550	90	0.202				0.266
2853	115	45.0	2.55	550	89	0.202			0.236	0.240
2862	115	45.0	2.55	546	90	0.202			0.234	0.213
2697	113	44.5	2.54	552	91	0.202	0.590		0.289	0.246
2858	115	45.0	2.55	569	94	0.202			0.239	
839	126	49.0	2.58	535	138	0.202	0.588			0.283
2847	116	45.0	2.57	542	133	0.202			0.314	0.312
2854	115	45.0	2.55	542	132	0.202			0.287	0.298
2857	115	45.0	2.55	563	138	0.202			0.284	0.286
840	126	49.0	2.58	500	173	0.202	0.607			0.313
2848	116	45.0	2.57	543	175	0.202			0.319	0.331
2855	115	45.0	2.55	541	175	0.202			0.329	0.322
2856	115	45.0	2.55	549	175	0.202			0.317	0.320
841	126	49.0	2.58	500	208	0.202	0.615			0.327
2936	123	48.5	2.51	880	13	0.202	0.273	0.085		0.031
2937	123	48.5	2.51	875	9	0.202	0.196	0.067		0.014
2938	123	48.5	2.51	875	9	0.202	0.199	0.066		0.014
2939	123	48.5	2.51	873	12	0.202	0.259	0.071		0.019
3012	126	48.5	2.58	963	10	0.202	0.247	0.073		0.035
3013	126	48.5	2.58	961	10	0.202	0.253	0.082		0.042
2935	123	48.5	2.51	860	18	0.202	0.329	0.108	0.021	0.043
2987	125	48.5	2.55	967	18	0.202	0.346	0.094		0.061
3011	126	48.5	2.58	969	20	0.202	0.370	0.112	0.045	0.060
3014	126	48.5	2.58	958	19	0.202	0.367	0.098		0.050
2931	123	48.5	2.51	884	42	0.202	0.487	0.186		0.138
2934	123	48.5	2.51	878	43	0.202	0.490	0.188		0.138
2986	125	48.5	2.55	964	41	0.202	0.501	0.175		0.142
3008	126	48.5	2.58	961	39	0.202	0.498	0.165	0.116	0.133
3010	126	48.5	2.58	965	41	0.202	0.505	0.168	0.122	0.136
2932	123	48.5	2.51	873	50	0.202	0.509	0.201	0.129	0.149
2933	123	48.5	2.51	872	50	0.202	0.506	0.199		0.150
2834	117	45.0	2.59	882	67	0.202	0.479		0.202	0.212
2843	117	45.0	2.59	877	69	0.202	0.486		0.204	0.194
2844	117	45.0	2.59	873	69	0.202	0.483		0.209	0.188
3009	126	48.5	2.58	954	64	0.202	0.563	0.185		0.191
2835	117	45.0	2.59	875	76	0.202	0.496		0.239	0.224
2842	117	45.0	2.59	881	79	0.202	0.498		0.215	0.213
2836	117	45.0	2.59	867	90	0.202	0.510		0.262	0.248
2841	117	45.0	2.59	889	95	0.202	0.522		0.237	0.251
2837	117	45.0	2.59	860	134	0.202	0.547		0.301	0.289
2840	117	45.0	2.59	883	139	0.202	0.549		0.296	0.293
2838	117	45.0	2.59	858	175	0.202	0.563		0.317	0.316
2839	117	45.0	2.59	866	175	0.202	0.565		0.311	0.321
2965	127	48.5	2.60	96	7	0.202	0.174	0.137	0.059	0.048
2964	127	48.5	2.60	96	16	0.202	0.361	0.193	0.108	0.083
2960	127	48.5	2.60	96	43	0.202	0.528	0.302	0.216	0.194
2963	127	48.5	2.60	96	45	0.202	0.537	0.312	0.230	0.207
2966	127	48.5	2.60	95	43	0.202	0.534	0.311	0.229	0.200
638	128	49.0	2.60	96	70	0.202	0.563	0.522		0.214
660	128	49.0	2.60	97	70	0.202	0.570	0.498		0.182
683	128	49.0	2.62	99	70	0.202	0.563			0.231
712	128	49.0	2.62	97	70	0.202	0.554			0.195
749	129	49.0	2.64	97	70	0.202	0.561			0.216
761	118	45.0	2.63	97	70	0.202	0.559			0.189
771	119	45.0	2.64	99	70	0.202	0.554			0.211
777	119	45.0	2.64	100	70	0.202	0.568			0.218
779	119	45.0	2.64	99	70	0.202	0.546			0.184
783	119	45.0	2.64	99	70	0.202	0.513			0.207
816	120	45.0	2.66	95	69	0.202	0.560			0.239
2753	117	44.5	2.63	96	70	0.202	0.597	0.352		0.309
2754	117	44.5	2.63	95	70	0.202	0.599	0.352		0.320
2782	117	45.0	2.61	95	68	0.202	0.590	0.337	0.304	0.296
2791	117	45.0	2.61	95	68	0.202	0.590	0.343	0.296	0.291
2891	129	49.0	2.63	96	69	0.202	0.575	0.378	0.276	0.280
2892	129	49.0	2.63	95	69	0.202	0.574	0.377	0.275	0.273
2961	127	48.5	2.60	95	65	0.202	0.577	0.348	0.270	0.245
2962	127	48.5	2.60	96	65	0.202	0.581	0.351	0.275	0.254
2976	127	48.5	2.60	96	65	0.202	0.584	0.349	0.266	0.252
2752	117	44.5	2.63	96	80	0.202	0.608	0.377		0.320
2755	117	44.5	2.63	96	77	0.202	0.605	0.360		0.320
2783	117	45.0	2.61	95	78	0.202	0.606	0.355	0.322	0.315
2790	117	45.0	2.61	95	79	0.202	0.608	0.364	0.317	0.306
2890	129	49.0	2.63	95	78	0.202	0.592	0.391	0.294	0.297
2893	129	49.0	2.63	95	77	0.202	0.589	0.392	0.292	0.289
2900	129	49.0	2.63	94	80	0.202	0.588	0.396	0.299	0.295
2901	129	49.0	2.63	94	80	0.202	0.585	0.393	0.295	0.285
639	128	49.0	2.60	96	86	0.202	0.594	0.535		0.247
713	128	49.0	2.62	97	87	0.202	0.588			0.244
750	129	49.0	2.64	96	86	0.202	0.591			0.253

Ser. Num.	Cal μm	B.W. g/m²	B_L cm³/g	Vel m/m	Load kN/m	Rad m	In-nip strain	Rec1 strain	Rec2 strain	Perm. strain
772	119	45.0	2.64	99	86	0.202	0.585			0.264
784	119	45.0	2.64	98	86	0.202	0.555			0.254
817	120	45.0	2.66	94	86	0.202	0.584			0.279
2751	117	44.5	2.63	96	95	0.202	0.619	0.386		0.340
2756	117	44.5	2.63	96	91	0.202	0.617	0.386		0.337
2784	117	45.0	2.61	95	92	0.202	0.622	0.378	0.334	0.337
2789	117	45.0	2.61	95	95	0.202	0.621	0.380	0.355	0.331
2894	129	49.0	2.63	94	91	0.202	0.607	0.407	0.310	0.317
2899	129	49.0	2.63	95	94	0.202	0.605	0.410	0.316	0.309
751	129	49.0	2.64	96	113	0.202	0.613			0.298
640	128	49.0	2.60	96	137	0.202	0.630	0.588		0.312
685	128	49.0	2.62	98	135	0.202	0.635			0.329
714	128	49.0	2.62	96	137	0.202	0.631			0.310
773	119	45.0	2.64	98	136	0.202	0.623			0.322
785	119	45.0	2.64	98	136	0.202	0.600			0.315
818	120	45.0	2.66	94	136	0.202	0.622			0.338
2747	117	44.5	2.63	96	138	0.202	0.650	0.411		0.387
2750	117	44.5	2.63	96	140	0.202	0.649	0.428		0.388
2785	117	45.0	2.61	95	137	0.202	0.654	0.416	0.387	0.374
2788	117	45.0	2.61	95	140	0.202	0.652	0.416	0.394	0.366
2895	129	49.0	2.63	93	135	0.202	0.641	0.442	0.352	0.356
2898	129	49.0	2.63	97	139	0.202	0.644	0.441	0.355	0.357
641	128	49.0	2.60	96	173	0.202	0.644	0.601		0.331
686	128	49.0	2.62	98	172	0.202	0.650			0.365
715	128	49.0	2.62	97	172	0.202	0.645			0.331
752	129	49.0	2.64	96	172	0.202	0.640			0.350
774	119	45.0	2.64	98	173	0.202	0.640			0.350
786	119	45.0	2.64	98	172	0.202	0.619			0.343
819	120	45.0	2.66	94	173	0.202	0.638			0.370
2748	117	44.5	2.63	96	177	0.202	0.674	0.445		0.414
2749	117	44.5	2.63	96	177	0.202	0.674	0.445		0.424
2786	117	45.0	2.61	95	177	0.202	0.680	0.442	0.413	0.398
2787	117	45.0	2.61	95	177	0.202	0.680	0.440	0.416	0.398
2896	129	49.0	2.63	90	176	0.202	0.662	0.464	0.380	0.387
2897	129	49.0	2.63	92	175	0.202	0.661	0.460	0.378	0.391
642	128	49.0	2.60	96	208	0.202	0.656	0.621		0.344
687	128	49.0	2.62	98	209	0.202	0.661			0.382
716	128	49.0	2.62	96	207	0.202	0.655			0.353
753	129	49.0	2.64	97	208	0.202	0.651			0.365
775	119	45.0	2.64	98	208	0.202	0.648			0.367
787	119	45.0	2.64	98	208	0.202	0.631			0.360
820	120	45.0	2.66	94	209	0.202	0.644			0.383
2806	119	45.0	2.64	185	30	0.202	0.497			0.191
643	128	49.0	2.60	169	71	0.202	0.542	0.513		0.181
717	128	49.0	2.62	171	70	0.202	0.536			0.183
755	129	49.0	2.64	171	70	0.202	0.533			0.187
767	119	45.0	2.64	173	70	0.202	0.558			0.202
768	119	45.0	2.64	173	69	0.202	0.551			0.194
776	119	45.0	2.64	173	70	0.202	0.541			0.181
2796	119	45.0	2.64	189	67	0.202	0.587			0.288
2805	119	45.0	2.64	186	68	0.202	0.596			0.276
2807	119	45.0	2.64	185	68	0.202	0.585			0.265
2884	129	49.0	2.63	188	68	0.202	0.570	0.363	0.263	0.263
2888	129	49.0	2.63	189	68	0.202	0.574	0.366	0.262	0.264
2797	119	45.0	2.64	185	77	0.202	0.601			0.304
2804	119	45.0	2.64	186	80	0.202	0.610			0.297
2885	129	49.0	2.63	184	79	0.202	0.592	0.381	0.278	0.293
2889	129	49.0	2.63	185	78	0.202	0.590	0.381	0.280	0.283
644	128	49.0	2.60	169	87	0.202	0.569	0.574		0.215
718	128	49.0	2.62	169	87	0.202	0.567			0.229
754	129	49.0	2.64	173	90	0.202	0.575			0.248
756	129	49.0	2.64	169	87	0.202	0.565			0.242
769	119	45.0	2.64	173	86	0.202	0.578			0.241
770	119	45.0	2.64	173	86	0.202	0.575			0.236
2798	119	45.0	2.64	183	92	0.202	0.619			0.319
2803	119	45.0	2.64	186	95	0.202	0.624			0.317
2886	129	49.0	2.63	185	92	0.202	0.606	0.391	0.296	0.298
645	128	49.0	2.60	169	136	0.202	0.607	0.597		0.258
719	128	49.0	2.62	171	135	0.202	0.607			0.285
757	129	49.0	2.64	169	136	0.202	0.604			0.298
2799	119	45.0	2.64	183	138	0.202	0.652			0.354
2802	119	45.0	2.64	186	141	0.202	0.658			0.354
2887	129	49.0	2.63	180	136	0.202	0.639	0.421	0.340	0.348
646	128	49.0	2.60	169	173	0.202	0.621	0.595		0.285
720	128	49.0	2.62	171	174	0.202	0.623			0.312
758	129	49.0	2.64	169	173	0.202	0.622			0.335
2800	119	45.0	2.64	185	177	0.202	0.685			0.386
2801	119	45.0	2.64	185	177	0.202	0.683			0.389
721	128	49.0	2.62	169	209	0.202	0.627			0.331
759	129	49.0	2.64	169	208	0.202	0.633			0.356
656	128	49.0	2.60	299	70	0.202	0.555			0.159
657	128	49.0	2.60	297	70	0.202	0.543			0.156
661	128	49.0	2.60	299	70	0.202	0.542			0.156
760	129	49.0	2.64	298	71	0.202	0.512			0.184
778	119	45.0	2.64	304	69	0.202	0.550			0.181
780	119	45.0	2.64	304	70	0.202	0.530			0.231
898	129	49.0	2.62	299	69	0.202	0.573			0.209
2823	117	45.0	2.60	328	66	0.202	0.574	0.298	0.255	0.240
2874	128	49.0	2.60	323	69	0.202	0.566	0.331	0.223	0.239
2833	128	49.0	2.60	323	71	0.202	0.561	0.332	0.226	0.230
2824	117	45.0	2.60	317	76	0.202	0.594	0.316	0.267	0.254
2831	117	45.0	2.60	318	78	0.202	0.601	0.316	0.268	0.244
2875	128	49.0	2.60	322	79	0.202	0.582	0.345	0.240	0.248
2882	128	49.0	2.60	324	82	0.202	0.579	0.349	0.244	0.256
658	128	49.0	2.60	301	84	0.202	0.578			0.201
662	128	49.0	2.60	301	86	0.202	0.579	0.588		0.189
781	119	45.0	2.64	301	85	0.202	0.561			0.289

Ser. Num.	Cal μm	B.W. g/m²	B_L cm³/g	Vel m/m	Load kN/m	Rad m	In-nip strain	Rec1 strain	Rec2 strain	Perm. strain
899	129	49.0	2.62	301	86	0.202	0.606			0.256
908	129	49.0	2.62	299	88	0.202	0.537			0.253
917	118	45.0	2.61	304	86	0.202	0.603			0.233
2825	117	45.0	2.60	316	90	0.202	0.612	0.336	0.295	0.272
2830	117	45.0	2.60	324	94	0.202	0.621	0.335	0.292	0.266
2876	128	49.0	2.60	319	93	0.202	0.600	0.362	0.263	0.276
2881	128	49.0	2.60	328	97	0.202	0.600	0.368	0.266	0.280
782	119	45.0	2.64	301	136	0.202	0.604			0.312
900	129	49.0	2.62	299	136	0.202	0.640			0.319
909	129	49.0	2.62	294	138	0.202	0.577			0.315
918	118	45.0	2.61	297	137	0.202	0.648			0.294
2826	117	45.0	2.60	311	134	0.202	0.643	0.372	0.340	0.314
2829	117	45.0	2.60	324	138	0.202	0.643	0.364	0.329	0.305
2877	128	49.0	2.60	318	137	0.202	0.636	0.399	0.313	0.316
2880	128	49.0	2.60	325	142	0.202	0.637	0.400		0.330
901	129	49.0	2.62	280	173	0.202	0.646			0.352
910	129	49.0	2.62	294	174	0.202	0.589			0.335
919	118	45.0	2.61	299	173	0.202	0.663			0.319
2827	117	45.0	2.60	311	175	0.202	0.663	0.396	0.364	0.343
2828	117	45.0	2.60	317	175	0.202	0.663	0.391	0.345	0.340
2878	128	49.0	2.60	317	177	0.202	0.653	0.413		0.350
2879	128	49.0	2.60	320	177	0.202	0.655	0.415		0.349
920	118	45.0	2.61	299	208	0.202	0.668			0.336
2972	127	48.5	2.60	560	7	0.202	0.170	0.097		0.034
2973	127	48.5	2.60	556	7	0.202	0.181	0.104		0.048
2980	127	48.5	2.60	557	9	0.202	0.226	0.104	0.014	0.031
2981	127	48.5	2.60	555	9	0.202	0.227	0.102		0.041
2971	127	48.5	2.60	564	16	0.202	0.343	0.138	0.054	0.070
2974	127	48.5	2.60	552	16	0.202	0.348	0.134	0.039	0.060
2979	127	48.5	2.60	565	17	0.202	0.353	0.143	0.054	0.072
2982	127	48.5	2.60	551	17	0.202	0.354	0.137		0.073
2967	127	48.5	2.60	561	43	0.202	0.514	0.241	0.161	0.159
2970	127	48.5	2.60	559	44	0.202	0.517	0.230	0.155	0.163
2975	127	48.5	2.60	547	42	0.202	0.515	0.217	0.123	0.139
2978	127	48.5	2.60	562	43	0.202	0.510	0.224	0.142	0.156
2983	127	48.5	2.60	544	41	0.202	0.506	0.209	0.122	0.144
722	128	49.0	2.62	524	70	0.202	0.488			0.178
727	128	49.0	2.62	500	70	0.202	0.535			0.179
788	119	45.0	2.64	500	70	0.202	0.527			0.163
789	119	45.0	2.64	535	70	0.202	0.514			0.167
2759	116	44.5	2.60	566	66	0.202	0.572			0.238
2764	116	44.5	2.60	555	68	0.202	0.578			0.237
2792	117	45.0	2.61	564	68	0.202	0.578	0.278	0.242	0.247
2815	117	45.0	2.60	563	67	0.202	0.569	0.261		0.250
2819	117	45.0	2.60	556	67	0.202	0.572	0.242		0.239
2871	128	49.0	2.60	564	69	0.202	0.566	0.303		0.234
2968	127	48.5	2.60	552	65	0.202	0.569	0.287	0.214	0.207
2969	127	48.5	2.60	557	65	0.202	0.570	0.280	0.208	0.209
2977	127	48.5	2.60	559	65	0.202	0.569	0.274		0.217
2984	127	48.5	2.60	544	65	0.202	0.564	0.257	0.177	0.192
2760	116	44.5	2.60	550	74	0.202	0.587			0.249
2763	116	44.5	2.60	556	76	0.202	0.591			0.251
2793	117	45.0	2.61	555	77	0.202	0.587	0.285		0.249
2816	117	45.0	2.60	553	76	0.202	0.583	0.272		0.262
2820	117	45.0	2.60	551	77	0.202	0.586	0.265	0.234	0.250
2872	128	49.0	2.60	552	79	0.202	0.577	0.315		0.242
723	128	49.0	2.62	500	85	0.202	0.520			0.212
728	128	49.0	2.62	528	86	0.202	0.568			0.217
790	119	45.0	2.64	539	86	0.202	0.544			0.189
846	129	49.0	2.63	528	86	0.202	0.471			0.217
850	129	49.0	2.63	524	87	0.202	0.406			0.196
902	129	49.0	2.62	543	85	0.202	0.547			0.232
905	129	49.0	2.62	531	87	0.202	0.528			0.236
921	118	45.0	2.61	528	88	0.202	0.584			0.204
2757	117	44.5	2.63	562	90	0.202	0.606	0.283		0.291
2761	116	44.5	2.60	552	89	0.202	0.601			0.277
2762	116	44.5	2.60	555	89	0.202	0.605			0.266
2794	117	45.0	2.61	550	91	0.202	0.606	0.305	0.269	0.277
2817	117	45.0	2.60	552	91	0.202	0.606	0.289		0.280
2821	117	45.0	2.60	552	91	0.202	0.602	0.277		0.260
2873	128	49.0	2.60	551	94	0.202	0.596	0.332		0.261
724	128	49.0	2.62	528	135	0.202	0.558			0.270
729	128	49.0	2.62	528	136	0.202	0.621			0.279
791	119	45.0	2.64	535	136	0.202	0.592			0.258
847	129	49.0	2.63	520	137	0.202	0.525			0.272
851	129	49.0	2.63	517	137	0.202	0.460			0.259
903	129	49.0	2.62	500	137	0.202	0.618			0.301
906	129	49.0	2.62	500	137	0.202	0.569			0.296
922	118	45.0	2.61	535	139	0.202	0.624			0.261
2758	117	44.5	2.63	548	134	0.202	0.635	0.326		0.326
2795	117	45.0	2.61	543	135	0.202	0.638	0.338	0.311	0.312
2818	117	45.0	2.60	545	134	0.202	0.639	0.327	0.309	0.315
2822	117	45.0	2.60	545	134	0.202	0.636	0.315	0.311	0.294
725	128	49.0	2.62	500	173	0.202	0.582			0.289
730	128	49.0	2.62	500	172	0.202	0.640			0.314
848	129	49.0	2.63	500	174	0.202	0.544			0.306
852	129	49.0	2.63	513	174	0.202	0.484			0.287
904	129	49.0	2.62	535	173	0.202	0.642			0.330
907	129	49.0	2.62	539	173	0.202	0.588			0.330
923	118	45.0	2.61	528	173	0.202	0.642			0.280
731	128	49.0	2.62	528	207	0.202	0.647			0.336
849	129	49.0	2.63	528	208	0.202	0.555			0.332
853	129	49.0	2.63	500	208	0.202	0.496			0.304
2767	116	44.5	2.60	884	64	0.202	0.512	0.231		0.235
2772	116	44.5	2.60	876	65	0.202	0.512	0.231		0.245
2768	116	44.5	2.60	874	74	0.202	0.519	0.240		0.254
2771	116	44.5	2.60	878	75	0.202	0.528	0.240		0.255

Ser. Num.	Cal µm	B.W. g/m^2	B$_3$ cm^3/g	Vel m/m	Load kN/m	Rad m	In-nip strain	Rec1 strain	Rec2 strain	Perm. strain
2773	116	44.5	2.60	870	74	0.202	0.523	0.240		0.242
2769	116	44.5	2.60	868	88	0.202	0.539	0.257		0.271
2770	116	44.5	2.60	871	88	0.202	0.539	0.257		0.272
2774	116	44.5	2.60	867	88	0.202	0.540	0.257		0.272
2775	116	44.5	2.60	862	134	0.202	0.564			0.310
2776	116	44.5	2.60	861	176	0.202	0.574			0.325
2777	116	44.5	2.60	870	176	0.202	0.573			0.315
3188	113	42.4	2.67	97	65	0.202	0.577			
3250	110	42.2	2.60	187	18	0.202	0.252	0.135	0.112	0.013
3251	110	42.2	2.60	187	15	0.202	0.191	0.129	0.106	0.009
3252	110	42.2	2.60	186	19	0.202	0.270	0.139	0.113	0.014
3246	110	42.2	2.60	186	41	0.202	0.496	0.214	0.187	0.078
3249	110	42.2	2.60	187	43	0.202	0.503	0.216	0.189	0.101
3253	110	42.2	2.60	185	41	0.202	0.498	0.211	0.185	0.084
3247	110	42.2	2.60	188	65	0.202	0.557	0.266	0.249	0.147
3248	110	42.2	2.60	187	65	0.202	0.558	0.265	0.249	0.151
3191	113	42.4	2.67	326	40	0.202	0.487	0.136	0.130	0.075
3189	113	42.4	2.67	321	65	0.202	0.574	0.218	0.230	0.167
3190	113	42.4	2.67	320	65	0.202	0.564	0.203	0.205	0.187
854	122	45.0	2.71	94	69	0.202	0.523			0.221
2706	121	44.5	2.71	96	72	0.202	0.529	0.387	0.359	0.307
2707	121	44.5	2.71	96	72	0.202	0.524	0.380	0.351	0.304
2705	121	44.5	2.71	95	80	0.202	0.546	0.396	0.378	0.327
2708	121	44.5	2.71	95	78	0.202	0.534	0.390	0.386	0.314
2863	121	45.0	2.68	95	80	0.202	0.461	0.265	0.281	0.269
855	122	45.0	2.71	94	87	0.202	0.546			0.271
888	121	45.0	2.69	101	87	0.202	0.514			0.256
2704	121	44.5	2.71	95	95	0.202	0.572	0.416	0.392	0.334
2709	121	44.5	2.71	95	91	0.202	0.553	0.405	0.371	0.326
2725	121	44.5	2.71	95	93	0.202	0.497		0.393	0.320
856	122	45.0	2.71	94	135	0.202	0.589			0.335
2700	121	44.5	2.71	96	137	0.202	0.647	0.459	0.442	0.376
2703	121	44.5	2.71	96	139	0.202	0.623	0.448	0.428	0.371
857	122	45.0	2.71	93	173	0.202	0.605			0.361
2701	121	44.5	2.71	96	176	0.202	0.673	0.477	0.466	0.397
2702	121	44.5	2.71	96	176	0.202	0.670	0.477	0.466	0.397
800	122	45.0	2.70	171	70	0.202	0.551			0.183
809	122	45.0	2.70	173	70	0.202	0.509			0.166
828	121	45.0	2.68	175	69	0.202	0.573			0.226
2680	119	44.5	2.67	179	73	0.202	0.604	0.302	0.270	0.259
2681	119	44.5	2.67	174	73	0.202	0.606	0.303	0.265	0.251
2717	121	44.5	2.71	187	70	0.202	0.504	0.353	0.337	0.284
2718	121	44.5	2.71	186	70	0.202	0.501	0.349	0.337	0.277
2679	119	44.5	2.67	174	82	0.202	0.617	0.319	0.293	0.283
2716	121	44.5	2.71	187	79	0.202	0.520	0.365	0.344	0.294
2719	121	44.5	2.71	186	77	0.202	0.513	0.361	0.340	0.288
2864	121	45.0	2.68	194	80	0.202	0.457	0.245	0.277	0.254
801	122	45.0	2.70	171	86	0.202	0.575			0.226
810	122	45.0	2.70	171	87	0.202	0.538			0.201
880	121	45.0	2.69	174	86	0.202	0.546			0.265
883	121	45.0	2.69	177	87	0.202	0.512			0.256
886	121	45.0	2.69	177	88	0.202	0.509			0.243
2673	119	44.5	2.67	176	95	0.202	0.623	0.327	0.295	0.309
2678	119	44.5	2.67	178	98	0.202	0.622	0.339	0.319	0.312
2710	121	44.5	2.71	186	91	0.202	0.537	0.380	0.358	0.310
2715	121	44.5	2.71	186	93	0.202	0.541	0.380	0.360	0.313
802	122	45.0	2.70	171	136	0.202	0.616			0.274
811	122	45.0	2.70	171	136	0.202	0.577			0.255
825	121	45.0	2.68	173	137	0.202	0.617			0.333
827	121	45.0	2.68	173	137	0.202	0.601			0.318
881	121	45.0	2.69	174	136	0.202	0.579			0.327
884	121	45.0	2.69	177	136	0.202	0.551			0.322
887	121	45.0	2.69	178	137	0.202	0.548			0.295
2674	119	44.5	2.67	175	140	0.202	0.636	0.374	0.362	0.355
2677	119	44.5	2.67	177	144	0.202	0.634	0.374	0.370	0.356
2711	121	44.5	2.71	187	133	0.202	0.592	0.421	0.413	0.348
2714	121	44.5	2.71	188	137	0.202	0.595	0.421	0.422	0.359
803	122	45.0	2.70	171	172	0.202	0.631			0.300
812	122	45.0	2.70	170	173	0.202	0.595			0.285
885	121	45.0	2.69	178	173	0.202	0.562			0.334
2675	119	44.5	2.67	174	178	0.202	0.639	0.392	0.372	0.373
2676	119	44.5	2.67	171	178	0.202	0.639	0.395	0.391	0.377
2712	121	44.5	2.71	187	174	0.202	0.632	0.442	0.445	0.380
2713	121	44.5	2.71	187	173	0.202	0.631	0.442	0.450	0.385
804	122	45.0	2.70	171	208	0.202	0.641			0.312
813	122	45.0	2.70	169	208	0.202	0.605			0.295
805	122	45.0	2.70	323	70	0.202	0.516			0.169
829	121	45.0	2.68	304	69	0.202	0.561			0.205
2722	121	44.5	2.71	320	69	0.202	0.480	0.299	0.304	0.238
2723	121	44.5	2.71	320	69	0.202	0.481	0.303	0.307	0.249
2733	121	44.5	2.71	320	72	0.202	0.449		0.292	0.249
2734	121	44.5	2.71	319	71	0.202	0.446	0.262	0.268	0.243
2732	121	44.5	2.71	321	80	0.202	0.465		0.299	0.259
2735	121	44.5	2.71	318	78	0.202	0.459	0.268	0.281	0.245
2865	121	45.0	2.68	333	80	0.202	0.455	0.226	0.265	0.236
806	122	45.0	2.70	323	86	0.202	0.544			0.198
872	121	45.0	2.69	306	86	0.202	0.520			0.235
876	121	45.0	2.69	309	87	0.202	0.513			0.245
2720	121	44.5	2.71	317	90	0.202	0.521	0.344	0.340	0.291
2726	121	44.5	2.71	324	93	0.202	0.492		0.331	0.301
2731	121	44.5	2.71	324	96	0.202	0.488	0.292	0.308	0.272
2736	121	44.5	2.71	317	92	0.202	0.483		0.308	0.256
807	122	45.0	2.70	321	136	0.202	0.581			0.246
873	121	45.0	2.69	301	136	0.202	0.557			0.308
877	121	45.0	2.69	309	139	0.202	0.549			0.299
2727	121	44.5	2.71	313	137	0.202	0.549		0.379	0.342
2730	121	44.5	2.71	321	141	0.202	0.548		0.361	0.323

Ser. Num.	Cal µm	B.W. g/m^2	B_L cm^3/g	Vel m/m	Load kN/m	Rad m	In-nip strain	Rec1 strain	Rec2 strain	Perm. strain
2737	121	44.5	2.71	317	135	0.202	0.545		0.360	0.313
808	122	45.0	2.70	323	173	0.202	0.603			0.286
874	121	45.0	2.69	304	173	0.202	0.565			0.326
878	121	45.0	2.69	306	175	0.202	0.557			0.335
2721	121	44.5	2.71	320	173	0.202	0.607		0.423	0.339
2724	121	44.5	2.71	320	172	0.202	0.608		0.407	0.330
2728	121	44.5	2.71	318	177	0.202	0.588		0.402	0.376
2729	121	44.5	2.71	320	177	0.202	0.585		0.397	0.351
879	121	45.0	2.69	304	210	0.202	0.567			0.350
797	122	45.0	2.70	535	69	0.202	0.539			0.133
2866	121	45.0	2.68	562	80	0.202	0.449		0.246	0.224
798	122	45.0	2.70	528	87	0.202	0.561			0.171
858	122	45.0	2.71	528	87	0.202	0.523			0.221
861	122	45.0	2.71	543	87	0.202	0.595			0.221
865	122	45.0	2.71	543	88	0.202	0.623			0.236
3183	118	42.4	2.78	96	41	0.202	0.531	0.235	0.231	
3184	118	42.4	2.78	96	39	0.202	0.528	0.239	0.238	
3180	118	42.4	2.78	320	20	0.202	0.296	0.110	0.110	
3186	118	42.4	2.78	322	20	0.202	0.311	0.126	0.116	0.070
3187	118	42.4	2.78	320	20	0.202	0.313	0.124	0.115	0.084
3179	118	42.4	2.78	321	40	0.202	0.509	0.181	0.182	
3182	118	42.4	2.78	324	41	0.202	0.513	0.193	0.193	
3185	118	42.4	2.78	321	39	0.202	0.515	0.197	0.197	
3181	118	42.4	2.78	322	65	0.202	0.584	0.262	0.259	
1546	96	48.0	2.01	169	50	0.254	0.456			0.016
1556	96	48.0	2.01	169	51	0.254	0.447			0.029
1547	96	48.0	2.01	165	69	0.254	0.485			0.043
1555	96	48.0	2.01	169	70	0.254	0.477			0.068
1548	96	48.0	2.01	168	85	0.254	0.497			0.048
1554	96	48.0	2.01	170	85	0.254	0.487			0.067
1549	96	48.0	2.01	167	135	0.254	0.539			0.112
1553	96	48.0	2.01	171	136	0.254	0.531			0.113
1550	96	48.0	2.01	167	177	0.254	0.558			0.143
1552	96	48.0	2.01	170	179	0.254	0.558			0.144
1551	96	48.0	2.01	167	201	0.254	0.565			0.158
1236	115	48.0	2.39	96	84	0.254	0.571			0.230
1290	118	48.0	2.45	95	85	0.254	0.590			0.242
1426	115	48.0	2.40	93	86	0.254	0.586			0.193
1431	115	48.0	2.40	94	86	0.254	0.593			0.184
1237	115	48.0	2.39	95	137	0.254	0.617			0.299
1291	118	48.0	2.45	95	136	0.254	0.641			0.313
1427	115	48.0	2.40	93	136	0.254	0.641			0.255
1432	115	48.0	2.40	93	137	0.254	0.653			0.247
1238	115	48.0	2.39	96	175	0.254	0.639			0.329
1292	118	48.0	2.45	95	175	0.254	0.663			0.332
1428	115	48.0	2.40	93	175	0.254	0.674			0.298
1430	115	48.0	2.40	93	178	0.254	0.676			0.294
1433	115	48.0	2.40	93	175	0.254	0.682			0.276
1239	115	48.0	2.39	95	209	0.254	0.646			0.347
1293	118	48.0	2.45	95	209	0.254	0.679			0.344
1429	115	48.0	2.40	93	209	0.254	0.692			0.321
1434	115	48.0	2.40	93	209	0.254	0.702			0.306
1256	114	48.0	2.38	167	85	0.254	0.589			0.233
1297	118	48.0	2.45	167	85	0.254	0.592			0.220
1435	115	48.0	2.40	166	86	0.254	0.609			0.162
1441	115	48.0	2.40	165	87	0.254	0.613			0.165
1257	114	48.0	2.38	204	137	0.254	0.635			0.302
1296	118	48.0	2.45	168	139	0.254	0.648			0.288
1436	115	48.0	2.40	163	136	0.254	0.671			0.244
1440	115	48.0	2.40	165	140	0.254	0.671			0.240
1258	114	48.0	2.38	160	176	0.254	0.660			0.330
1295	118	48.0	2.45	167	179	0.254	0.665			0.319
1437	115	48.0	2.40	164	175	0.254	0.695			0.276
1439	115	48.0	2.40	164	179	0.254	0.696			0.279
1259	114	48.0	2.38	167	208	0.254	0.671			0.347
1294	118	48.0	2.45	169	209	0.254	0.680			0.345
1438	115	48.0	2.40	163	209	0.254	0.709			0.291
1268	113	48.0	2.36	292	87	0.254	0.562			0.207
1279	118	48.0	2.45	288	84	0.254	0.612			0.232
1269	113	48.0	2.36	289	138	0.254	0.612			0.274
1280	118	48.0	2.45	290	137	0.254	0.670			0.296
1270	113	48.0	2.36	290	176	0.254	0.639			0.309
1281	118	48.0	2.45	280	176	0.254	0.694			0.330
1271	113	48.0	2.36	290	209	0.254	0.653			0.331
1282	118	48.0	2.45	292	210	0.254	0.707			0.357
1240	115	48.0	2.39	523	87	0.254	0.556			0.198
1283	118	48.0	2.45	515	86	0.254	0.617			0.238
1410	115	48.0	2.40	520	85	0.254	0.599			0.184
1241	115	48.0	2.39	500	139	0.254	0.605			0.265
1274	113	48.0	2.36	518	139	0.254	0.606			0.266
1284	118	48.0	2.45	500	138	0.254	0.664			0.298
1411	115	48.0	2.40	500	134	0.254	0.665			0.255
1415	115	48.0	2.40	500	140	0.254	0.674			0.260
1242	115	48.0	2.39	515	175	0.254	0.626			0.295
1273	113	48.0	2.36	513	179	0.254	0.633			0.301
1285	118	48.0	2.45	520	177	0.254	0.681			0.307
1412	115	48.0	2.40	512	176	0.254	0.696			0.289
1414	115	48.0	2.40	500	178	0.254	0.698			0.285
1243	115	48.0	2.39	520	209	0.254	0.641			0.310
1272	113	48.0	2.36	518	210	0.254	0.646			0.311
1413	115	48.0	2.40	509	210	0.254	0.712			0.308
1244	115	48.0	2.39	939	86	0.254	0.489			0.172
1390	115	48.0	2.40	921	85	0.254	0.516			0.175
1396	115	48.0	2.40	900	87	0.254	0.466			0.175
1404	115	48.0	2.40	939	87	0.254	0.574			0.184
1421	115	48.0	2.40	939	88	0.254	0.572			0.137
1245	115	48.0	2.39	900	138	0.254	0.542			0.253

Ser. Num.	Cal µm	B.W. g/m²	B_i cm³/g	Vel m/m	Load kN/m	Rad m	In-nip strain	Rec1 strain	Rec2 strain	Perm. strain
1391	115	48.0	2.40	900	137	0.254	0.558			0.240
1395	115	48.0	2.40	900	140	0.254	0.532			0.236
1405	115	48.0	2.40	900	137	0.254	0.634			0.248
1416	115	48.0	2.40	939	136	0.254	0.650			0.219
1420	115	48.0	2.40	930	139	0.254	0.642			0.204
1246	115	48.0	2.39	900	176	0.254	0.570			0.269
1392	115	48.0	2.40	900	176	0.254	0.573			0.264
1394	115	48.0	2.40	900	179	0.254	0.562			0.272
1417	115	48.0	2.40	948	175	0.254	0.677			0.249
1419	115	48.0	2.40	900	177	0.254	0.670			0.235
1247	115	48.0	2.39	900	209	0.254	0.586			0.296
1393	115	48.0	2.40	900	210	0.254	0.581			0.289
1418	115	48.0	2.40	939	208	0.254	0.696			0.265
1482	124	48.0	2.59	308	50	0.254	0.516			0.193
1483	124	48.0	2.59	308	69	0.254	0.545			0.220
1484	124	48.0	2.59	307	84	0.254	0.564			0.250
1485	124	48.0	2.59	307	135	0.254	0.606			0.312
1486	124	48.0	2.59	306	177	0.254	0.621			0.332
1487	124	48.0	2.59	307	201	0.254	0.628			0.344
1488	124	48.0	2.59	513	50	0.254	0.531			0.163
1489	124	48.0	2.59	514	69	0.254	0.572			0.208
1518	127	48.0	2.65	93	51	0.254	0.525			0.192
1499	127	48.0	2.65	93	70	0.254	0.514			0.251
1519	127	48.0	2.65	93	69	0.254	0.558			0.225
1058	128	48.0	2.66	96	82	0.254	0.510			0.195
937	126	48.0	2.63	97	85	0.254	0.634			0.224
1500	127	48.0	2.65	93	85	0.254	0.531			0.257
1520	127	48.0	2.65	93	84	0.254	0.576			0.249
938	126	48.0	2.63	97	136	0.254	0.661			0.296
1059	128	48.0	2.66	96	135	0.254	0.584			0.288
1521	127	48.0	2.65	93	135	0.254	0.620			0.299
939	126	48.0	2.63	97	176	0.254	0.675			0.335
1060	128	48.0	2.66	96	174	0.254	0.618			0.320
1522	127	48.0	2.65	94	177	0.254	0.647			0.326
940	126	48.0	2.63	97	210	0.254	0.688			0.344
1061	128	48.0	2.66	96	209	0.254	0.647			0.335
1523	127	48.0	2.65	93	201	0.254	0.656			0.335
1503	127	48.0	2.65	172	51	0.254	0.481			0.189
1508	127	48.0	2.65	173	51	0.254	0.547			0.191
1502	127	48.0	2.65	170	70	0.254	0.515			0.234
1501	127	48.0	2.65	172	84	0.254	0.528			0.259
1509	127	48.0	2.65	170	85	0.254	0.602			0.256
1510	127	48.0	2.65	171	85	0.254	0.600			0.243
1512	127	48.0	2.65	291	50	0.254	0.548			0.180
1511	127	48.0	2.65	290	70	0.254	0.585			0.209
1038	128	48.0	2.66	303	87	0.254	0.525			0.206
1513	127	48.0	2.65	288	84	0.254	0.595			0.236
1514	127	48.0	2.65	290	84	0.254	0.595			0.236
1539	128	48.0	2.66	298	83	0.254	0.616			0.232
1540	128	48.0	2.66	296	84	0.254	0.595			0.258
1039	128	48.0	2.66	297	138	0.254	0.601			0.294
1040	128	48.0	2.66	297	175	0.254	0.631			0.321
1041	128	48.0	2.66	299	209	0.254	0.653			0.343
1517	127	48.0	2.65	514	51	0.254	0.538			0.154
1516	127	48.0	2.65	510	71	0.254	0.579			0.197
1034	128	48.0	2.66	500	86	0.254	0.527			0.191
1515	127	48.0	2.65	518	84	0.254	0.593			0.209
1035	128	48.0	2.66	529	137	0.254	0.609			0.286
1036	128	48.0	2.66	500	175	0.254	0.641			0.315
1037	128	48.0	2.66	532	209	0.254	0.668			0.337
1000	130	48.0	2.71	101	85	0.254	0.584			0.257
1016	130	48.0	2.71	99	85	0.254	0.549			0.237
1091	121	45.0	2.68	95	83	0.254	0.527			0.232
1115	121	45.0	2.68	93	83	0.254	0.533			0.234
1117	121	45.0	2.68	94	84	0.254	0.533			0.222
1172	121	45.0	2.70	93	84	0.254	0.544			0.207
1001	130	48.0	2.71	100	136	0.254	0.644			0.328
1017	130	48.0	2.71	99	136	0.254	0.605			0.309
1092	121	45.0	2.68	90	138	0.254	0.613			0.319
1116	121	45.0	2.68	93	137	0.254	0.616			0.297
1118	121	45.0	2.68	93	138	0.254	0.616			0.298
1136	122	45.0	2.71	95	132	0.254	0.619			0.302
1173	121	45.0	2.70	94	138	0.254	0.607			0.288
1002	130	48.0	2.71	100	175	0.254	0.679			0.352
1018	130	48.0	2.71	98	175	0.254	0.638			0.329
1093	121	45.0	2.68	90	177	0.254	0.645			0.350
1119	121	45.0	2.68	94	174	0.254	0.644			0.321
1137	122	45.0	2.71	95	177	0.254	0.656			0.343
1174	121	45.0	2.70	92	178	0.254	0.632			0.311
1003	130	48.0	2.71	100	209	0.254	0.706			0.368
1019	130	48.0	2.71	99	210	0.254	0.666			0.345
1094	121	45.0	2.68	94	211	0.254	0.664			0.366
1120	121	45.0	2.68	94	211	0.254	0.666			0.342
1138	122	45.0	2.71	95	209	0.254	0.673			0.360
976	128	48.0	2.67	174	87	0.254	0.499			0.232
1004	130	48.0	2.71	177	87	0.254	0.583			0.242
1020	130	48.0	2.71	172	87	0.254	0.545			0.227
1107	121	45.0	2.68	160	85	0.254	0.543			0.238
1152	122	45.0	2.71	169	84	0.254	0.561			0.228
1160	122	45.0	2.71	167	84	0.254	0.535			0.216
977	128	48.0	2.67	173	137	0.254	0.559			0.294
1005	130	48.0	2.71	176	137	0.254	0.639			0.309
1021	130	48.0	2.71	172	138	0.254	0.601			0.289
1108	121	45.0	2.68	164	136	0.254	0.617			0.302
1153	122	45.0	2.71	166	138	0.254	0.634			0.295
1161	122	45.0	2.71	166	137	0.254	0.613			0.295
978	128	48.0	2.67	174	175	0.254	0.593			0.309

Ser. Num.	Cal µm	B.W. g/m^2	B_L cm^3/g	Vel m/m	Load kN/m	Rad m	In-nip strain	Rec1 strain	Rec2 strain	Perm. strain
1006	130	48.0	2.71	175	176	0.254	0.672			0.343
1022	130	48.0	2.71	171	175	0.254	0.630			0.319
1109	121	45.0	2.68	165	175	0.254	0.646			0.338
1154	122	45.0	2.71	166	176	0.254	0.664			0.324
1162	122	45.0	2.71	166	175	0.254	0.641			0.323
979	128	48.0	2.67	173	209	0.254	0.621			0.334
1007	130	48.0	2.71	176	209	0.254	0.694			0.362
1023	130	48.0	2.71	172	209	0.254	0.654			0.335
1110	121	45.0	2.68	165	208	0.254	0.665			0.350
1155	122	45.0	2.71	166	209	0.254	0.686			0.342
1163	122	45.0	2.71	165	210	0.254	0.662			0.337
980	128	48.0	2.67	305	86	0.254	0.487			0.217
1008	130	48.0	2.71	307	84	0.254	0.569			0.220
1114	121	45.0	2.68	284	84	0.254	0.530			0.206
1151	122	45.0	2.71	280	84	0.254	0.554			0.224
1167	122	45.0	2.71	293	86	0.254	0.537			0.192
1189	121	45.0	2.69	285	84	0.254	0.519			0.197
981	128	48.0	2.67	303	137	0.254	0.548			0.282
1009	130	48.0	2.71	313	135	0.254	0.632			0.285
1113	121	45.0	2.68	287	137	0.254	0.615			0.279
1166	122	45.0	2.71	290	139	0.254	0.610			0.274
1190	121	45.0	2.69	288	137	0.254	0.587			0.273
982	128	48.0	2.67	305	177	0.254	0.581			0.306
1010	130	48.0	2.71	311	177	0.254	0.664			0.320
1112	121	45.0	2.68	287	179	0.254	0.646			0.318
1165	122	45.0	2.71	296	177	0.254	0.639			0.294
1191	121	45.0	2.69	280	176	0.254	0.616			0.306
1212	128	48.0	2.67	300	176	0.254	0.698			0.291
1213	128	48.0	2.67	300	177	0.254	0.675			0.291
1214	128	48.0	2.67	300	176	0.254	0.648			0.291
1215	128	48.0	2.67	300	176	0.254	0.633			0.291
1216	128	48.0	2.67	300	176	0.254	0.625			0.291
1217	128	48.0	2.67	300	176	0.254	0.622			0.291
983	128	48.0	2.67	303	209	0.254	0.605			0.326
1011	130	48.0	2.71	305	209	0.254	0.688			0.333
1111	121	45.0	2.68	280	208	0.254	0.666			0.341
1164	122	45.0	2.71	296	210	0.254	0.663			0.316
1192	121	45.0	2.69	285	208	0.254	0.578			0.330
1098	121	45.0	2.68	500	82	0.254	0.513			0.204
1133	122	45.0	2.70	520	82	0.254	0.441			0.174
974	128	48.0	2.67	550	85	0.254	0.504			0.214
984	128	48.0	2.67	500	87	0.254	0.469			0.199
1099	121	45.0	2.68	515	83	0.254	0.508			0.200
1143	122	45.0	2.71	520	85	0.254	0.525			0.199
1208	122	45.0	2.72	529	85	0.254	0.523			0.196
975	128	48.0	2.67	547	138	0.254	0.574			0.278
985	128	48.0	2.67	535	138	0.254	0.534			0.269
1100	121	45.0	2.68	512	139	0.254	0.599			0.276
1134	122	45.0	2.70	500	137	0.254	0.532			0.255
1144	122	45.0	2.71	512	138	0.254	0.606			0.280
1201	122	45.0	2.72	500	139	0.254	0.618			0.293
1209	122	45.0	2.72	500	138	0.254	0.593			0.270
986	128	48.0	2.67	538	176	0.254	0.569			0.297
1101	121	45.0	2.68	500	175	0.254	0.626			0.305
1145	122	45.0	2.71	520	175	0.254	0.632			0.307
1202	122	45.0	2.72	500	177	0.254	0.652			0.327
1210	122	45.0	2.72	500	177	0.254	0.632			0.303
987	128	48.0	2.67	541	209	0.254	0.592			0.322
1146	122	45.0	2.71	518	209	0.254	0.655			0.334
1203	122	45.0	2.72	500	210	0.254	0.674			0.339
1211	122	45.0	2.72	515	210	0.254	0.645			0.311
1177	121	45.0	2.69	921	85	0.254	0.475			0.202
1185	121	45.0	2.69	900	85	0.254	0.520			0.191
1207	122	45.0	2.72	939	83	0.254	0.540			0.186
1178	121	45.0	2.69	939	137	0.254	0.545			0.265
1186	121	45.0	2.69	948	136	0.254	0.589			0.259
1206	122	45.0	2.72	921	139	0.254	0.618			0.254
1179	121	45.0	2.69	912	192	0.254	0.581			0.299
1187	121	45.0	2.69	900	176	0.254	0.623			0.288
1205	122	45.0	2.72	930	178	0.254	0.653			0.293
1180	121	45.0	2.69	900	210	0.254	0.591			0.307
1188	121	45.0	2.69	900	209	0.254	0.647			0.299
1204	122	45.0	2.72	958	210	0.254	0.681			0.316
2586	96	45.0	2.14	91	97	0.355	0.463	0.207		0.084
2610	96	45.0	2.12	91	132	0.355	0.462	0.228		0.161
2159	96	44.5	2.17	297	97	0.355	0.475	0.129		0.015
2160	96	44.5	2.17	302	97	0.355	0.482	0.123		0.016
2167	96	44.5	2.17	303	98	0.355	0.477	0.135		0.016
2587	96	45.0	2.14	303	97	0.355	0.454	0.175		0.071
2593	94	45.0	2.08	304	97	0.355	0.421	0.100		0.082
2594	94	45.0	2.08	302	97	0.355	0.422	0.106		0.085
2600	96	45.0	2.12	296	98	0.355	0.420	0.155		0.091
2601	96	45.0	2.12	304	99	0.355	0.424	0.160		0.094
2161	96	44.5	2.17	302	133	0.355	0.501	0.161		0.045
2166	96	44.5	2.17	306	135	0.355	0.496	0.155		0.039
2588	94	45.0	2.08	301	137	0.355	0.498	0.144		0.102
2592	94	45.0	2.08	300	135	0.355	0.460	0.129		0.096
2599	96	45.0	2.12	297	135	0.355	0.461	0.180		0.122
2602	96	45.0	2.12	301	134	0.355	0.458	0.182		0.109
2604	96	45.0	2.12	302	135	0.355	0.458	0.185		0.120
2606	96	45.0	2.12	313	135	0.355	0.462	0.191		0.123
2162	96	44.5	2.17	300	178	0.355	0.525	0.183		0.064
2165	96	44.5	2.17	301	180	0.355	0.533	0.186		0.074
2589	94	45.0	2.08	303	185	0.355	0.533	0.170		0.137
2603	96	45.0	2.12	300	181	0.355	0.497	0.205		0.141
2605	96	45.0	2.12	302	181	0.355	0.496	0.205		0.132
2609	96	45.0	2.12	302	185	0.355	0.501	0.216		0.149

Ser. Num.	Cal μm	B.W. g/m²	B_v cm³/g	Vel m/m	Load kN/m	Rad m	In-nip strain	Rec1 strain	Rec2 strain	Perm. strain
2163	96	44.5	2.17	301	209	0.355	0.537	0.196		0.088
2164	96	44.5	2.17	302	209	0.355	0.547	0.205		0.090
2590	94	45.0	2.08	302	211	0.355	0.550	0.180		0.136
2591	94	45.0	2.08	303	210	0.355	0.547	0.178		0.133
2607	96	45.0	2.12	303	210	0.355	0.519	0.224		0.156
2608	96	45.0	2.12	302	210	0.355	0.516	0.218		0.141
2168	96	44.5	2.17	519	94	0.355	0.504	0.186		0.041
2174	96	44.5	2.17	525	96	0.355	0.561	0.159		0.031
2169	96	44.5	2.17	516	130	0.355	0.559	0.203		0.060
2173	96	44.5	2.17	523	133	0.355	0.593	0.184		0.067
2175	96	44.5	2.17	517	129	0.355	0.578	0.177		0.061
2611	96	45.0	2.12	530	131	0.355	0.452	0.177		0.142
2616	96	45.0	2.12	524	135	0.355	0.450	0.157		0.143
2617	96	45.0	2.12	519	135	0.355	0.451	0.157		0.134
2170	96	44.5	2.17	523	174	0.355	0.636	0.228		0.096
2172	96	44.5	2.17	525	178	0.355	0.617	0.217		0.081
2176	96	44.5	2.17	518	173	0.355	0.595	0.189		0.089
2612	96	45.0	2.12	516	177	0.355	0.484	0.186		0.149
2615	96	45.0	2.12	523	181	0.355	0.492	0.185		0.160
2171	96	44.5	2.17	519	208	0.355	0.640	0.219		0.106
2177	96	44.5	2.17	519	207	0.355	0.610	0.207		0.109
2613	96	45.0	2.12	522	209	0.355	0.510	0.200		0.172
2614	96	45.0	2.12	522	208	0.355	0.511	0.199		0.172
2618	96	45.0	2.12	514	208	0.355	0.513	0.201		0.165
2619	96	45.0	2.12	521	208	0.355	0.507	0.195		0.155
2654	114	45.0	2.53	91	11	0.355	0.272	0.137	0.138	0.074
2655	114	45.0	2.53	91	11	0.355	0.280	0.146	0.174	0.074
2656	114	45.0	2.53	92	24	0.355	0.391	0.211	0.217	0.126
2657	114	45.0	2.53	91	24	0.355	0.398	0.217	0.224	0.147
2653	114	45.0	2.53	91	98	0.355	0.537	0.341	0.324	0.269
2663	114	45.0	2.53	92	96	0.355	0.534	0.362	0.354	0.276
2664	114	45.0	2.53	174	95	0.355	0.528	0.332		0.250
2659	114	45.0	2.53	302	12	0.355	0.279	0.146	0.152	0.076
2660	114	45.0	2.53	301	13	0.355	0.271	0.137	0.160	0.063
2658	114	45.0	2.53	303	25	0.355	0.385	0.196	0.199	0.101
2661	114	45.0	2.53	301	25	0.355	0.382	0.197	0.187	0.088
2666	114	45.0	2.53	922	28	0.355	0.388		0.132	0.112
2667	114	45.0	2.53	921	16	0.355	0.292		0.083	0.072
2668	114	45.0	2.53	921	16	0.355	0.297		0.096	0.077
2669	114	45.0	2.53	919	28	0.355	0.392		0.136	0.098
2670	114	45.0	2.53	923	28	0.355	0.397		0.135	
2665	114	45.0	2.53	927	94	0.355	0.508		0.246	0.219
2029	121	45.9	2.64	90	24	0.355	0.431	0.181		0.137
2291	117	44.5	2.63	88	20	0.355	0.507			0.107
2300	116	44.0	2.64	89	19	0.355	0.429			0.156
2317	116	44.0	2.64	88	25	0.355				0.137
2318	116	44.0	2.64	89	22	0.355				0.117
2319	116	44.0	2.64	89	22	0.355				0.122
2320	116	44.0	2.64	89	25	0.355				0.123
2333	116	44.0	2.64	89	22	0.355				0.117
2334	116	44.0	2.64	89	22	0.355				0.115
2523	117	45.0	2.60	92	26	0.355	0.381	0.163		0.141
2524	117	45.0	2.60	90	17	0.355	0.315	0.132		0.116
2525	117	45.0	2.60	91	25	0.355	0.379	0.167		0.141
2022	121	45.9	2.64	89	96	0.355	0.600	0.304		0.296
2028	121	45.9	2.64	91	96	0.355	0.574	0.315		0.304
2030	121	45.9	2.64	86	95	0.355	0.561	0.318		0.297
2286	117	44.5	2.63	89	97	0.355	0.558			0.268
2290	117	44.5	2.63	89	97	0.355	0.552			0.256
2297	116	44.0	2.64	89	97	0.355	0.541			0.305
2299	116	44.0	2.64	89	98	0.355	0.534			0.299
2308	116	44.0	2.64	89	96	0.355				0.296
2309	116	44.0	2.64	90	96	0.355				0.300
2316	116	44.0	2.64	89	95	0.355				0.265
2321	116	44.0	2.64	90	94	0.355				0.246
2331	116	44.0	2.64	89	93	0.355				0.255
2023	121	45.9	2.64	90	133	0.355	0.634	0.338		0.338
2027	121	45.9	2.64	89	136	0.355	0.611	0.344		0.339
2287	117	44.5	2.63	90	134	0.355	0.580			0.289
2310	116	44.0	2.64	89	133	0.355				0.323
2315	116	44.0	2.64	89	134	0.355				0.302
2469	118	45.0	2.63	90	131	0.355	0.571	0.320		0.302
2512	120	45.0	2.66	93	129	0.355	0.585	0.290		
2522	117	45.0	2.60	92	136	0.355	0.548	0.316		0.328
2024	121	45.9	2.64	89	179	0.355				0.376
2026	121	45.9	2.64	90	182	0.355	0.655	0.359		0.363
2288	117	44.5	2.63	89	179	0.355	0.599			0.312
2311	116	44.0	2.64	89	179	0.355				0.329
2314	116	44.0	2.64	89	180	0.355				0.328
2470	118	45.0	2.63	89	175	0.355	0.597	0.351		0.325
2025	121	45.9	2.64	89	210	0.355		0.398		0.383
2289	117	44.5	2.63	89	209	0.355	0.611	0.299		0.319
2298	116	44.0	2.64	90	211	0.355	0.596			0.372
2312	116	44.0	2.64	89	210	0.355				0.346
2313	116	44.0	2.64	89	210	0.355				0.339
2332	116	44.0	2.64	89	210	0.355				0.330
2335	116	44.0	2.64	88	210	0.355				0.323
2336	116	44.0	2.64	89	210	0.355				0.318
2328	116	44.0	2.64	171	23	0.355				0.098
2329	116	44.0	2.64	174	23	0.355				0.094
2459	118	45.0	2.63	175	23	0.355	0.386	0.125		0.103
2460	118	45.0	2.63	174	20	0.355	0.363	0.114		0.101
2461	118	45.0	2.63	175	20	0.355	0.361	0.116		0.094
2462	118	45.0	2.63	175	23	0.355	0.385	0.128		0.095
2527	117	45.0	2.60	175	25	0.355	0.368	0.149		0.122
2528	117	45.0	2.60	176	18	0.355	0.306	0.117		0.088
2529	117	45.0	2.60	177	25	0.355	0.366	0.148		0.115

Ser. Num.	Cal µm	B.W. g/m²	B_s cm³/g	Vel m/m	Load kN/m	Rad m	In-nip strain	Rec1 strain	Rec2 strain	Perm. strain
2322	116	44.0	2.64	177	94	0.355				0.223
2327	116	44.0	2.64	172	94	0.355				0.220
2330	116	44.0	2.64	176	94	0.355				0.214
2526	117	45.0	2.60	177	98	0.355	0.509	0.273		0.267
2458	118	45.0	2.63	175	131	0.355	0.559	0.315		0.293
2324	116	44.0	2.64	174	174	0.355				0.299
2325	116	44.0	2.64	174	208	0.355				0.301
2326	116	44.0	2.64	174	208	0.355				0.304
2011	122	45.9	2.65	309	22	0.355	0.371			0.108
2012	122	45.9	2.65	299	22	0.355	0.375			0.115
2464	118	45.0	2.63	298	22	0.355	0.376			0.107
2465	118	45.0	2.63	301	20	0.355	0.350			0.094
2466	118	45.0	2.63	300	20	0.355	0.356			0.095
2467	118	45.0	2.63	300	22	0.355	0.379			0.100
2004	122	45.9	2.65	301	98	0.355	0.621			0.283
2010	122	45.9	2.65	303	99	0.355	0.605			0.276
2013	122	45.9	2.65	292	98	0.355	0.586			0.264
2005	122	45.9	2.65	299	134	0.355				0.310
2009	122	45.9	2.65	303	137	0.355	0.658			0.298
2463	118	45.0	2.63	301	133	0.355	0.575			0.293
2468	118	45.0	2.63	300	133	0.355	0.571	0.294		0.276
2006	122	45.9	2.65	302	179	0.355				0.345
2008	122	45.9	2.65	303	182	0.355				0.335
2007	122	45.9	2.65	301	210	0.355				0.352
2072	121	45.9	2.64	534	20	0.355	0.467	0.341		0.094
2306	116	44.0	2.64	513	18	0.355	0.364			0.124
2307	116	44.0	2.64	520	22	0.355	0.389			0.128
2474	118	45.0	2.63	519	28	0.355	0.385			0.089
2475	118	45.0	2.63	524	25	0.355	0.373			0.085
2476	118	45.0	2.63	519	25	0.355	0.369			0.092
2477	118	45.0	2.63	520	27	0.355	0.383			0.102
2479	118	45.0	2.63	521	27	0.355	0.387			0.085
2480	118	45.0	2.63	520	25	0.355	0.371			0.080
2481	118	45.0	2.63	520	25	0.355	0.371			0.081
2482	118	45.0	2.63	520	27	0.355	0.382			0.084
2514	120	45.0	2.66	526	29	0.355	0.419	0.092		0.086
2515	120	45.0	2.66	522	26	0.355	0.396	0.077		0.066
2516	120	45.0	2.66	524	26	0.355	0.395	0.073		0.078
2517	120	45.0	2.66	523	29	0.355	0.416	0.085		0.098
2518	120	45.0	2.66	526	26	0.355	0.396	0.069		0.086
2519	120	45.0	2.66	522	29	0.355	0.413	0.074		0.095
2065	121	45.9	2.64	522	99	0.355	0.562	0.456		0.236
2071	121	45.9	2.64	526	100	0.355	0.544	0.450		0.243
2301	116	44.0	2.64	517	97	0.355	0.520			0.254
2302	116	44.0	2.64	519	97	0.355	0.526			0.247
2304	116	44.0	2.64	515	97	0.355	0.501			0.283
2478	118	45.0	2.63	521	91	0.355	0.507			0.207
2483	118	45.0	2.63	521	91	0.355	0.509			0.198
2513	120	45.0	2.66	536	93	0.355	0.538			0.195
2520	120	45.0	2.66	516	91	0.355	0.534			0.185
2066	121	45.9	2.64	519	136	0.355	0.580	0.476		0.276
2070	121	45.9	2.64	527	139	0.355	0.571	0.468		0.270
2473	118	45.0	2.63	527	127	0.355	0.542			0.250
2067	121	45.9	2.64	520	182	0.355	0.598	0.487		0.295
2069	121	45.9	2.64	526	186	0.355	0.595	0.482		0.303
2068	121	45.9	2.64	521	211	0.355	0.604	0.492		0.310
2303	116	44.0	2.64	521	210	0.355	0.586			0.306
2305	116	44.0	2.64	522	211	0.355	0.566			0.343
2095	121	45.9	2.63	937	23	0.355	0.475			0.106
2088	121	45.9	2.63	928	96	0.355	0.569			
2094	121	45.9	2.63	930	98	0.355	0.551			0.251
2096	121	45.9	2.63	912	97	0.355	0.559			0.239
2097	121	45.9	2.63	921	97	0.355	0.555			0.225
2098	121	45.9	2.63	926	97	0.355	0.552			0.213
2089	121	45.9	2.63	924	133	0.355	0.592			
2093	121	45.9	2.63	924	137	0.355	0.583			0.269
2090	121	45.9	2.63	913	179	0.355	0.614			
2092	121	45.9	2.63	931	183	0.355	0.612			0.314
2091	121	45.9	2.63	919	210	0.355	0.619			0.330
2651	123	45.0	2.73	91	11	0.355	0.302			0.067
2049	123	45.9	2.67	88	23	0.355	0.465	0.196		0.150
2124	120	44.5	2.69	92	23	0.355	0.468	0.153		0.150
2236	123	45.0	2.73	95	22	0.355	0.404	0.125		0.134
2043	123	45.9	2.67	90	97	0.355	0.538	0.328		0.300
2048	123	45.9	2.67	91	97	0.355	0.519	0.335		0.313
2117	120	44.5	2.69	89	98	0.355	0.534	0.305		0.324
2123	120	44.5	2.69	90	98	0.355	0.516	0.290		0.300
2133	120	44.5	2.69	89	96	0.355	0.513	0.279		0.282
2134	120	44.5	2.69	89	96	0.355	0.510	0.276		0.274
2229	123	45.0	2.73	90	94	0.355	0.547	0.262		0.278
2235	123	45.0	2.73	92	95	0.355	0.539	0.267		0.271
2237	123	45.0	2.73	86	94	0.355	0.533	0.271		0.280
2244	123	45.0	2.73	90	92	0.355	0.631	0.272		0.280
2340	120	44.0	2.73	89	97	0.355	0.552			0.299
2343	120	44.0	2.73	90	97	0.355	0.551			
2346	120	45.0	2.67	89	96	0.355	0.530	0.234		
2347	120	45.0	2.67	89	96	0.355	0.609			0.314
2348	120	45.0	2.67	89	97	0.355	0.486			0.316
2352	120	45.0	2.67	89	95	0.355	0.470			0.299
2356	121	45.0	2.70	90	96	0.355	0.512			0.290
2367	122	45.0	2.72	89	98	0.355	0.566	0.412		0.338
2368	122	45.0	2.72	89	97	0.355	0.563	0.404		0.316
2396	119	44.0	2.71	89	96	0.355	0.539	0.437		0.269
2398	119	44.0	2.71	89	95	0.355	0.540	0.431		0.268
2401	119	44.0	2.71	89	94	0.355	0.530	0.425		0.246
2431	124	45.0	2.76	90	95	0.355	0.543	0.308		0.286
2622	122	45.0	2.71	91	98	0.355	0.504			

Ser. Num.	Cal μm	B.W. g/m²	B_s cm³/g	Vel m/m	Load kN/m	Rad m	In-nip strain	Rec1 strain	Rec2 strain	Perm. strain
2623	122	45.0	2.71	91	98	0.355	0.497			
2647	123	45.0	2.73	92	98	0.355	0.565	0.346	0.267	0.257
2044	123	45.9	2.67	89	133	0.355	0.559	0.354		0.339
2118	120	44.5	2.69	88	134	0.355	0.557	0.332		0.352
2122	120	44.5	2.69	91	137	0.355	0.554			0.356
2230	123	45.0	2.73	89	130	0.355	0.584	0.294		0.311
2234	123	45.0	2.73	92	133	0.355	0.576	0.292		0.299
2648	123	45.0	2.73	91	135	0.355	0.596	0.375	0.297	0.283
2045	123	45.9	2.67	89	179	0.355	0.572	0.379		0.368
2119	120	44.5	2.69	87	180	0.355	0.580			0.379
2121	120	44.5	2.69	91	183	0.355	0.581			0.389
2231	123	45.0	2.73	89	175	0.355	0.617			0.330
2233	123	45.0	2.73	90	178	0.355	0.613	0.315		0.326
2649	123	45.0	2.73	91	181	0.355	0.630	0.398	0.321	0.308
2046	123	45.9	2.67	89	210	0.355	0.584	0.462		0.385
2120	120	44.5	2.69	88	211	0.355	0.590			0.394
2232	123	45.0	2.73	88	209	0.355		0.333		0.345
2650	123	45.0	2.73	92	209	0.355	0.650	0.416	0.325	0.330
2125	120	44.5	2.69	174	97	0.355	0.517	0.275		0.289
2349	120	45.0	2.67	174	97	0.355	0.480			
2357	121	45.0	2.70	175	96	0.355	0.498			0.267
2126	120	44.5	2.69	175	132	0.355	0.541			0.312
2432	124	45.0	2.76	175	129	0.355	0.562	0.300		0.297
2127	120	44.5	2.69	173	177	0.355	0.564			0.345
2128	120	44.5	2.69	173	209	0.355	0.576			0.357
2409	119	44.0	2.71	298	26	0.355	0.390	0.232		0.097
2410	119	44.0	2.71	300	23	0.355	0.367	0.219		0.085
2411	119	44.0	2.71	299	23	0.355	0.367	0.218		0.086
2412	119	44.0	2.71	299	26	0.355	0.392	0.235		0.091
2050	123	45.9	2.67	312	96	0.355	0.512	0.267		0.272
2129	120	44.5	2.69	306	97	0.355	0.514			0.267
2137	123	44.5	2.76	294	100	0.355		0.374		0.194
2138	123	44.5	2.76	301	99	0.355		0.365		0.194
2139	123	44.5	2.76	302	99	0.355	0.641	0.359		0.194
2140	123	44.5	2.76	301	98	0.355	0.613	0.352		0.194
2141	123	44.5	2.76	302	98	0.355	0.594	0.347		0.194
2142	123	44.5	2.76	304	98	0.355	0.581	0.341		0.194
2143	123	44.5	2.76	301	97	0.355	0.576	0.336		0.194
2145	123	44.5	2.76	300	97	0.355	0.551	0.322		0.194
2146	123	44.5	2.76	301	97	0.355	0.539	0.315		0.194
2147	123	44.5	2.76	300	96	0.355	0.529	0.309		0.194
2344	120	44.0	2.73	296	97	0.355	0.551			
2350	120	45.0	2.67	298	96	0.355	0.473			0.287
2354	120	45.0	2.67	301	96	0.355	0.464			0.252
2358	121	45.0	2.70	297	96	0.355	0.490			0.254
2392	119	44.0	2.71	301	97	0.355	0.540	0.392		0.233
2393	119	44.0	2.71	302	97	0.355	0.538	0.396		0.234
2397	119	44.0	2.71	301	95	0.355	0.533	0.392		0.231
2399	119	44.0	2.71	300	94	0.355	0.533	0.386		0.242
2408	119	44.0	2.71	299	95	0.355	0.526	0.373		0.218
2413	119	44.0	2.71	303	94	0.355	0.527	0.377		0.210
2430	124	45.0	2.76	302	95	0.355	0.535	0.258		0.265
2574	123	45.0	2.73	302	94	0.355	0.571	0.313		0.216
2575	123	45.0	2.73	302	94	0.355	0.570	0.314		0.216
2576	123	45.0	2.73	302	93	0.355	0.564	0.318		0.216
2577	123	45.0	2.73	301	93	0.355	0.562	0.318		0.216
2578	123	45.0	2.73	301	93	0.355	0.558	0.316		0.216
2579	123	45.0	2.73	301	92	0.355	0.555	0.313		0.216
2580	123	45.0	2.73	301	92	0.355	0.551	0.309		0.216
2581	123	45.0	2.73	301	91	0.355	0.551	0.308		0.216
2582	123	45.0	2.73	301	91	0.355	0.549	0.301		0.216
2583	123	45.0	2.73	301	91	0.355	0.548	0.295		0.216
2051	123	45.9	2.67	295	132	0.355	0.530	0.318		0.315
2130	120	44.5	2.69	295	131	0.355	0.536			0.296
2394	119	44.0	2.71	300	134	0.355	0.572	0.424		0.256
2400	119	44.0	2.71	301	131	0.355	0.568	0.417		0.271
2402	119	44.0	2.71	301	130	0.355	0.565	0.417		0.252
2407	119	44.0	2.71	301	133	0.355	0.564	0.410		0.256
2052	123	45.9	2.67	301	177	0.355	0.556	0.331		0.336
2131	120	44.5	2.69	298	176	0.355	0.555			0.316
2395	119	44.0	2.71	301	180	0.355	0.605	0.448		0.281
2403	119	44.0	2.71	297	176	0.355	0.597	0.437		0.283
2406	119	44.0	2.71	301	179	0.355	0.599	0.437		0.297
2053	123	45.9	2.67	301	209	0.355	0.565			0.340
2132	120	44.5	2.69	299	209	0.355	0.568			0.332
2404	119	44.0	2.71	299	209	0.355	0.616	0.453		0.310
2405	119	44.0	2.71	300	209	0.355	0.612	0.446		0.305
2266	123	45.0	2.73	541	19	0.355	0.467			0.093
2274	123	45.0	2.73	534	16	0.355				0.130
2275	123	45.0	2.73	524	16	0.355				0.125
2531	121	45.0	2.69	534	24	0.355	0.368	0.120		0.135
2532	121	45.0	2.69	521	19	0.355	0.324	0.099		0.112
2533	121	45.0	2.69	525	19	0.355	0.323	0.097		0.109
2534	121	45.0	2.69	523	24	0.355	0.362	0.106		0.123
2255	123	45.0	2.73	527	90	0.355	0.601			0.215
2055	123	45.9	2.67	532	96	0.355	0.496			0.247
2114	120	44.5	2.69	533	97	0.355	0.549			0.275
2135	120	44.5	2.69	533	96	0.355	0.502			0.230
2245	123	45.0	2.73	532	91	0.355	0.622			0.234
2263	123	45.0	2.73	538	98	0.355	0.589			0.241
2265	123	45.0	2.73	526	101	0.355	0.539			0.244
2267	123	45.0	2.73	505	99	0.355	0.543			0.242
2273	123	45.0	2.73	537	100	0.355				0.280
2276	123	45.0	2.73	503	99	0.355				0.260
2277	123	45.0	2.73	543	98	0.355	0.581			
2278	123	45.0	2.73	537	98	0.355	0.598			
2279	123	45.0	2.73	526	98	0.355	0.585			

Ser. Num.	Cal µm	B.W. g/m²	B_L cm³/g	Vel m/m	Load kN/m	Rad m	In-nip strain	Rec1 strain	Rec2 strain	Perm. strain
2280	123	45.0	2.73	518	98	0.355	0.586			
2351	120	45.0	2.67	515	95	0.355	0.469			0.264
2353	120	45.0	2.67	533	95	0.355	0.465			0.243
2359	121	45.0	2.70	518	96	0.355	0.486			0.247
2535	121	45.0	2.69	514	97	0.355	0.520	0.245		0.247
2115	120	44.5	2.69	515	133	0.355	0.574			0.307
2246	123	45.0	2.73	514	127	0.355	0.656			0.261
2256	123	45.0	2.73	517	126	0.355	0.638			0.238
2530	121	45.0	2.69	529	134	0.355	0.557			0.317
2536	121	45.0	2.69	531	133	0.355	0.558			0.293
2537	121	45.0	2.69	523	133	0.355	0.556			0.284
2247	123	45.0	2.73	519	171	0.355				0.289
2054	123	45.9	2.67	516	209	0.355	0.560			0.342
2248	123	45.0	2.73	519	207	0.355				0.307
2249	123	45.0	2.73	522	207	0.355				0.299
2264	123	45.0	2.73	507	211	0.355				0.316
2268	123	45.0	2.73	505	210	0.355	0.599			0.299
2632	122	45.0	2.71	922	13	0.355	0.232			0.094
2633	122	45.0	2.71	920	13	0.355	0.225			0.080
2441	124	45.0	2.76	927	28	0.355	0.384			0.105
2442	124	45.0	2.76	919	28	0.355	0.385			0.102
2631	122	45.0	2.71	924	26	0.355	0.335			0.134
2634	122	45.0	2.71	921	25	0.355	0.327			0.121
2643	122	45.0	2.71	927	27	0.355	0.341			0.114
2644	122	45.0	2.71	921	27	0.355	0.346			0.117
2238	123	45.0	2.73	935	94	0.355	0.513			0.223
2360	121	45.0	2.70	926	96	0.355	0.470			0.226
2439	124	45.0	2.76	923	94	0.355	0.512			0.216
2440	124	45.0	2.76	919	94	0.355	0.507			
2443	124	45.0	2.76	910	92	0.355	0.509			0.212
2444	124	45.0	2.76	923	92	0.355	0.508			0.206
2630	122	45.0	2.71	926	98	0.355	0.478			0.263
2635	122	45.0	2.71	916	96	0.355	0.473			0.234
2642	122	45.0	2.71	927	97	0.355	0.476			0.224
2645	122	45.0	2.71	914	95	0.355	0.471			0.209
2361	121	45.0	2.70	918	126	0.355	0.498			0.264
2433	124	45.0	2.76	931	128	0.355	0.548			0.258
2438	124	45.0	2.76	923	132	0.355	0.543			0.249
2624	122	45.0	2.71	928	132	0.355	0.509			0.288
2629	122	45.0	2.71	925	136	0.355	0.509			0.287
2636	122	45.0	2.71	922	132	0.355	0.510			0.269
2641	122	45.0	2.71	926	135	0.355	0.511			0.265
2362	121	45.0	2.70	915	164	0.355	0.522			0.274
2364	121	45.0	2.70	924	168	0.355	0.526			0.267
2434	124	45.0	2.76	915	172	0.355	0.580			0.280
2437	124	45.0	2.76	923	176	0.355	0.580			0.278
2625	122	45.0	2.71	920	177	0.355	0.546			0.311
2628	122	45.0	2.71	927	181	0.355	0.546			0.323
2637	122	45.0	2.71	918	176	0.355	0.540			0.293
2640	122	45.0	2.71	926	180	0.355	0.548			0.295
2363	121	45.0	2.70	916	198	0.355				0.292
2435	124	45.0	2.76	917	207	0.355	0.598			0.295
2436	124	45.0	2.76	923	207	0.355	0.598			0.292
2626	122	45.0	2.71	918	209	0.355	0.566			0.334
2627	122	45.0	2.71	923	209	0.355	0.560			0.329
2638	122	45.0	2.71	921	208	0.355	0.563			0.312
2639	122	45.0	2.71	922	208	0.355	0.561			0.310
2448	126	45.0	2.79	90	22	0.355	0.413	0.186		0.143
2449	126	45.0	2.79	89	19	0.355	0.394	0.176		0.139
2450	126	45.0	2.79	90	20	0.355	0.395	0.178		0.150
2451	126	45.0	2.79	90	23	0.355	0.421	0.192		0.159
2486	126	45.0	2.81	90	18	0.355	0.381	0.204		0.103
2487	126	45.0	2.81	90	16	0.355	0.359	0.195		
2488	126	45.0	2.81	89	16	0.355	0.360	0.194		0.088
2489	126	45.0	2.81	90	19	0.355	0.384	0.209		0.098
2492	126	45.0	2.79	89	23	0.355	0.427	0.229		0.142
2493	126	45.0	2.79	90	20	0.355	0.404	0.214		0.120
2494	126	45.0	2.79	90	20	0.355	0.405	0.214		0.129
2495	126	45.0	2.79	90	24	0.355	0.425	0.226		0.132
2373	122	44.0	2.78	90	97	0.355	0.600			0.344
2419	125	44.0	2.84	90	96	0.355	0.545	0.321		0.324
2447	126	45.0	2.79	90	98	0.355	0.563	0.356		0.296
2457	126	45.0	2.79	90	97	0.355	0.555	0.339		0.272
2485	126	45.0	2.81	90	101	0.355	0.555	0.348		0.226
2490	126	45.0	2.81	90	98	0.355	0.551	0.362		0.228
2491	126	45.0	2.79	90	97	0.355	0.553	0.349		0.266
2496	126	45.0	2.79	89	95	0.355	0.553	0.353		0.243
2497	126	45.0	2.79	90	133	0.355	0.604	0.354		
2499	126	45.0	2.79	90	127	0.355	0.603	0.355		0.323
2503	126	45.0	2.79	89	128	0.355	0.607	0.349		0.314
2511	126	45.0	2.79	92	125	0.355	0.598	0.326		0.293
2382	122	44.0	2.78	176	23	0.355	0.426	0.319		0.143
2383	122	44.0	2.78	175	20	0.355	0.402	0.301		0.127
2384	122	44.0	2.78	175	20	0.355	0.401	0.297		0.124
2385	122	44.0	2.78	174	23	0.355	0.424	0.320		0.150
2389	122	44.0	2.78	173	21	0.355	0.401	0.294		0.105
2428	125	44.0	2.84	174	25	0.355	0.418	0.152		0.142
2429	125	44.0	2.84	174	22	0.355	0.397	0.139		0.120
2452	126	45.0	2.79	176	23	0.355	0.410	0.175		0.139
2453	126	45.0	2.79	175	20	0.355	0.390	0.158		0.127
2454	126	45.0	2.79	175	20	0.355	0.394	0.164		0.130
2455	126	45.0	2.79	175	23	0.355	0.415	0.175		0.142
2374	122	44.0	2.78	175	97	0.355	0.589			0.313
2381	122	44.0	2.78	174	97	0.355	0.566			0.278
2386	122	44.0	2.78	174	95	0.355	0.554	0.457		0.267
2388	122	44.0	2.78	173	96	0.355	0.555	0.458		0.248
2390	122	44.0	2.78	176	95	0.355	0.554	0.452		0.237

Ser. Num.	Cal µm	B.W. g/m^2	B_i cm^3/g	Vel m/m	Load kN/m	Rad m	In-nip strain	Rec1 strain	Rec2 strain	Perm. strain
2420	125	44.0	2.84	174	96	0.355	0.542	0.308		0.290
2427	125	44.0	2.84	175	96	0.355	0.541	0.300		0.256
2456	126	45.0	2.79	176	96	0.355	0.557	0.323		0.254
2375	122	44.0	2.78	175	127	0.355	0.616			0.330
2380	122	44.0	2.78	174	130	0.355	0.589	0.499		0.300
2421	125	44.0	2.84	176	132	0.355	0.576	0.334		0.325
2426	125	44.0	2.84	174	134	0.355	0.569	0.321		0.303
2500	126	45.0	2.79	173	127	0.355	0.595	0.323		0.310
2504	126	45.0	2.79	175	127	0.355	0.601	0.314		0.292
2376	122	44.0	2.78	175	166	0.355	0.633			0.349
2379	122	44.0	2.78	175	169	0.355	0.620			0.329
2422	125	44.0	2.84	175	177	0.355	0.601	0.354		0.344
2425	125	44.0	2.84	175	178	0.355	0.598	0.350		0.333
2377	122	44.0	2.78	175	200	0.355	0.645	0.550		0.353
2378	122	44.0	2.78	175	200	0.355	0.643	0.543		0.348
2387	122	44.0	2.78	173	204	0.355	0.632	0.525		0.334
2423	125	44.0	2.84	176	210	0.355	0.617	0.368		0.359
2424	125	44.0	2.84	175	210	0.355	0.618	0.368		0.354
2498	126	45.0	2.79	300	130	0.355	0.599	0.319		0.287
2501	126	45.0	2.79	300	127	0.355	0.596	0.311		0.294
2505	126	45.0	2.79	305	127	0.355	0.603	0.292		0.279
2510	126	45.0	2.79	303	129	0.355	0.597	0.288		0.281
2506	126	45.0	2.79	305	171	0.355	0.632	0.310		0.298
2509	126	45.0	2.79	304	173	0.355	0.629	0.306		0.303
2507	126	45.0	2.79	304	206	0.355	0.652	0.318		0.329
2508	126	45.0	2.79	303	206	0.355	0.648	0.317		0.334

Appendix A2: Computer programs for data acquisition and control

```
/*                      File AQSUBS2.C                                  */
/*                    Global definitions                                */
/*                     and subroutines                                  */
/*                        for AQ2.C                                     */
/*              Last modification: 27 February  1992                    */
/*              Modified for 2 A/D boards,  May 1992                    */

#define   apply_load_mask   1       /* digital output to apply load */
#define   raise_load_mask   8       /* digital output to relieve load */
#define   brake_reel_mask   4       /* digital output to apply brake */
#define   emerg_stop_mask   12      /* relieve load and apply brake */
#define   num_chans  8              /* 8 channels per board */
#define   num_scans  2048           /* read each channel 2048 times */
#define   num_avg 4                 /* continuous averaging parameter */
#define   num_saved 512             /* num_scans/num_avg */
#define   tenschan  5               /* winder tension is board 1, channel 5 */
#define   loadchan  6               /* nip load is board 1, channel 6 */
#define   contactload  120          /* load cell output when roll contacts;
                                        525 for 711 rolls and 4" cylinder,
                                        -50 for 404 rolls and 4" cylinder,
                                        120 for 404 rolls and 2" cylinder*/
#define   trigger  0                /* initiate A/D; 1 for hardware trigger */
#define   board1  1                      /* board addresses */
#define   board2  2
#define   lift_time  1.0            /* time in sec to lift at end of exprmnt;
                                       longer for large rolls/small cylinder */
#define   motor_bits_per_vel  2.143033   /* 4.043256 bits/(m/min), 60:30  */
#define   motor_bits_offset   -20.45419  /* 14.19529 bits, 60:30  */
#define   trim_bits_per_vel   44.045435  /* trim bits/(m/min) */
#define   trim_bits_offset    249.16481  /* trim bits offset */
#define   load_bits_per_kN    2235.597   /* bits/kN/m, loading, log fit */
                                         /* for 711 rolls only */
#define   load_bits_offset    -9574.39   /* bits, loading, log fit */
#define   relief_bits_per_kN  -325.18    /* bits/kN/m, lifting, log fit */
#define   relief_bits_offset  1578.596   /* bits, lifting, log fit */
#define   min_load_bits 0               /* limits on analog output */
#define   max_load_bits 4095
#define   load_sel_min 0                /* indices for load select array */
#define   load_sel_max 3
#define   load_start 2                  /* initial load selection */
#define   vel_sel_min 0                 /* indices for velocity select array */
#define   vel_sel_max 5
#define   min_trim_bits 0               /* limits on analog output */
#define   max_trim_bits 4095
#define   d_v  1                        /* vel increment, bits */
#define   d_t  110                      /* time increment, ms */
#define   minrevs 25                    /* min acq time in roll revs */
#define   xerror  15                    /* x, y coords for error messages */
#define   yerror  60
#define   TMid 950                      /* target winder tension in bits */
#define   smoothfact  0.4               /* filtering for tension control */
#define   gain_adjust 1.50              /* factor to alter gains on the fly */
#define   ctr1  1                       /* counter addresses */
#define   ctr5  5
#define   source1  6
#define   source5  10
#define   NumEdgeIn 10                  /* number of rising edges */
#define   NumEdgeOut 10

int    huge *exp_buff1,                 /* raw data buffers */
       huge *exp_buff2;
double    outbuff1[num_saved][num_chans], /* converted data buffers */
          outbuff2[num_saved][num_chans],
          avg_data1[num_chans],
          avg_data2[num_chans];
int       motor_bits,                   /* main motor output, bits */
          trim_bits,                    /* trim motor output, bits */
```

```
        load_bits,                      /* load control output, bits */
        LMid,
        vel_array[6] = {90,175,300,500,900,1100},
        vel_sel = 0,                    /* index for velocities */
        load_array[6] = {10,20,40,65,15,50},
                        /* for 404 rolls and 4" cylinder:
                           {70,80,95,135,175,175}, */
        load_array_bin[6] = {1450,600,1100,3000,1250,1825},
                        /* for 404 rolls and 4" cylinder:
                           {700,971,1253,1865,2346,2346},*/
        load_dir[6] = {8,8,1,1,8,1},    /* 8 for relief, 1 for load */
        load_sel = 2,                   /* index for loading */
        mask = 0,                       /* digital output mask */
        firstrun = 1,           /* number of runs saved in a file */
        num_samples,            /* num_scans * num_channels */
        endfile = 11111,        /* flag at the end of a file */
        endblock = 10000,       /* flag at the end of a block */
        AQStatus,               /* end of acquisition flag */
        AQerrNum,               /* error handling */
        tenserr[3],             /* tension deviation from setpoint */
        avg_tens = 0,           /* averaging for tension control */
        loaderr[3],
        monitor_buff[2*num_chans];   /* most recent block of data */
unsigned int buff_index,        /* index to most recent block of data */
            VinCount,           /* count from ingoing square wave */
            VoutCount,          /* count from outgoing square wave */
            ClockCount;         /* count in ms from clock */
char    par_file[12] = "info2.txt",         /* parameter file name */
        calibr_file[12]  = "calibr2.txt",
        control_file[12] = "control.txt",  /* PID gains */
        firstprn[50] = "c:\\phd\\calcs\\data\\",   /* converted data files */
        prn[5] = ".prn",        /* converted data files */
        dta[5] = ".dta",        /* raw data files */
        sum[5] = ".sum";        /* summary file */
float   cons[3][16],            /* calibration constants */
        Tp,                     /* PID controller coefficients */
        Ti,
        Td,
        Lp,
        Li,
        Ld,
        deltaT,                             /* PID control dt */
        deltaV,                             /* speed change due to stretch */
        tensadj[3],                         /* PID controller coefficients */
        loadadj[3],
        DRollIn = 0.06335,                  /* idler roll diameters */
        DRollOut = 0.06334;

struct  dosdate_t ddate;
struct  dostime_t dtime;
struct  {
          float dry_bulb,           /* laboratory ambient temp */
                dew_pt,             /* laboratory dew point */
                baro,               /* laboratory barometric pressure */
                rel_hum,            /* laboratory relative humidity */
                bas_wt,             /* basis weight */
                volt_seq[7],        /* sequence of supply voltages */
                calroll_d1,
                calroll_d2,         /* calender reel diameters in m */
                i_vel;              /* velocity in meters/min */
          int   file_no,            /* file identification number */
                calroll_n1,
                calroll_n2,         /* calender roll id numbers */
                chan_seq1[8],       /* sequence channels read */
                gain_seq1[8],       /* sequence of gains */
                chan_seq2[8],       /* sequence channels read */
                gain_seq2[8],       /* sequence of gains */
```

```
            sens_seq[7];          /* sequence of sensor connections */
        char  pap_type[30];       /* type of paper */
        double s_rate,            /* rate between channels, Hz */
               scan_rate;         /* rate between consecutive scans, Hz */
      } data;



/*************************************************************************/
/*                Subroutines begin here                                 */
/*************************************************************************/

int motor()                       /* ramp motor up to desired speed */
{
  int dd_v,
      exitNum = 0,
      eltime,                     /* time spent in loop */
      over,
      old_time,                   /* time when loop starts */
      new_time,                   /* time when loop finishes */
      new_motor_bits;             /* desired velocity in bits */
  new_motor_bits = (data.i_vel*motor_bits_per_vel+motor_bits_offset)*1;
  if (new_motor_bits>4095) new_motor_bits=4095;
  if (motor_bits>new_motor_bits) dd_v = -d_v;
  else dd_v = d_v;
  while (((motor_bits <= (new_motor_bits-d_v))
      || (motor_bits >= (new_motor_bits+d_v))) && (exitNum != 27))
  {
    eltime=0;
    if ((AQerrNum = CTR_EvCount(board1,5,4,1))!=0)   /* start timer */
      DAQ_error("CTR_EvCount",1000);
    if ((AQerrNum = CTR_EvRead(board1,5,&over,&old_time))!=0)
      DAQ_error("CTR_EvRead",1010);
    while ((eltime<d_t) && (exitNum != 27))
    {
      if (kbhit()) exitNum = getch();
      if (exitNum != 27)
      {
        get_last_data();
        display_last_data();
        trim_control(exitNum);
        load_control(exitNum);
        exitNum = 0;
        if ((AQerrNum = CTR_EvRead(board1,5,&over,&new_time))!=0)
          DAQ_error("CTR_EvRead",1020);
        eltime = new_time-old_time;
      }
    }
    motor_bits=motor_bits+dd_v;
    if ((AQerrNum = AO_Write(board1,0,motor_bits))!=0)
      DAQ_error("AO_Write",1030);
  }
  if ((AQerrNum = CTR_Stop(board1,5))!=0)         /* stop the timer */
    DAQ_error("CTR_Stop",1040);
    if ((AQerrNum = AO_Write(board1,0,new_motor_bits))!=0)
      DAQ_error("AO_Write",1050);
  return exitNum;
}

/*************************************************************************/

int wait()        /* wait for a keypress while reading and controlling */
{
  int exitNum=0;
  _settextposition(2,1);
  printf(" \"A\"  - begin ACQUISITION                                  ");
```

```
  _settextposition(20,1);
  printf("requested speed reached of %6.2f m/min              ",data.i_vel);
  while ((exitNum!=27) && (exitNum!=97) && (exitNum!=65))
  { if (kbhit()) exitNum = getch();
    else exitNum = 0;
    get_last_data();
    display_last_data();
    trim_control(exitNum);
    load_control(exitNum);
  }
  return exitNum;
}

/*************************************************************************/

int exprmnt()             /* acquire the data and store in two arrays */
{
  int exitNum = 0,
      scan_int;

  if ((AQerrNum = AI_Clear(board1))!=0)
    DAQ_error("AI_Clear 1",1120);
  if ((AQerrNum = AI_Clear(board2))!=0)
    DAQ_error("AI_Clear 2",1130);
  if ((AQerrNum = DAQ_Config(board1,trigger,0))!=0)
    DAQ_error("DAQ_Config 1",1140);
  if ((AQerrNum = DAQ_Config(board2,trigger,0))!=0)
    DAQ_error("DAQ_Config 2",1150);
  if ((AQerrNum = DAQ_DB_Config(board1,0))!=0)
    DAQ_error("DAQ_DB_Config 1",1160);
  if ((AQerrNum = DAQ_DB_Config(board2,0))!=0)
    DAQ_error("DAQ_DB_Config 2",1170);
  buff_index = 1;
  _settextposition(20,1);
  printf("acquiring data . . . .                                          ");
  scan_int = 1000000.0/data.scan_rate;
  if ((AQerrNum = SCAN_Setup(board1,num_chans,data.chan_seq1,
        data.gain_seq1))!=0)
    DAQ_error("SCAN_Setup 1",1180);
  if ((AQerrNum = SCAN_Setup(board2,num_chans,data.chan_seq2,
        data.gain_seq2))!=0)
    DAQ_error("SCAN_Setup 2",1190);
  if ((AQerrNum = SCAN_Start(board1,exp_buff1,num_samples,1,50,1,
        scan_int)) != 0)
  { DAQ_error("SCAN_Start 1",1200);
    exitNum=4;
    return exitNum;
  }
  if ((AQerrNum = SCAN_Start(board2,exp_buff2,num_samples,1,50,1,
        scan_int)) != 0)
  { DAQ_error("SCAN_Start 2",1210);
    exitNum=4;
    return exitNum;
  }
  while (buff_index < 2*num_chans)
    if ((AQerrNum = DAQ_Check(board1, &AQStatus,&buff_index))!=0)
      DAQ_error("DAQ_Check",1220);
  do            /* Check acquisition progress, display and control */
  { if((AQerrNum = DAQ_Monitor(board1,-1,0,num_chans,monitor_buff,
          &buff_index,&AQStatus))!=0)
      DAQ_error("DAQ_Monitor 1",1230);
    if((AQerrNum = DAQ_Monitor(board2,-1,0,num_chans,
          &monitor_buff[num_chans],&buff_index,&AQStatus))!=0)
      DAQ_error("DAQ_Monitor 2",1240);
    if (kbhit()) exitNum=getch();
    display_last_data();
    trim_control(exitNum);
```

```
    load_control(exitNum);
    if (exitNum != 27) exitNum = 0;
  } while ((!AQStatus) && (exitNum != 27));
  if ((AQerrNum = DAQ_Clear(board1))!=0)
    DAQ_error("DAQ_Clear 1",1250);
  if ((AQerrNum = DAQ_Clear(board2))!=0)
    DAQ_error("DAQ_Clear 2",1260);
  return exitNum;
}

/*********************************************************************/

int trim_control(Num)       /* adjust trim as necessary */
int Num;
{
  int ii;
  if (Num > 0)
  { switch (Num)
    {
      case 56:
        Tp *= gain_adjust;
        tensadj[0] = Tp + 0.5*Ti*deltaT + Td/deltaT;
        tensadj[1] = -Tp + 0.5*Ti*deltaT - 2*Td/deltaT;
        tensadj[2] = Td*deltaT;
        break;
      case 53:
        Tp /= gain_adjust;
        tensadj[0] = Tp + 0.5*Ti*deltaT + Td/deltaT;
        tensadj[1] = -Tp + 0.5*Ti*deltaT - 2*Td/deltaT;
        tensadj[2] = Td*deltaT;
        break;
      case 57:
        Ti *= gain_adjust;
        tensadj[0] = Tp + 0.5*Ti*deltaT + Td/deltaT;
        tensadj[1] = -Tp + 0.5*Ti*deltaT - 2*Td/deltaT;
        tensadj[2] = Td*deltaT;
        break;
      case 54:
        Ti /= gain_adjust;
        tensadj[0] = Tp + 0.5*Ti*deltaT + Td/deltaT;
        tensadj[1] = -Tp + 0.5*Ti*deltaT - 2*Td/deltaT;
        tensadj[2] = Td*deltaT;
        break;
    }
    _settextposition (23,40);
    printf("Trim gains: Tp= %f, Ti = %f",Tp,Ti);
  }
  avg_tens = smoothfact*avg_tens + (1-smoothfact)*monitor_buff[tenschan];
  tenserr[0] = TMid - avg_tens;              /* compute deviation */
  for (ii=0;ii<3;ii++)
    trim_bits -= tensadj[ii]*tenserr[ii];    /* compute corection */
  if (trim_bits > max_trim_bits) trim_bits = max_trim_bits;
  else if (trim_bits < min_trim_bits) trim_bits = min_trim_bits;
  tenserr[2] = tenserr[1];                 /* save current deviation . . . */
  tenserr[1] = tenserr[0];                 /* . . . for next loop */
  if ((AQerrNum = AO_Write(board2, 0, trim_bits))!=0)
    DAQ_error("AO_Write",1300);            /* Output new value to trim */
  _settextposition(22,62);
  printf("trimming %d bits   ",trim_bits);
}

/*********************************************************************/

int load_control(Num)       /* adjust load as necessary */
int Num;
{
  int ii;
```

```
  float load_corr = 0.0250;

  if (Num > 0 )
  { switch (Num)
    {
      case 43:
        if (load_dir[load_sel] == 1)  /* adjust gains if neccessary */
          load_bits *= (1+load_corr); /* remove once controller fully */
        else                          /* debugged. */
          load_bits *= (1-load_corr);
        break;
      case 45:
        if (load_dir[load_sel] == 1)
          load_bits *= (1-load_corr);
        else
          load_bits *= (1+load_corr);
        break;
    }
    _settextposition(22,40);
    printf("loading %d bits; ",load_bits);
  }
  loaderr[0] = LMid - monitor_buff[loadchan];
  if (load_dir[load_sel] = 8)
  { for (ii=0;ii<3;ii++)
      load_bits -= loadadj[ii]*loaderr[ii];
  }
  if (load_bits > max_load_bits) load_bits = load_bits;
  else if (load_bits < min_load_bits) load_bits = min_load_bits;
  loaderr[2] = loaderr[1];
  loaderr[1] = loaderr[0];
  if ((AQerrNum = AO_Write(board1, 1, load_bits))!=0)
    DAQ_error("AO_Write",1350);
}

/*************************************************************************/

get_last_data()
{
int ii;

  for (ii=0; ii<num_chans;ii++)
    if ((AQerrNum = AI_Read(board1,ii,data.gain_seq1[ii],
                        &monitor_buff[ii]))!=0)
      DAQ_error("AI_Read 1",1420);          /* read 8 channels from each board */
  for (ii=num_chans; ii<(2*num_chans);ii++)
    if ((AQerrNum = AI_Read(board2,(ii-num_chans),
                        data.gain_seq2[ii-num_chans],&monitor_buff[ii]))!=0)
    DAQ_error("AI_Read 2",1430);
  return;
}


/*************************************************************************/

display_last_data()      /* convert and display latest data */
{
int ii;

  _settextposition(13,1);
  for (ii=0; ii<(2*num_chans);ii++)
    printf("%4.0f ",(cons[0][ii]+monitor_buff[ii]*(cons[1][ii]
          +cons[2][ii]*monitor_buff[ii])));
  _settextposition(21,30);
  printf("%6u",buff_index);
  return;
}
```

```
/*************************************************************************/

write_data()                    /* update parameter file */
{
  FILE *x;
  int i,
      j,
      endblock = 10000;

  if ((x=fopen(par_file,"wt")) != NULL)
  { fprintf(x,"%5.3f\n",data.dry_bulb);
    fprintf(x,"%5.3f\n",data.dew_pt);
    fprintf(x,"%5.3f\n",data.baro);
    fprintf(x,"%5.3f\n",data.rel_hum);
    fprintf(x,"%5.3f\n",data.calroll_d1);
    fprintf(x,"%d\n",data.calroll_n1);
    fprintf(x,"%5.3f\n",data.calroll_d2);
    fprintf(x,"%d\n",data.calroll_n2);
    fprintf(x,"%5.3f\n",data.bas_wt);
    fprintf(x,"%s\n",data.pap_type);
    fprintf(x,"%8.2lf\n",data.s_rate);
    fprintf(x,"%8.2lf\n",data.scan_rate);
    for (i=0; i<num_chans; i++)
      fprintf(x,"%1d\t",data.chan_seq1[i]);
    fprintf(x,"\n");
    for (i=0; i<num_chans; i++)
      fprintf(x,"%3d\t",data.gain_seq1[i]);
    fprintf(x,"\n");
    for (i=0; i<num_chans; i++)
      fprintf(x,"%1d\t",data.chan_seq2[i]);
    fprintf(x,"\n");
    for (i=0; i<num_chans; i++)
      fprintf(x,"%3d\t",data.gain_seq2[i]);
    fprintf(x,"\n");
    for (i=0; i<7 ; i++)
      fprintf(x,"%1d\t",data.sens_seq[i]);
    fprintf(x,"\n");
    for (i=0; i<7 ; i++)
      fprintf(x,"%5.2f\t",data.volt_seq[i]);
    fprintf(x,"\n%6.2f",data.i_vel);
    fprintf(x,"\n%.4d\n",data.file_no);
  }
  else
  { perror("write error: can't open INFO2.TXT for writing");
    exit(1);
  }
  fclose(x);
  return;
}

/*************************************************************************/

data_screen()             /* display parameters */
{
  _clearscreen(_GCLEARSCREEN);
  printf(" World's Narrowest Calender Data Acquisition Program\n");
  printf("C. THESE VALUES ARE CORRECT\n");
  printf("1. Dry bulb temperature                    \t\t\t%5.3f
                              \n",data.dry_bulb);
  printf("2. Dew point temperature                   \t\t\t%5.3f
                              \n",data.dew_pt);
  printf("3. Barometric pressure                     \t\t\t%5.3f
                              \n",data.baro);
  printf("4. Relative humidity                       \t\t\t%5.3f
                              \n",data.rel_hum);
  printf("5. top calender reel - diameter (cm):      \t\t\t%5.3f
                              \n",data.calroll_d1);
```

```
  printf("6.                    - id #:          \t\t\t  %d
                                \n",data.calroll_n1);
  printf("7. bottom calender reel -diameter (cm): \t\t\t%5.3f
                                \n",data.calroll_d2);
  printf("8.                      -id #:         \t\t\t  %d
                                \n",data.calroll_n2);
  printf("9. basis weight (Kg):                  \t\t\t%5.3f \n",data.bas_wt);
  printf("10. paper type:                        \t\t\t %s\n",data.pap_type);
  printf("11. scan rate-one channel (scan/sec):  \t\t\t%8.2lf\n",data.s_rate);
  printf("12.          -all channels (scan/sec): \t\t\t%8.2lf
                                \n",data.scan_rate);
  printf("\n--      Edit INFO.TXT to alter Gain vector       --\n\n\n");
  printf("17. initial velocity (m/min):          \t\t\t%6.2f\n",data.i_vel);
  printf("18. file number:                       \t\t\t    %4d",data.file_no);
  _settextposition(22,1);
  return;
}

/*************************************************************************/

int change(ch1)                 /* alter selected parameter */
char ch1;                       /* first character of inputted choice */
{
  int   ascii,x,i;
  char  temp[100],y[3];         /* final choice to input data */
  strcpy(y, &ch1);
  ch1 = getche();
  ascii = toascii(ch1);
  if (ascii != 13)
  { strcpy (y + 1, &ch1);
    ch1 = getch();
  }
  x=atoi(y);
  if ((x>0) && (x<=18))
  { clearl((x+2),40,38);
    _settextposition((x+2),66);
    if ((x!=11) && (x!=12))
      scanf("%s", temp );
    if (x==1)
      data.dry_bulb=atof( temp );
    else if (x==2)
      data.dew_pt = atof( temp );
    else if (x==3)
      data.baro = atof( temp );
    else if (x==4)
      data.rel_hum = atof( temp );
    else if (x==5)
      data.calroll_d1 = atof( temp );
    else if (x==6)
      data.calroll_n1 = atoi( temp );
    else if (x==7)
      data.calroll_d2 = atof( temp );
    else if (x==8)
      data.calroll_n2 = atoi( temp );
    else if (x==9)
      data.bas_wt = atoi( temp );
    else if (x==10)
      strcpy(data.pap_type, temp);
    else if (x==11)
      scanf("%lf",&data.s_rate);
    else if (x==12)
      scanf("%lf",&data.scan_rate);
    else if (x==17)
    { data.i_vel = atof( temp );
      data.scan_rate = 20*ceil(0.05*num_scans*data.i_vel/
                       (3.1416*60*data.calroll_d1*minrevs));
      clearl((14),40,38);
```

```
      _settextposition((14),66);
      printf("%8.2lf",data.scan_rate);
    }
    else if (x==18)
      data.file_no = atoi( temp );
  }
  return;
}

/*********************************************************************/

int txconvert (filenum)            /* convert raw binary file . . . */
int filenum;                       /* . . . to .PRN files */

{
  FILE *dtabin;
  int i,
      end[8],
      temp,
      trial = 0,
      ch = 96;
  char file_[10];

  _settextposition (21,1);
  printf("Reading file: %s                                    ",file_name);
  if ((dtabin = fopen(file_name, "rb")) == NULL)
  { printf("error opening file");
    exit(1);
  }
  itoa(filenum,file_,10);
  fread (end, sizeof(end), 1, dtabin);
  do
  { trial++;
    ch++;
    clearl(22,1,78);
    printf("Reading trial %d; ",trial);
    fread (&ddate, sizeof(ddate), 1, dtabin);
    fread (&dtime, sizeof(dtime), 1, dtabin);
    fread (&data, sizeof(data), 1, dtabin);
    fread (cons, sizeof(cons), 1, dtabin);
    fread (&deltaV, sizeof(deltaV), 1, dtabin);
    fread (&VinCount, sizeof(VinCount), 1, dtabin);
    fread (&VoutCount, sizeof(VoutCount), 1, dtabin);
    fread (&ClockCount, sizeof(ClockCount), 1, dtabin);
    for (i=0; i<4; i++)
      fread (&temp, sizeof(temp), 1, dtabin);
    fread (&exp_buff1[0], sizeof(exp_buff1[0]), num_samples, dtabin);
    fread (&exp_buff2[0], sizeof(exp_buff2[0]), num_samples, dtabin);
    fread (end, sizeof(end), 1, dtabin);
    average();
    svetxt(file_,ch);
  } while (end[3] != 11111);
  fclose(dtabin);
}

/*********************************************************************/

average()          /* average and de-multiplex data  */
{
  int divisor,
      ch,
      sc,
      i;
  printf ("adding; ");
  sc = 0;
  for (ch=0;ch<num_chans;ch++)  /* First channel scan */
  { outbuff1[sc][ch]=0.0;
```

```
  outbuff2[sc][ch]=0.0;
  avg_data1[ch]=0.0;
  avg_data2[ch]=0.0;
  for (i=0;i<num_avg+1;i++)   /* data from first num_avg+1 scans */
  { outbuff1[sc][ch] += exp_buff1[i*num_chans+ch];
    outbuff2[sc][ch] += exp_buff2[i*num_chans+ch];
    avg_data1[ch] += exp_buff1[i*num_chans+ch];
    avg_data2[ch] += exp_buff2[i*num_chans+ch];
  }
}
for (sc=1;sc<(num_saved-1);sc++)    /* Scans 2 through 2047 */
{ for (ch=0;ch<num_chans;ch++)
  { outbuff1[sc][ch]=0.0;
    outbuff2[sc][ch]=0.0;
    for (i=-num_avg;i<num_avg+1;i++)   /* data near current one */
    {
      outbuff1[sc][ch] += exp_buff1[(num_avg*sc+i)*num_chans+ch];
      outbuff2[sc][ch] += exp_buff2[(num_avg*sc+i)*num_chans+ch];
      avg_data1[ch] += exp_buff1[i*num_chans+ch];
      avg_data2[ch] += exp_buff2[i*num_chans+ch];
    }
  }
}
sc = num_saved-1;
for (ch=0;ch<num_chans;ch++)          /* last channel scan */
{ outbuff1[sc][ch]=0;
  outbuff2[sc][ch]=0;
  for (i=-num_avg;i<num_avg;i++)     /* add data from last scans */
  {
    outbuff1[sc][ch] += exp_buff1[(num_avg*sc+i)*num_chans+ch];
    outbuff2[sc][ch] += exp_buff2[(num_avg*sc+i)*num_chans+ch];
    avg_data1[ch] += exp_buff1[i*num_chans+ch];
    avg_data2[ch] += exp_buff2[i*num_chans+ch];
  }
}
printf ("averaging; ");             /* divide sums by appropriate divisors */
divisor = num_avg+1;
sc = 0;
for (ch=0;ch<num_chans;ch++)        /* and convert to real variables */
{ outbuff1[sc][ch] = cons[0][ch]
                  +outbuff1[sc][ch]*(cons[1][ch]+
                  cons[2][ch]*outbuff1[sc][ch]/divisor)/divisor;
  outbuff2[sc][ch] = cons[0][ch+num_chans]
                  +outbuff2[sc][ch]*(cons[1][ch+num_chans]+
                  cons[2][ch+num_chans]*outbuff2[sc][ch]/divisor)/divisor;
  avg_data1[ch] = avg_data1[ch]/num_scans;
  avg_data2[ch] = avg_data2[ch]/num_scans;
}

divisor = 2*num_avg+1;
for (sc=1;sc<(num_saved-1);sc++)
{ for (ch=0;ch<num_chans;ch++)
  { outbuff1[sc][ch] = cons[0][ch]
                    +outbuff1[sc][ch]*(cons[1][ch]+
                    cons[2][ch]*outbuff1[sc][ch]/divisor)/divisor;
    outbuff2[sc][ch] = cons[0][ch+num_chans]
                    +outbuff2[sc][ch]*(cons[1][ch+num_chans]+
                    cons[2][ch+num_chans]*outbuff2[sc][ch]/divisor)/divisor;
  }
}
divisor = 2*num_avg;
sc = num_saved-1;
for (ch=0;ch<num_chans;ch++)
{ outbuff1[sc][ch] = cons[0][ch]
                  +outbuff1[sc][ch]*(cons[1][ch]+
                  cons[2][ch]*outbuff1[sc][ch]/divisor)/divisor;
  outbuff2[sc][ch] = cons[0][ch+num_chans]
```

```
                    +outbuff2[sc][ch]*(cons[1][ch+num_chans]+
                    cons[2][ch+num_chans]*outbuff2[sc][ch]/divisor)/divisor;
  }
}

/*********************************************************************/

svetxt(file1,chext)          /* save converted data after averaging */
char file1[50];
char chext;
{
  FILE *dtatxt;
  int length,
      pdest,
      divisor,
      ch,
      sc,
      j, k;
  char ext[5],
       file[50];

  strcpy (firstprn,"c:\\phd\\calcs\\data\\");
  strcpy (prn,".prn");
  strcpy(file,file1);

  pdest = strcpy( firstprn + 18, file );
  length = strlen(firstprn);
  pdest = strcpy( firstprn + length, &chext );
  length = strlen(firstprn);
  pdest = strcpy( firstprn + length, prn );
  pdest = strcpy( file , firstprn);

  dtatxt = fopen(file, "wt");
  save_data(file,chext,dtatxt);

  for (sc=0;sc<num_saved;sc++)
  { for (ch=0;ch<num_chans;ch++)
      fprintf(dtatxt,"%4.8f, ",outbuff1[sc][ch]);
    for (ch=0;ch<num_chans;ch++)
      fprintf(dtatxt,"%4.8f, ",outbuff2[sc][ch]);
    fprintf (dtatxt,"\n");
  }
  fclose(dtatxt);
}

/*********************************************************************/

save_data(file,ext,dtatxt)     /* save parameters with converted data */
char file[50],ext;
FILE *dtatxt;
{
int j, k;
  printf("writing file: %s\n",file);
  fprintf(dtatxt,"\"DATE: \"\"%u/%u/%u\"\t\"TIME: \"\"%u/%u/%u\"\n",ddate.day,
            ddate.month,ddate.year,dtime.hour, dtime.minute,dtime.second);
  fprintf(dtatxt,"\"Dry bulb  \"      %5.3f  \n",data.dry_bulb);
  fprintf(dtatxt,"\"Dew point \"      %5.3f \n",data.dew_pt);
  fprintf(dtatxt,"\"Barometer \"      %5.3f \n",data.baro);
  fprintf(dtatxt,"\"R.H.      \"      %5.3f \n",data.rel_hum);
  fprintf(dtatxt,"\"TrollD    \"   %5.3f \n",data.calroll_d1);
  fprintf(dtatxt,"\"id        \"    %d \n",data.calroll_n1);
  fprintf(dtatxt,"\"BrollD    \" %5.3f \n",data.calroll_d2);
  fprintf(dtatxt,"\"id        \"   %d \n",data.calroll_n2);
  fprintf(dtatxt,"\"BW        \"  %5.3f \n",data.bas_wt);
  fprintf(dtatxt,"\"paper type\"\" %s\"\n",data.pap_type);
  fprintf(dtatxt,"\"CRate     \" %8.2lf\n",data.s_rate);
  fprintf(dtatxt,"\"SRate     \"%8.2lf,  %8.2lf\n",data.scan_rate,
```

```
                                                    data.scan_rate/num_avg);
  fprintf(dtatxt,"\"channel v:\"");
  for (j=0; j<8 ; j++)
    fprintf(dtatxt,"%1d       ",data.chan_seq1[j]);
  for (j=0; j<8 ; j++)
    fprintf(dtatxt,"%1d       ",data.chan_seq2[j]);
  fprintf(dtatxt,"\n\"gain v: \"");
  for (j=0; j<8 ; j++)
    fprintf(dtatxt,"%3d     ",data.gain_seq1[j]);
  for (j=0; j<8 ; j++)
    fprintf(dtatxt,"%3d     ",data.gain_seq2[j]);
  fprintf(dtatxt,"\n\"sensor v: \"");
  for (j=0; j<7 ; j++)
    fprintf(dtatxt,"%1d       ",data.sens_seq[j]);
  fprintf(dtatxt,"\n\"Vin,Vout,Clock,DeltaV:\" %5u %5u %5u %6.6f",
                      VinCount,VoutCount,ClockCount,deltaV);
  fprintf(dtatxt,"\n\"Vel\"           %6.2f  %6.2f",data.i_vel,data.i_vel);
  fprintf(dtatxt,"\n\"file:\" %.4d  \" %c \"\n",data.file_no, ext);
  fprintf(dtatxt,"\n\"calibration \" \n");
  for (j=0;j<3;j++)
  { for (k=0;k<(2*num_chans);k++)
      fprintf(dtatxt,"%.8f,",cons[j][k]);
    fprintf(dtatxt,"\n");
  }
  fprintf(dtatxt,"\n\"N0\"\t\"N1\"\t\"C2\"\t\"C3\"\t\"T4\"\t\"T5\"\t\"
                                                    L 6 \ " \ t \ " V 7 \ " \ t " ) ;
fprintf(dtatxt,"\"N10\"\t\"N11\"\t\"C12\"\t\"C13\"\t\"X14\"\t\"X15\"\t\"
                X16\"\t\"V17\"\t\n");
}

/*************************************************************************/

int DAQ_error(err_msg, location)    /* general error message handler */
char err_msg[30];
int location;
{
  _settextposition(xerror,yerror);
  printf("%s error # %d at %d",err_msg,AQerrNum,location);
  return;
}

/*************************************************************************/

int eexit(int x)        /* emergency exit subroutine */
{
  time_t etstart, etstop;
  float emerg_time;

  if ((AQerrNum = DIG_Out_Port(board1,1,emerg_stop_mask))!=0)
    DAQ_error("DIG_Out_Port",3000);
  if ((AQerrNum = AO_Write(board1,0,0))!=0)
    DAQ_error("AO_Write 1",3010);
  if ((AQerrNum = AO_Write(board1,1,4000))!=0)
    DAQ_error("AO_Write 1",3020);
  if ((AQerrNum = AO_Write(board2,0,0))!=0)
    DAQ_error("AO_Write 2",3030);
  if ((AQerrNum = AO_Write(board2,1,4000))!=0)
    DAQ_error("AO_Write 2",3040);
  motor_bits= 0;
  _settextposition(xerror,yerror);
  printf ("Emergency stop");
  _settextposition(xerror+1,yerror);
  printf ("error # %d",x);
  _settextposition(xerror+2,yerror);
  if (x==1)
    printf("subroutine EXPRMNT");
  else if (x==2)
```

```
    printf("subroutine WAIT");
  else if (x==3)
    printf("subroutine MOTOR");
  else if (x==4)
    printf("subroutine SCAN_Start");
  else if (x==5)
    printf("subroutine MAIN");
  _settextposition (xerror+3,yerror);
  time (&etstart);
  do                                /* Wait */
  { time (&etstop);
    emerg_time = difftime(etstop,etstart);
  }
  while (emerg_time < lift_time);
  if((AQerrNum = AO_Write(board1,1,brake_reel_mask))!=0)/* Load off, brake on */
    DAQ_error("AO_Write Load",3050);

  printf("Press a key to exit:");
  return x;
}

/*************************************************************************/

int clear(row,column,num)             /* Clear n lines */
int row,
    column,
    num;
{
  int i,j;
  _settextposition(row,column);
  for (j=column;j<79;j++)
    printf(" ");
  printf("\n");
  for (i=1;i<num;i++)
  { for (j=0;j<79;j++)
      printf(" ");
    printf("\n");
  }
  _settextposition(row,column);
  return;
}

/*************************************************************************/

int clear1(row,column,num)            /* Clear n spaces */
int row,
    column,
    num;
{
  int i;
  _settextposition(row,column);
  for (i=0;i<num;i++)
    printf(" ");
  _settextposition(row,column);
  return;
}

/*************************************************************************/
/*                Subroutines end here                                   */
/*************************************************************************/
```

```
/* AQ2.C: Main acquisition program;                                    */
/* Data Acquisition and control program for World's Narrowest Calender */
/*              Written by Miles Sherman, August 1990                  */
/*       Modified for 2 A/D boards, May 1992, by Thomas Browne         */
/*  Automatic trim control installed, June/July 1992, by Thomas Browne */
/*  Counters for draw installed July 1992, by Thomas Browne            */
/*  Global variable definitions are in the file AQSUBS2.C              */

#include <doslbdrv.h>          /* header file for LABDRIVER routines */
#include <conio.h>
#include <stdio.h>
#include <stdlib.h>
#include <dos.h>
#include <malloc.h>
#include <graph.h>
#include <ctype.h>
#include <float.h>
#include <math.h>
#include <time.h>
#include "aqsubs2.c"

main()
{
  FILE   *outfbin,              /* data file */
         *inftxt,               /* parameter file */
         *outftxt;
  double el_time;
  int    cont,
         ascii,                 /* ascii value */
         i,j,
         press,                 /* value read from nip load cell */
         errNum,
         pdest,
         length,
         overflow,
         cr;                    /* carriage return */
  char   quit,                  /* first character entered for vel */
         vel_char,              /* next character entered for vel */
         vel_temp[100],         /* temporary velocity as char string */
         firstdta[5] = "f:\\";
  time_t tstart,
         tstop;
  float  DeltaVFact;


/*************************************************************************/
/*                Main program begins here                               */
/*************************************************************************/

  _clearscreen(_GCLEARSCREEN);
  num_samples = num_scans*num_chans;      /* allocate data buffers */
  exp_buff1 = NULL;
  exp_buff2 = NULL;
  if (!(exp_buff1=(int huge *) halloc ((unsigned long)num_samples,
                          sizeof(int))))
  { perror ("error allocating memory for buffer 1");
    printf("ending program....");
    exit(1);
  }
  if (!(exp_buff2=(int huge *) halloc ((unsigned long)num_samples,
                          sizeof(int))))
  { perror ("error allocating memory for buffer 2");
    printf("ending program....");
    exit(1);
  }
  if ((inftxt=fopen(par_file,"rt")) != NULL)
```

```
{ fscanf(inftxt,"%f",&data.dry_bulb);   /* Open and read INFO2.TXT */
  fscanf(inftxt,"%f",&data.dew_pt);
  fscanf(inftxt,"%f",&data.baro);
  fscanf(inftxt,"%f",&data.rel_hum);
  fscanf(inftxt,"%f",&data.calroll_d1);
  fscanf(inftxt,"%d",&data.calroll_n1);
  fscanf(inftxt,"%f",&data.calroll_d2);
  fscanf(inftxt,"%d",&data.calroll_n2);
  fscanf(inftxt,"%f",&data.bas_wt);
  fscanf(inftxt,"%s",data.pap_type);
  fscanf(inftxt,"%lf",&data.s_rate);
  fscanf(inftxt,"%lf",&data.scan_rate);
  for (i=0; i<num_chans; i++)
    fscanf(inftxt,"%d",&data.chan_seq1[i]);
  for (i=0; i<num_chans; i++)
    fscanf(inftxt,"%d",&data.gain_seq1[i]);
  for (i=0; i<num_chans; i++)
    fscanf(inftxt,"%d",&data.chan_seq2[i]);
  for (i=0; i<num_chans; i++)
    fscanf(inftxt,"%d",&data.gain_seq2[i]);
  for (i=0; i<num_chans-1; i++)
    fscanf(inftxt,"%d",&data.sens_seq[i]);
  for (i=0; i<num_chans-1; i++)
    fscanf(inftxt,"%f",&data.volt_seq[i]);
  fscanf(inftxt,"\n%f",&data.i_vel);
  fscanf(inftxt,"\n%d",&data.file_no);
  fclose(inftxt);
}
else
{ perror("error opening INFO2.TXT");
  exit(1);
}
if ((inftxt=fopen(calibr_file,"rt")) != NULL)
{ for (i=0;i<3;i++)
  { for (j=0;j<num_chans;j++)
      fscanf(inftxt,"%f",&cons[i][j]);
  }
  for (i=0;i<3;i++)
  { for (j=num_chans;j<(2*num_chans);j++)
      fscanf(inftxt,"%f",&cons[i][j]);
  }
}
else
{ perror("error opening CALIBR2.TXT");
  exit(1);
}

if ((inftxt=fopen(control_file,"rt")) != NULL)
{ fscanf(inftxt,"%f",&Tp);     /* Open and read CONTROL.TXT */
  fscanf(inftxt,"%f",&Ti);
  fscanf(inftxt,"%f",&Td);
  fscanf(inftxt,"%f",&Lp);
  fscanf(inftxt,"%f",&Li);
  fscanf(inftxt,"%f",&Ld);
  fscanf(inftxt,"%f",&deltaT);
  fclose(inftxt);
}
else
{ perror("error opening CONTROL.TXT");
  exit(1);
}
tensadj[0] = Tp + 0.5*Ti*deltaT + Td/deltaT;      /* PID constants */
tensadj[1] = -Tp + 0.5*Ti*deltaT - 2*Td/deltaT;
tensadj[2] = Td*deltaT;
loadadj[0] = Lp + 0.5*Li*deltaT + Ld/deltaT;
loadadj[1] = -Lp + 0.5*Li*deltaT - 2*Ld/deltaT;
loadadj[2] = Ld/deltaT;
```

```
for (i=0; i<3; i++)
{ tenserr[i] = 0;
  loaderr[i] = 0;
}
_dos_getdate(&ddate);
_dos_gettime(&dtime);
if ((AQerrNum = AO_Config(board1,0,1,10.0,0))!=0)
  DAQ_error("AO_Config 1, channel 0",10);
if ((AQerrNum = AO_Config(board1,1,1,10.0,0))!=0)
  DAQ_error("AO_Config 1, channel 1",20);
if ((AQerrNum = AO_Config(board2,0,1,10.0,0))!=0)
  DAQ_error("AO_Config 2, channel 0",30);
if ((AQerrNum = AO_Config(board2,1,1,10.0,0))!=0)
  DAQ_error("AO_Config 2, channel 1",40);
if ((AQerrNum = AI_Config(board1,0,5,0))!=0)
  DAQ_error("AI_Config 1",50);
if ((AQerrNum = AI_Config(board2,0,10,1))!=0)
  DAQ_error("AI_Config 2",60);
if ((AQerrNum = DIG_Prt_Config(board1,0,0,0))!=0)
  DAQ_error("DIG_Prt_Config 1",70);
if ((AQerrNum = DIG_Prt_Config(board1,1,0,1))!=0)
  DAQ_error("DIG_Prt_Config 1",80);
if ((AQerrNum = DIG_Prt_Config(board2,0,0,0))!=0)
  DAQ_error("DIG_Prt_Config 2",90);
if ((AQerrNum = DIG_Prt_Config(board2,1,0,1))!=0)
  DAQ_error("DIG_Prt_Config 2",100);
motor_bits = 0;
trim_bits = 0;
load_bits = 0;
DeltaVFact = DRollOut*NumEdgeIn/(DRollIn*NumEdgeOut);
if ((AQerrNum = AO_Write(board1,0,motor_bits))!=0)/* Motor off */
  DAQ_error("AO_Write Main",110);
if ((AQerrNum = AO_Write(board1,1,load_bits))!=0) /* load off */
  DAQ_error("AO_Write Load",120);
if ((AQerrNum = AO_Write(board2,0,trim_bits))!=0) /* Trim motor off */
  DAQ_error("AO_Write Trim",130);
mask = mask & 11;                                 /* leave load alone */
if ((AQerrNum = DIG_Out_Port(board1,1,mask))!=0)   /* Release brake */
  DAQ_error("DIG_Out_Port",140);
data_screen();                          /* displays current parameters */
_settextposition(22,1);
printf("         Ent\" choice:\n\t>");
cr = getche();
while ((cr != 'c') && (cr != 'C'))
{ change(cr);                             /* change selected parameter */
  clear(23,10,2);
  cr = getche();
}
_settextposition(24,1);
printf ("Lowering roll . . .");
mask = raise_load_mask;
load_bits = 1575;
if ((AQerrNum = AO_Write(board1,1,load_bits))!=0)
  DAQ_error("AO_Write",150);
if ((AQerrNum = DIG_Out_Port(board1,1,mask))!=0)       /* pressure . . . */
  DAQ_error("DIG_Out_Port",160);
do
  if ((AQerrNum = AI_Read (board1,loadchan,data.gain_seq1[loadchan],
                           &press))!=0)
     DAQ_error("AI_Read",170);
while ((press > contactload) && (!kbhit()));  /* until contact or keypress. */
mask = 0;
if ((AQerrNum = DIG_Out_Port(board1,1,mask))!=0)     /* then release */
  DAQ_error("DIG_Out_Port",180);
if ((AQerrNum = AO_Write(board1,1,0))!=0)
  DAQ_error("AO_Write",190);
_clearscreen(_GCLEARSCREEN);
```

```
_settextposition(10,1);
printf(" N0   N1   C2   C3   T4    T5   L6   V7  N10  N11  C12  C13
          X14  X15  X16  V17\n");
printf(" um   um   um   um  N/m   N/m  kN/m  m/m  um   um   um   um
     m/m");
do                  /* experiment loop begins here */
{  cont = 1;
  _settextposition(2,1);
  printf(" \"C\"  - CONTINUE                                          ");
  _settextposition (4,52);
  printf("Velocity: %8.2f m/min",data.i_vel);
  _settextposition (5,52);
  printf("Load:     %6d kN/m",load_array[load_sel]);
  _settextposition(4,1);
  printf("Press V for Velocity, L for Load; ");
  _settextposition(5,1);
  printf("Press GREY + or - to increment or decrement:");
  quit = 0;
  while (quit != 'C')   /* Get new sheet speed and load */
  { while (!kbhit())
    { get_last_data();              /* read latest data */
      display_last_data();          /* display */
      if (firstrun > 1)
       trim_control(0);            /* control */
    }                               /* key has been hit */
    quit = getch();                 /* get the key */
    ascii = toupper(quit);          /* convert to upper case */
    quit = ascii;
    if ((ascii == 'L') || (ascii == 'V'))
    { _settextposition (5,45);
      printf("%1c",ascii);
      while (!kbhit())
      { get_last_data();            /* read latest data */
        display_last_data();        /* display */
        if (firstrun > 1)           /* while waiting for second key */
          trim_control(0);          /* control */
      }                             /* key has been hit */
      quit = getch();               /* get the key */
      if (quit == '+')
      { _settextposition (5,46);
        printf ("+");
        if (ascii == 'L')
        { load_sel++;
          if (load_sel > load_sel_max) load_sel = load_sel_max;
        }
        else
        { vel_sel++;
          if (vel_sel > vel_sel_max) vel_sel = vel_sel_max;
          data.i_vel = vel_array[vel_sel];
          data.scan_rate = 20*ceil(0.05*num_scans*data.i_vel/
                           (3.1416*60*data.calroll_d1*minrevs));
        }
      }
      else if (quit = '-')
      { _settextposition (5,46);
        printf("-");
        if (ascii == 'L')
        { load_sel--;
          if (load_sel < load_sel_min) load_sel = load_sel_min;
        }
        else
        { vel_sel--;
          if (vel_sel < vel_sel_min) vel_sel = vel_sel_min;
          data.i_vel = vel_array[vel_sel];
          data.scan_rate = 20*ceil(0.05*num_scans*data.i_vel/
                           (3.1416*60*data.calroll_d1*minrevs));
        }
```

```
    }
    _settextposition (4,52);
    printf("Velocity: %8.2f m/min   ",data.i_vel);
    _settextposition (5,52);
    printf("Load:     %6d kN/m   ",load_array[load_sel]);
    _settextposition (5,45);
    printf("  ");
  }
}                  /* End get sheet speed and load*/
load_bits = load_array_bin[load_sel];
clearl (4,1,45);
clearl (5,1,45);
_dos_gettime(&dtime);
_settextposition (1,1);
printf("\"ESC\" - EMERGENCY EXIT");
_settextposition(7,1);
printf("File number: %4d;  Run: %4d    \n",data.file_no,firstrun);
printf("Acq. rate:   %8.2lf Hz         \n",data.scan_rate);
_settextposition (20,1);
printf("starting motor....");
errNum = 0;
mask = apply_load_mask;                                  /* apply load */
if ((AQerrNum = AO_Write(board1,1,load_array_bin[load_sel]))!=0)
  DAQ_error("AO_Write",280);
if ((AQerrNum = DIG_Out_Port(board1,1,mask))!=0)
  DAQ_error("DIG_Out_Port",290);
if ((cont = motor()) != 27)    /* if motor() returns without ESC pressed */
{ if ((AQerrNum = AO_Write(board1,1,load_array_bin[load_sel]))!=0)
    DAQ_error("AO_Write",292);
  if ((AQerrNum = DIG_Out_Port(board1,1,load_dir[load_sel]))!=0)
    DAQ_error("DIG_Out_Port",294);
  if ((cont = wait()) != 27)   /* if wait() returns without ESC pressed */
  { if ((AQerrNum = CTR_EvCount(board1,ctr5,4,1))!=0)
      DAQ_error("CTR_EvCount clk",300);          /* start clock */
    if ((AQerrNum = CTR_EvCount(board2,ctr1,source1,1))!=0)
      DAQ_error("CTR_EvCount Vin",310);          /* start in counter */
    if ((AQerrNum = CTR_EvCount(board2,ctr5,source5,1))!=0)
      DAQ_error("CTR_EvCount Vou",320);          /* start out counter */
    if ((cont = exprmnt())==27)
      errNum = eexit(1);     /* if exprmnt() returns with ESC */
    if ((AQerrNum = CTR_EvRead(board1,ctr5,&overflow,&ClockCount))!=0)
      DAQ_error("CTR_EvRead clk",330);           /* Read clock */
    if ((AQerrNum = CTR_EvRead(board2,ctr1,&overflow,&VinCount))!=0)
      DAQ_error("CTR_EvRead Vin",340);           /* Read pulses in */
    if ((AQerrNum = CTR_EvRead(board2,ctr5,&overflow,&VoutCount))!=0)
      DAQ_error("CTR_EvRead Vou",350);           /* Read pulses out */
    if ((AQerrNum = CTR_Stop(board1,ctr1))!=0)
      DAQ_error("CTR_Stop clk",360);             /* Stop clock */
    if ((AQerrNum = CTR_Stop(board2,ctr1))!=0)
      DAQ_error("CTR_Stop Vin",370);             /* Stop in count */
    if ((AQerrNum = CTR_Stop(board2,ctr5))!=0)
      DAQ_error("CTR_Stop Vou",380);             /* Stop out count */
    if (VinCount > 0)
      deltaV = 100*(VoutCount*DeltaVFact/VinCount-1);
    else deltaV = 9999;
    get_last_data();              /* read latest data */
    display_last_data();          /* display */
    trim_control(0);                   /* control */
  }
  else errNum = eexit(2);    /* if wait() returns with ESC */
}
else errNum = eexit(3);      /* if motor() returns with ESC */

if (errNum < 2)            /* save whatever data was acquired */
{ itoa(data.file_no, file_name,10);
  pdest =strcpy( firstdta + 3, file_name );
  length=strlen(firstdta);
```

```
      pdest =strcpy( firstdta + length, dta );
      pdest=strcpy( file_name , firstdta);
      _settextposition(20,1);
      printf("writing file %s, data set # %d",file_name,firstrun);
      if ((outfbin = fopen(file_name, "ab")) != NULL )
      { for (i=0; i<8; i++)
          fwrite (&endblock, sizeof(endblock), 1, outfbin);
        fwrite (&ddate, sizeof(ddate), 1, outfbin);
        fwrite (&dtime, sizeof(dtime), 1, outfbin);
        fwrite (&data, sizeof(data), 1, outfbin);
        fwrite (cons, sizeof(cons), 1, outfbin);
        fwrite (&deltaV, sizeof(deltaV), 1, outfbin);
        fwrite (&VinCount, sizeof(VinCount), 1, outfbin);
        fwrite (&VoutCount, sizeof(VoutCount), 1, outfbin);
        fwrite (&ClockCount, sizeof(ClockCount), 1, outfbin);
        for (i=0; i<4; i++)
          fwrite (&endblock, sizeof(endblock), 1, outfbin);
        fwrite (&exp_buff1[0], sizeof(exp_buff1[0]), num_samples,
                                                     outfbin);
        fwrite (&exp_buff2[0], sizeof(exp_buff2[0]), num_samples,
                                                     outfbin);
        fclose(outfbin);
      }
      clear(20,1,1);
      firstrun++;
    }
    if (!errNum)
    { _settextposition(1,1);
      printf(" \"E\"  - END                                    \n");
      printf(" \"C\"  - CHANGE VELOCITY OR LOAD AND CONTINUE");
      while ((cont != 69) && (cont != 67))
      { get_last_data();
        trim_control(0);
        display_last_data();
        if (kbhit())
        { cont = getch();
          ascii = toascii(cont);
          if (ascii == 27)
          { cont = 69;            /* ASCII 69 = 'E', for exit */
            errNum = eexit(5);
          }
          else cont = toupper(cont);
        }
      }
    } else cont = 69;           /* force exit if errNum */
  } while (cont == 67);         /* end experiment loop unless C pressed */
  data.file_no++;
  write_data();
  if (firstrun>1)               /* If this is not the first run */
  { outfbin = fopen(file_name,"ab");
    for (i=0; i<8; i++)
      fwrite(&endfile,sizeof(endfile),1,outfbin);
    fclose(outfbin);
  }
  if (errNum)                   /* If emergency exit . . . */
  { do {} while (!kbhit());     /* don't release brake until keypressed */
    cont = getch();
  }
  else                          /* Otherwise normal exit, lift roll */
  { _settextposition(21,1);
    printf("Raising upper roll . . .            \n");
    time (&tstart);
    if ((AOerrNum = DIG_Out_Port(board1,1,(raise_load_mask)))!=0)
      DAQ_error("DIG_Out_Prt",480);
    if ((AOerrNum = AO_Write(board1,1,4000))!=0)
      DAQ_error("AO_Write",490);
    do                          /* Wait */
```

```
    { time (&tstop);
      el_time = difftime(tstop,tstart);
    }
    while (el_time < lift_time);
  }
  if((AQerrNum = AO_Write(board1,0,0))!=0)      /* Main motor off */
    DAQ_error("AO_Write Main",500);
  if((AQerrNum = AO_Write(board1,1,0))!=0)      /* Load off */
    DAQ_error("AO_Write Load",510);
  if ((AQerrNum = AO_Write(board2,0,0))!=0)     /* Trim motor off */
    DAQ_error("AO_Write Trim",520);
  if ((AQerrNum = DIG_Out_Port(board1,1,0))!=0)
    DAQ_error("DIG_Out_Prt 1",530);
  if ((AQerrNum = DIG_Out_Port(board2,1,0))!=0)
    DAQ_error("DIG_Out_Prt 2",540);
  if ((AQerrNum = AI_Clear(board1))!=0)
    DAQ_error("AI_Clear 1",570);
  if ((AQerrNum = AI_Clear(board2))!=0)
    DAQ_error("AI_Clear 2",580);
  data.file_no--;
  txconvert(data.file_no);
  if ((outftxt = fopen(control_file,"wt")) != NULL)
  { fprintf(outftxt,"%10.8f\n",Tp);
    fprintf(outftxt,"%10.8f\n",Ti);
    fprintf(outftxt,"%10.8f\n",Td);
    fprintf(outftxt,"%10.8f\n",Lp);
    fprintf(outftxt,"%10.8f\n",Li);
    fprintf(outftxt,"%10.8f\n",Ld);
    fprintf(outftxt,"%10.8f\n",deltaT);
    fclose(outftxt);
  }
  hfree(exp_buff1);              /* frees allocated memory */
  hfree(exp_buff2);
  printf("\n");
}

/*************************************************************************/
/*                      END MAIN PROGRAM                                 */
/*************************************************************************/
```

Appendix A3: Constitutive equations for linear viscoelastic models in a rolling nip

A3.1 Nip geometry

Refering to Figure A3.1, a cartesian coordinate system is defined with origin at the intersection of the plane of the undeformed sheet and the centreline joining the rolls. The x-axis is positive in the MD, while the z-axis is positive downwards. The sheet mid-plane is assumed to be a plane of symmetry. Time is measured from the point of first contact between sheet and roll: t=0 when x=-a. Distances z_i, z_n and z_f are the initial, in-nip and final recovered sheet half-thicknesses, $z(t)$ is the downward deflection of a point P(x,z) on the surface of the paper, $z_o = z_i - z_n$ is the maximum value of $z(t)$, and z_e is the half-thickness at the nip exit. Distances a and b are the ingoing and outgoing nip lengths; b_{max} is the largest possible value of b. Calendering variables are the roll radius R, sheet velocity V and line load L. If the roll radius R is much larger than z_o-$z(t)$, then

$$z(t) = \frac{Vt}{2R}(2a - Vt) \qquad [A3.1]$$

Strain is the change in thickness divided by the initial thickness:

$$\varepsilon_1(t) = \frac{Vt}{2Rz_i}(2a - Vt) \qquad [A3.2]$$

In-nip and permanent strains are defined as follows:

$$\varepsilon_n = \frac{z_i - z_n}{z_i} \qquad [A3.3]$$

$$\varepsilon_p = \frac{z_i - z_f}{z_i} \qquad [A3.4]$$

The ingoing and maximum outgoing nip lengths a and b_{max} are then

$$a^2 = 2Rz_i\varepsilon_n \qquad [A3.5]$$

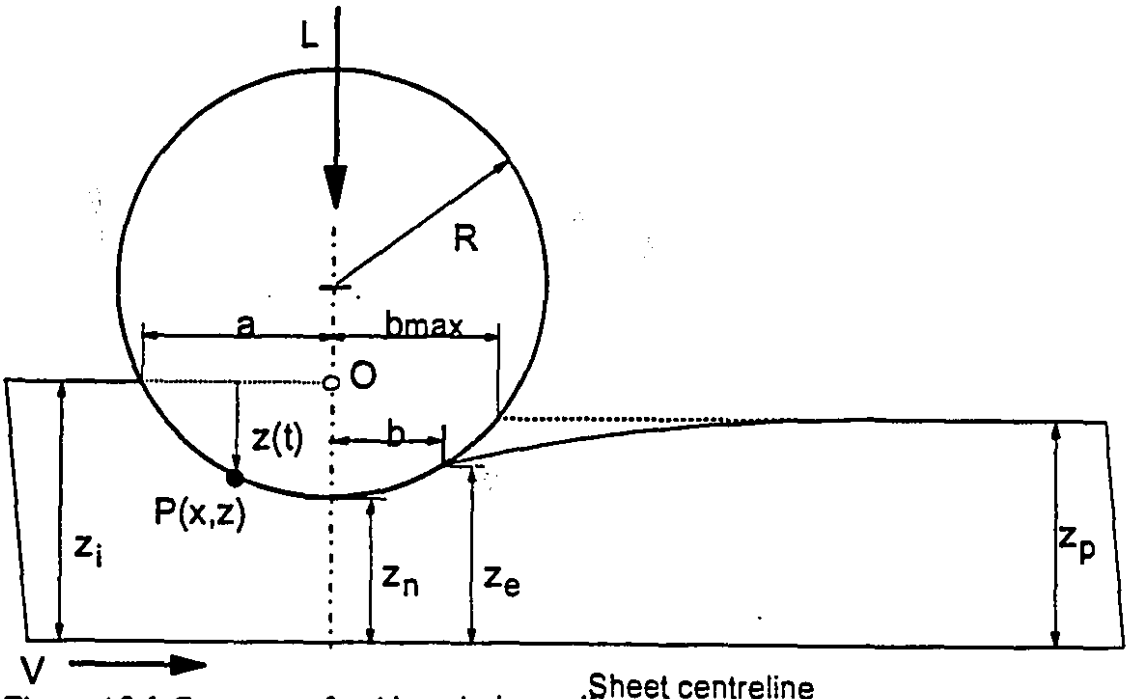

Figure A3.1 Geometry of a thin strip in a rolling nip.

$$b_{max}^2 = 2Rz_i\,(\varepsilon_n - \varepsilon_p) \qquad [A3.6]$$

The strain and strain rate while paper remains in contact with the rolls are then

$$\varepsilon_1(t) = \varepsilon_n \left(\frac{Vt}{a}\right)\left(2 - \frac{Vt}{a}\right) \qquad [A3.7]$$

$$\frac{\partial \varepsilon_1(t)}{\partial t} = \frac{2\varepsilon_n V}{a}\left(1 - \frac{Vt}{a}\right) \qquad [A3.8]$$

The strain rate is thus a maximum at the nip entrance, when t=0:

$$\left(\frac{\partial \varepsilon_1(t)}{\partial t}\right)_{max} = \frac{2\varepsilon_n V}{a} \qquad [A3.9]$$

A3.2 Model definitions

The two models discussed here are the standard linear liquid and Burger's four-element model. They are shown in Figures A3.2 and A3.3, and are composed of elastic elements G_M and G_K (with units Pa) and viscous elements η_M and η_K (with units Pa s).

The analysis is based on the following assumptions:

1. Roll radius ≪ web thickness; roll deformation ≪ web deformation.
2. Web roughness ≪ web thickness.
3. The web is a continuum in the z-direction.
4. Moduli G_i and viscosities η_j are material constants unaffected by stress, strain, or stress or strain rates.
5. MD and CD deformations are small; Poisson's ratio ≈ 0.
6. Shear stresses are negligible.

Numerical solution methods for root-finding can fail when the order of the coefficients is significantly different from 1. Although the analysis here will not use these substitutions, the analysis can proceed using non-dimensional model parameters:

$$\eta_1 = \frac{V}{L}\eta_M \qquad \eta_2 = \frac{V}{L}\eta_K \qquad [A3.10]$$

$$G_1 = \frac{a}{L}G_M \qquad G_2 = \frac{a}{L}G_K$$

Two other non-dimensional numbers are used. The Devorah number is the ratio of a material time to a typical processing time:

$$\xi = \frac{\tau}{a/V} \qquad [A3.11]$$

where the time constant τ is defined in the analysis. The nip length ratio β is

$$\beta = \frac{a + b}{a} \qquad [A3.12]$$

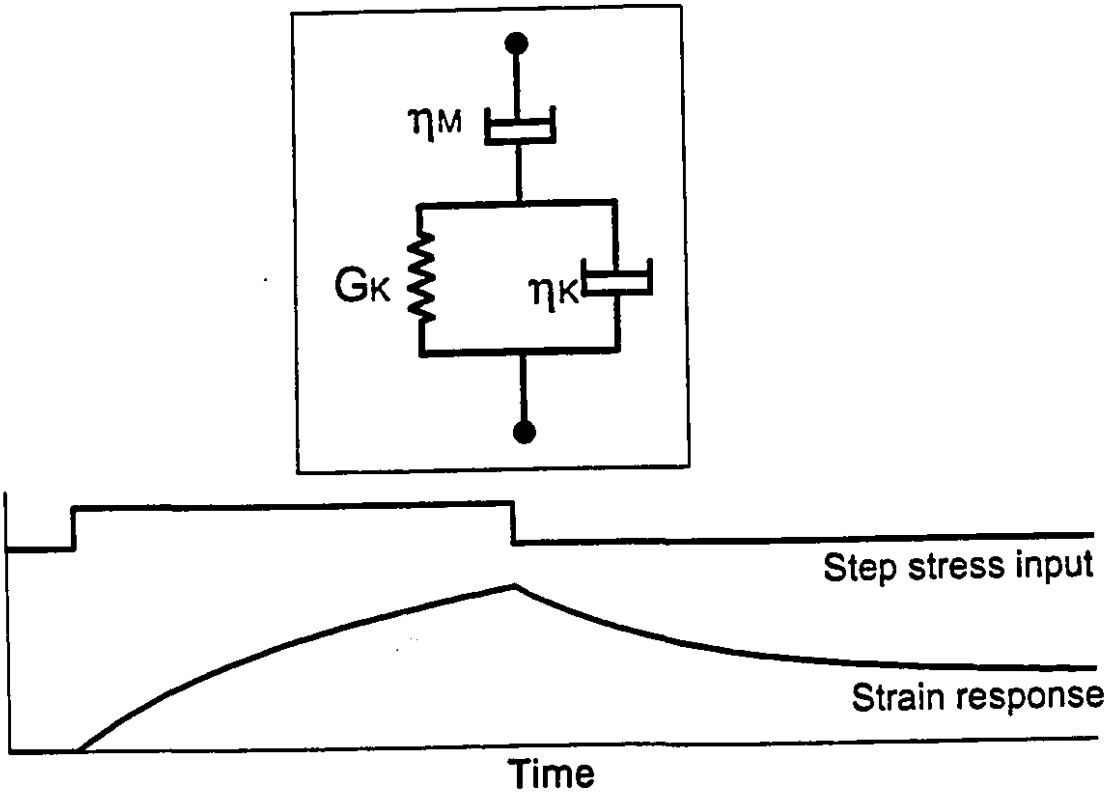

Figure A3.2 A linear liquid showing partial time-delayed recovery.

When b is small, β approaches 1; as b approaches b_{max}, β approaches β_{max}:

$$\beta_{max} = 1 + \sqrt{1 - \frac{\varepsilon_p}{\varepsilon_n}} \qquad [A3.13]$$

As the permanent strain ε_p approaches zero, β_{max} approaches 2.

For linear materials the Boltzmann superposition principle states

$$\sigma(t) = - \int_0^t \psi(t-t') \frac{\partial \varepsilon_1(t')}{\partial t'} dt' \qquad [A3.14]$$

When t_e is the elapsed time at the nip exit, the strain recovery for $t > t_e$ is

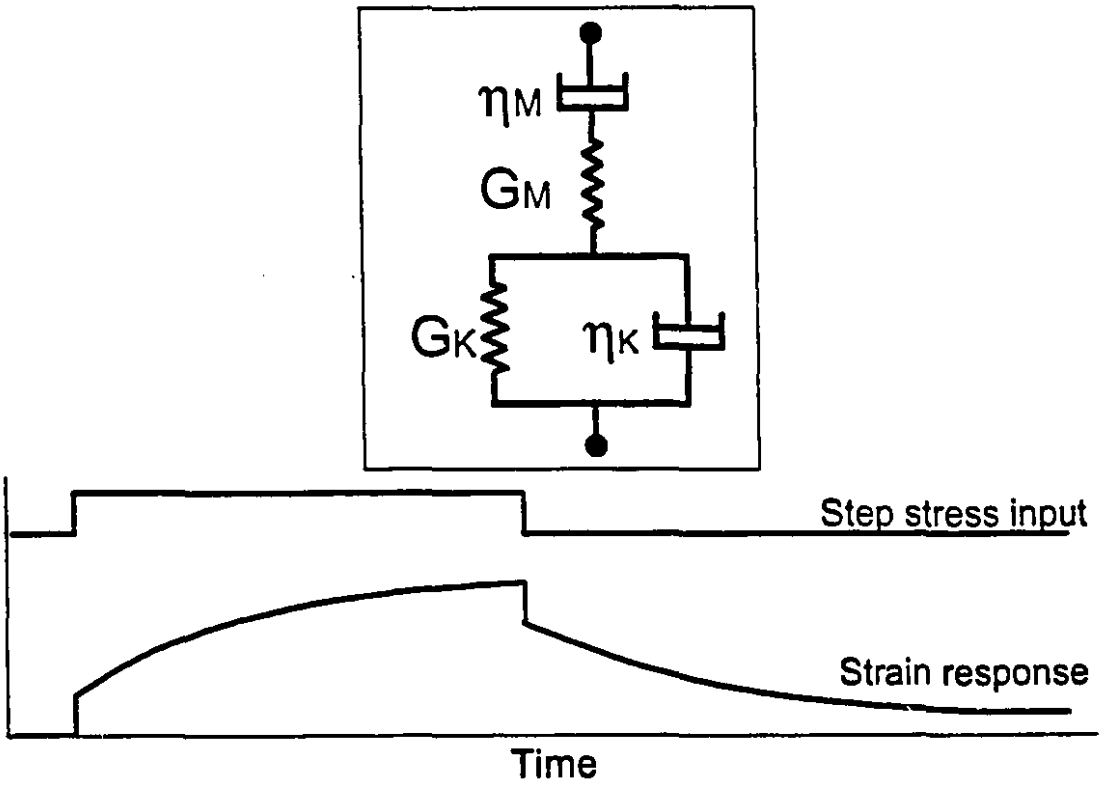

Figure A3.3 Burger's model showing instantaneous elasticity and delayed partial recovery.

$$\varepsilon_2(t) = \int_0^{t_e} \phi(t-t') \frac{\partial \sigma(t')}{\partial t'} dt' \qquad [A3.15]$$

where

$$t_e = \frac{a+b}{V} \qquad [A3.16]$$

The relaxation function $\psi(t)$ and the retardation function $\phi(t)$ are functions of the model parameters, as detailed next.

A3.3 Equations describing the standard linear liquid

A3.3.1 Relaxation and retardation functions

The relaxation function $\psi(t)$ is derived following Findley et al. [27]. The total strain is the sum of the strains in the Kelvin element ε_K and in the viscous element ε_M:

$$\varepsilon = \varepsilon_M + \varepsilon_K \qquad [A3.17]$$

where the strains are related to the overall stress σ by

$$\begin{aligned} \sigma &= \eta_M \dot{\varepsilon}_M \\ \sigma &= \eta_K \dot{\varepsilon}_K + G_K \varepsilon_K \end{aligned} \qquad [A3.18]$$

Substitute A3.18 into A3.17, rearrange and transform to the Laplace domain:

$$\varepsilon(s) = \left[\frac{1}{\eta_M s} + \frac{1}{\eta_2 (s + G_K/\eta_K)}\right]\sigma(s) \qquad [A3.19]$$

Multiply through by $\eta_M\eta_K(s + G_K/\eta_M)$, solve for $\sigma(s)$, and transform back to the time domain:

$$\sigma(t) + \left(\frac{\eta_M + \eta_K}{G_K}\right)\dot{\sigma}(t) = \eta_M \dot{\varepsilon}(t) + \left(\frac{\eta_M \eta_K}{G_K}\right)\ddot{\varepsilon}(t) \qquad [A3.20]$$

Define the relaxation time and two temporary variables q_1 and q_2:

$$\tau = \frac{\eta_M + \eta_K}{G_K} \qquad [A3.21]$$

$$q_1 = \eta_M \qquad q_2 = \frac{\eta_M \eta_K}{G_K} \qquad [A3.22]$$

Rewrite Equation A3.20 with a step strain input of magnitude ε_o, then retransform (Tschoegl [79], p.569):

$$\sigma(t) + \tau\dot{\sigma}(t) = q_1\varepsilon_o\delta(t) + q_2\varepsilon_o\frac{\partial}{\partial t}\delta(t) \qquad [A3.23]$$

$$\begin{aligned}\sigma(s) &= \varepsilon_o\left[\frac{q_1 + q_2 s}{1 + \tau s}\right] \\ &= \varepsilon_o\left[\frac{q_1}{\tau}\left(\frac{\tau}{1 + \tau s}\right) + \frac{q_2}{\tau}\left(\frac{\tau s}{1 + ts}\right)\right]\end{aligned} \qquad [A3.24]$$

$$\sigma(t) = \varepsilon_o\frac{q_2}{\tau}\left[\left(\frac{q_1}{q_2} - \frac{1}{\tau}\right)e^{-t/\tau} + \delta(t)\right] \qquad [A3.25]$$

Define the equivalent viscosity η_e and equivalent time constant τ_e:

$$\begin{aligned}\frac{q_2}{\tau} &= \frac{\eta_M\eta_K}{\eta_M + \eta_K} \\ &= \eta_e\end{aligned} \qquad [A3.26]$$

$$\begin{aligned}\frac{q_1}{q_2} - \frac{1}{\tau} &= \frac{1}{\tau_K} - \frac{1}{\tau} \\ &= \frac{1}{\tau_e}\end{aligned} \qquad [A3.27]$$

where the Kelvin time constant $\tau_K = \eta_K/G_K$. Then the relaxation function is the response to the step strain ε_o:

$$\psi(t) = \eta_e\left[\frac{e^{-t/\tau}}{\tau_e} + \delta(t)\right] \qquad [A3.28]$$

The retardation function for this model is given by Findley et al. [27]:

$$\phi(t) = \frac{t}{\eta_M} + \frac{1}{G_K}\left(1 - e^{-t/\tau_k}\right) \qquad [A3.29]$$

A3.3.2 Standard linear liquid: explicit expressions for stress and strain

Substitute the relaxation function, Equation A3.28, and the strain rate, Equation A3.8, into the Boltzmann integral, Equation A3.14, and integrate:

$$\sigma(t) = \int_0^t \eta_e \left[\frac{1}{\tau_e} \exp\left(\frac{-(t-t')}{\tau} \right) + \delta(t-t') \right] \frac{2\varepsilon_n V}{a} \left(1 - \frac{Vt'}{a} \right) dt'$$

$$= \frac{2\varepsilon_n V}{a} \frac{\eta_e}{\tau_e} e^{-t/\tau} \left[\int_0^t e^{t'/\tau} \, dt' - \frac{V}{a} \int_0^t e^{t'/\tau} \, t' \, dt' \right] \qquad [A3.30]$$

$$+ \frac{2\varepsilon_n V}{a} \eta_e \int_0^t \delta(t-t') \left(1 - \frac{Vt'}{a} \right) dt'$$

A solution for the second integral can be found in published tables of integrals:

$$\int u e^{\alpha u} du = \frac{(\alpha u - 1)}{\alpha^2} e^{\alpha u} + C \qquad [A3.31]$$

The third integral can be solved by noting that $\delta(t-t')$ is different from 0 only when $t = t'$. Therefore

$$\int_0^\infty \delta(t-t') \, f(t') \, dt' = f(t) \int_0^\infty \delta(t-t') \, dt' \qquad [A3.32]$$

$$= f(t)$$

and

$$I_3 = \left(1 - \frac{Vt}{a} \right) \qquad [A3.33]$$

Performing the other two integrations gives

$$\sigma(t) = \frac{2\varepsilon_n V}{a}\frac{\eta_M^2}{\eta_M+\eta_K}\left[(1+\xi)(1-e^{-t/\tau})-\frac{Vt}{a}\right]+\frac{2\varepsilon_n V}{a}\left(1-\frac{Vt}{a}\right)\frac{\eta_M\eta_K}{\eta_M+\eta_K} \qquad [A3.34]$$

where the Devorah number ξ is as defined in Equation A3.11. The stress rate is therefore

$$\frac{\partial\sigma(t)}{\partial t} = \frac{2\varepsilon_n V}{a}\left[\frac{\eta_c^2}{\eta_K\tau_K}(1+\xi)e^{-t/\tau}-\eta_M\frac{V}{a}\right] \qquad [A3.35]$$

Substitute A3.29 and the stress rate in the nip, A3.35, into A3.15 and integrate:

$$\varepsilon_2(t) = \int_0^{t_c}\left[\frac{t-t'}{\eta_M}+\frac{1-e^{-(t-t')/\tau_K}}{G_K}\right]\frac{\partial\sigma(t')}{\partial t'}\,dt' \qquad [A3.36]$$

Collect terms:

$$\varepsilon_2(t) = \left[\frac{t}{\eta_M}+\frac{1}{G_K}\right]\int_0^{t_c}\frac{\partial\sigma(t')}{\partial t'}\,dt' - \int_0^{t_c}\left[\frac{t'}{\eta_M}+\frac{e^{-t/\tau_K}e^{t'/\tau_K}}{G_K}\right]\frac{\partial\sigma(t')}{\partial t'}\,dt' \qquad [A3.37]$$

The first integral is zero, since

$$\int_0^{t_c}\frac{\partial\sigma(t)}{\partial t}\,dt = \sigma(t_c)-\sigma(0) \qquad [A3.38]$$

Evaluating the second integral gives an expression with a time-dependent term and a constant term:

$$\varepsilon_2(t) = C_0 - C_1 e^{-t/\tau_K} \qquad [A3.39]$$

where the constant term is equal to the fully recovered strain ε_p:

$$C_0 = \varepsilon_p$$

$$= \frac{2\varepsilon_n V}{a}\,\frac{\eta_M}{G_K}\left[(1+\xi) - (1+\xi)\left(\frac{\beta}{\xi}+1\right)e^{\beta/\xi} - \frac{a\eta_M\beta^2}{2VG_K} - \xi_K\left(e^{\beta/\xi_K}-1\right)\right] \qquad \text{[A3.40]}$$

and where

$$C_1 = 2\varepsilon_n\left(\frac{\eta_M}{\eta_M+\eta_K}\right)^2\frac{\xi(1+\xi)}{1-\xi/\xi_K}\left(e^{-\frac{\beta}{\xi}\left(1-\frac{\xi}{\xi_K}\right)}-1\right) \qquad \text{[A3.41]}$$

A3.4 Equations describing Burger's model

A3.4.1 Relaxation and retardation functions

The relaxation function is derived by Findley et al. [27]:

$$\psi(t) = K_1 e^{-t/\tau_1} - K_2 e^{-t/\tau_2} \qquad [A3.42]$$

where K_1, K_2, τ_1 and τ_2 are functions of the model parameters G_M, G_K, η_M, and η_K:

$$p_1 = \frac{\eta_M}{G_M} + \frac{\eta_K}{G_K} + \frac{\eta_M}{G_K} \qquad (r_1, r_2) = \frac{p_1 \pm A}{2p_2}$$

$$p_2 = \frac{\eta_M \eta_K}{G_M G_K} \qquad (\tau_1, \tau_2) = \left(\frac{1}{r_1}, \frac{1}{r_2}\right)$$

$$q_1 = \eta_M \qquad (\xi_1, \xi_2) = \left(\frac{V\tau_1}{a}, \frac{V\tau_2}{a}\right) \qquad [A3.43]$$

$$q_2 = \frac{\eta_M \eta_K}{G_K} \qquad K_1 = \frac{q_1 - q_2 r_1}{A}$$

$$A = \sqrt{p_1^2 - 4p_2} \qquad K_2 = \frac{q_1 - q_2 r_2}{A}$$

The retardation function $\phi(t)$ is also derived by Findley et al [27]:

$$\phi(t) = \frac{1}{G_M} + \frac{t}{\eta_M} + \frac{1 - e^{-t/\tau_K}}{G_K} = \frac{1}{G_M}\left[1 + \frac{t}{\tau_M} + \frac{G_M}{G_K}\left(1 - e^{-t/\tau_K}\right)\right] \qquad [A3.44]$$

where the Maxwell and Kelvin time constants τ_M and τ_K are given by

$$\tau_M = \frac{\eta_M}{G_M} \qquad \tau_K = \frac{\eta_K}{G_K} \qquad [A3.45]$$

A3.4.2 Burger's model: explicit expressions for stress and strain

The derivation proceeds as for the standard linear liquid, Section A3.3.2, with the appropriate response functions substituted. The stress profile in the nip is obtained by substituting the relaxation function, Equation A3.42, and the strain rate, Equation A3.8, into the Boltzmann equation, A3.14:

$$\sigma(t) = -2\varepsilon_n \left[K_1\xi_1(1+\xi_1)\left(1-e^{-t/\tau_1}\right) - K_2\xi_2(1+\xi_2)\left(1-e^{-t/\tau_2}\right) - (K_1\xi_1-K_2\xi_2)\frac{Vt}{a} \right] \quad [A3.46]$$

Differentiating the stress profile, Equation A3.46, and substituting into A3.15 along with the retardation equation, A3.44, gives the strain after the nip exit:

$$\varepsilon_2(t) = \frac{1}{G_M}\int_0^{t_e} \left[1 + \frac{t-t'}{\tau_M} + \frac{G_M}{G_K}\left(1 - e^{-(t-t')/\tau_K}\right) \right] \frac{\partial\sigma(t')}{\partial t'}\, dt' \quad [A3.47]$$

Separating terms in t from terms in t′ gives

$$\varepsilon_2(t) = \frac{1}{G_M}\left[1 + \frac{t}{\tau_M} + \frac{G_M}{G_K}\right]\int_0^{t_e} \frac{\partial\sigma(t')}{\partial t'}\, dt' - \frac{1}{G_M}\int_0^{t_e}\left[\frac{t'}{\tau} + e^{-t/\tau_K}e^{t'/\tau_K}\right]\frac{\partial\sigma(t')}{\partial t'}\, dt' \quad [A3.48]$$

As for the standard linear liquid, the first integral is zero. Evaluating the second integral gives

$$\varepsilon_2(t) = C_0 - C_1 e^{-t/\tau_K} \qquad \text{[A3.49]}$$

where the constant term is equal to the fully recovered strain ε_p:

$$\begin{aligned} C_0 &= \varepsilon_p \\ &= \frac{2\varepsilon_n a}{V\eta_M}\left[K_2\xi_2(1+\xi_2)(\beta+\xi_2)e^{-\beta/\xi_2} - K_1\xi_1(1+\xi_1)(\beta+\xi_1)e^{-\beta/\xi_1}\right. \\ &\qquad \left. + \left(K_1\xi_1^2(1+\xi_1) - K_2\xi_2^2(1+\xi_2)\right) - \left(K_1\xi_1 - K_2\xi_2\right)\frac{\beta^2}{2}\right] \end{aligned} \qquad \text{[A3.50]}$$

and where

$$\begin{aligned} C_1 = \frac{2\varepsilon_n}{G_K}\left[\frac{K_1\xi_1(1+\xi_1)}{1-\xi_1/\xi_K}\left(e^{-\frac{\beta}{\xi_1}\left(1-\frac{\xi_1}{\xi_k}\right)}-1\right) - \frac{K_2\xi_2(1+\xi_2)}{1-\xi_2/\xi_K}\left(e^{-\frac{\beta}{\xi_2}\left(1-\frac{\xi_2}{\xi_k}\right)}-1\right)\right. \\ \left. - \xi_k\left(K_1\xi_1 - K_2\xi_2\right)\left(1-e^{\beta/\xi_k}\right)\right] \end{aligned} \qquad \text{[A3.51]}$$